

MICROCOPY RESOLUTION TEST CHART
NATIONAL BUREAU OF STANDARDS-1963-A

AD-A160 657

RADC-TR-85-107
Phase Report
July 1985



12

MODELING CROSSTALK ON PRINTED CIRCUIT BOARDS

Georgia Institute of Technology

Clayton R. Paul and Woodrow W. Everett, III

DTIC
ELECTE
OCT 28 1985
S B

APPROVED FOR PUBLIC RELEASE; DISTRIBUTION UNLIMITED

DTIC FILE COPY

**ROME AIR DEVELOPMENT CENTER
Air Force Systems Command
Griffiss Air Force Base, NY 13441-5700**

85 10 28 023

This report has been reviewed by the RADC Public Affairs Office (PA) and is releasable to the National Technical Information Service (NTIS). At NTIS it will be releasable to the general public, including foreign nations.

RADC-TR-85-107 has been reviewed and is approved for publication.

APPROVED: *Roy F. Stratton*

ROY F. STRATTON
Project Engineer

APPROVED:

W.S. Tuthill
W.S. TUTHILL, Colonel, USAF
Chief, Reliability & Compatibility Division

FOR THE COMMANDER:

John A. Ritz

JOHN A. RITZ
Plans Office

If your address has changed or if you wish to be removed from the RADC mailing list, or if the addressee is no longer employed by your organization, please notify RADC (RBCT) Griffiss AFB NY 13441-5700. This will assist us in maintaining a current mailing list.

Do not return copies of this report unless contractual obligations or notices on a specific document requires that it be returned.

REPORT DOCUMENTATION PAGE

1a. REPORT SECURITY CLASSIFICATION UNCLASSIFIED			1b. RESTRICTIVE MARKINGS N/A		
2a. SECURITY CLASSIFICATION AUTHORITY N/A			3. DISTRIBUTION / AVAILABILITY OF REPORT Approved for public release; distribution unlimited		
2b. DECLASSIFICATION / DOWNGRADING SCHEDULE N/A					
4. PERFORMING ORGANIZATION REPORT NUMBER(S) N/A			5. MONITORING ORGANIZATION REPORT NUMBER(S) RADC-TR-85-107		
6a. NAME OF PERFORMING ORGANIZATION Georgia Institute of Technology		6b. OFFICE SYMBOL (If applicable) 	7a. NAME OF MONITORING ORGANIZATION Rome Air Development Center (RBCT)		
6c. ADDRESS (City, State, and ZIP Code) 206 O'Keefe Building Atlanta GA 30332			7b. ADDRESS (City, State, and ZIP Code) Griffiss AFB NY 13441-5700		
8a. NAME OF FUNDING / SPONSORING ORGANIZATION Rome Air Development Center		8b. OFFICE SYMBOL (If applicable) RBCT	9. PROCUREMENT INSTRUMENT IDENTIFICATION NUMBER F30602-81-C-0185		
8c. ADDRESS (City, State, and ZIP Code) Griffiss AFB NY 13441-5700			10. SOURCE OF FUNDING NUMBERS		
			PROGRAM ELEMENT NO. 62702F	PROJECT NO. 2338	TASK NO. 03
			WORK UNIT ACCESSION NO. PW		
11. TITLE (Include Security Classification) MODELING CROSSTALK ON PRINTED CIRCUIT BOARDS					
12. PERSONAL AUTHOR(S) Clayton R. Paul, Woodrow W. Everett, III					
13a. TYPE OF REPORT Phase		13b. TIME COVERED FROM Feb 84 TO Dec 84		14. DATE OF REPORT (Year, Month, Day) July 1985	
15. PAGE COUNT 176					
16. SUPPLEMENTARY NOTATION Work was performed at the University of Kentucky, Lexington KY (Electrical Engineering Department) under the RADC Post Doctoral Program					
17. COSATI CODES			18. SUBJECT TERMS (Continue on reverse if necessary and identify by block number)		
FIELD	GROUP	SUB-GROUP			
09	03		Printed circuit board, Transmission Lines,		
09	01		Crosstalk, Ribbon Cable,		
			Coupling, Electromagnetic Compatibility		
19. ABSTRACT (Continue on reverse if necessary and identify by block number)					
<p>The modeling of crosstalk on printed circuit boards is investigated. The emphasis is on simple models for use in CAD/CAM codes. Several simple models are developed. Their predictions are assessed for typical printed circuit board dimensions and interfering signals.</p> <p>The model predictions are compared to those of conventional lumped-circuit iterative models as well as experimental results. Also included are similar results for a ribbon cable.</p> <p><i>K. Paul, W. Everett, III</i></p>					
20. DISTRIBUTION / AVAILABILITY OF ABSTRACT <input checked="" type="checkbox"/> UNCLASSIFIED/UNLIMITED <input type="checkbox"/> SAME AS RPT <input type="checkbox"/> DTIC USERS			21. ABSTRACT SECURITY CLASSIFICATION UNCLASSIFIED		
22a. NAME OF RESPONSIBLE INDIVIDUAL Ray E. Stratton			22b. TELEPHONE (Include Area Code) (315) 330-2563		22c. OFFICE SYMBOL RADC (RBCT)

B

TABLE OF CONTENTS

	Page
I. Introduction	1
1.1. The Conventional, Transmission-Line Model	8
1.1.1. The Transmission-Line Equations--Lossless Lines	9
1.1.2. The Transmission-Line Equations--Lossy	13
1.2. Incorporating the Terminal Constraints	18
1.3. Report Summary	19
II. Survey of Previous Methods	20
2.1. Lumped Circuit Iterative Models	20
2.2. Direct, Time-Domain Solution of the Transmission-Line Equations	28
2.3. Frequency-Domain Methods	35
2.4. Summary	37
III. A Simple, Time-Domain Prediction Model	38
3.1. Inductive and Capacitive Coupling Models	40
3.2. A Simple, Time-Domain Crosstalk Prediction Model	50
3.3. An Improved, Time-Domain Crosstalk Prediction Model	54
3.3.1. Solution for Trapezoidal (Clock) Pulses	63
3.4. Implementation in CAD Codes	76
3.5. A Further Improvement	78
IV. Experimental Results	83
4.1. Printed Circuit Board	84
4.1.1. Frequency-Domain Results	87
4.1.2. Time-Domain Results	87
4.2. Ribbon Cables	108
4.2.1. Frequency-Domain Results	108
4.2.2. Time-Domain Results	126
4.3. Summary	151
V. Summary and Conclusions	164
REFERENCES	166

☒
☐
☐



Dist

A-1

for

60303

I. Introduction

Compact packaging of electronic circuits has had an extraordinary impact on the electronics industry. Small scale, integrated circuits allow the placement of a large number of discrete components on a single chip. However these small packages must be interconnected in order to perform specific tasks.

The common medium for interconnecting these packages is the printed circuit board (PCB). PCB's consist of a thin, substrate material on which rectangular conductors (lands) are placed. The most common type of substrate or board is glass-epoxy having a relative permittivity of approximately $\epsilon_r \doteq 5$. Typical board thicknesses are on the order of 25-100 mils with the typical thickness being 1/16 inch or 62.5 mils. The conductors are "etched" on either one side (single-sided boards), or on both sides (double-sided boards) and connected through holes known as "vias". Another type of board which is somewhat less common has lands on one side and a ground plane on the other and is often referred to as microstrip. There is also an increasing use of multilayer boards although these will not be considered in this report.

The metal which is deposited on the board surface is typically copper. The thicknesses are characterized by weight per unit surface area. The common thicknesses are 1 ounce and 2 ounce which means a weight of 1 or 2 ounces of copper per square foot. The 1 ounce copper thickness is 0.356 mm (1.4 mils). The thickness of 2 ounce copper is double that of 1 ounce copper or .0711 mm (2.8 mils).

Land widths vary depending on the intended use of that land. Signal lands have widths ranging from 5 to 25 mils. Lands intended for carrying large currents such as motor drivers are typically 50 mils in width and

larger. Land spacings range from 5 mils to well over 100 mils depending on layout constraints. In short, one can say very little about "typical" land widths and spacings. In fact, on most PCB's there exist areas in which no definable land lengths exist; sections are filled with metallic areas to reduce ground noise due to return path inductance. Typical practice uses a "gridded ground" to aid in minimizing "ground shifts" due to inductive surges caused by switching currents.

This wide variability in land widths, spacing and shape is only one reason for the difficulty in characterizing electrical properties of a PCB. Perhaps the major problem is the enormous number of lands (and interconnected components) on a typical PCB. If one wishes to model a PCB for the purposes of analyzing functional, electrical performance, one is faced with a modeling as well as computational task of considerable magnitude.

Of perhaps equal importance is the analysis of the electrical performance of a PCB layout for the purpose of determining nonfunctional performance such as crosstalk, ringing, etc. which may affect functional performance. Two boards intended to perform the same task but which have different layouts may perform quite differently. One of the major reasons for this is crosstalk or electromagnetic coupling between lands. The current and voltage associated with a pair of lands generate electric and magnetic fields which interact with neighboring lands. These electromagnetic fields induce signals in other lands which appear across the terminals of components attached to these lands. These induced signals may cause the devices to malfunction or may reduce their performance to marginal levels. In other words, on-board interference may be caused by this crosstalk.

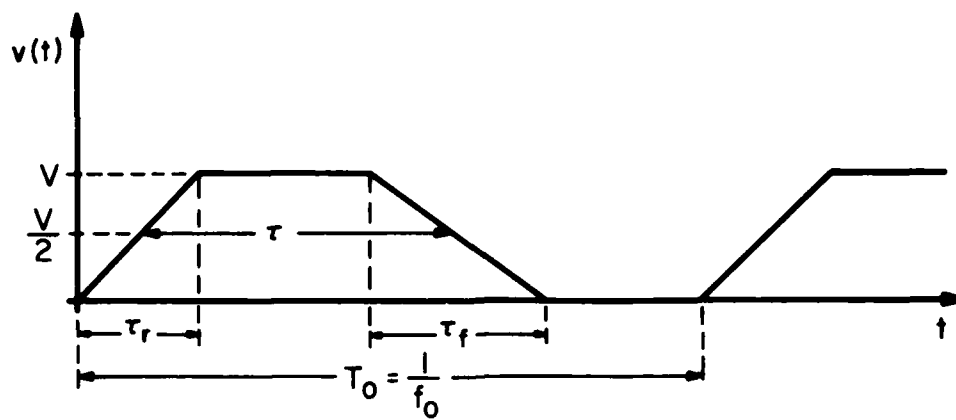
There exist a large number of digital computer programs which are intended to model the electrical performance of interconnected electronic components. In the majority of these codes, the effect of the inter-connecting lands are neglected. There is the inherent ability to consider these effects via lumped circuit approximate models of the lands but this is rarely done by the user.

The speeds of clock circuits (and the associated rise/fall times) on PCB's are increasing at a dramatic rate. Present clock speeds are on the order of 10 to 25 MHz. However, speeds of 100 MHz are not far away. As the basic speeds of the clock circuits increase, so do the associated rise/fall times. It is not uncommon to find rise/fall times of pulses on the order of 1 to 10 ns. Subnanosecond rise/fall times are certainly in the near future.

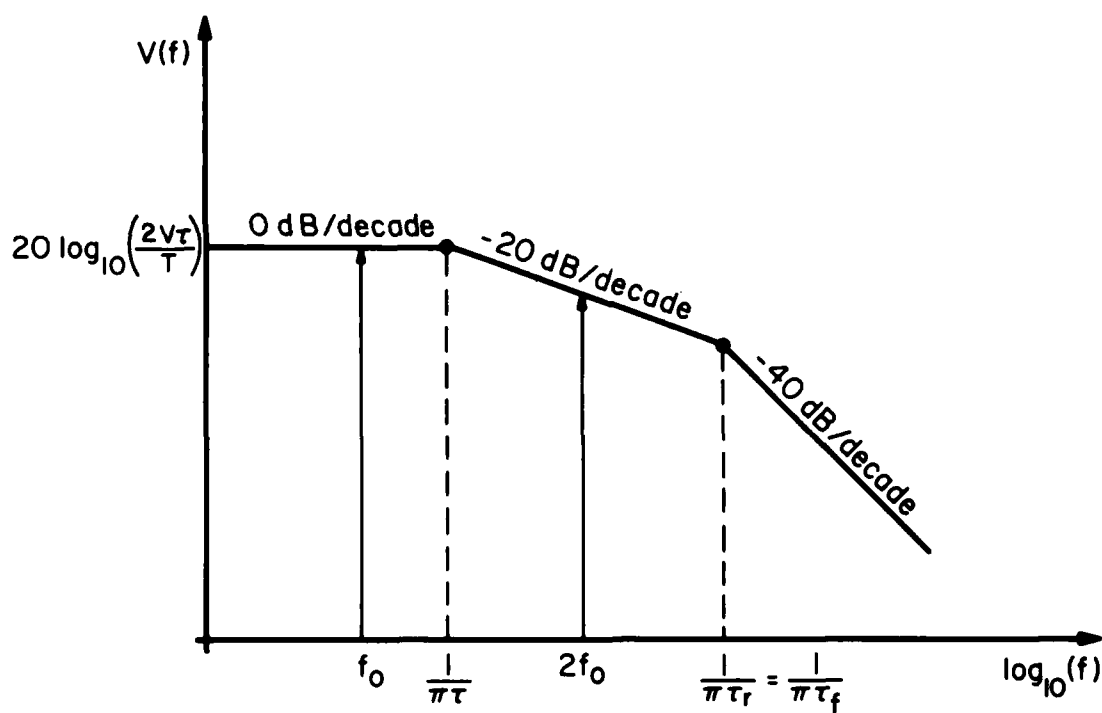
As the speeds and associated rise/fall times increase so do their high frequency spectral content. For example, consider a typical clock signal approximated as a periodic, trapezoidal waveform shown in Fig. 1-1(a). The repetition frequency is denoted as f_o with the bit rate or period being $T_o = 1/f_o$. The pulse width (between 50% points) is denoted as τ . The rise and fall times are denoted as τ_r and τ_f , respectively. For equal rise and fall times, one can obtain the Fourier series coefficients as

$$c_n = \frac{2V\tau}{T_o} \frac{\sin(\frac{n\pi\tau}{T_o})}{(\frac{n\pi\tau}{T_o})} \frac{\sin(\frac{n\pi\tau_r}{T_o})}{(\frac{n\pi\tau_r}{T_o})} \quad (1.1)$$

The amplitudes of these spectral components can be bounded as shown in Fig. 1.1(b). The spectra are approximately constant out to a frequency of $1/\pi\tau$. Between this and $1/\pi\tau_r$ they fall off at -20 dB/decade. Above



(a)



(b)

Fig. 1.1. Bounds on trapezoidal pulse spectra.

$1/\pi\tau_r$ they fall off at -40 dB/decade. Thus the high-frequency spectral content of the signal is primarily determined by the rise/fall time of the pulse.

For example, consider a typical 10 MHz signal with 50% duty cycle having 5 ns rise/fall times. The breakpoints are at 1.6 MHz and 63.7 MHz. A pair of lands of typical length of 10 cm on a glass epoxy board will be 1/10 of a wavelength and electrically short at approximately 170 MHz. Thus the lands will be electrically short at frequencies below the breakpoints. In this range, the crosstalk typically increases at +20 dB/decade. The spectrum of the crosstalk signal can then be found as the product of the spectrum of the clock signal and the spectrum of the crosstalk transfer function as shown in Fig. 1.2. Note that the resulting spectrum of the crosstalk pulse is constant between the above two frequencies. Reducing the pulse rise/fall time directly increases the high frequency content of the crosstalk spectrum. It will be shown that this results in an increased amplitude of the time-domain crosstalk pulse. Thus the potential interference of this crosstalk pulse increases directly as the rise/fall time of the source pulse decreases.

This concept will be addressed in more detail in later chapters. However it is sufficient to point out here that potential crosstalk problems will increase with anticipated pulse rise/fall time reductions. Crosstalk which, with present speeds, cause few problems will generate an ever increasing set of interference problems in the future.

It is therefore becoming increasingly important to consider crosstalk on PCB's. Present computer-aided design (CAD) programs do not generally include modeling capabilities for the purpose of including crosstalk. There are inherent capabilities via lumped circuit approximations of the

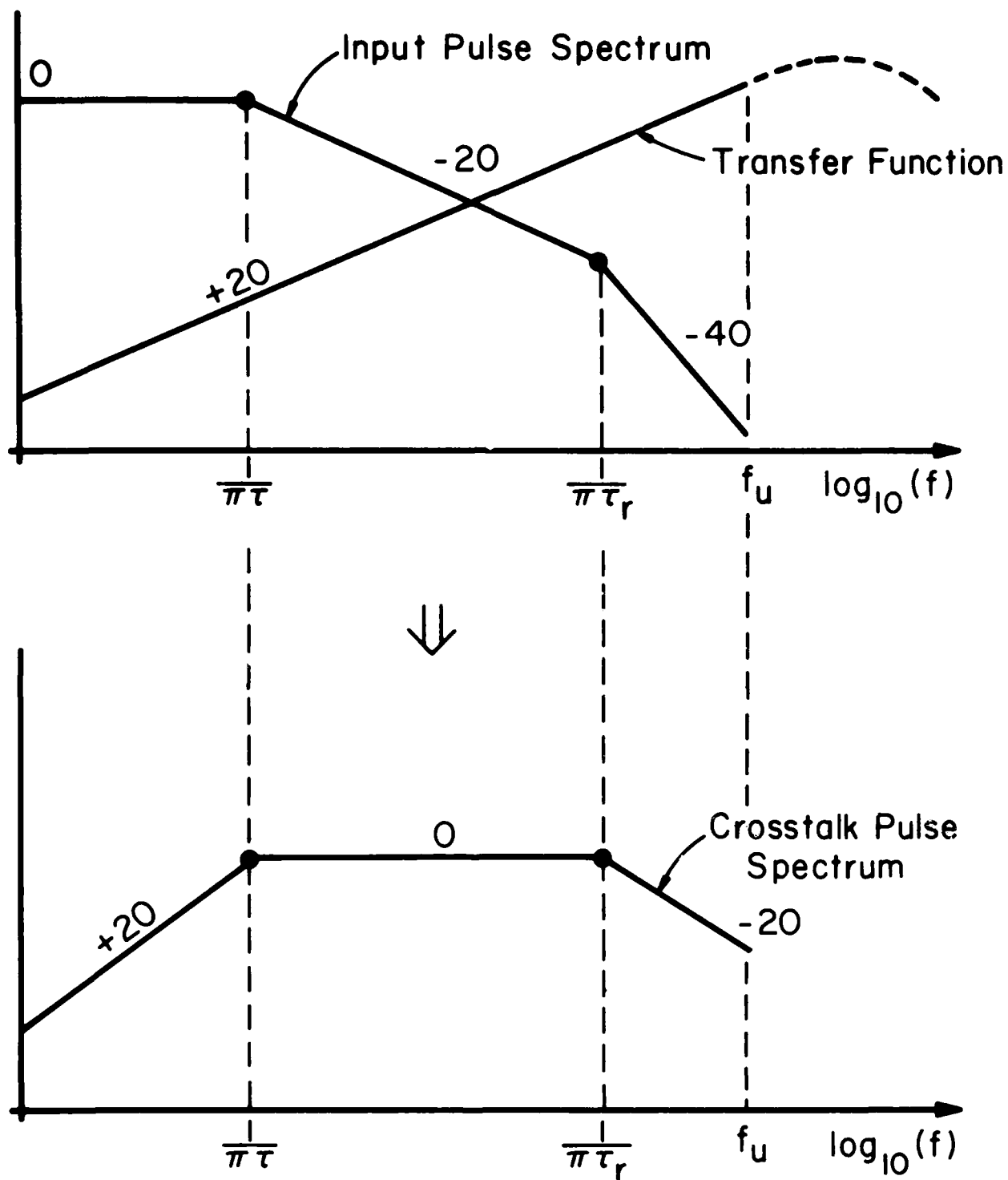


Fig. 1.2. The net spectrum of the crosstalk pulse.

land-circuits as will be discussed in later chapters. However, a circuit designer who uses these codes to check functional performance of a board will not be predisposed to include crosstalk considerations because preparation of crosstalk models for use in the program will require a large effort on the analyst's part. For example, the analyst will generally not have information readily available as to the land dimensions or configuration; functional schematics do not include this. Thus the first major problem which the analyst will face if he/she intends to include a crosstalk analysis in the functional performance analysis is gathering these physical layout data. Generally these data are computerized since the board layout was probably done by automated design techniques.

Once the analyst gathers this physical layout data, he/she is faced with a more formidable problem; translating that physical data into mathematical models suitable for use in the intended CAD program. If gathering the physical layout data is not a sufficient deterrent to including crosstalk analysis in the CAD program, this latter aspect of the problem--preparing a mathematical model--generally is. What would be highly desirable if we desire crosstalk analysis to be integrated into functional analysis would be to make the inclusion of these crosstalk models as simple as possible for the analyst.

The primary purposes of this report are (1) to examine the available time-domain, crosstalk prediction models and to determine their suitability for inclusion in CAD programs and (2) to develop a model which minimizes the implementation difficulty while providing reasonable estimates of PCB crosstalk and is suitable for inclusion in typical CAD programs. It is certainly not possible to determine an all-inclusive prediction model

which is simple and at the same time will handle general, transmission lines of any dimensions driven by completely general signals. We will evaluate models using criteria such as typical board/land dimensions and typical driving signals. Within these limitations we will find that one can develop fairly simple models which yield quite accurate predictions. Within these restrictions we will find that the only limitation to realizing our goal of making crosstalk analysis a simple matter in CAD programs is translating the physical layout dimensions to the appropriate per-unit-length line parameters.

1.1. The Conventional, Transmission-Line Model

The usual method for modelling electromagnetic coupling between parallel conductors is the distributed-parameter, transmission line model [1]. The model assumes that the mode of propagation on the line is the Transverse Electro Magnetic (TEM) mode. For lines which have (1) imperfect conductors and/or (2) an inhomogeneous surrounding medium, a pure TEM mode is not possible. However the dominant mode of propagation resembles the TEM mode and is referred to as the "quasi-TEM" mode. Assuming a TEM mode of propagation for these structures, while technically not correct, nevertheless has been shown to provide accurate representation for (1) typical conductor materials and (2) typical dielectric inhomogeneities so long as the frequency(s) of excitation is small enough. For typical PCB's, the transmission line model will provide an accurate characterization for frequencies up to the GHz range. Therefore the fundamental model which we will use is the distributed parameter transmission-line model.

1.1.1. The Transmission-Line Equations - Lossless Lines

Consider a general transmission line consisting of $(n+1)$ lossless conductors immersed in a lossless, surrounding medium. We will assume the line to be uniform; that is, cross-sectional views at any two points along the line will be identical in dimensions as well as conductor and medium properties. Thus we consider $(n+1)$ parallel conductors. The conductors will be parallel to the x axis. An electrically small Δx length of the line is modeled as shown in Fig. 1.3. with per-unit-length self inductances (capacitances) ℓ_{ii} (c_{ii}) and mutual inductances (capacitances) ℓ_{ij} (c_{ij}) for $i, j=1, \dots, n$. These per-unit-length parameters are calculated from static (DC) configurations of the cross-sectional fields [1]. Line voltages, $\underline{V}_i(x, t)$, are defined for n of the conductors with respect to the $(n+1)$ st (reference) conductor. We refer to this conductor as the 0 conductor. Line currents, $\underline{J}_i(x, t)$ are defined for the n conductors in the positive x direction and return in the reference conductor so that the net current in the $+x$ direction at each point along the line is zero. These notions are exact for the TEM mode and are reasonable approximations for the "quasi-TEM" mode [1].

From the circuit in Fig. 1.3 one can obtain the transmission-line equations, in the limit as $\Delta x \rightarrow 0$ as a coupled set of $2n$ partial differential equations [1]:

$$\frac{\partial \underline{V}(x, t)}{\partial x} = - \underline{L} \frac{\partial \underline{J}(x, t)}{\partial t} \quad (1.2a)$$

$$\frac{\partial \underline{J}(x, t)}{\partial x} = - \underline{C} \frac{\partial \underline{V}(x, t)}{\partial t} \quad (1.2b)$$

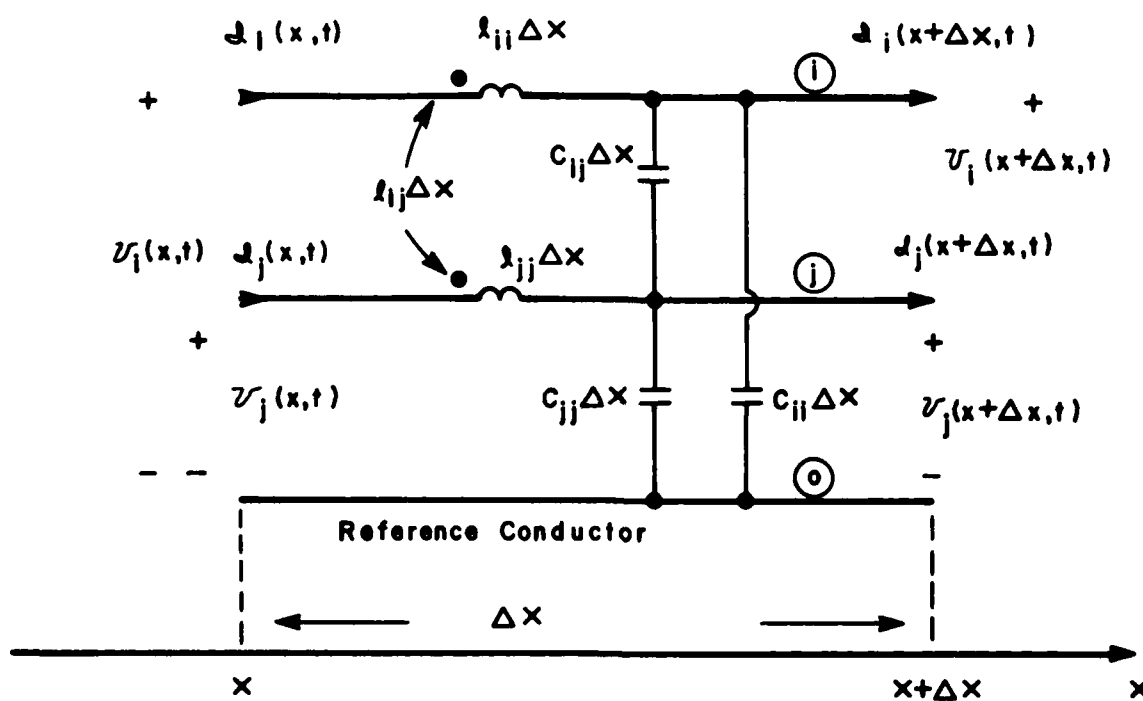


Fig. 1.3. The per-unit-length, distributed parameter, transmission line model.

The $n \times 1$ vectors $\underline{V}(x,t)$ and $\underline{I}(x,t)$ are

$$\underline{V}(x,t) = \begin{bmatrix} V_1(x,t) \\ \vdots \\ V_i(x,t) \\ \vdots \\ V_n(x,t) \end{bmatrix} \quad (1.3a)$$

$$\underline{I}(x,t) = \begin{bmatrix} I_1(x,t) \\ \vdots \\ I_i(x,t) \\ \vdots \\ I_n(x,t) \end{bmatrix} \quad (1.3b)$$

The $n \times n$ matrices \underline{L} and \underline{C} are referred to as the per-unit-length inductance and capacitance matrices, respectively, with entries

$$[\underline{L}]_{ii} = \ell_{ii} \quad (1.4a)$$

$$[\underline{L}]_{ij} = \ell_{ij} \quad (1.4b)$$

$i \neq j$

$$[\underline{C}]_{ii} = \sum_{k=1}^n c_{ik} \quad (1.4c)$$

$$[\underline{C}]_{ij} = -c_{ij} \quad (1.4d)$$

$i \neq j$

For sinusoidal, steady-state excitation we assume

$$V_i(x,t) = V_i(x)e^{j\omega t} \quad (1.5a)$$

$$I_i(x,t) = I_i(x)e^{j\omega t} \quad (1.5b)$$

where the complex, phasor voltages and currents are denoted as $V_i(x)$ and $I_i(x)$, respectively, and $\omega = 2\pi f$ is the radian frequency of excitation. For this case, the transmission line equations become [1]

$$\underline{V}(x) = -j\omega \underline{L} \underline{I}(x) \quad (1.6a)$$

$$\underline{I}(x) = -j\omega \underline{C} \underline{V}(x) \quad (1.6b)$$

where $[\underline{V}(x)]_i = V_i(x)$ and $[\underline{I}(x)]_i = I_i(x)$.

For a homogeneous surrounding medium (which is not the case for PCB's)[1]

$$\underline{L} \underline{C} = \mu \epsilon \underline{1}_n \quad (1.7)$$

where $\underline{1}_n$ is the $n \times n$ identity matrix and $\mu(\epsilon)$ is the permeability (permittivity) of the surrounding medium. The velocity of propagation in this homogeneous medium is

$$\underline{v} = \frac{1}{\sqrt{\mu \epsilon}} \quad (1.8)$$

Equation (1.7) shows that we need only determine one parameter matrix. For example, if we obtain the per-unit-length capacitance matrix \underline{C} from static field considerations, then the per-unit-length inductance matrix is easily obtainable in terms of the inverse of the capacitance matrix as

$$\underline{L} = \frac{1}{v^2} \underline{C}^{-1} \quad (1.9)$$

For an inhomogeneous medium we can obtain both parameter matrices from only capacitance calculations as

$$\underline{L} = \frac{1}{v_o^2} \underline{C}_o^{-1} \quad (1.10)$$

where \underline{C}_0 is the per-unit-length capacitance matrix with the dielectric insulation removed and $v_0 = 1/\sqrt{\mu_0 \epsilon_0} = 3 \times 10^8$ m/s is the velocity of propagation in free space.

The matrices \underline{L} and \underline{C} contain all of the information concerning the cross-sectional, physical configuration of the line. For the purposes of this report, we will assume that these parameters have been calculated (or measured) and are known. The primary thrust of this report is to develop a simple solution of (1.2) suitable for implementation in CAD programs.

1.1.2. The Transmission-Line Equations - Lossy Lines

The previous formulation assumed perfect conductors and a lossless medium. Losses in the surrounding, inhomogeneous medium pose no problems in so far as representation in the per-unit-length model of Fig. 1.3. In order to consider a lossy surrounding medium we add per-unit-length conductances between each of the n conductors and between each of the n conductors and the reference conductor. Similarly, imperfect conductors may be considered in the per-unit-length model by adding per-unit-length impedances in series with each conductor. For typical PCB's losses in the medium are neglectable for frequencies below 1 GHz. However, conductor losses may be significant for all frequencies. A simple example is the resistance of the reference conductor. Currents of the other circuits pass through this reference conductor and the resulting voltage drop across this reference conductor appears directly in all the other circuits. This phenomenon is referred to as "common impedance coupling" or "ground loop coupling" and may be important at very low frequencies. In ribbon cables where all circuits share a common return wire, this component of

crosstalk coupling has been shown to be dominant below frequencies as high as 10 kHz [2,3]. Thus conductor losses are not necessarily neglectable.

However, if we include imperfect conductors, we are faced with several formidable modeling problems. The first of these is determining a suitable model for characterizing these losses. In the case of sinusoidal, steady-state excitation of the line, it is a rather straightforward task to model the effects of conductor losses; simply add frequency dependent impedances in series with each conductor [1]. These impedances are frequency dependent as a result of skin effect and vary typically as the square root of frequency. Thus we add

$$Z_i(f) = Z_{i0} + Z_{i1} \sqrt{f} \quad \Omega/\text{m} \quad (1.11)$$

in series with each conductor (including the reference conductor). The constants Z_{i0} and Z_{i1} are dependent on the conductor cross-section and physical properties. Similarly losses in the medium are frequency dependent and may be modeled by adding a frequency dependent conductance, $g_{ij}(f)$ between each conductor. This results in modifying the transmission-line equations for sinusoidal steady-state excitation in (1.6) as

$$\underline{V}(x) = -[\underline{\tilde{Z}}(f) + j\omega\underline{L}] \underline{I}(x) \quad (1.12a)$$

$$\underline{I}(x) = -[\underline{\tilde{G}}(f) + j\omega\underline{C}] \underline{V}(x) \quad (1.12b)$$

where

$$[\underline{\tilde{Z}}(f)]_{ii} = Z_i(f) + Z_0(f) \quad (1.13a)$$

$$[\underline{\tilde{Z}}(f)]_{ij} = Z_0(f) \quad (1.13b)$$

$i \neq j$

where $Z_0(f)$ is the per-unit-length impedance of the reference conductor and

$$[\tilde{G}(f)]_{ij} = g_{ij}(f) \quad (1.13)$$

Including losses in the transmission-line model is therefore not conceptually difficult in the case of sinusoidal, steady-state excitation. Of course, determining the constants Z_{i0} and Z_{i1} in (1.11) and the function $g_{ij}(f)$ in (1.13) requires analysis but once that is concluded, there is no difficulty in including these effects in the transmission-line model.

On the other hand, including lossy conductors and media in the time-domain, transmission-line model and the resulting equations in (1.2) presents considerable difficulty. For example, how does one represent frequency dependent losses $Z_i(f)$ and $g_{ij}(f)$ in the time domain? The usual method of doing this is to omit the frequency dependence of the losses and assume constant, per-unit-length resistances in series with each conductor and conductances between each line. The time-domain, transmission-line equations in (1.2) become [1]

$$\frac{\partial \underline{V}(x,t)}{\partial x} = - [\underline{R} + j\omega \underline{L}] \frac{\partial \underline{I}(x,t)}{\partial t} \quad (1.14a)$$

$$\frac{\partial \underline{I}(x,t)}{\partial x} = - [\underline{G} + j\omega \underline{C}] \underline{V}(x,t) \quad (1.14b)$$

where

$$[\underline{R}]_{ii} = r_i + r_0 \quad (1.15a)$$

$$[\underline{R}]_{ij} = r_0 \quad (1.15b)$$

$i \neq j$

$$[\underline{G}]_{ij} = g_{ij} \quad (1.15c)$$

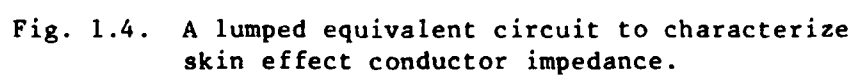
and these parameters are constants.

Solution of the time-domain transmission-line equations without losses has been considered in numerous instances [4-8]. Inclusion of frequency independent losses as in (1.14) has been the usual method of including losses in time-domain solutions [9-11]. However frequency independent losses as in (1.14) are a gross simplification. Frequency independent losses are usually assumed simply because they are easier to model than are frequency dependent losses. A recent attempt at including frequency dependent losses in the time-domain model is given in [12]. However this requires measurements of the line under study and as such is not satisfactory as a prediction model.

A recent, promising approach to modeling frequency dependent losses in the time-domain model is given in [13]. This model uses a lumped circuit to approximate the \sqrt{f} impedance dependence of the conductors as shown in Fig. 1.4. The values of the resistors and inductors are chosen such that as frequency is increased each branch "opens up" thereby increasing the resistance in such a way that it becomes a function of \sqrt{f} up to an upper frequency limit. For example, consider $m=3$ in Fig. 1.4. The input admittance is

$$Y = \frac{1}{R_1} + \frac{1}{j\omega L_2 + \frac{1}{\frac{1}{R_2} + \frac{1}{R_3 + \frac{1}{j\omega L_3}}}} \quad (1.16)$$

At DC the impedance is the parallel combination of R_1 , R_2 , R_3 . As frequency is increased the limiting value is R_1 . For intermediate frequencies the impedance approximates a \sqrt{f} dependence [13].



The advantage of this circuit is that it can be included in a time-domain CAD model directly with no translation between frequency domain dependence and time-domain dependence. Nevertheless this model does not show how the time-domain, transmission-line equations in (1.2) can be modified to include frequency dependent losses. Thus inclusion of frequency dependent losses in the time-domain, transmission-line equations is still an open problem.

1.2. Incorporating the Terminal Constraints

The exact solution to the transmission line equations in (1.2) is (even without regard to implementation in CAD programs) not a simple matter. An exact solution will be shown in the next chapter. Traditionally solutions to these equations are obtained via approximations also discussed in the next chapter.

Nevertheless the general solution to the transmission line equations involve $4n$ undetermined constants. The final step in the complete solution to these equations is the incorporation of the terminal constraints at the two ends of the line. Consider a line of length \mathcal{L} extending from $x=0$ to $x=\mathcal{L}$. At $x=0$, the voltages and currents are related or constrained in some fashion:

$$\underline{f}_0(\underline{v}(0,t), \underline{I}(0,t)) = \underline{0} \quad (1.17a)$$

Similarly at $x = \mathcal{L}$

$$\underline{f}_{\mathcal{L}}(\underline{v}(\mathcal{L},t), \underline{I}(\mathcal{L},t)) = \underline{0} \quad (1.17b)$$

If the terminations are linear (as they generally are not on PCB's) then (1.17) can be represented as linear constraints. For sinusoidal, steady-

state excitation, linear termination networks are usually represented as generalized Thevenin or Norton equivalents [1]. Nevertheless, the complete solution to the transmission-line equations involves incorporating the line terminal constraints into the general solution. This final, important part of the solution process will be the most difficult part. Nonlinear termination networks as is usually the case for PCB's complicate the process considerably simply because, for nonlinear terminations, we cannot write simple, terminal constraint equations.

1.3. Report Summary

Chapter II will be devoted to a discussion of previous methods for direct, time-domain solution. The advantages as well as the limitations and disadvantages for implementation in CAD codes will be discussed.

In Chapter III, a simple, time-domain model which is suitable for inclusion into CAD codes will be developed. Although an approximation, the simplicity of the model will allow the analysis of large, practical PCB's. The various limitations and restrictions of this model will be investigated fully.

Experimental results will be given in Chapter IV which show the prediction accuracy of the simple model as well as its limitations.

A summary of the report will be given in Chapter V along with recommendations for future investigations.

II. Survey of Previous Methods

The purpose of this chapter is to summarize the methods for direct, time-domain analysis of transmission lines for the purpose of predicting crosstalk. Each of these methods will be discussed from the standpoint of their limitations, advantages and disadvantages and their suitability for inclusion in CAD codes.

It should be kept in mind that the fundamental model of the transmission line which all models strive to approximate is the TEM mode, distributed parameter model discussed in the previous chapter and represented, for the lossless case, by equations (1.2). Therefore there are no "new theoretical" models but only methods for solving or approximating the solution to the transmission-line equations.

2.1. Lumped Circuit Iterative Models

Lumped circuit iterative models are the most common forms of models of transmission lines [1]. Of all the various methods which are used in CAD codes for modeling transmission lines, the lumped circuit iterative models are the most common. There exist only a few exceptions to this.

The philosophy of lumped circuit iterative models is as follows. It is well known that lumped circuit elements are valid representations of an object so long as the physical dimensions are electrically small. The basic TEM mode model of a line assumes that the cross-sectional dimensions of the line are electrically small otherwise higher order modes are possible. Thus the transmission line is divided into N sections each of which is electrically short at the frequency of interest as shown in Fig. 2.1. Traditionally the line is divided into N equal length sections

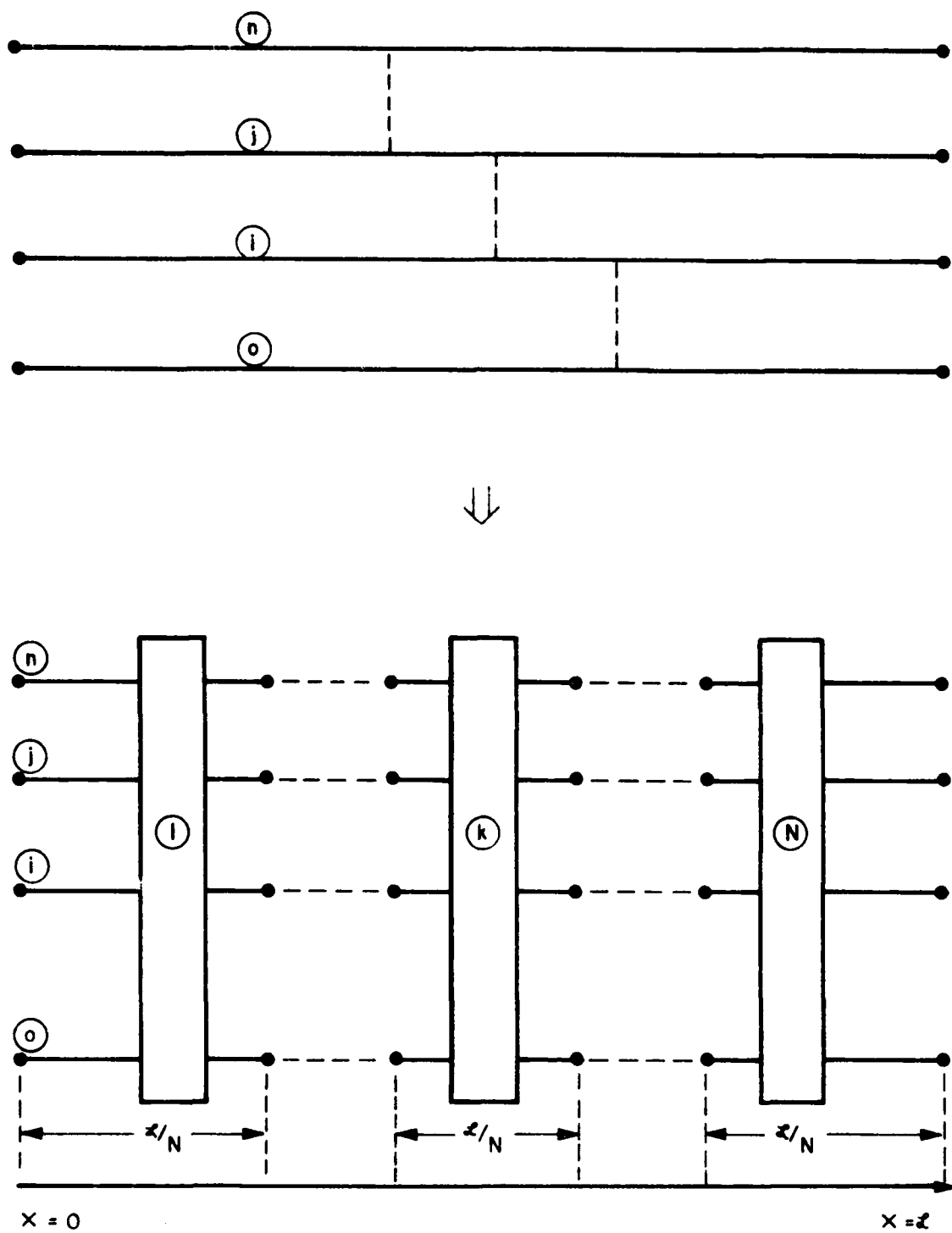


Fig. 2.1. Segmenting a line into electrically short sections.

each of length l/N such that

$$l/N \ll \lambda \quad (2.1)$$

where

$$\lambda = v/f \quad (2.2)$$

is a wavelength at the frequency of interest.

Once this is done, each section is modelled with a lumped circuit model to represent the distributed parameter model of the line in Fig. 1.3. There are typically four topologies which one finds. These are arrived at by either placing all parallel elements on the left or on the right of the series elements or placing half the parallel elements on the left and right of the series elements or placing half the series elements on the left and right of the parallel elements and are referred to as the lumped Γ , Π , Pi and Tee circuits, respectively. These are shown in Fig. 2.2, 2.3, 2.4 and 2.5.

The various approximation capabilities of these lumped circuit iterative models was investigated in [14]. For lossless lines, one can characterize the performance of these models in terms of the ratio l/λ rather than frequency. It was found that one section of each model provided an accurate approximation of the transmission line for frequencies up to a point where the line is approximately $\frac{1}{10}\lambda$ long. Adding sections increases the coverage in a nonlinear fashion. For example, it was found that 10 sections do not uniformly increase the prediction accuracy to frequencies where the line is one λ long.

In addition, it was found that the prediction frequency range was dependent on the termination impedances. For example, suppose the

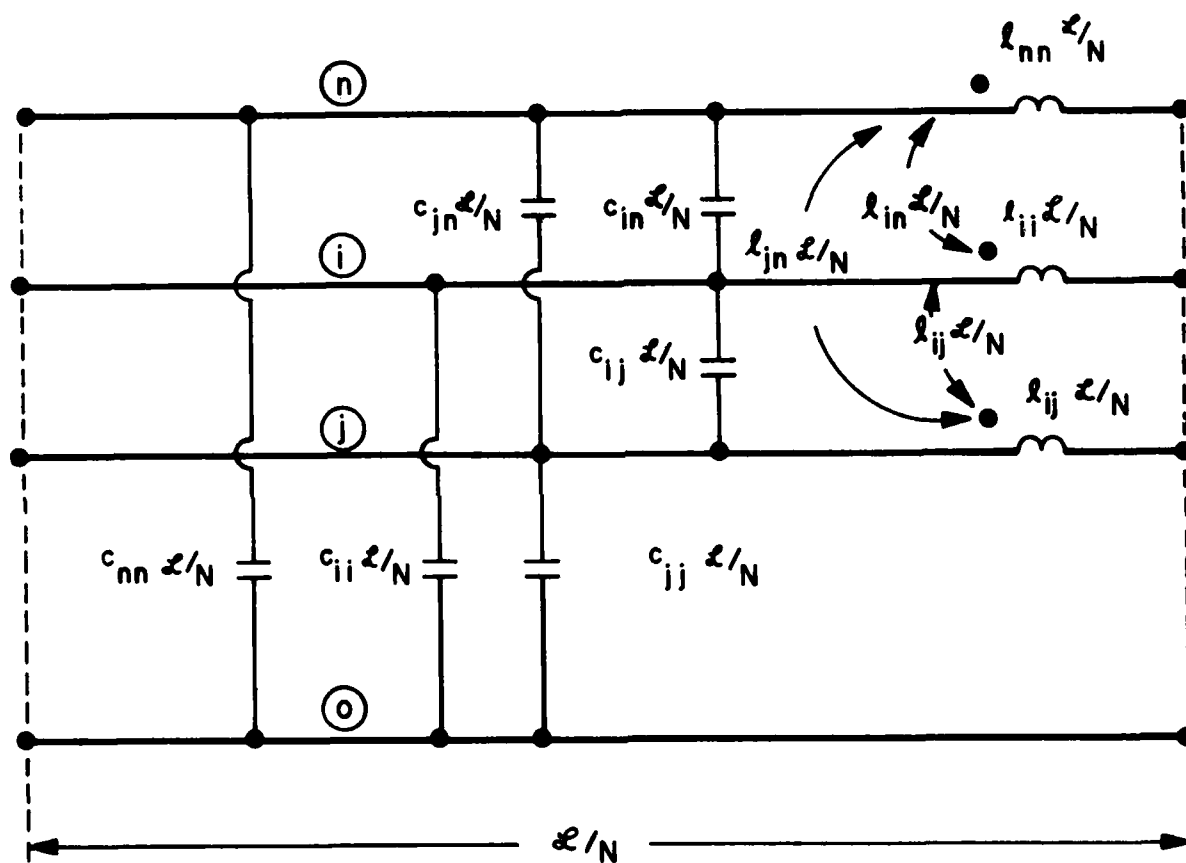


Fig. 2.2. The lumped Γ circuit.

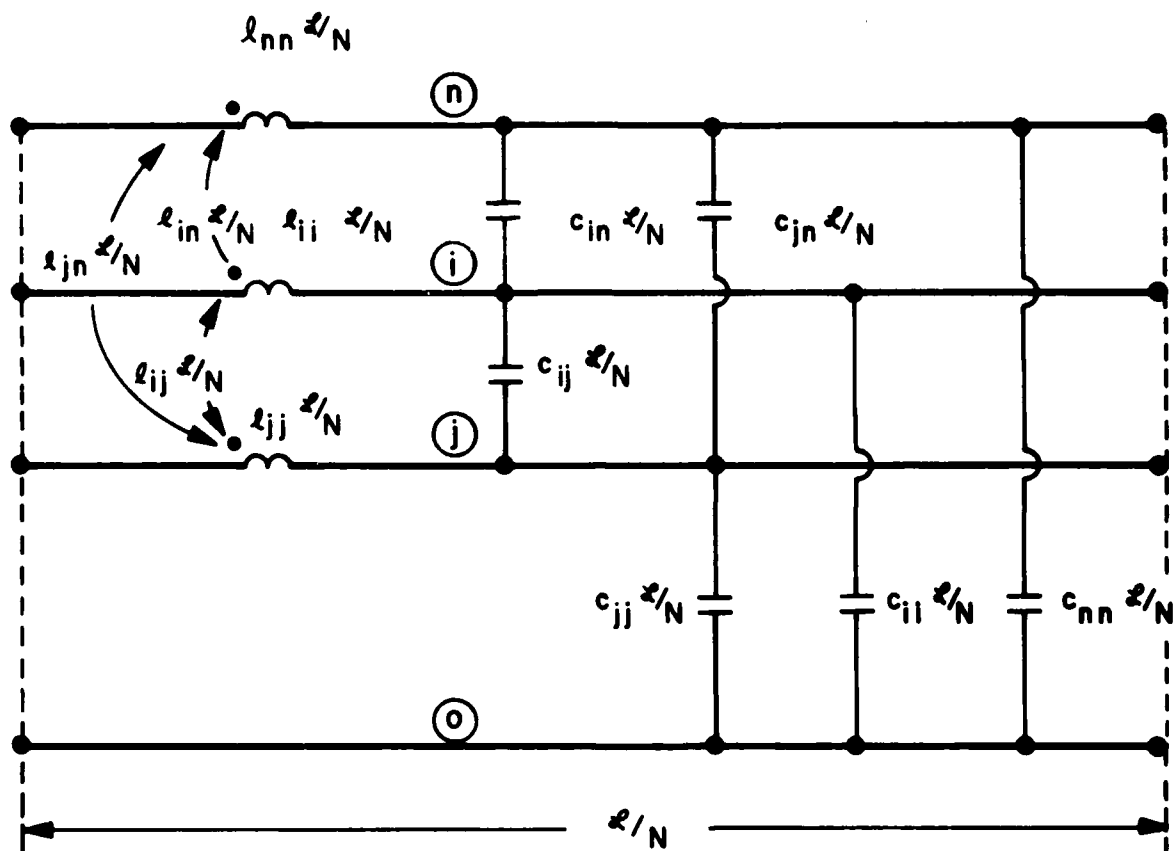


Fig. 2.3. The lumped Γ circuit.

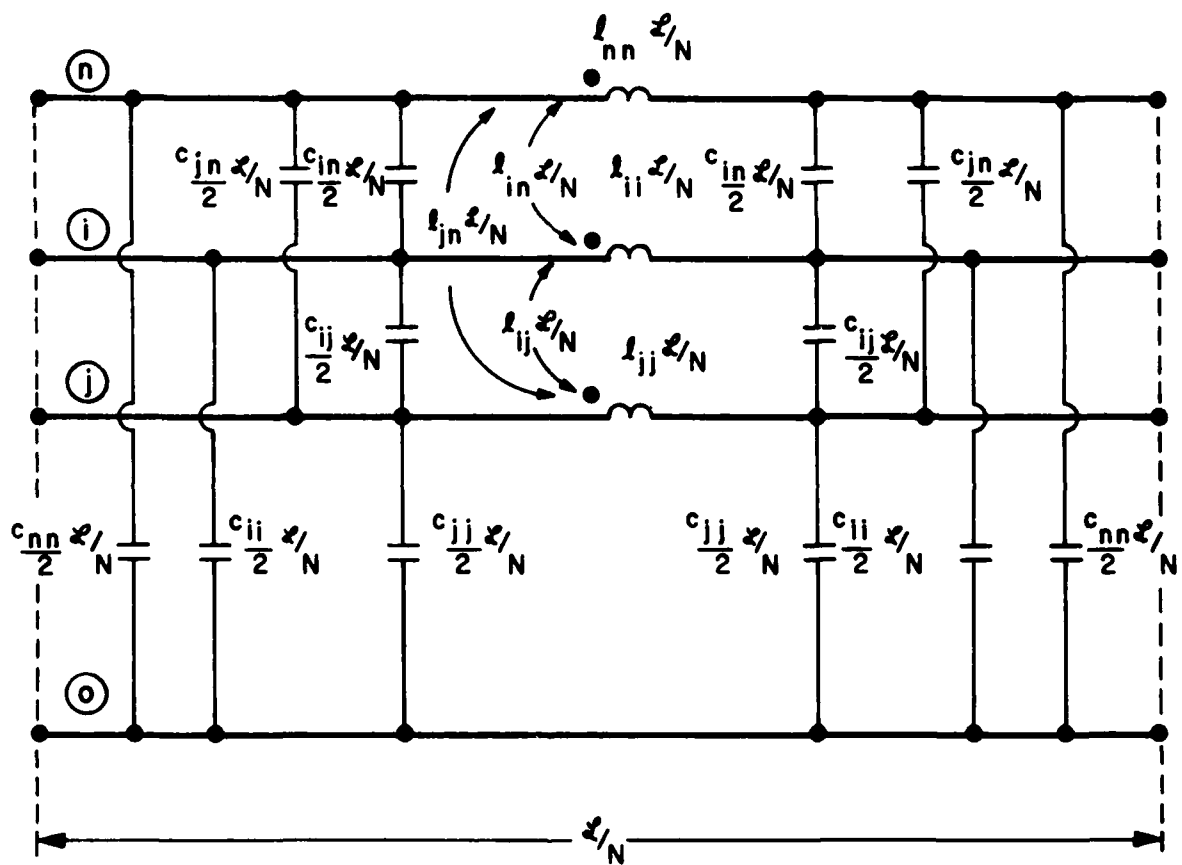


Fig. 2.4. The lumped Pi circuit.

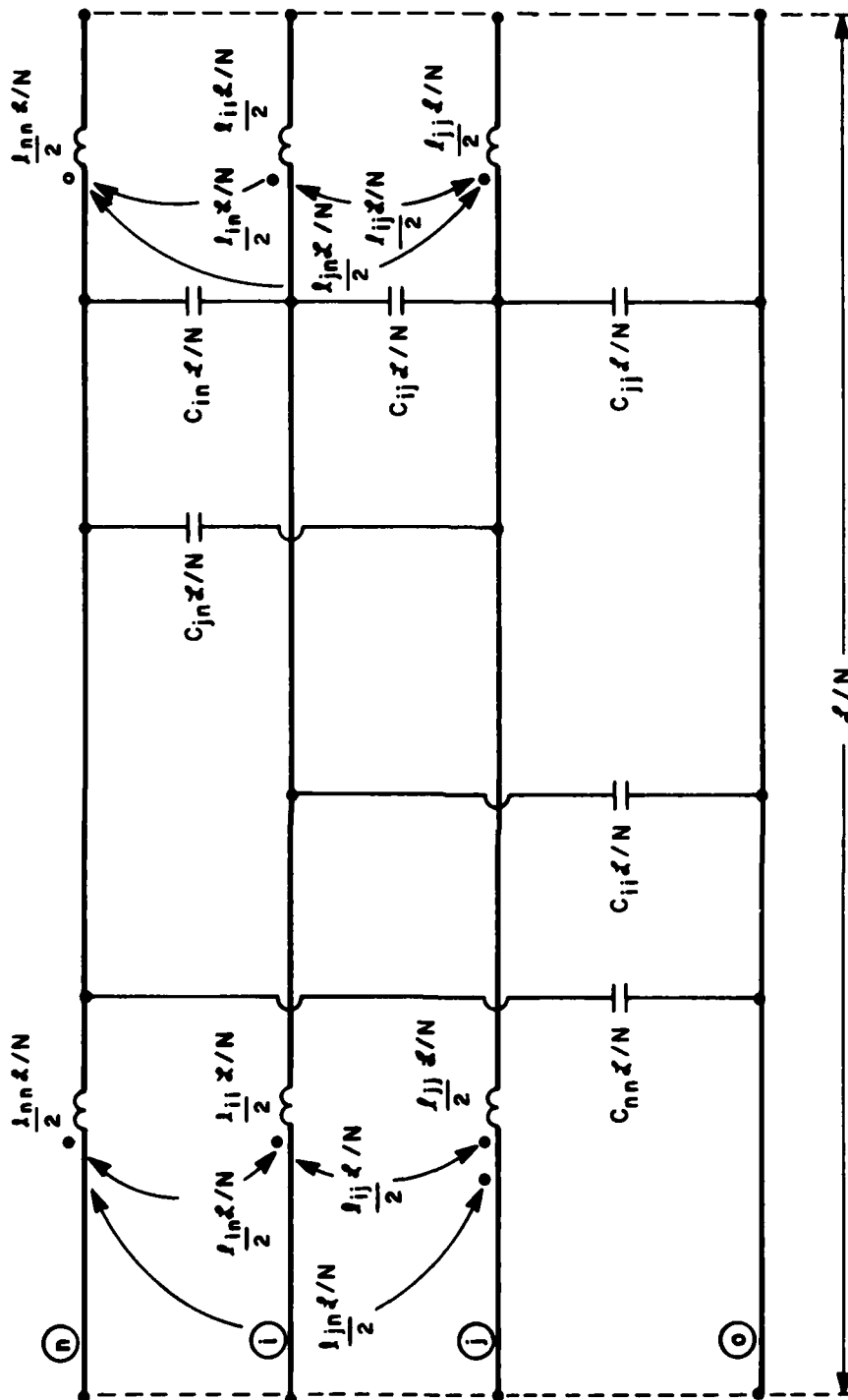


Fig. 2.5. The lumped Tee circuit.

termination impedances are small in value. Then the capacitances on the right of the Pi model are effectively of no consequence and the Pi model essentially reduces to the Γ model.

Thus the precise frequency range for which lumped-circuit iterative models provide an adequate approximation to the transmission line model is (1) very difficult to predict, (2) dependent on the terminations, and (3) not significantly increased with the addition of more sections. These deficiencies make the lumped-circuit iterative models difficult to apply in CAD codes. In addition, if the line is electrically long at the frequency of interest, a large lumped circuit is needed to model the line. For PCB's which contain a very large number of coupled lands, one is essentially restricted to modeling frequencies where all the traces on the board (or most of them) are electrically short. In the case of pulse excitation, such as clock or trapezoidal pulses discussed in Chapter I, one is restricted to rise/fall times for which the second break point in Fig. 1.1, $1/\pi\tau_r$, is much less than the frequency at which the lands are, say, $\frac{1}{10} \lambda$ in length. For a typical PCB land length of 10 cm one can consider rise/fall times no shorter than 10 to 20 ns. In the next chapter we will consider a much simpler model which has essentially the same restriction.

However, the main advantage of the lumped-circuit iterative models is that they require no understanding of specialized solution methods and, given the per-unit-length capacitances and inductances, one can readily implement the models in a CAD program using lumped-circuit elements which are already available in the CAD program in a fashion very similar to the process the analyst is presently using to model the functional modules.

2.2. Direct, Time-Domain Solution of the Transmission-Line Equations

The conventional method for direct solution of the time-domain transmission-line equations in (1.2) is usually referred to as "modal analysis". With this technique one uses a change of variables to transform the actual line voltages and currents to their modal values. For example, define a change of variables as

$$\underline{V}(x,t) = \underline{T}_V \underline{\hat{V}}(x,t) \quad (2.3a)$$

$$\underline{I}(x,t) = \underline{T}_I \underline{\hat{I}}(x,t) \quad (2.3b)$$

Substitution into (1.2) yields

$$\underline{T}_V \frac{\partial}{\partial x} \underline{\hat{V}}(x,t) = - \underline{L} \underline{T}_I \frac{\partial}{\partial t} \underline{\hat{I}}(x,t) \quad (2.4a)$$

$$\underline{T}_I \frac{\partial}{\partial x} \underline{\hat{I}}(x,t) = - \underline{C} \underline{T}_V \frac{\partial}{\partial t} \underline{\hat{V}}(x,t) \quad (2.4b)$$

For nonsingular transformations (a necessity) we obtain

$$\frac{\partial}{\partial x} \underline{\hat{V}}(x,t) = - \underline{T}_V^{-1} \underline{L} \underline{T}_I \frac{\partial}{\partial t} \underline{\hat{I}}(x,t) \quad (2.5a)$$

$$\frac{\partial}{\partial x} \underline{\hat{I}}(x,t) = - \underline{T}_I^{-1} \underline{C} \underline{T}_V \frac{\partial}{\partial t} \underline{\hat{V}}(x,t) \quad (2.5b)$$

If transformations \underline{T}_V and \underline{T}_I can be found such that

$$\underline{T}_V^{-1} \underline{L} \underline{T}_I = \underline{\Lambda}_L \quad (2.6a)$$

$$\underline{T}_I^{-1} \underline{C} \underline{T}_V = \underline{\Lambda}_C \quad (2.6b)$$

where $\underline{\Lambda}_L$ and $\underline{\Lambda}_C$ are diagonal, then (2.5) are sets of uncoupled, differential equations.

Although there are several such transformations which have been used [5,6] an example is

$$\underline{T}_V = \underline{L} \underline{T} \quad (2.7a)$$

$$\underline{T}_I = \underline{T} \quad (2.7b)$$

where

$$\underline{T}^{-1} \underline{C} \underline{L} \underline{T} = \underline{\Lambda} \quad (2.8)$$

is diagonal. The columns of \underline{T} are the eigenvectors of the matrix product $\underline{C} \underline{L}$, and the entries along the main diagonal of $\underline{\Lambda}$ are the associated eigenvalues [1]. For this transformation, (2.5) becomes

$$\frac{\partial}{\partial x} \underline{\hat{V}}(x,t) = - \frac{\partial}{\partial t} \underline{\hat{J}}(x,t) \quad (2.9a)$$

$$\frac{\partial}{\partial x} \underline{\hat{J}}(x,t) = - \underline{\Lambda} \frac{\partial}{\partial t} \underline{\hat{V}}(x,t) \quad (2.9b)$$

Thus we have reduced n coupled lines to a set of n uncoupled, two-conductor lines each of which are characterized by

$$\frac{\partial}{\partial x} \hat{V}_i(x,t) = - \frac{\partial}{\partial t} \hat{J}_i(x,t) \quad (2.10a)$$

$$\frac{\partial}{\partial x} \hat{J}_i(x,t) = - \Lambda_i \frac{\partial}{\partial t} \hat{V}_i(x,t) \quad (2.10b)$$

Thus we have, in terms of these modal variables, n sets of uncoupled, two-conductor lines each of which have a characteristic impedance of

$$\hat{Z}_{C_i} = \frac{1}{\sqrt{\Lambda_i}} \quad (2.11)$$

and velocity of propagation

$$\hat{v}_i = \frac{1}{\sqrt{\Lambda_i}} \quad (2.12)$$

as shown in Fig. 2.6.

Consider a two-conductor, lossless line with characteristic impedance Z_C and velocity of propagation v . The transmission-line equations are

$$\frac{\partial V(x,t)}{\partial x} = -L \frac{\partial I(x,t)}{\partial t} \quad (2.13a)$$

$$\frac{\partial I(x,t)}{\partial x} = -C \frac{\partial V(x,t)}{\partial t} \quad (2.13b)$$

where

$$Z_C = \sqrt{\frac{L}{C}} \quad (2.14a)$$

$$v = \frac{1}{\sqrt{LC}} \quad (2.14b)$$

The general solution to these equations is

$$V(x,t) = V^+(t-x/v) + V^-(t+x/v) \quad (2.15a)$$

$$I(x,t) = \frac{1}{Z_C} V^+(t-x/v) - \frac{1}{Z_C} V^-(t+x/v) \quad (2.15b)$$

At the terminals we have

$$V(0,t) = V^+(t) + V^-(t) \quad (2.16a)$$

$$I(0,t) = \frac{1}{Z_C} V^+(t) - \frac{1}{Z_C} V^-(t) \quad (2.16b)$$

and

$$V(l,t) = V^+(t-\tau) + V^-(t+\tau) \quad (2.17a)$$

$$I(l,t) = \frac{1}{Z_C} V^+(t-\tau) - \frac{1}{Z_C} V^-(t+\tau) \quad (2.17b)$$

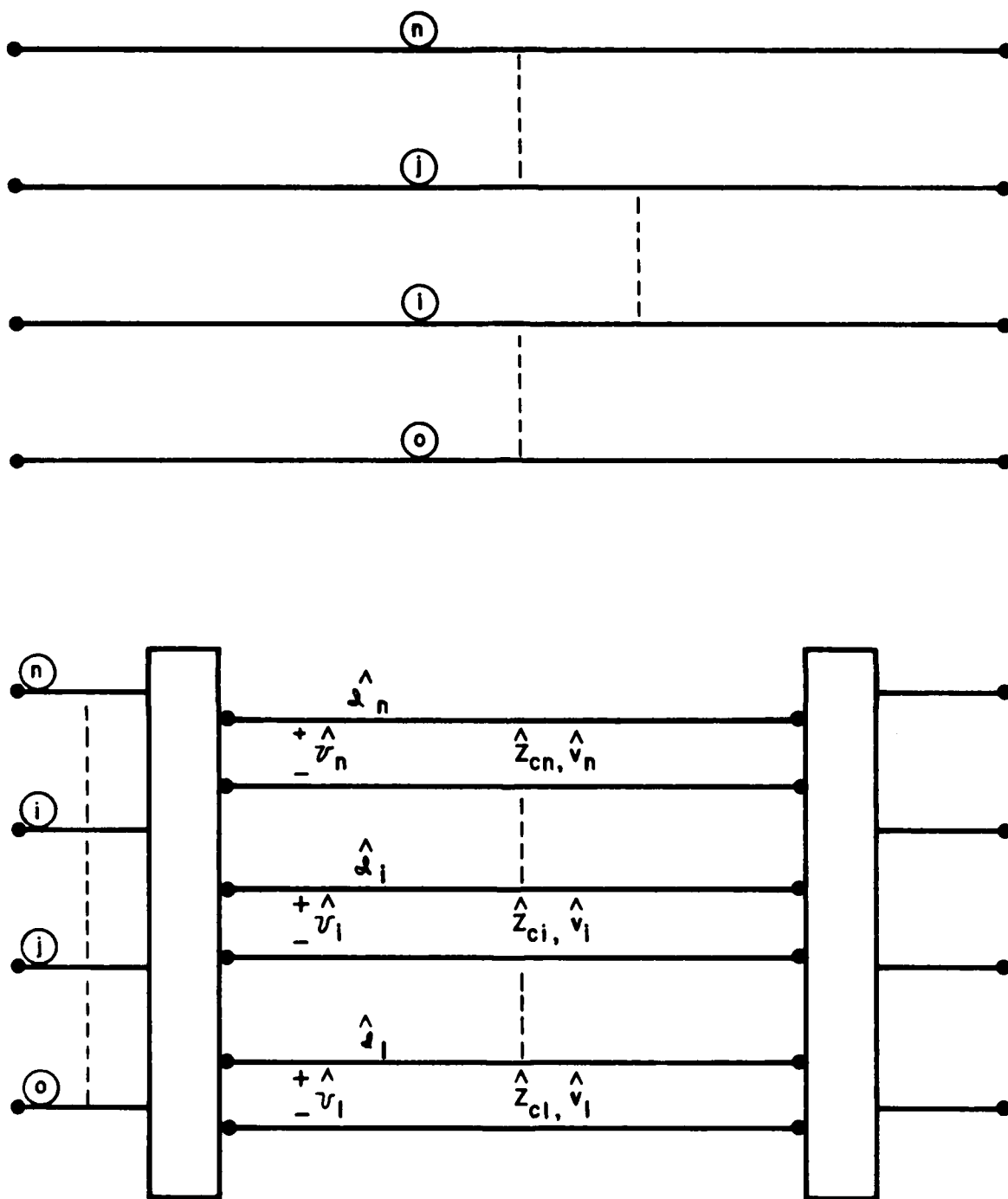


Fig. 2.6. Separating n coupled lines into n uncoupled lines.

where the one-way line delay is

$$\tau = \ell/v \quad (2.18)$$

Solving (2.16) and (2.17) yields

$$V(0,t) + Z_C I(0,t) = V(\ell,t-\tau) + Z_C I(\ell,t+\tau) \quad (2.19a)$$

$$V(0,t) - Z_C I(0,t) = V(\ell,t-\tau) - Z_C I(\ell,t-\tau) \quad (2.19b)$$

$$V(\ell,t) + Z_C I(\ell,t) = V(0,t-\tau) + Z_C I(0,t-\tau) \quad (2.19c)$$

$$V(\ell,t) - Z_C I(\ell,t) = V(0,t+\tau) - Z_C I(0,t+\tau) \quad (2.19d)$$

Equation (2.19b) yields

$$V(0,t) = [V(\ell,t-\tau) - Z_C I(\ell,t-\tau)] + Z_C I(0,t) \quad (2.20)$$

Similarly equation (2.19c) yields

$$V(\ell,t) = [V(0,t-\tau) + Z_C I(0,t-\tau)] - Z_C I(\ell,t) \quad (2.21)$$

This yields the equivalent circuit shown in Fig. 2.7 involving controlled sources with time delay as first proposed by Branin [15] and later extended to include frequency independent losses by Liu [16]. This model has been used by a host of others for two-conductor lines in one form or another [17] and extended to multiconductor lines with the above modal transformation by Chang [5]. The technique gives an extremely efficient numerical computation technique [15]. Its principle disadvantage is in CAD implementation for multiconductor lines which, according to the above, requires determination of the modal transformation matrices (eigenvectors) of certain matrices as in (2.6). Thus implementation of this technique for multiconductor lines

requires the writing of specialized codes for executing this method.

In addition this method is not well suited to the analysis of lossy lines. First consider sinusoidal excitation of the line. The transmission-line equations are given in (1.12). In order to apply modal analysis, we transform the phasor voltages and currents to modal, phasor variables

$$\underline{V}(x) = \underline{T}_V \hat{\underline{V}}(x) \quad (2.22a)$$

$$\underline{I}(x) = \underline{T}_I \hat{\underline{I}}(x) \quad (2.22b)$$

Substitution into (1-12) yields

$$\hat{\underline{V}}(x) = \underline{T}_V^{-1} [\underline{Z}(f) + j\omega \underline{L}] \underline{T}_I \hat{\underline{I}}(x) \quad (2.23a)$$

$$\hat{\underline{I}}(x) = \underline{T}_I^{-1} [\underline{G}(f) + j\omega \underline{C}] \underline{T}_V \hat{\underline{V}}(x) \quad (2.23b)$$

We must obtain \underline{T}_V and \underline{T}_I which uncouple both sets of equations. It was shown in [1] that choice of

$$\underline{T}_V = [\underline{Z}(f) + j\omega \underline{L}] \underline{T} \quad (2.24a)$$

$$\underline{T}_I = \underline{T} \quad (2.24b)$$

where

$$\underline{T}^{-1} [\underline{G}(f) + j\omega \underline{C}] [\underline{Z}(f) + j\omega \underline{L}] \underline{T} = \underline{\Lambda} \quad (2.25)$$

and $\underline{\Lambda}$ is diagonal will uncouple (2.23). However, the columns of \underline{T} will be eigenvectors which are frequency dependent. Thus, unless certain special cases are considered as outlined in [1], we must perform the modal decomposition and equation decoupling at each frequency being considered. This

can be very time consuming, computationally, even for small numbers of coupled lines.

In the case of direct, time-domain analysis of lossy lines, we are faced with the usual problem of how to include these frequency dependent losses in the time-domain transmission line equations.

2.3. Frequency-Domain Methods

Perhaps the method for time-domain analysis which is second in popularity to the lumped-circuit iterative models is referred to as the frequency domain method. First one determines (through calculation or measurement) the frequency-domain transfer function (magnitude and phase) relating the input signal to the desired crosstalk signal, $T(f)$. Then one determines, via Fourier methods, the spectrum (magnitude and phase) of the input pulse. Multiplying the magnitude functions and adding the phase functions gives the spectrum (magnitude and phase) of the crosstalk pulse as shown in Fig. 2.8. The spectrum of this crosstalk pulse is then transformed via the inverse Fourier transform to yield the time-domain crosstalk pulse.

This method is quite popular but not suited to implementation in CAD codes. A major advantage of this method is that frequency-dependent losses are readily modeled. A major disadvantage is that the transfer function must represent a linear system since the method inherently relies on the principle of superposition to process the individual spectral components of the input pulse. Thus, although the line may be linear, an important part of the overall transfer function is the line terminations. If these are nonlinear, the overall system is nonlinear and this method cannot be

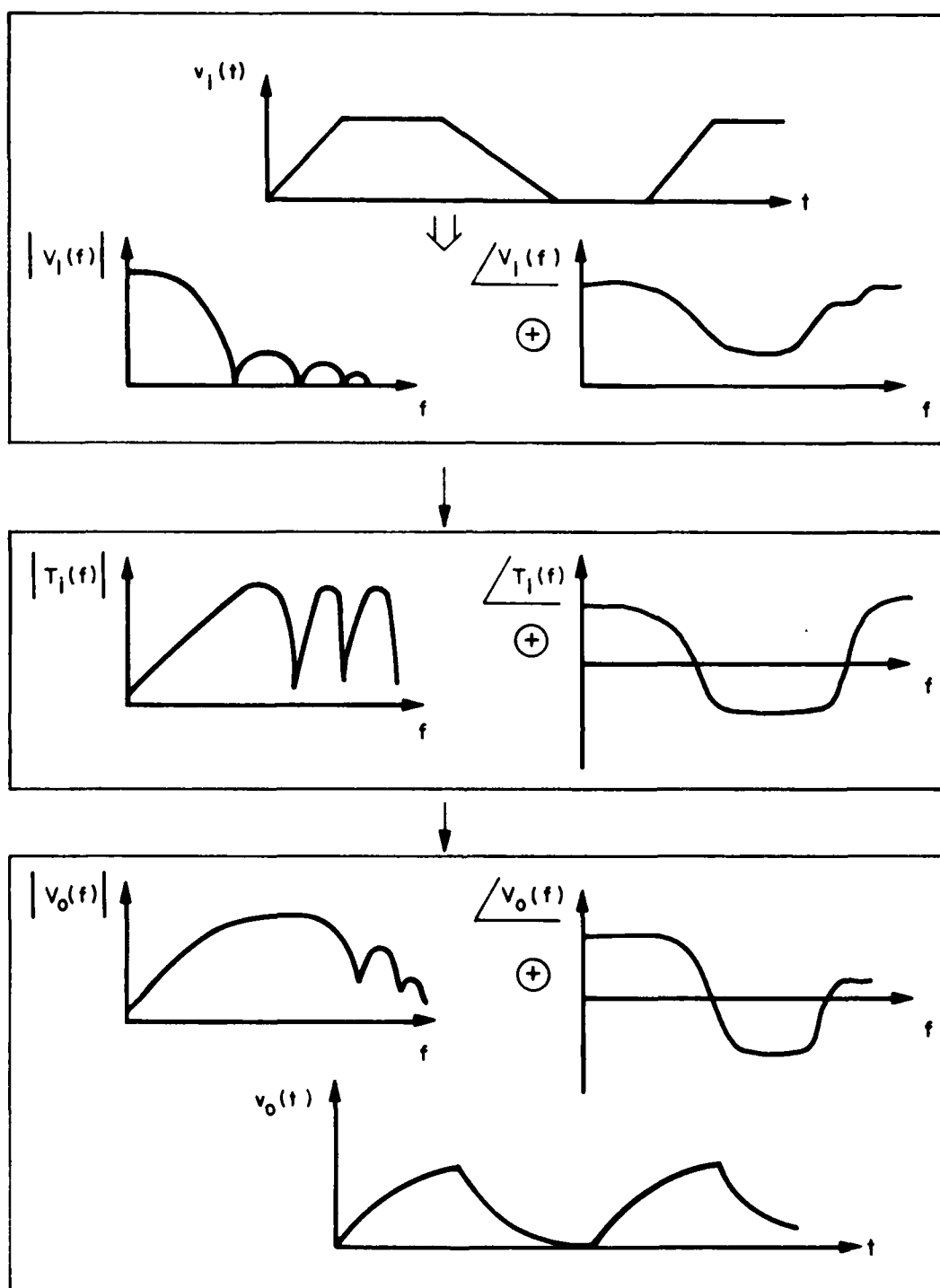


Fig. 2.8. Illustration of the computation of time-domain crosstalk using frequency-domain techniques.

used. Since the terminations on PCB lands are electronic modules which are inherently nonlinear (highly nonlinear in their digital mode of operation), this method is not a viable one.

2.4. Summary

Of all the models considered, only the lumped-circuit iterative models are appropriate for use in CAD codes when multiconductor lines are involved. A number of numerical computation techniques have been proposed in the literature for analyzing "transmission lines" directly in the time domain [15-18]. However, with the exception of the modal method proposed by Chang, none of these methods are capable of handling multiconductor lines, i.e., predicting crosstalk.

The predictive ability of the lumped-circuit iterative models will be investigated in Chapter IV with reference to experimental results.

III. A Simple, Time-Domain Prediction Model

Methods for the solution of the transmission-line equations were given in the previous chapter. Only one method--the lumped-circuit, iterative model--was suitable for inclusion into CAD codes. The lumped-circuit, iterative model relied on dividing the line into electrically short lengths and modeling those sections with lumped circuits which resembled the per-unit-length model from which the transmission line equations were derived.

The primary advantage of this technique is that, given the per-unit-length parameters of the line, it is a simple matter to incorporate these models into lumped-circuit, CAD codes using the available model elements of the code (resistors, inductors, mutual inductors and capacitors). The primary disadvantage of this method is that one must divide the line into electrically short sections and model each section with a fairly complex lumped circuit. If the entire line is electrically short (say, less than $\frac{1}{10} \lambda$ in length), then one section will usually suffice. However, further segmentation of the line usually does not increase the frequency coverage significantly. Even if one could satisfactorily model a line by dividing it into sections $\frac{1}{10} \lambda$ in length, a one wavelength section of line would require 10 sections which is a very complex circuit. Modeling all lands on typical PCB's in this fashion will generally result in an overall, lumped circuit which is prohibitively complex either in computation time or required array storage. So, even with the lumped circuit iterative models, one is typically restricted to electrically short lines.

If we consider typical PCB land dimensions and pulse rise/fall times, it is found that requiring the lands to be electrically short is not a serious restriction. For example, suppose we consider trapezoidal pulse signals such as are shown in Fig. 1.1 and are typical of clock signals. Suppose we consider 10 ns rise/fall times. The second break frequency in the spectrum occurs at 31.8 MHz. Suppose we require that the spectrum decay by 10 dB at some point after this second break frequency. This point becomes 100 MHz. If we now consider land lengths which are no longer than $\frac{1}{10} \lambda$ at 100 MHz, this means that we are restricted to analyzing land lengths no longer than 15 cm. If the pulse rise/fall time is reduced to 1 ns, the maximum line lengths reduce to 1.5 cm. Therefore typical board dimensions will be capable of being analyzed with one lumped-circuit iterative model per set of lands so long as the pulse rise/fall times are not much less than 10 ns.

In the above frequency-domain criterion we are assuming that the high frequency components of the spectrum (those above the second break point, $1/\pi\tau_r$) have decayed sufficiently at some upper point, f_u , such that incorrect prediction of them will result in negligible errors in the prediction of the crosstalk pulse. This can be equivalently related to the time domain.

For example suppose that we require that the line be electrically short at some frequency f_u

$$L = k\lambda \quad (3.1)$$

$$= k \frac{v}{f_u}$$

For example, choose $k = \frac{1}{10}$. Next, suppose that this frequency is well above the second break point of the input pulse spectrum:

$$f_u \geq \frac{1}{\pi \tau_r} \quad (3.2)$$

For a fall-off of 10 dB from the level of $1/\pi \tau_r$, we require $\alpha = 3.16$. The one-way time delay of the line is

$$\tau_d = \frac{L}{v} \quad (3.3)$$

Substituting (3.3) and (3.2) into (3.1) yields

$$\tau_r, \tau_f \geq \frac{\alpha}{k\pi} \tau_d \quad (3.4)$$

Thus the rise/fall time of the pulse must be much longer than the one-way delay time of the line. For $k = \frac{1}{10}$, $\alpha = 3.16$,

$$\tau_r, \tau_f \geq 10 \tau_d \quad (3.5)$$

This result shows that, so long as the pulse rise/fall time is, say, a factor of ten larger than the one-way delay of the line, one can model the line as though it is electrically short.

For the model which we will develop, we will assume that the line is electrically short. In other words, the time-domain constraint in (3.5) will place a bound on the signals which may be analyzed with this method.

3.1. Inductive and Capacitive Coupling Models

Consider a uniform three-conductor, lossless line immersed in a lossless, homogeneous medium. This represents the simplest possible configuration in which crosstalk is possible. Lands on a printed circuit

board approximate this situation to some degree with the primary difference being that the medium surrounding the conductors for a PCB is inhomogeneous (glass-epoxy, air). Nevertheless this model provides considerable insight into the PCB crosstalk mechanism, and moreover, the resulting transmission line equations are solvable in literal form [19].

The general, physical configuration is shown in Fig. 3.1. One conductor, the generator conductor, with the reference conductor forms the generator circuit. This circuit is driven at the left end with a (pulse) source $v_S(t)$ having a source resistance R_S and is terminated to the reference conductor at the other end with a resistor R_L . Another conductor, the receptor conductor with the reference conductor forms the receptor circuit. This circuit is terminated at the end near the source (the near end) in a resistor R_{NE} and at the end opposite the source (the far end) in a resistor R_{FE} . The object here is, given the physical dimensions and properties of the conductors and the surrounding medium, the terminal resistors and the time-domain pulse source, $v_S(t)$, predict the time-domain induced voltages $v_{NE}(t)$ and $v_{FE}(t)$.

This is, of course, a special case of the general, $(n+1)$ conductor uniform line discussed previously where $n=2$. The generator and receptor line voltages with respect to the reference conductor are denoted as $v_G(x,t)$ and $v_R(x,t)$, respectively. The generator and receptor line currents are denoted as $i_G(x,t)$ and $i_R(x,t)$, respectively. Again it is assumed that these currents return through the reference conductor such that the net current in the $+x$ direction at any point on the line is zero.

The per-unit-length transmission-line model is shown in Fig. 3.2. Once again the per-unit-length self inductances (capacitances) are denoted

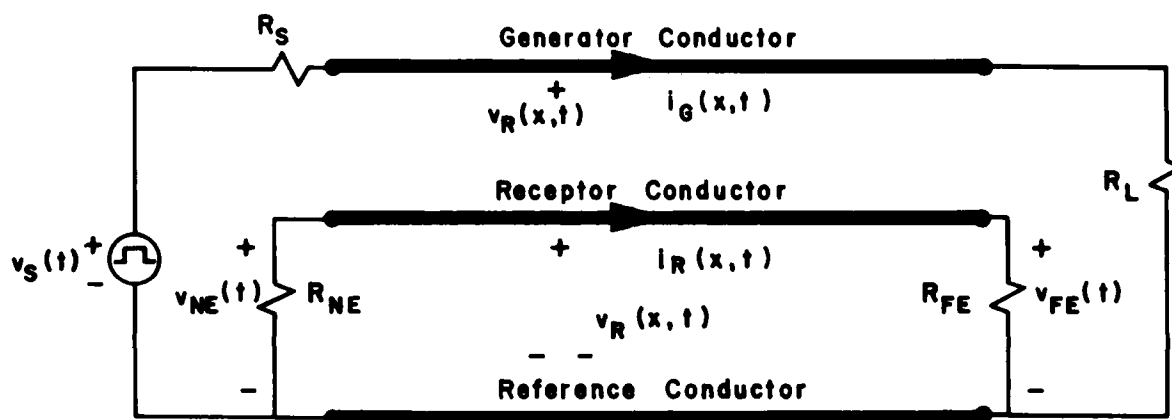


Fig. 3.1. A three-conductor line.

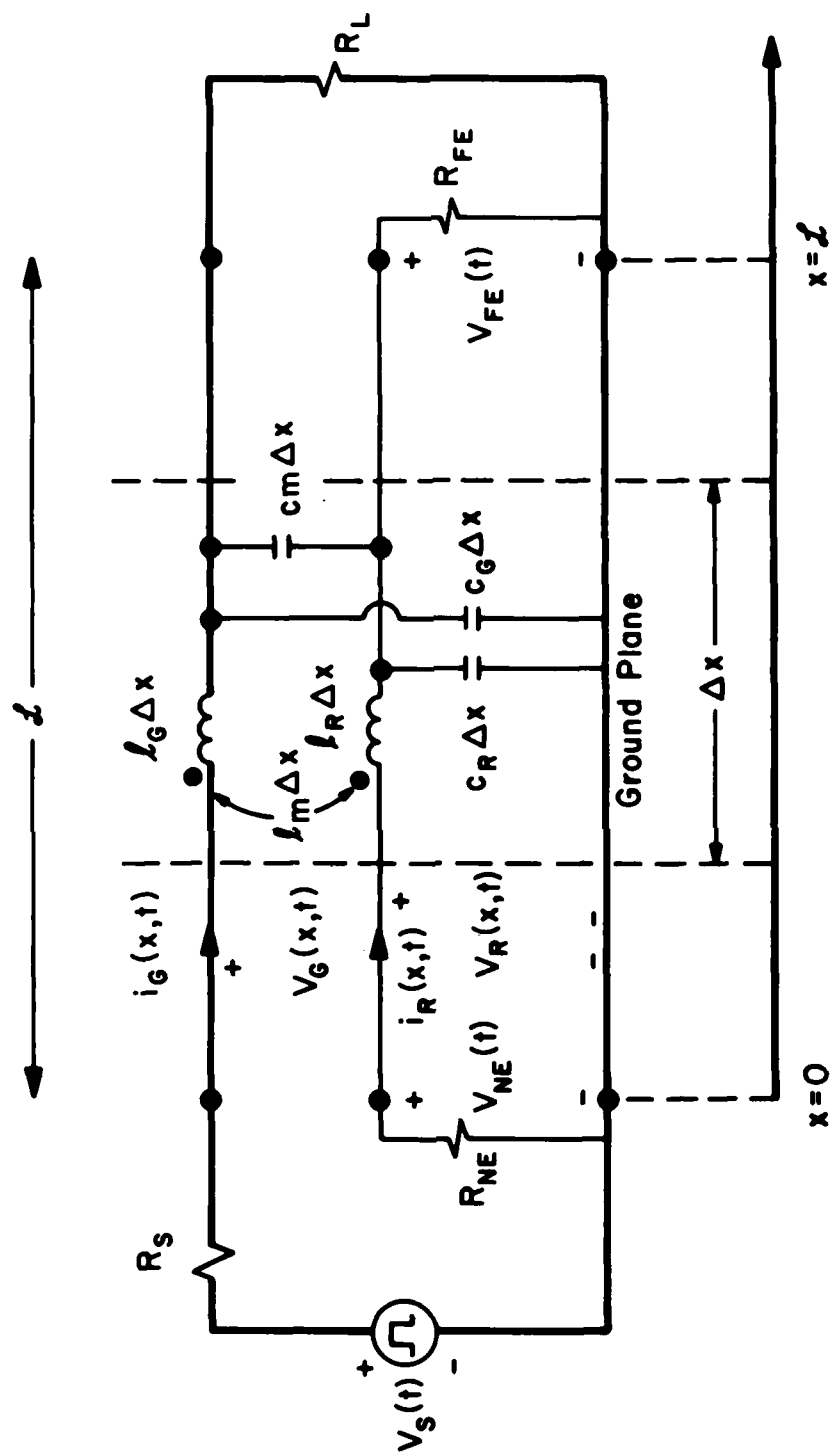


Fig. 3.2. The per-unit-length equivalent circuit for a three-conductor line.

as $\ell_G, \ell_R (c_G, c_R)$. The per-unit-length mutual inductance (capacitance) is denoted as $\ell_m (c_m)$. The transmission line equations can be obtained from Fig. 3.2 in the limit as $\Delta x \rightarrow 0$ as

$$\frac{\partial v_G(x,t)}{\partial x} = -\ell_G \frac{\partial i_G(x,t)}{\partial t} - \ell_m \frac{\partial i_R(x,t)}{\partial t} \quad (3.6a)$$

$$\frac{\partial v_R(x,t)}{\partial x} = -\ell_m \frac{\partial i_G(x,t)}{\partial t} - \ell_R \frac{\partial i_R(x,t)}{\partial t} \quad (3.6b)$$

$$\frac{\partial i_R(x,t)}{\partial x} = -(c_G + c_m) \frac{\partial v_G(x,t)}{\partial t} + c_m \frac{\partial v_R(x,t)}{\partial t} \quad (3.6c)$$

$$\frac{\partial i_G(x,t)}{\partial x} = c_m \frac{\partial v_G(x,t)}{\partial t} - (c_R + c_m) \frac{\partial v_R(x,t)}{\partial t} \quad (3.6d)$$

Direct solution of (3.6) in the time-domain and incorporation of the terminal constraints is quite difficult [1]. However, an exact literal solution can be obtained for sinusoidal, steady-state excitation. For sinusoidal, steady-state excitation, (3.6) becomes a set of ordinary differential equations [1]:

$$\frac{dV_G(x)}{dx} = -j\omega\ell_G I_G(x) - j\omega\ell_m I_R(x) \quad (3.7a)$$

$$\frac{dV_R(x)}{dx} = -j\omega\ell_m I_G(x) - j\omega\ell_R I_R(x) \quad (3.7b)$$

$$\frac{dI_G(x)}{dx} = -j\omega(c_G + c_m) V_G(x) + j\omega c_m V_R(x) \quad (3.7c)$$

$$\frac{dI_R(x)}{dx} = j\omega c_m V_G(x) - j\omega(c_R + c_m) V_R(x) \quad (3.7d)$$

where the phasor line voltages and currents are V_G, V_R, I_G, I_R and

$$v_G(x,t) = v_R(x)e^{j\omega t} \quad (3.8a)$$

$$v_R(x,t) = v_R(x)e^{j\omega t} \quad (3.8b)$$

$$i_G(x,t) = I_G(x)e^{j\omega t} \quad (3.8c)$$

$$i_R(x,t) = I_R(x)e^{j\omega t} \quad (3.8d)$$

The terminal constraints at the ends of the line, $x = 0$ and $x = l$, are

$$v_G(0) = v_S - R_S I_G(0) \quad (3.9a)$$

$$v_R(0) = -R_{NE} I_R(0) \quad (3.9b)$$

$$v_G(l) = R_L I_G(l) \quad (3.9c)$$

$$v_R(l) = R_{FE} I_R(l) \quad (3.9d)$$

where the source is assumed to be sinusoidal:

$$v_S(t) = v_S e^{j\omega t} \quad (3.10)$$

The exact solution of (3.7) with the terminal constraints in (3.9) incorporated was obtained in literal form in [19] for homogeneous media. The terminal voltages of the receptor circuit are

$$v_{FE} = \frac{S}{\text{Den}} \left[-\left(\frac{R_{FE}}{R_{NE} + R_{FE}} \right) (j\omega l_m) I_{GDC} + \left(\frac{R_{NE} R_{FE}}{R_{NE} + R_{FE}} \right) (j\omega c_m) v_{GDC} \right] \quad (3.11a)$$

$$V_{NE} = \frac{S}{\text{Den}} \left[\left(\frac{R_{NE}}{R_{NE}+R_{FE}} \right) (j\omega \ell_m) \left(C + \frac{j2\pi(\ell/\lambda)}{\sqrt{1-k^2}} \frac{R_L}{R_{CG}} S \right) I_{G_{DC}} \right. \\ \left. + \left(\frac{R_{NE}R_{FE}}{R_{NE}+R_{FE}} \right) (j\omega c_m) \left(C + \frac{j2\pi(\ell/\lambda)}{\sqrt{1-k^2}} \frac{R_{CG}}{R_L} S \right) V_{G_{DC}} \right] \quad (3.11b)$$

where

$$S = \frac{\sin\left(\frac{2\pi\ell}{\lambda}\right)}{\left(\frac{2\pi\ell}{\lambda}\right)} \quad (3.12a)$$

$$C = \cos\left(\frac{2\pi\ell}{\lambda}\right) \quad (3.12b)$$

The coupling coefficient k is

$$k = \frac{\ell_m}{\sqrt{\ell_G \ell_R}} \quad (3.13) \\ = \frac{c_m}{\sqrt{(c_G+c_m)(c_R+c_m)}}$$

and the characteristic impedances of the respective circuits are

$$R_{CG} = v \ell_G \sqrt{1-k^2} \quad (3.14a)$$

$$R_{CR} = v \ell_R \sqrt{1-k^2} \quad (3.14b)$$

The terms $V_{G_{DC}}$ and $I_{G_{DC}}$ are the generator line voltage and current computed from DC considerations:

$$V_{G_{DC}} = \frac{R_L}{R_S+R_L} V_S \quad (3.15a)$$

$$I_{G_{DC}} = \frac{1}{R_S+R_L} V_S \quad (3.15b)$$

The denominator term, Den, is

$$\text{Den} = C^2 - S^2 \omega^2 \tau_R \tau_G \left[1 - k^2 \frac{(1 - \alpha_{NG} \alpha_{FR})(1 - \alpha_{FG} \alpha_{NR})}{(1 + \alpha_{NR} \alpha_{FR})(1 + \alpha_{NG} \alpha_{FG})} \right] + j\omega CS [\tau_R + \tau_G] \quad (3.16)$$

The α terms are defined by

$$\begin{aligned} \alpha_{NG} &= \frac{R_S}{R_{CG}} & \alpha_{FG} &= \frac{R_L}{R_{CG}} \\ \alpha_{NR} &= \frac{R_{NE}}{R_{CR}} & \alpha_{FR} &= \frac{R_{FE}}{R_{CR}} \end{aligned} \quad (3.17)$$

and the circuit time constants are

$$\tau_G = \frac{\ell_G \mathcal{L}}{R_S + R_L} + (c_G + c_m) \mathcal{L} \left(\frac{R_S R_L}{R_S + R_L} \right) \quad (3.18a)$$

$$\tau_R = \frac{\ell_R \mathcal{L}}{R_{NE} + R_{FE}} + (c_R + c_m) \mathcal{L} \left(\frac{R_{NE} R_{FE}}{R_{NE} + R_{FE}} \right) \quad (3.18b)$$

The above equations represent the exact solution of the transmission-line equations with the terminal constraints incorporated for sinusoidal steady-state excitation. They are the only known literal solutions of the transmission-line equations for lines consisting of more than two conductors, i.e., $n > 1$. A great deal of insight can be gained from these equations [20,21]. However a considerable simplification of them can be obtained if we assume (1) weakly coupled circuits and (2) line lengths which are electrically short. If the coupling coefficient, k , is sufficiently small, the denominator term, Den, in (3.16) simplifies to

$$\text{Den} = (C + j\omega S\tau_G)(C + j\omega S\tau_R) \quad (3.19)$$

If the line is electrically short, $l \ll \lambda$, then

$$C = 1$$

$$S = 1$$

The results in (3.11) simplify to

$$V_{FE} = \frac{-\left(\frac{R_{FE}}{R_{NE}+R_{FE}}\right)(j\omega l_m) I_{G_{DC}} + \left(\frac{R_{NE}R_{FE}}{R_{NE}+R_{FE}}\right)(j\omega c_m) V_{G_{DC}}}{(1+j\omega\tau_G)(1+j\omega\tau_R)} \quad (3.20a)$$

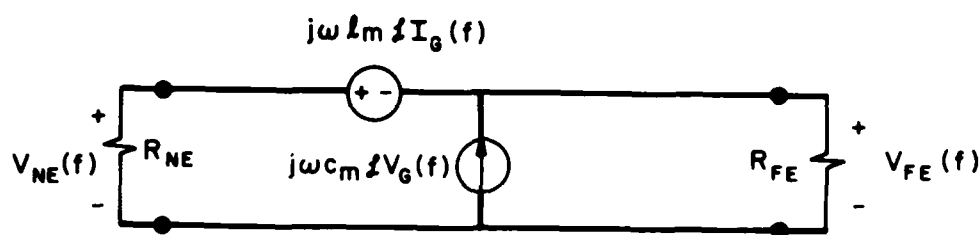
$$V_{NE} = \frac{\left(\frac{R_{NE}}{R_{NE}+R_{FE}}\right)(j\omega l_m) I_{G_{DC}} + \left(\frac{R_{NE}R_{FE}}{R_{NE}+R_{FE}}\right)(j\omega c_m) V_{G_{DC}}}{(1+j\omega\tau_G)(1+j\omega\tau_R)} \quad (3.20b)$$

If, in addition to being electrically short, the frequency of excitation is small enough such that $\omega\tau_G \ll 1$ and $\omega\tau_R \ll 1$ then (3.20) simplifies to

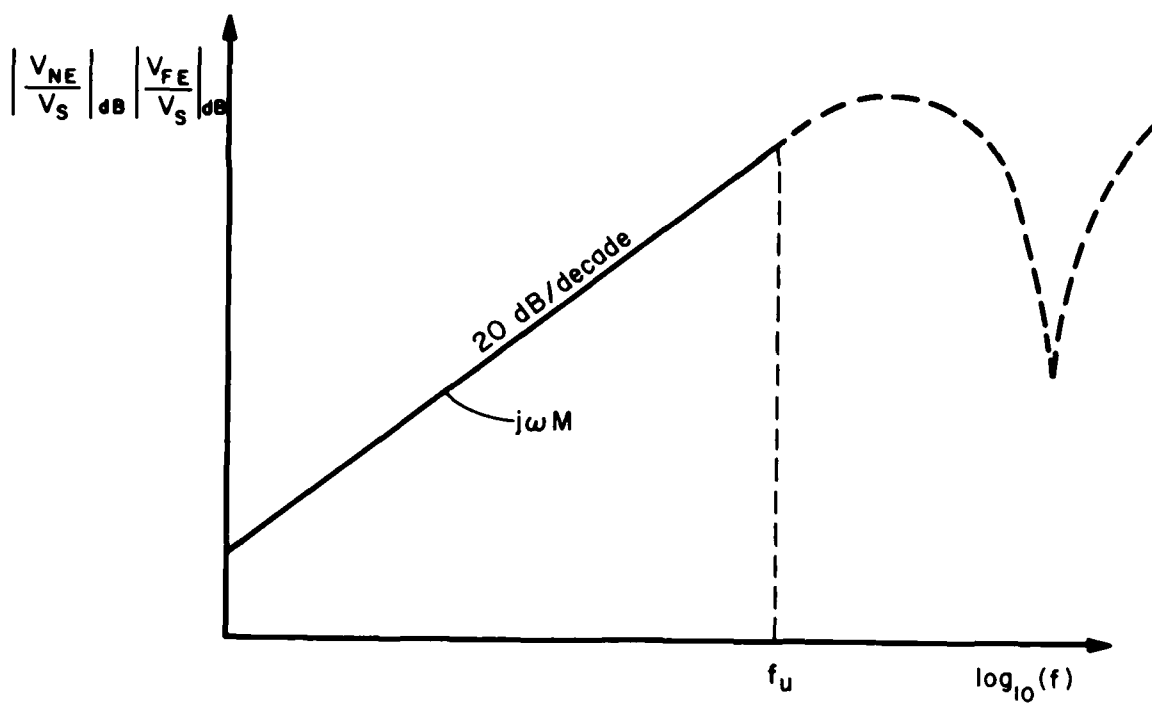
$$V_{FE} = -\left(\frac{R_{FE}}{R_{NE}+R_{FE}}\right)j\omega l_m I_{G_{DC}} + \left(\frac{R_{NE}R_{FE}}{R_{NE}+R_{FE}}\right)j\omega c_m V_{G_{DC}} \quad (3.21a)$$

$$V_{NE} = \left(\frac{R_{NE}}{R_{NE}+R_{FE}}\right)j\omega l_m I_{G_{DC}} + \left(\frac{R_{NE}R_{FE}}{R_{NE}+R_{FE}}\right)j\omega c_m V_{G_{DC}} \quad (3.21b)$$

These induced crosstalk voltages can be calculated from the equivalent receptor circuit shown in Fig. 3.3(a). There are two contributions to the induced voltage. One source, the voltage source, depends on the mutual inductance between the two circuits, l_m , and is referred to as the inductive coupling contribution. The other source, the current source, depends on the mutual capacitance between the two circuits, c_m , and is referred to as



(a)



(b)

Fig. 3.3. A low-frequency, crosstalk circuit.

the capacitive coupling contribution. The net induced crosstalk is the sum of the inductive and capacitive coupling contributions.

Both the inductive and capacitive coupling contributions vary linearly with frequency (20 dB/decade) up to some upper frequency limit, f_u . In addition, the phase angle is $+90^\circ$ represented by $j = \sqrt{-1}$. This type of behavior is typical for crosstalk. The upper limit, f_u , is simply the point at which the increase deviates from 20 dB/decade. This was shown to be a function of the terminal impedances in [21]. Nevertheless, this frequency range can cover a large portion of the spectrum of the input pulse, and its extent can be determined either from frequency response measurements of the actual line (with loads) or from calculation with (3.11). It is this simple, low-frequency region which we will concentrate on modeling.

3.2. A Simple, Time-Domain Crosstalk Prediction Model

One can determine the time-domain crosstalk pulse using frequency-domain methods as outlined in Chapter II. Determine the frequency-domain crosstalk transfer function (magnitude and phase) via calculation or measurements and the spectrum of the input pulse, $v_S(t)$, (magnitude and phase) via Fourier methods. Multiply the magnitudes of these spectra together to yield the magnitude of the crosstalk pulse spectrum, and add the phases of these spectra to obtain the phase of the crosstalk pulse spectrum. Then obtain, via the inverse Fourier transform, the time-domain crosstalk pulse.

This frequency-domain method, although potentially exact, has a number of drawbacks. It is not suitable for direct implementation in CAD codes, cannot handle nonlinear terminations, and requires computation at a potentially large number of frequency points. It would be desirable to

bypass this time-domain to frequency-domain to time-domain conversion process and compute the crosstalk pulse directly in the time domain based on the time domain input pulse. This will be our objective along with any simplification of that process.

First let us suppose that the frequency-domain transfer function varies linearly with frequency and has a $\pm 90^\circ$ phase angle:

$$V_{NE}(f) = j\omega M_{NE} V_S(f) \quad (3.22a)$$

$$V_{FE}(f) = j\omega M_{FE} V_S(f) \quad (3.22b)$$

Then it is a simple matter to show that the time-domain crosstalk voltage is simply each M multiplied by the time derivative of $v_S(t)$:

$$v_{NE}(t) = M_{NE} \frac{dv_S(t)}{dt} \quad (3.23a)$$

$$v_{FE}(t) = M_{FE} \frac{dv_S(t)}{dt} \quad (3.23b)$$

A typical response for trapezoidal $v_S(t)$ is shown in Fig. 3.4. The slopes of the transfer functions, M_{NE} and M_{FE} , can be found either from measurement or from calculation. From Fig. 3.3 we obtain

$$M_{NE} = \left(\frac{R_{NE}}{R_{NE} + R_{FE}} \right) \ell_m \angle I_{GDC} + \left(\frac{R_{NE} R_{FE}}{R_{NE} + R_{FE}} \right) c_m \angle V_{GDC} \quad (3.24a)$$

$$M_{FE} = - \left(\frac{R_{FE}}{R_{NE} + R_{FE}} \right) \ell_m \angle I_{GDC} + \left(\frac{R_{NE} R_{FE}}{R_{NE} + R_{FE}} \right) c_m \angle V_{GDC} \quad (3.24b)$$

where

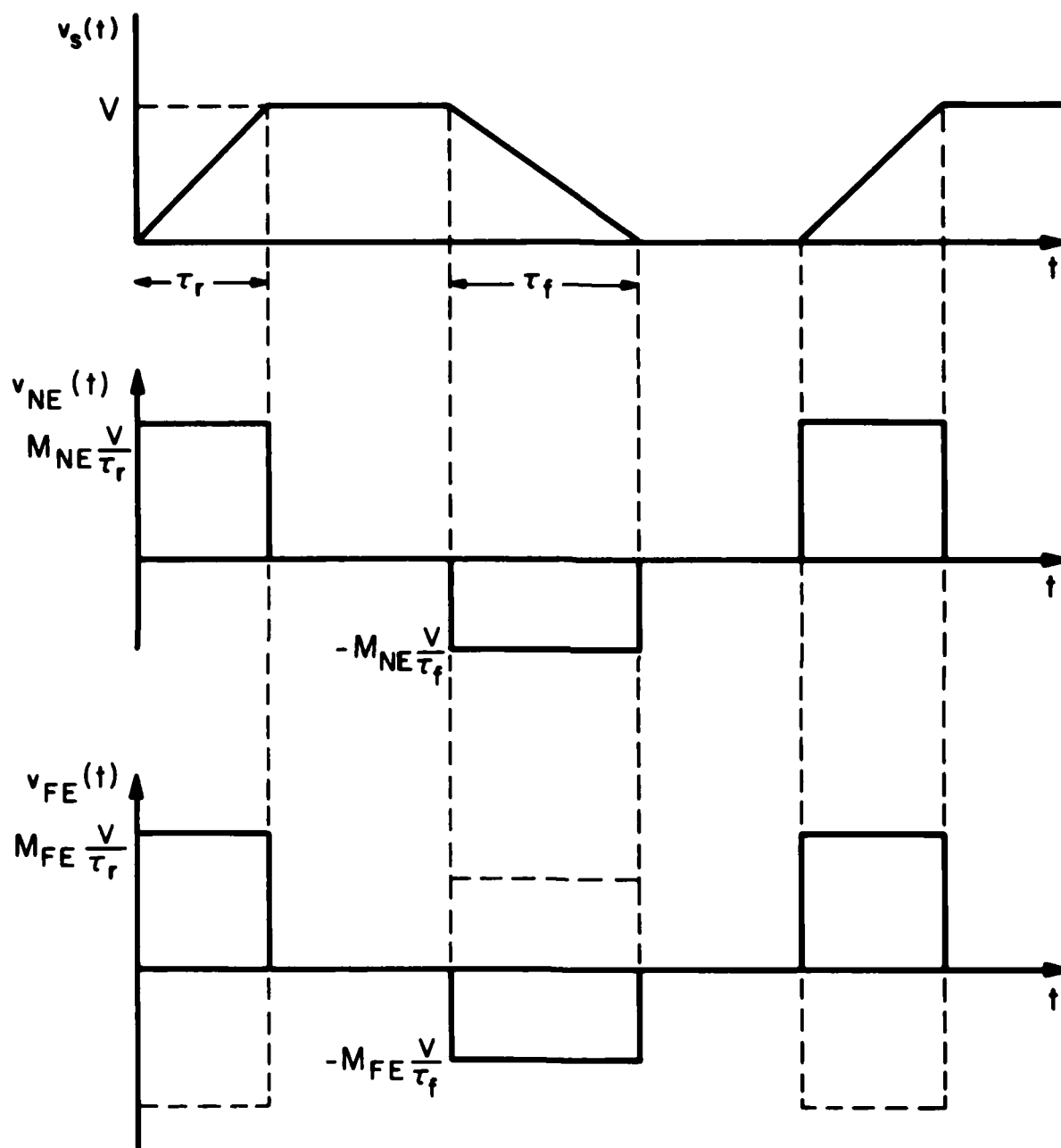


Fig. 3.4. Crosstalk prediction in the time domain.

$$V_{G_{DC}} = \frac{R_L}{R_S + R_L} V_S \quad (3.25a)$$

$$I_{G_{DC}} = \frac{1}{R_S + R_L} V_S \quad (3.25b)$$

Note that the near end and far end crosstalk consist of pulses occurring during the transition times of the input pulse. The heights of these pulses are dependent on the slopes of these transitions, i.e., the slew rates of the input pulse, and the slopes of the frequency-domain transfer functions, M_{NE} and M_{FE} . Note also that the near end and far end crosstalk pulses can be the same or opposite in polarity. This is because M_{FE} can be positive or negative depending on whether capacitive or inductive coupling is dominant, respectively. Thus for small load impedances, one would expect inductive coupling to dominate capacitive coupling and the near end and far end crosstalk pulses would be opposite in polarity. For large load impedances, one would expect capacitive coupling to dominate inductive coupling and the near end and far end crosstalk pulses would be the same polarity. This will be shown to be true in the experimental results of the next chapter.

In order to prove the result in (3.23) we presume the input voltage to be periodic (although this is not necessary) with period T_0 . It need not be trapezoidal in shape; any pulse shape is acceptable. Thus we represent the input pulse in the frequency domain via a Fourier series:

$$v_S(t) = \sum_{n=-\infty}^{\infty} V_S(\omega) e^{jn\omega_0 t} \quad (3.26)$$

where $\omega_0 = 2\pi/T_0$. Note that the time derivative is

$$\frac{dv_S(t)}{dt} = \sum_{n=-\infty}^{\infty} (jn\omega_o) V_S(\omega) e^{jn\omega_o t} \quad (3.27)$$

The near end and far end crosstalk pulses will also be periodic and represented by

$$v_{NE}(t) = \sum_{n=-\infty}^{\infty} V_{NE}(\omega) e^{jn\omega_o t} \quad (3.28a)$$

$$v_{FE}(t) = \sum_{n=-\infty}^{\infty} V_{FE}(\omega) e^{jn\omega_o t} \quad (3.28b)$$

Substituting (3.22) into (3.28) yields

$$v_{NE}(t) = \sum_{n=-\infty}^{\infty} jn\omega_o M_{NE} V_S(\omega) e^{jn\omega_o t} \quad (3.29a)$$

$$v_{FE}(t) = \sum_{n=-\infty}^{\infty} jn\omega_o M_{FE} V_S(\omega) e^{jn\omega_o t} \quad (3.29b)$$

where we have substituted $\omega = n\omega_o$. Comparing (3.29) and (3.27) yields the result in (3.23).

3.3. An Improved, Time-Domain Crosstalk Prediction Model

In the previous section we made a major, simplifying assumption. The frequency domain transfer function was assumed to vary linearly with frequency and have a $\pm 90^\circ$ phase angle for all frequencies. Clearly this is not realistic although, as we will show in the next chapter, this very simple model can yield quite accurate results for a wide range of practical problems involving PCB's as well as crosstalk in cables.

An important secondary effect is that of "common impedance coupling" as illustrated in Fig. 3.5. Consider DC excitation of the line, i.e., $\omega=0$. The generator circuit sees a net resistance of

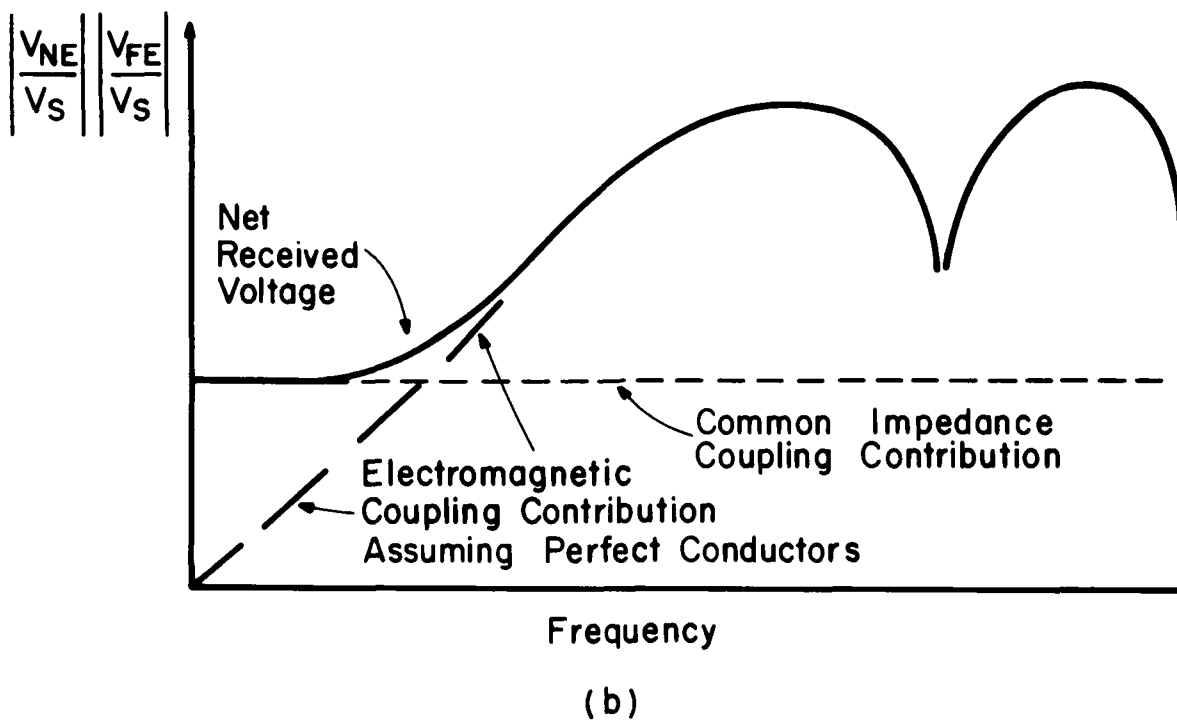
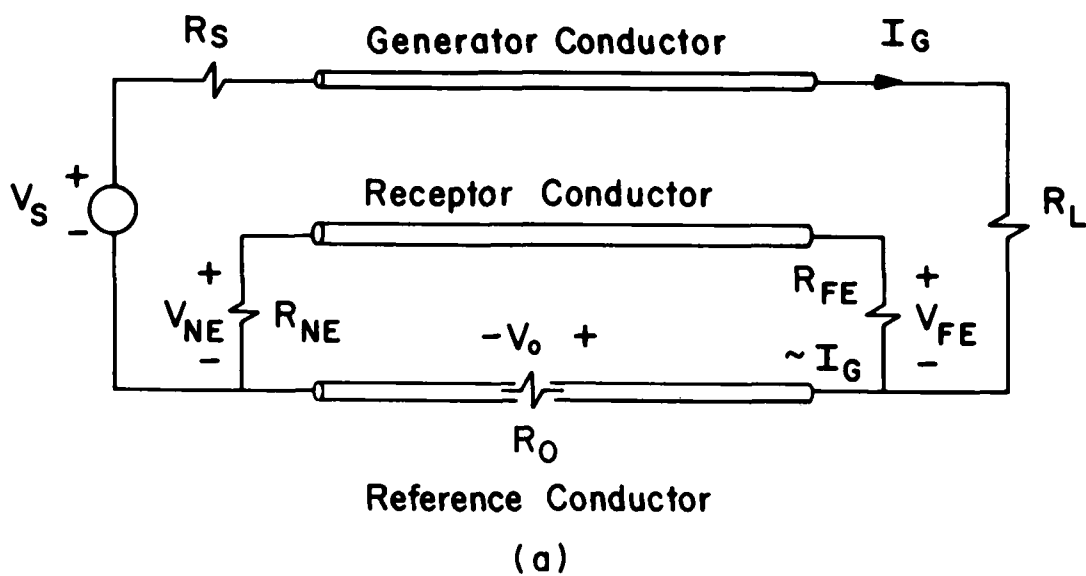


Fig. 3.5. Illustration of common impedance coupling.

$$R_{in} = R_L + (R_{NE} + R_{FE}) || R_0 \quad (3.30)$$

$$= R_L + R_0$$

$$= R_L$$

where R_0 is the total DC resistance of the reference conductor which is assumed to be much less than R_L and $R_{NE} + R_{FE}$. Thus the DC generator circuit current is

$$I_{GDC} = \frac{V_S}{R_S + R_L} \quad (3.31)$$

The fraction of this current which returns through the reference conductor is, by current division,

$$I_0 = \frac{(R_{NE} + R_{FE})}{R_0 + (R_{NE} + R_{FE})} I_{GDC} \quad (3.32)$$

$$= I_{GDC}$$

Thus, for practical load resistance values, virtually the entire generator circuit current returns in the reference conductor.

This results in a voltage drop across the reference conductor of

$$V_0 = R_0 I_0 \quad (3.33)$$

This voltage is divided across the receptor circuit loads as

$$V_{NE}^{CI} = \frac{R_{NE}}{R_{NE} + R_{FE}} V_0 \quad (3.34a)$$

$$= \frac{R_{NE}}{R_{NE} + R_{FE}} R_0 \frac{V_S}{R_S + R_L}$$

$$V_{FE}^{CI} = - \frac{R_{FE}}{R_{NE} + R_{FE}} R_0 \frac{V_S}{R_S + R_L} \quad (3.34b)$$

This induced voltage is due to the impedance of the reference conductor being common to both circuits and is referred to as common impedance coupling. It tends to be the dominant coupling mechanism at the lower frequencies where it dominates the electromagnetic coupling computed assuming perfect conductors as shown in Fig. 3.5(b). Depending on (1) the type of reference conductor and (2) the bit rate or period of the signal, it may represent an important coupling mechanism. If the fundamental ($f_0 = 1/T_0$) frequency of the generator signal occurs below the frequency at which the two coupling mechanisms are equal, common impedance coupling cannot be neglected. In the case of ribbon cables and data baud rates below 10 kHz, this was shown to be an important consideration [2,3].

Another important consideration occurs at the higher frequencies. The crosstalk does not continue to increase at a 20 dB/decade rate but replicates causing nulls and maxima to appear in the frequency response. The magnitude of the maxima and the locations of the nulls are difficult to predict but occur above the point at which the line becomes $\frac{1}{4} \lambda$ in length. Other, secondary minima (not nulls) can occur below this point [20]. We propose to bound this high frequency region with a constant coupling level rather than have it increase with frequency indefinitely. Thus, above f_u in Fig. 3.3 we choose a constant coupling level at the level existing at f_u and zero phase angle.

Combining these two practical considerations yields the proposed frequency-domain crosstalk model shown in Fig. 3.6. The curve is defined by

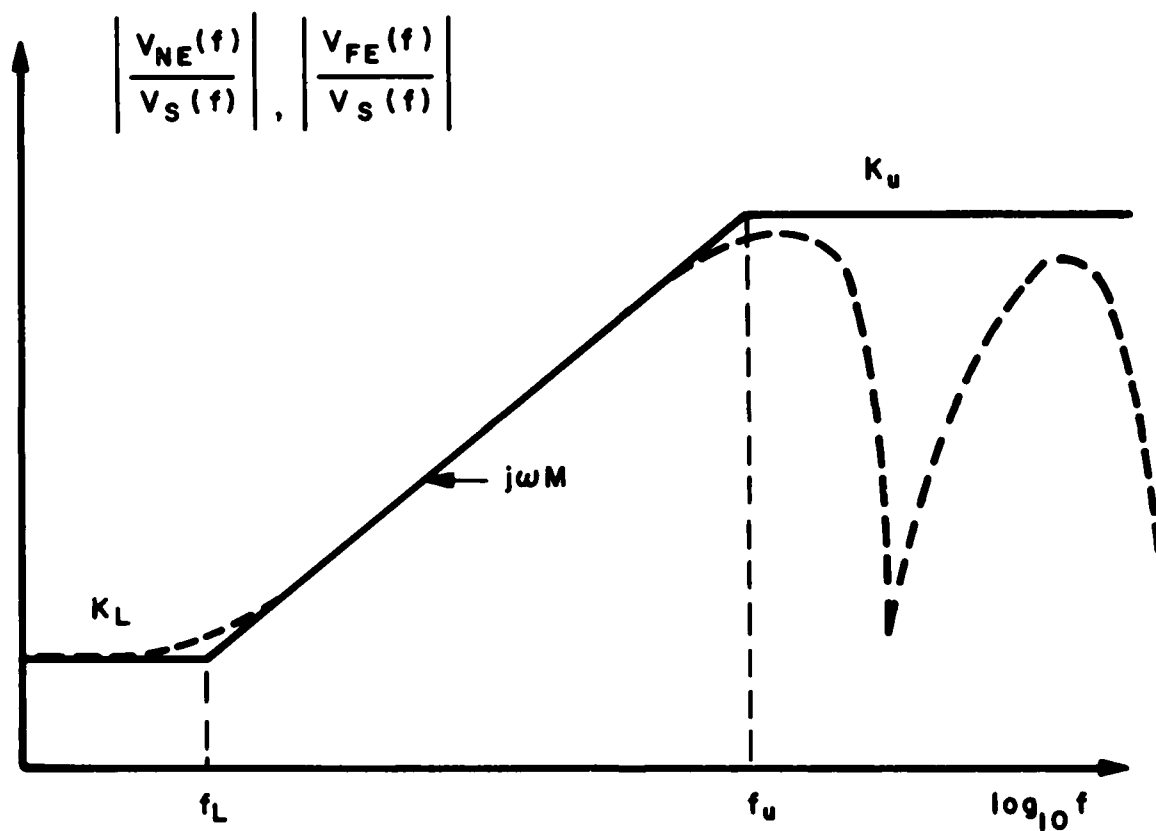


Fig. 3.6. An improved frequency response model incorporating common impedance coupling K_L , and finite, high-frequency response, K_u .

$$\frac{V(f)}{V_S(f)} = \begin{cases} K_L & f \leq f_L \\ j\omega M & f_L \leq f \leq f_u \\ K_u & f \geq f_u \end{cases} \quad (3.35)$$

where $V(f)$ denotes V_{NE} or V_{FE} as appropriate. The transfer function for this becomes

$$\frac{V(f)}{V_S(f)} = K_L \frac{(1 + j \frac{\omega}{\omega_L})}{(1 + j \frac{\omega}{\omega_u})} \quad (3.36)$$

The time-domain, differential equation relating $v(t)$ to $v_S(t)$ can be obtained by replacing $j\omega$ with the differential operator $p = \frac{d}{dt}$:

$$\frac{v(t)}{v_S(t)} = K_L \frac{(1 + \frac{p}{\omega_L})}{(1 + \frac{p}{\omega_u})} \quad (3.37)$$

This yields

$$(\frac{p}{\omega_u} + 1) v(t) = K_L (\frac{p}{\omega_L} + 1) v_S(t) \quad (3.38)$$

The differential equation becomes

$$\frac{dv(t)}{dt} + \omega_u v(t) = \frac{\omega_u}{\omega_L} K_L \frac{dv_S(t)}{dt} + \omega_u K_L v_S(t) \quad (3.39)$$

The solution to this becomes, using state variable theory [1],

$$v(t) = e^{-\omega_u t} v(0) + \int_0^t e^{-\omega_u(t-\lambda)} \frac{\omega_u}{\omega_L} K_L \dot{v}_S(\lambda) d\lambda$$

(3.40)

$$+ \int_0^t e^{-\omega_u(t-\lambda)} \omega_u K_L v_S(\lambda) d\lambda$$

where \dot{v}_S denotes $\frac{dv_S}{dt}$. Substituting

$$M = \frac{K_u}{\omega_u}$$

(3.41)

$$= \frac{K_L}{\omega_L}$$

yields

$$v(t) = e^{-\omega_u t} v(0) + \int_0^t e^{-\omega_u(t-\lambda)} \omega_u M \dot{v}_S(\lambda) d\lambda$$

(3.42)

$$+ \int_0^t e^{-\omega_u(t-\lambda)} \omega_u K_L v_S(\lambda) d\lambda$$

For a general $v_S(t)$ this requires direct integration (or convolution). However if $\omega_u \rightarrow \infty$; that is, the frequency response is assumed to increase at 20 dB/decade indefinitely but common impedance coupling is retained, we obtain

$$\frac{v(t)}{v_S(t)} = K_L \left(1 + \frac{p}{\omega_L}\right)$$

(3.43)

or

$$v(t) = K_L v_S(t) + M \frac{dv_S(t)}{dt}$$

(3.44)

as in the previous section.

An alternative derivation of (3.42) can be obtained by viewing the frequency response given in Fig. 3.6 as an analogue to that obtained by a high-pass filter. This is not to imply a physical correspondence but only a mathematical analogue for the purposes of deriving (3.42). For example, the high-pass filter shown in Fig. 3.7 has the frequency response transfer function

$$\frac{V_o(f)}{V_i(f)} = \left(\frac{R_a}{R + R_a + R_b} \right) \frac{(1 + j\omega RC)}{(1 + j\omega R \parallel (R_a + R_b)C)} \quad (3.45)$$

Comparing (3.45) and (3.36) shows that, for this analogue,

$$K_L = \frac{R_a}{R + R_a + R_b} \quad (3.46a)$$

$$\omega_L = \frac{1}{RC} \quad (3.46b)$$

$$\omega_u = \frac{1}{C[R \parallel (R_a + R_b)]} \quad (3.46c)$$

Thus, if one desires, the circuit shown in Fig. 3.7 may be used to simulate the time-domain line response once the analogous quantities R , R_a , R_b , C are calculated from measured (or calculated [19]) results from the following.

There are three independent parameters in Fig. 3.6, for example, K_L , ω_u and M . The circuit in Fig. 3.7 contains four parameters, R , C , R_a , R_b .

So we can constrain one and find the remaining three. A number of possibilities exist. One may choose C arbitrarily and compute R , R_a and R_b from (3.46). If we do so we find, using $M = K_L/\omega_L$

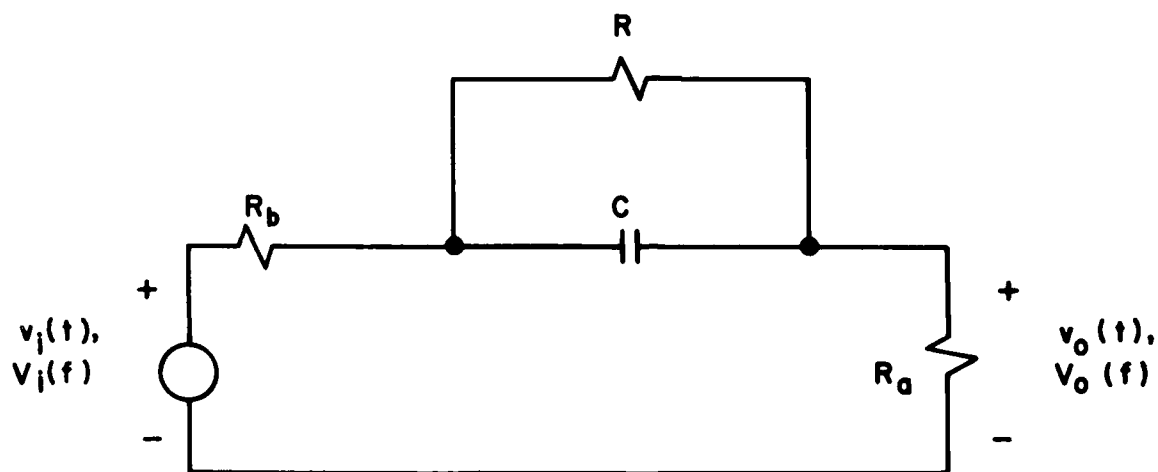


Fig. 3.7. A lumped, equivalent circuit for simulation of time-domain crosstalk.

$$R = \frac{M}{K_L C} \quad (3.47a)$$

$$R_a = \frac{M\omega_u}{(M\omega_u - K_L)} \frac{M}{C} \quad (3.47b)$$

$$R_b = \frac{(1 - \omega_u M)}{(M\omega_u - K_L)} \frac{M}{C} \quad (3.47c)$$

Note that $K_u = M\omega_u$. Since $K_u > K_L$ the denominators of R_a and R_b are positive. However it is possible to have $K_u > 1$. This would require R_b to be negative. Most CAD codes can handle negative resistors.

Thus one can use the lumped circuit of Fig.3.7 in any standard, lumped-circuit CAD code to calculate the induced, time-domain crosstalk pulses once the circuit parameters are calculated with (3.47) from frequency-domain measurements. It should be stressed again that no physical correspondence between the circuit in Fig. 3.7 and the actual transmission line are intended nor should be attempted. The circuit of Fig. 3.7 is only intended as an analogue which provides a convenient way of calculating the line time-domain crosstalk using a CAD code.

For known $v_s(t)$, use of the equivalent circuit is not necessary. In the next section we will give an explicit solution to (3.42) for a specific $v_s(t)$ --a periodic, trapezoidal pulse train--which is common on PCB's.

3.3.1. Solution for Trapezoidal (Clock) Pulses

Consider a periodic, trapezoidal pulse train shown in Fig. 1.1(a). This type of signal is commonly present on PCB lands and is meant to resemble clock signals. For this type of pulse we may obtain an explicit solution to (3.42). We will assume that the line is initially uncharged when the pulse is applied at $t=0$, $v(0)=0$. Thus (3.42) becomes

$$\begin{aligned}
v(t) = & \omega_u K_L \int_0^t e^{-\omega_u(t-\lambda)} v_S(\lambda) d\lambda \\
& + \omega_u M \int_0^t e^{-\omega_u(t-\lambda)} \dot{v}_S(\lambda) d\lambda
\end{aligned} \tag{3.48}$$

The result requires a determination of the convolution of $e^{-\omega_u t}$ and two signals, $\dot{v}_S(t)$ and $v_S(t)$:

$$\int_0^t e^{-\omega_u(t-\lambda)} v_S(\lambda) d\lambda = e^{-\omega_u t} * v_S(t) \tag{3.49a}$$

$$\int_0^t e^{-\omega_u(t-\lambda)} \dot{v}_S(\lambda) d\lambda = e^{-\omega_u t} * \dot{v}_S(t) \tag{3.49b}$$

where $*$ denotes convolution. The signal, $v_S(t)$, and its derivative $\dot{v}_S(t)$, are shown in Fig. 3.8. The convolutions in (3.49) are shown in Fig. 3.9. Each convolution requires the product of $e^{-\omega_u(t-\lambda)}$ and either $v_S(\lambda)$ or $\dot{v}_S(\lambda)$ as t progresses and the determination of the resulting area under the product curve. This interpretation shows three distinct regions over a complete period:

$$\begin{aligned}
0 & \leq t \leq t_1 \\
t_1 & \leq t \leq t_2 \\
t_2 & \leq t \leq t_3
\end{aligned} \tag{3.50}$$

where

$$\begin{aligned}
t_1 &= \tau_r \\
t_2 &= \tau - \frac{(\tau_r + \tau_f)}{2} \\
t_3 &= \tau + \frac{(\tau_r + \tau_f)}{2}
\end{aligned} \tag{3.51}$$

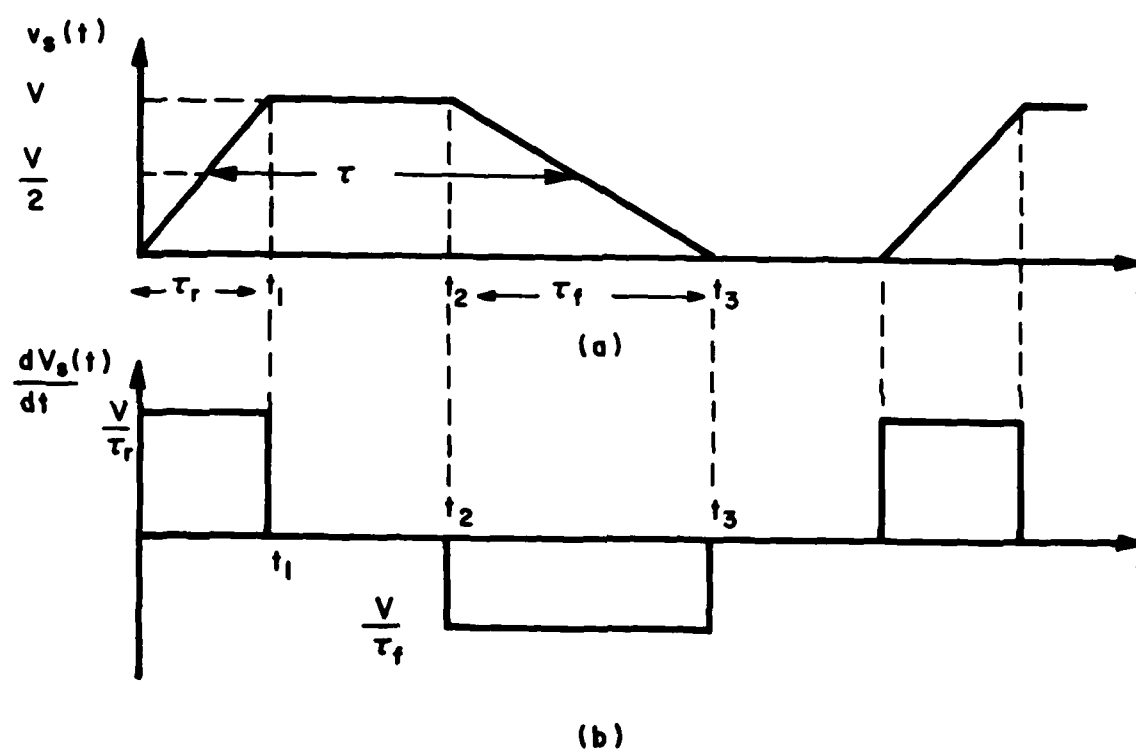


Fig. 3.8. The input signal and its derivative.

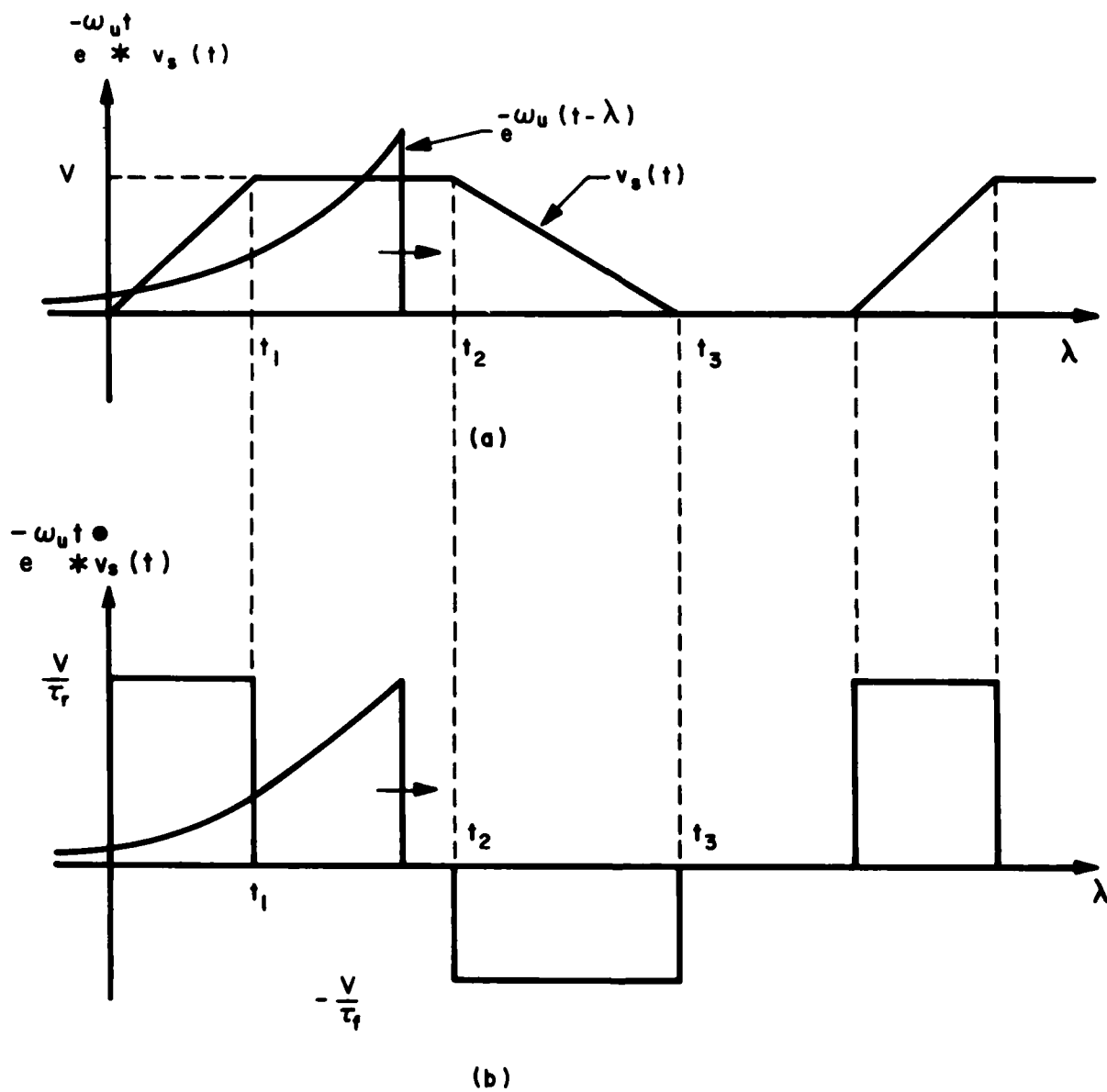


Fig. 3.9. Illustration of convolution.

and τ is the pulse width (between 50% points).

One of the simplest ways of determining the solution to (3.48) for this signal is to recognize that $\dot{v}_S(t)$ is a sequence of pulses and may be written in terms of the unit step function $u(t)$ over $0 \leq t \leq T$ as

$$\begin{aligned} \dot{v}_S(t) = & \frac{V}{\tau_r} [u(t) - u(t-t_1)] \\ & - \frac{V}{\tau_f} [u(t-t_2) - u(t-t_3)] \end{aligned} \quad (3.52)$$

$$0 \leq t \leq T$$

Similarly, $v_S(t)$ can be written in terms of unit ramp functions, $r(t)$, over $0 \leq t \leq T$ as

$$\begin{aligned} v_S(t) = & \frac{V}{\tau_r} [r(t) - r(t-t_1)] \\ & - \frac{V}{\tau_f} [r(t-t_2) - r(t-t_3)] \end{aligned} \quad (3.53)$$

$$0 \leq t \leq T$$

We will determine the basic convolutions in (3.49) in response to a unit step or a unit ramp and use (3.52) and (3.53) to determine the complete response.

The convolution of $e^{-\omega_u t}$ and a unit step is

$$\begin{aligned} e^{-\omega_u t} * u(t) &= e^{-\omega_u t} \int_0^t e^{\omega_u \lambda} u(\lambda) d\lambda \\ &= \frac{1}{\omega_u} (1 - e^{-\omega_u t}) u(t) \end{aligned} \quad (3.54)$$

The convolution of $e^{-\omega_u t}$ and a unit ramp is

$$\begin{aligned}
e^{-\omega_u t} * r(t) &= e^{-\omega_u t} \int_0^t e^{\omega_u \lambda} \lambda u(\lambda) d\lambda \\
&= \left\{ \frac{(\omega_u t - 1)}{\omega_u} + \frac{e^{-\omega_u t}}{\omega_u} \right\} u(t)
\end{aligned} \tag{3.55}$$

Note that (3.55) is the integral of (3.54) as it should be.

Thus, the solution to (3.48) is the appropriately weighted combination of these solutions delayed according to (3.52) and (3.53):

$$\begin{aligned}
v(t) &= \frac{VK_L}{\tau_r \omega_u} [\{ \omega_u t - 1 + e^{-\omega_u t} \} u(t) \\
&\quad - \{ \omega_u (t-t_1) - 1 + e^{-\omega_u (t-t_1)} \} u(t-t_1)] \\
&\quad - \frac{VK_L}{\tau_f \omega_u} [\{ \omega_u (t-t_2) - 1 + e^{-\omega_u (t-t_2)} \} u(t-t_2) \\
&\quad - \{ \omega_u (t-t_3) - 1 + e^{-\omega_u (t-t_3)} \} u(t-t_3)] \\
&\quad + \frac{VM}{\tau_r} [\{ 1 - e^{-\omega_u t} \} u(t) \\
&\quad - \{ 1 - e^{-\omega_u (t-t_1)} \} u(t-t_1)] \\
&\quad - \frac{VM}{\tau_f} [\{ 1 - e^{-\omega_u (t-t_2)} \} u(t-t_2) \\
&\quad - \{ 1 - e^{-\omega_u (t-t_3)} \} u(t-t_3)]
\end{aligned} \tag{3.56}$$

Although these equations appear to be complicated they may be broken down according to the appropriate time intervals of interest.

For $0 \leq t \leq t_1$, (3.56) becomes

$$\begin{aligned}
 v(t) &= \frac{VK_L}{\tau_r} t - \frac{VK_L}{\omega_u \tau_r} (1 - e^{-\omega_u t}) \\
 &\quad + \frac{VM}{\tau_r} (1 - e^{-\omega_u t}) \\
 &= \frac{VK_L}{\tau_r} + \frac{V}{\tau_r} \left(M - \frac{K_L}{\omega_u} \right) (1 - e^{-\omega_u t}) \quad (3.57) \\
 &\quad 0 \leq t \leq t_1
 \end{aligned}$$

The first term is simply the input signal multiplied by the common impedance coupling factor, K_L , which is sensible to expect. Since $K_u = M\omega_u$ and $K_u \gg K_L$ for typical boards, the second term may be simplified so that

$$\begin{aligned}
 v(t) &\approx K_L v_S(t) + \frac{VM}{\tau_r} (1 - e^{-\omega_u t}) \quad (3.58) \\
 &\quad 0 \leq t \leq t_1
 \end{aligned}$$

The second term is the result derived in the previous section where we neglected common impedance coupling and assumed the frequency response to increase indefinitely with frequency but is multiplied by the term $(1 - e^{-\omega_u t})$.

For $t_1 \leq t \leq t_2$ additional terms are added. The result is

$$\begin{aligned}
 v(t) &= \frac{VK_L}{\tau_r} t + \frac{V}{\tau_r} \left(M - \frac{K_L}{\omega_u} \right) (1 - e^{-\omega_u t}) \\
 &\quad - \frac{VK_L}{\omega_r} (t - t_1) + \frac{VK_L}{\tau_r \omega_u} [1 - e^{-\omega_u (t - t_1)}] \\
 &\quad - \frac{VM}{\tau_r} [1 - e^{-\omega_u (t - t_1)}] \quad (3.59) \\
 &\quad t_1 \leq t \leq t_2
 \end{aligned}$$

But this may be written as

$$\begin{aligned}
 v(t) &= VK_L + \frac{V}{\tau_r} \left(M - \frac{K_L}{\omega_u} \right) [1 - e^{-\omega_u t}] \\
 &\quad - \frac{V}{\tau_r} \left(M - \frac{K_L}{\omega_u} \right) [1 - e^{-\omega_u (t-t_1)}] \\
 &= VK_L + \frac{V}{\tau_r} \left(M - \frac{K_L}{\omega_u} \right) [1 - e^{-\omega_u t_1}] e^{-\omega_u (t-t_1)} \quad (3.60) \\
 &\quad t_1 \leq t \leq t_2
 \end{aligned}$$

Since we usually have $K_u \gg K_L$, this simplifies to

$$\begin{aligned}
 v(t) &= VK_L + \frac{VM}{\tau_r} [1 - e^{-\omega_u \tau_r}] e^{-\omega_u (t-\tau_r)} \\
 &\quad t_1 \leq t \leq t_2 \quad (3.61)
 \end{aligned}$$

The first term is the input signal over this interval multiplied by the common impedance coupling coefficient. The second term is the initial condition at $t = t_1 = \tau_r$ resulting from the second term of (3.58) multiplied by the decay term $e^{-\omega_u (t-\tau_r)}$:

$$\begin{aligned}
 v(t) &= K_L v_S(t) + v(t_1) e^{-\omega_u (t-\tau_r)} \quad (3.62) \\
 &\quad t_1 \leq t \leq t_2
 \end{aligned}$$

For $t_2 \leq t \leq t_3$ we obtain

$$\begin{aligned}
 v(t) &= VK_L + \frac{V}{\tau_r} \left(M - \frac{K_L}{\omega_u}\right) [1 - e^{-\omega_u t_1}] e^{-\omega_u(t-t_1)} \\
 &\quad - \frac{VK_L}{\tau_f} (t-t_2) \\
 &\quad - \frac{V}{\tau_f} \left(M - \frac{K_L}{\omega_u}\right) [1 - e^{-\omega_u(t-t_2)}] \\
 &\qquad\qquad\qquad t_2 \leq t \leq t_3 \\
 &= VK_L \left[1 - \frac{(t-t_2)}{\tau_f}\right] \\
 &\quad + \frac{V}{\tau_r} \left(M - \frac{K_L}{\omega_u}\right) [1 - e^{-\omega_u t_1}] e^{-\omega_u(t-t_1)} \\
 &\quad - \frac{V}{\tau_f} \left(M - \frac{K_L}{\omega_u}\right) [1 - e^{-\omega_u(t-t_2)}] \tag{3.63}
 \end{aligned}$$

The first term is simply the input signal over this interval multiplied by the common impedance coupling coefficient. The second and third terms can be written as

$$\begin{aligned}
 v(t) &= VK_L \left[1 - \frac{(t-t_2)}{\tau_f}\right] \\
 &\quad + \left\{ \frac{V}{\tau_r} \left(M - \frac{K_L}{\omega_u}\right) [1 - e^{-\omega_u t_1}] e^{-\omega_u(t_2-t_1)} \right\} e^{-\omega_u(t-t_2)} \\
 &\quad - \left\{ \frac{V}{\tau_f} \left(M - \frac{K_L}{\omega_u}\right) [1 - e^{-\omega_u(t-t_2)}] \right\} \tag{3.64}
 \end{aligned}$$

The second term is the initial condition at $t = t_2$ caused by the solution of the previous interval multiplied by the decay term $e^{-\omega_u(t-t_2)}$. The third term is similar to terms in other intervals. Once again, since $K_u \gg K_L$,

this can be simplified to

$$\begin{aligned}
 v(t) = & K_L v_S(t) + v(t_2) e^{-\omega_u(t-t_2)} \\
 & - \frac{VM}{\tau_f} [1 - e^{-\omega_u(t-t_2)}] \\
 & t_2 \leq t \leq t_3
 \end{aligned} \tag{3.65}$$

For $t_3 \leq t \leq T$ the result is

$$\begin{aligned}
 v(t) = & \frac{V}{\tau_r} (M - \frac{K_L}{\omega_u}) [1 - e^{-\omega_u \tau_r}] e^{-\omega_u(t-t_1)} \\
 & - \frac{V}{\tau_f} (M - \frac{K_L}{\omega_u}) [1 - e^{-\omega_u \tau_f}] e^{-\omega_u(t-t_3)} \\
 & t_3 \leq t \leq T
 \end{aligned} \tag{3.66}$$

The first term is part of the result due to the initial condition established on the previous interval as is the third term which decays by $e^{-\omega_u(t-t_3)}$.

Since $K_u \gg K_L$ we may again replace $(M - K_L/\omega_u)$ with M . Note that the usual term involving the product of K_L and $v_S(t)$ over this time interval is absent since $v_S(t) = 0$ over this time interval.

In summary, the response consists of three contributions:

$$v(t) = K_L v_S(t) + M f_1(t) + M f_2(t) \tag{3.67a}$$

The function $f_1(t)$ is the response of a first-order circuit with time constant $1/\omega_u$ to a square pulse of height v/τ_r occurring over $0 \leq t \leq t_1$. The function $f_2(t)$ is the response of a first-order circuit with time constant $1/\omega_u$ to a square pulse of height $-V/\tau_f$ occurring over $t_3 \leq t \leq t_2$. Thus

$$f_1(t) = \begin{cases} \frac{V}{\tau_r} (1 - e^{-\omega_u t}) & 0 \leq t \leq t_1 \\ \frac{V}{\tau_r} (1 - e^{-\omega_u \tau_r}) e^{-\omega_u (t-t_1)} & t_1 \leq t \leq T \end{cases} \quad (3.67b)$$

$$f_2(t) = \begin{cases} 0 & t \leq t_2 \\ \frac{V}{\tau_f} (1 - e^{-\omega_u (t-t_2)}) & t_2 \leq t \leq t_3 \\ \frac{V}{\tau_f} (1 - e^{-\omega_u \tau_f}) e^{-\omega_u (t-t_3)} & t_3 \leq t \leq T \end{cases} \quad (3.67c)$$

Note that f_1 and f_2 are the appropriate slew rates of the signal transitions multiplied by appropriate charging and discharging exponentials. The process is shown in Fig. 3.10.

If we assume for illustration that $K_L v_S(t)$ is small enough to be neglected (as we will show is typically the case), a typical crosstalk waveform is given in Fig. 3.11. If we assume that the interval $(t_2 - t_1)$ is sufficiently long such that the first pulse has decayed to essentially zero at t_2 , the maximum crosstalk can be calculated as

$$v_{\max} = \text{MAX} \left\{ \frac{VM}{\tau_r} (1 - e^{-\omega_u \tau_r}), \frac{VM}{\tau_f} (1 - e^{-\omega_u \tau_f}) \right\} \quad (3.68a)$$

Note that the maximum crosstalk is bounded by the simple result obtained assuming the frequency response increased indefinitely with frequency:

$$v_{\max} = \text{MAX} \left\{ \frac{VM}{\tau_r}, \frac{VM}{\tau_f} \right\} \quad (3.68b)$$

If the pulse rise/fall time is much longer than the line one-way delay then the exponential term in (3.68a) is negligible since

$$\omega_u \tau_r = (2\pi \frac{L}{\lambda_u}) \tau_d \tau_r \quad (3.68c)$$

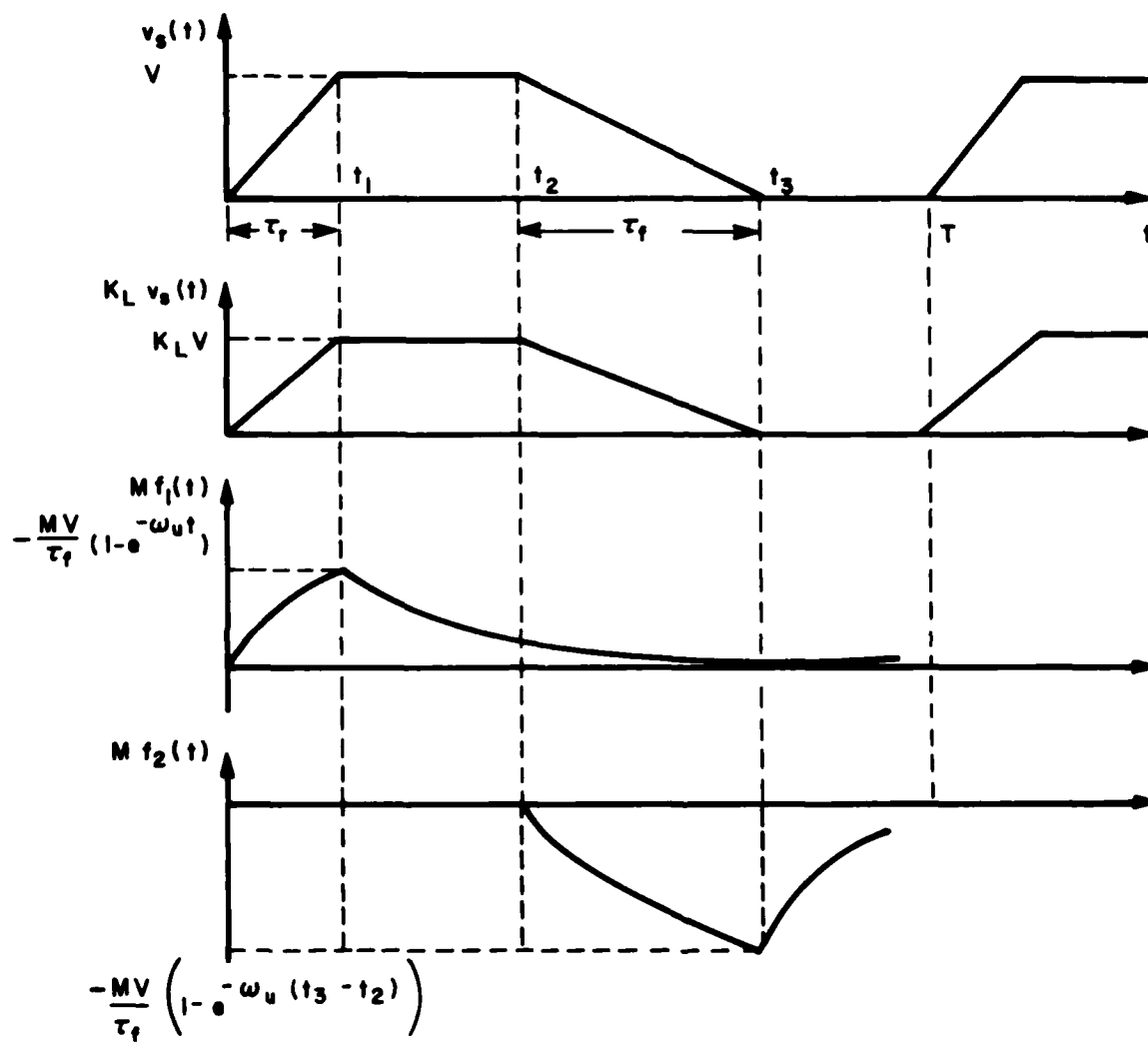


Fig. 3.10. The resulting contributions.

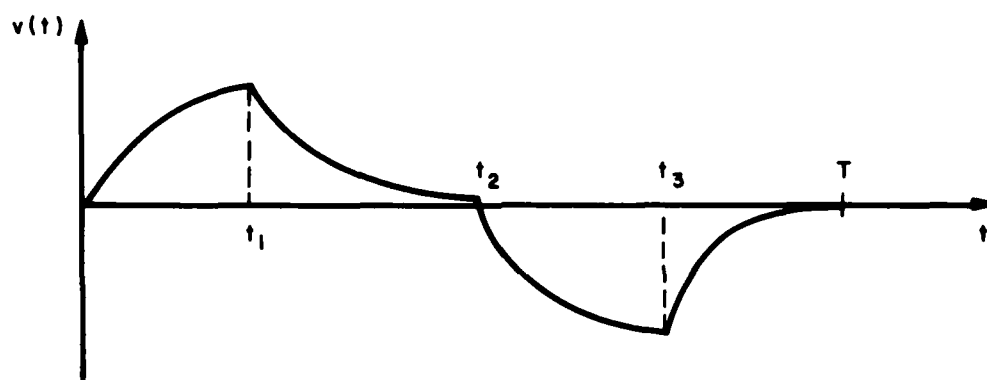


Fig. 3.11. The composite crosstalk pulse.

3.4. Implementation in CAD Codes

It should be emphasized that the intent in developing a model for use in CAD codes is to obtain one which (1) provides estimates of the time-domain crosstalk and (2) does not consume an excessive amount of computation time or array storage. The complexity of modern PCB's provides strong motivation for the latter criterion.

The simplest model would be the one addressed in section 3.2 in which we assumed $\omega_u \rightarrow \infty$; i.e., the frequency response of the transfer function increased linearly with frequency indefinitely. To implement this model we note that $j\omega$ in Fig. 3.3 may be replaced by $\frac{d}{dt}$ and the result in (3.23) will again be obtained. Thus equivalent sources may be inserted into all receptor circuits and the values of these equivalent sources depend only on land geometry (through ℓ_m and c_m) and the derivatives of the signals on the other lands. This is illustrated in Fig. 3.12. In this way, nonlinear load terminations may be handled since we only model the induced sources in the receptor line.

The degree to which this approximation is valid is usually difficult to determine. Nevertheless it represents a simple approach to estimating the solution to a difficult problem.

The question now arises as to whether it is worth implementing the improved model of section 3.3. In the author's opinion the answer is no. To do so would require multiplication of each term in each source by exponential decay terms. Each ω_u would depend on the generator circuit and would probably require more preliminary analysis than analysts would be willing to expend. In addition each ω_u depends, in addition to readily available parameters such as land geometry (through ℓ_m and c_m), on the loads of the

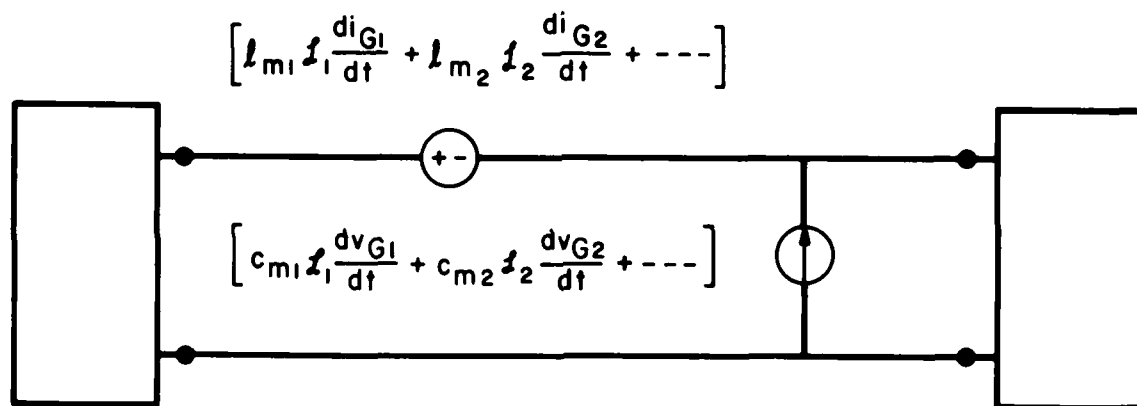


Fig. 3.12. A simplified equivalent circuit for CAD/CAM use.

receptor circuit. Thus one could not simply insert sources which depended only on land geometry.

Also it should be kept in mind that the simple model in Fig. 3.12 provides an upper bound on the crosstalk. Generally, one is interested in CAD codes in obtaining estimates of potential crosstalk problems. Culling the large number of those cases which will not provide crosstalk problems will be a significant contribution since the analyst can devote additional effort to determining whether those suspect cases in fact would provide problems.

When all of these factors are considered, it seems that the simple model in Fig. 3.12 provides the logical choice for CAD implementation.

3.5. A Further Improvement

The models of the previous sections represent approximations to the exact solution given in [19] and outlined in section 3.1. It is possible to find situations which do not satisfy the restrictions of those models even though the line is electrically short. For example, there exist cases which, even for resistive loads, the frequency response does not vary at 20 dB/decade in the region between f_L and f_u in Fig. 3.6 [20,21]. In order to handle these cases, we use the development given in [20].

The exact solution in [19] can be written as [20]

$$\frac{V_{NE}}{V_S} = \frac{j\omega(1 + j\omega T)}{1 + j\omega A + (j\omega)^2 B} M_{NE} \quad (3.69a)$$

$$\frac{V_{FE}}{V_S} = \frac{1}{\cos(2\pi l/\lambda)} \frac{j\omega}{1 + j\omega A + (j\omega)^2 B} M_{FE} \quad (3.69b)$$

where

$$\Theta = \frac{v}{\mathcal{L}} \tan (2\pi \mathcal{L}/\lambda) \quad (3.70)$$

and M_{NE} and M_{FE} are given, as before, by (3.24). The other terms in (3.69) are

$$T = \frac{\mathcal{L}}{v} \frac{1}{\sqrt{1-k^2}} \left[\frac{\alpha_{FG} + \alpha_{FR}}{1 + \alpha_{FG} \alpha_{FR}} \right] \quad (3.71a)$$

$$A = \tau_G + \tau_R \quad (3.71b)$$

$$B = \tau_G \tau_R (1-\psi) \quad (3.71c)$$

where τ_G and τ_R are given by (3.18) and

$$\psi = k^2 \frac{(1-\alpha_{NG} \alpha_{FR})(1-\alpha_{FG} \alpha_{NR})}{(1+\alpha_{NG} \alpha_{FR})(1+\alpha_{NR} \alpha_{FR})} \quad (3.72)$$

Suppose that we only consider frequencies of the excitation pulse, $v_S(t)$, such that the line is electrically short, $\mathcal{L} < \frac{1}{10} \lambda$. Then we may approximate Θ as

$$\Theta \approx 2\pi \frac{v}{\lambda}$$

$$= \omega$$

$$\text{and} \quad \cos(2\pi \mathcal{L}/\lambda) \approx 1. \quad (3.73)$$

Replacing $j\omega$ with the differential operator p we obtain the differential equations relating $v_{NE}(t)$ and $v_{FE}(t)$ to the input voltage $v_S(t)$ as

$$B \frac{d^2 v_{NE}(t)}{dt^2} + A \frac{dv_{NE}(t)}{dt} + v_{NE}(t) = M_{NE} \frac{dv_S(t)}{dt} + M_{NE} T \frac{d^2 v_S(t)}{dt^2} \quad (3.74a)$$

$$B \frac{d^2 v_{FE}(t)}{dt^2} + A \frac{dv_{FE}(t)}{dt} + v_{FE}(t) = M_{FE} \frac{dv_S(t)}{dt} \quad (3.74b)$$

These differential equations can be solved for $v_{NE}(t)$ and $v_{FE}(t)$ for $t > 0$ given the initial conditions at $t=0$:

$$\begin{aligned} v_{NE}(0), \left. \frac{dv_{NE}}{dt} \right|_{t=0} \\ v_{FE}(0), \left. \frac{dv_{FE}}{dt} \right|_{t=0} \end{aligned} \quad (3.75)$$

This form of solution can be used assuming that the initial conditions in (3.75) are all zero. Perhaps the assumption $v_{NE}(0) = v_{FE}(0) = 0$ is reasonable, but assuming the derivatives to be zero at $t=0$ is not an obviously valid result.

Nevertheless, if we assume all initial conditions are zero and write the equations in terms of their Laplace transforms, we obtain

$$V_{NE}(s) = \frac{s(1 + Ts)}{(Bs^2 + As + 1)} M_{NE} V_S(s) \quad (3.76a)$$

$$V_{FE}(s) = \frac{s}{(Bs^2 + As + 1)} M_{FE} V_S(s) \quad (3.76b)$$

If the two lines are weakly coupled, $\psi \ll 1$, then

$$1 + sA + s^2 B = (1 + s\tau_G)(1 + s\tau_R) \quad (3.77)$$

Thus the denominators of (3.76) factor into a product of two factors each of which involve the time constant of one circuit. Suppose we assume that

$v_S(t)$ is the step function

$$v_S(t) = V u(t) \quad (3.78)$$

The Laplace transform of this is

$$V_S(s) = \frac{V}{s} \quad (3.79)$$

The transfer functions in (3.76) become

$$V_{NE}(s) = \frac{(1 + Ts)}{(1 + s\tau_G)(1 + s\tau_R)} M_{NE} V \quad (3.80a)$$

$$V_{FE}(s) = \frac{1}{(1 + s\tau_G)(1 + s\tau_R)} M_{FE} V \quad (3.80b)$$

These can be factored as

$$\begin{aligned} V_{NE}(s) = & \frac{(\tau_G - T)}{\tau_G(\tau_G - \tau_R)} \frac{M_{NE} V}{(s + 1/\tau_G)} \\ & + \frac{(\tau_R - T)}{\tau_R(\tau_R - \tau_G)} \frac{M_{NE} V}{(s + 1/\tau_R)} \end{aligned} \quad (3.81a)$$

$$\begin{aligned} V_{FE}(s) = & \frac{1}{(\tau_G - \tau_R)} \frac{M_{FE} V}{(s + 1/\tau_G)} \\ & + \frac{1}{(\tau_R - \tau_G)} \frac{M_{FE} V}{(s + 1/\tau_R)} \end{aligned} \quad (3.81b)$$

The inverse Laplace transforms become

$$v_{NE}(t) = \left[\frac{(T - \tau_G)e^{-t/\tau_G}}{\tau_G} - \frac{(T - \tau_R)e^{-t/\tau_R}}{\tau_R} \right] \frac{M_{NE} V}{(\tau_R - \tau_G)} \quad (3.82a)$$

$$v_{FE}(t) = \left[-e^{-t/\tau_G} + e^{-t/\tau_R} \right] \frac{M_{FE} V}{(\tau_R - \tau_G)} \quad (3.82b)$$

The solution is therefore the familiar double exponential pulse similar to the overdamped solution of a second order circuit.

For practical, trapezoidal pulses typical of clock pulses, the solution is more complicated than for methods of the previous sections. Thus this additional refinement is not suitable for CAD implementation unless (1) a suitable analog circuit can be derived and (2) the initial conditions in (3.75) are known and translated to appropriate initial conditions on this analog circuit.

IV. Experimental Results

Experimental results were obtained to illustrate the prediction accuracies as well as the restrictions of the simple models developed in the previous chapter. Two types of lines were tested--a typical PCB and a ribbon cable. Although the primary intent of this report is to address crosstalk on PCB's, it is worthwhile to show that these models can predict time-domain crosstalk in fairly long cables so long as the pulse rise/fall times are sufficiently long as discussed previously.

This chapter will be organized into a discussion of (1) the line characteristics, (2) the frequency response data, and (3) the time-domain response data. Model predictions for both frequency-domain and time-domain results will be shown using (1) the lumped-circuit iterative models and (2) the simple prediction model of the previous chapter.

The lines will be driven and terminated as in Fig. 3.1. The input signal $v_S(t)$ will be monitored and set at the desired level. Thus $R_S=0$. The other three terminal resistors will be chosen equal:

$$R_L = R_{NE} = R_{FE} = R$$

Two values of R will be used

$$R = 50\Omega, 1\text{ k}\Omega$$

These two values were chosen for the investigation in order to enhance either inductive or capacitive coupling. We will find that both the frequency-domain and the time-domain crosstalk properties depend quite strongly on whether inductive or capacitive coupling is dominant.

The measurement and excitation equipment are as follows. For the frequency-domain results, the sources were standard sinusoidal oscillators which covered the measurement range of 10 kHz to 500 MHz for the PCB and 100 Hz to 100 MHz for the ribbon cable. The measurement equipment for the frequency-domain results consisted of HP 3400A RMS voltmeters for use below 1 MHz and a HP 8405A vector voltmeter for use above 1 MHz.

For the time-domain measurements, the excitation source was a HP 8015A pulse generator. The crosstalk voltages were measured with a Tektronix 7834 oscilloscope. For the PCB, P6201 active FET probes were used. Several values of rise/fall time were used. For the PCB, a 1 MHz trapezoidal waveform which transitioned from -1.25 V to + 1.25 V was used. The rise/fall times of the pulses which were investigated were 10 ns, 50 ns and 100 ns. The board one-way delay was on the order of 1.3 ns. Thus we will investigate rise/fall times which approach the limit discussed in Chapter 2.

For the ribbon cable, a 20 kHz trapezoidal waveform typical of RS-232C applications was used. The pulse transitioned from -1.25 V to + 1.25 V and had rise/fall times of 6 μ s, 1 μ s, 700 ns, 400 ns, 100 ns, 60 ns and 20 ns. The line one-way delay was approximately 32 ns.

4.1. Printed Circuit Board

The printed circuit board consisted of glass-epoxy substrate 62 mils in thickness with a ground plane on one side and lands on the other. A photograph is shown in Fig. 4.1. All conductors are 1 ounce copper (1.4 mils thickness). The lands are 100 mils in width and separated by 100 mils. The land lengths are 20 cm ($\lambda = 20$ cm).

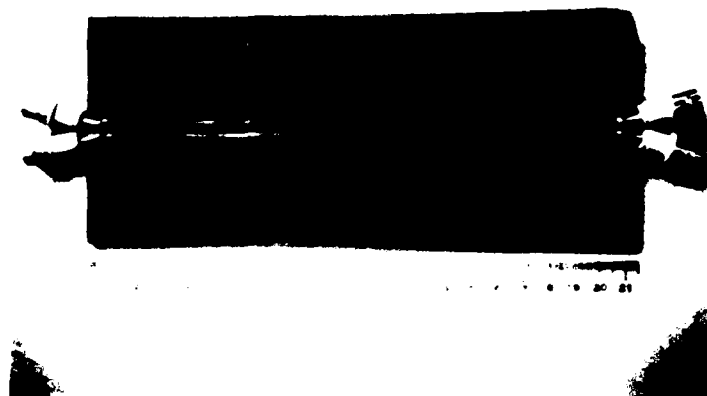


Fig. 4.1. The printed circuit board (PCB) used in the experiment.

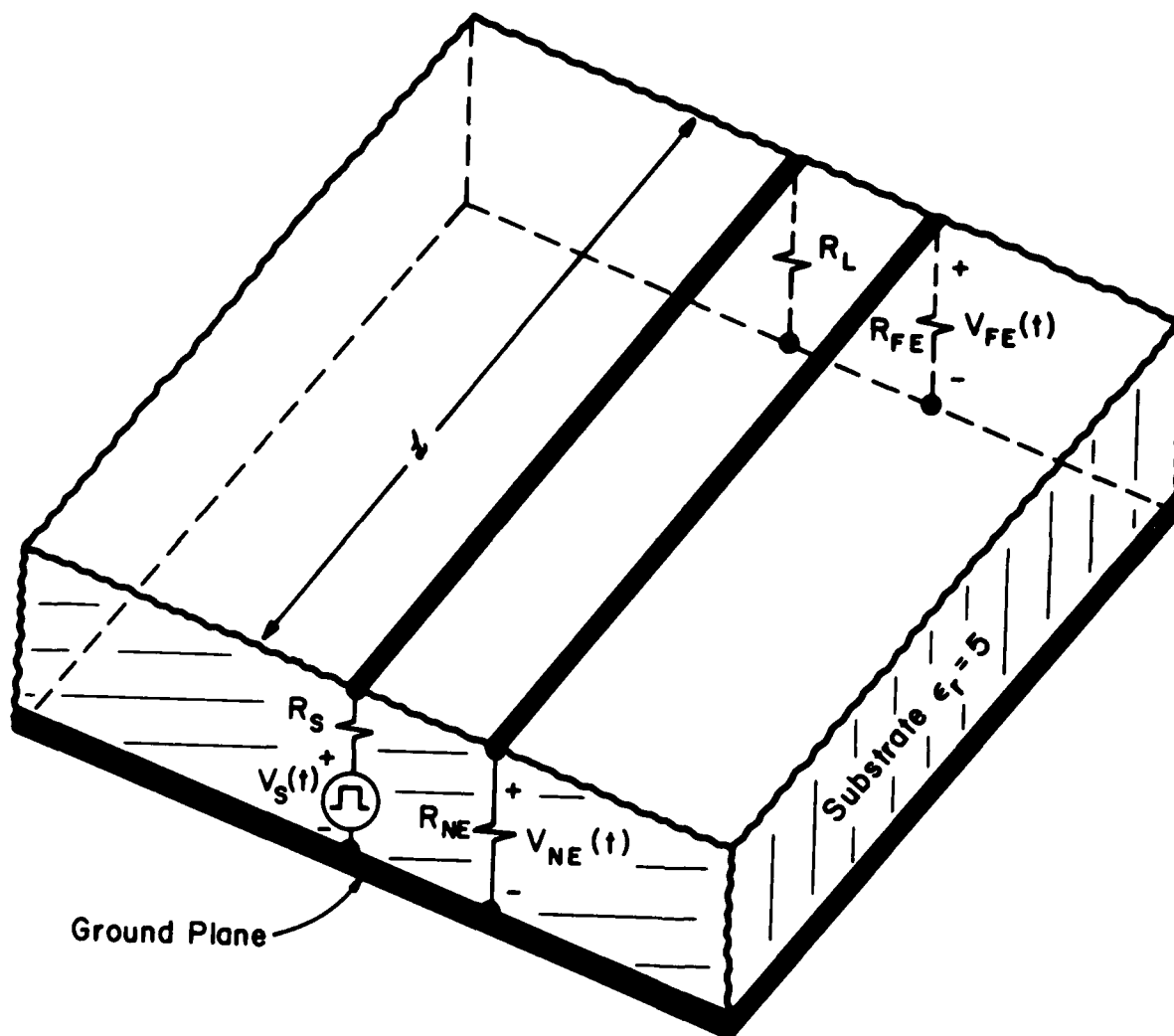


Fig. 4.2. A schematic of the PCB.

4.1.1. Frequency-Domain Results

The frequency-domain crosstalk was measured from 10 kHz to 500 MHz. The results are shown for near end crosstalk and $R=50\Omega$ in Fig. 4.3, for far end crosstalk and $R=50\Omega$ in Fig. 4.4, for near end crosstalk and $R=1\text{ k}\Omega$ in Fig. 4.5, and for far end crosstalk and $R=1\text{ k}\Omega$ in Fig. 4.6. The predictions of the multiconductor transmission line model are also shown [1,2].

From these results we obtain

Table 4.1

	R	K_L	M	ω_u
near end	50Ω	0	$1.06\text{E}-10$	$2\text{E}9$
	$1\text{ k}\Omega$	0	$6.37\text{E}-10$	$6.28\text{E}7$
far end	50Ω	0	$-4.46\text{E}-11$	$7\text{E}9$
	$1\text{ k}\Omega$	0	$6.37\text{E}-10$	$6.28\text{E}7$

The predictions of the lumped Pi and Tee models for 1 and 5 sections are shown in Fig. 4.7 through Fig. 4.14. These are compared against the predictions of the multiconductor transmission line model. Generally the lumped-circuit iterative models provide accurate predictions up to the point at which the line is $\frac{1}{10} \lambda$ (approximately 80 MHz). Note that increasing the number of lumped-circuit iterative model sections does not result in a dramatic increase in frequency coverage.

4.1.2. Time-Domain Results

A 1 MHz trapezoidal waveform which transitioned from -1.25 V to 1.25 V was applied. Three rise/fall times were investigated--100 ns, 50 ns, 10 ns. The board one-way delay was 1.3 ns. Thus the 10 ns rise/fall time represents

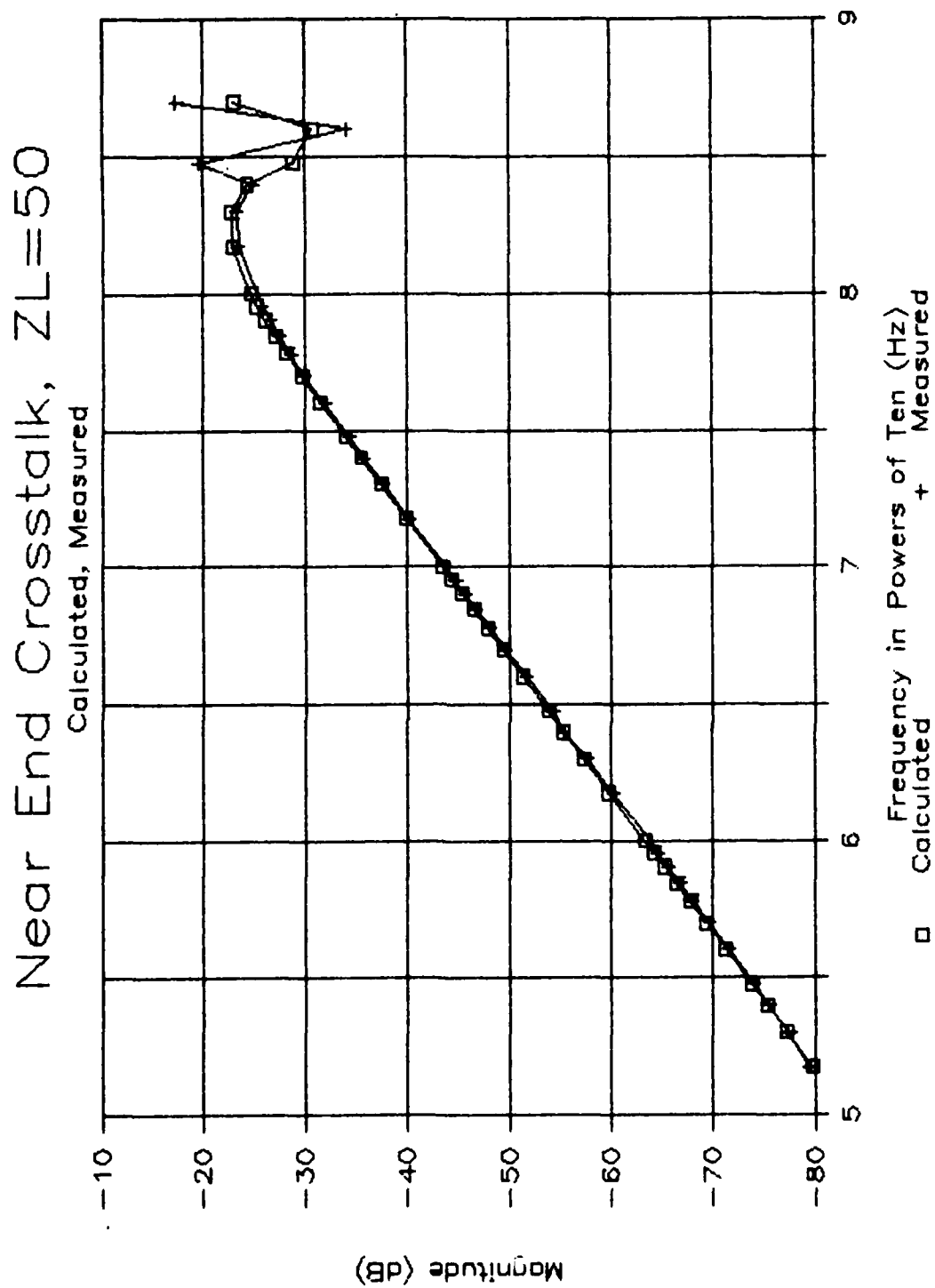


Fig. 4.3. Frequency response experimental data vs. predictions of the MTL model. Near End, 50 Ω .

Far End Crosstalk, ZL=50

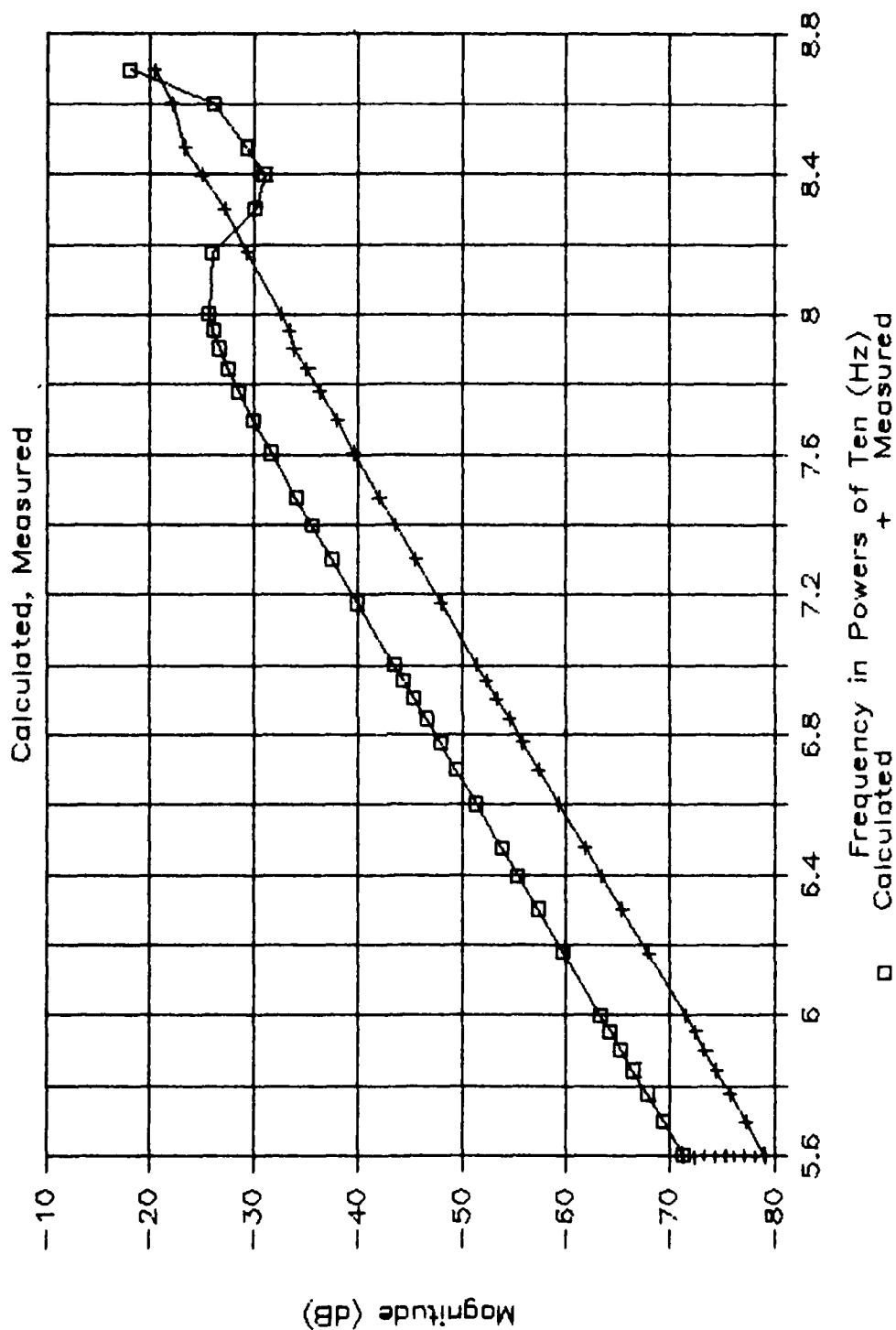


Fig. 4.4. Frequency response experimental data vs. predictions of the MTL model. Far end, 50 Ω .

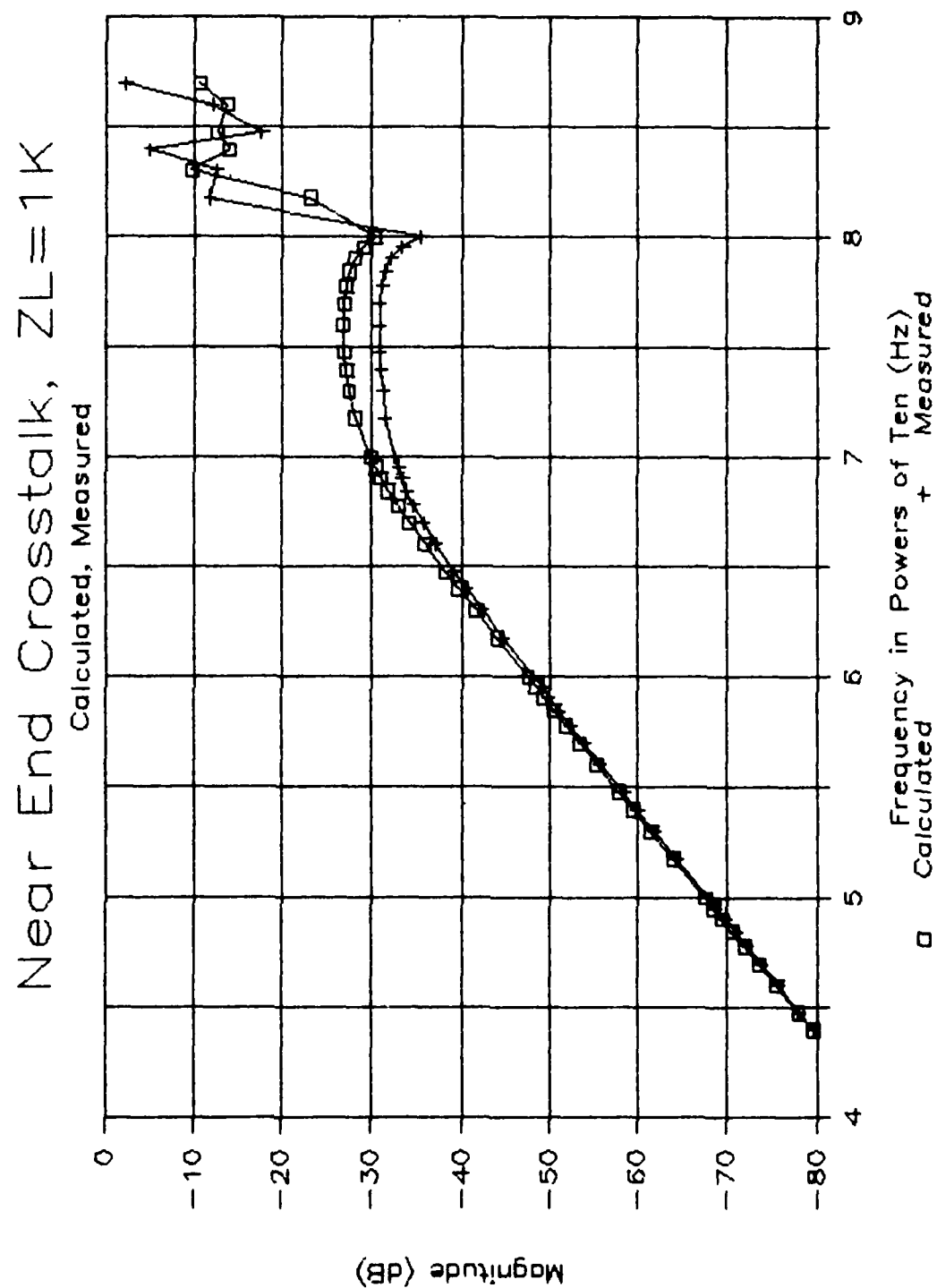


Fig. 4.5. Frequency response experimental data vs. predictions of the MTL model. Near End, 1 k Ω .

Far End Crosstalk, $Z_L=1K$

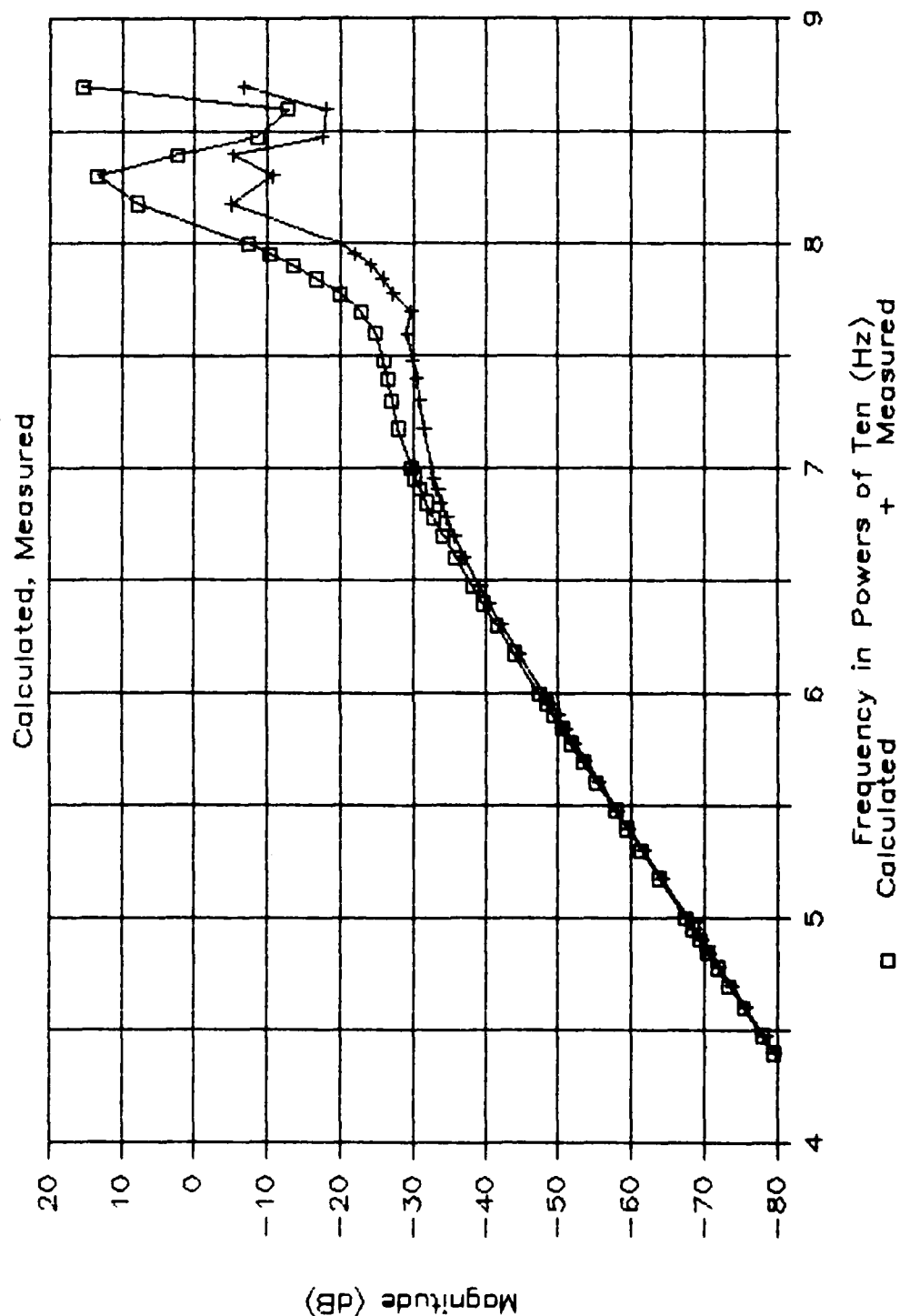


Fig. 4.6. Frequency response experimental data vs. predictions of the MTL model. Far End, 1 k Ω .

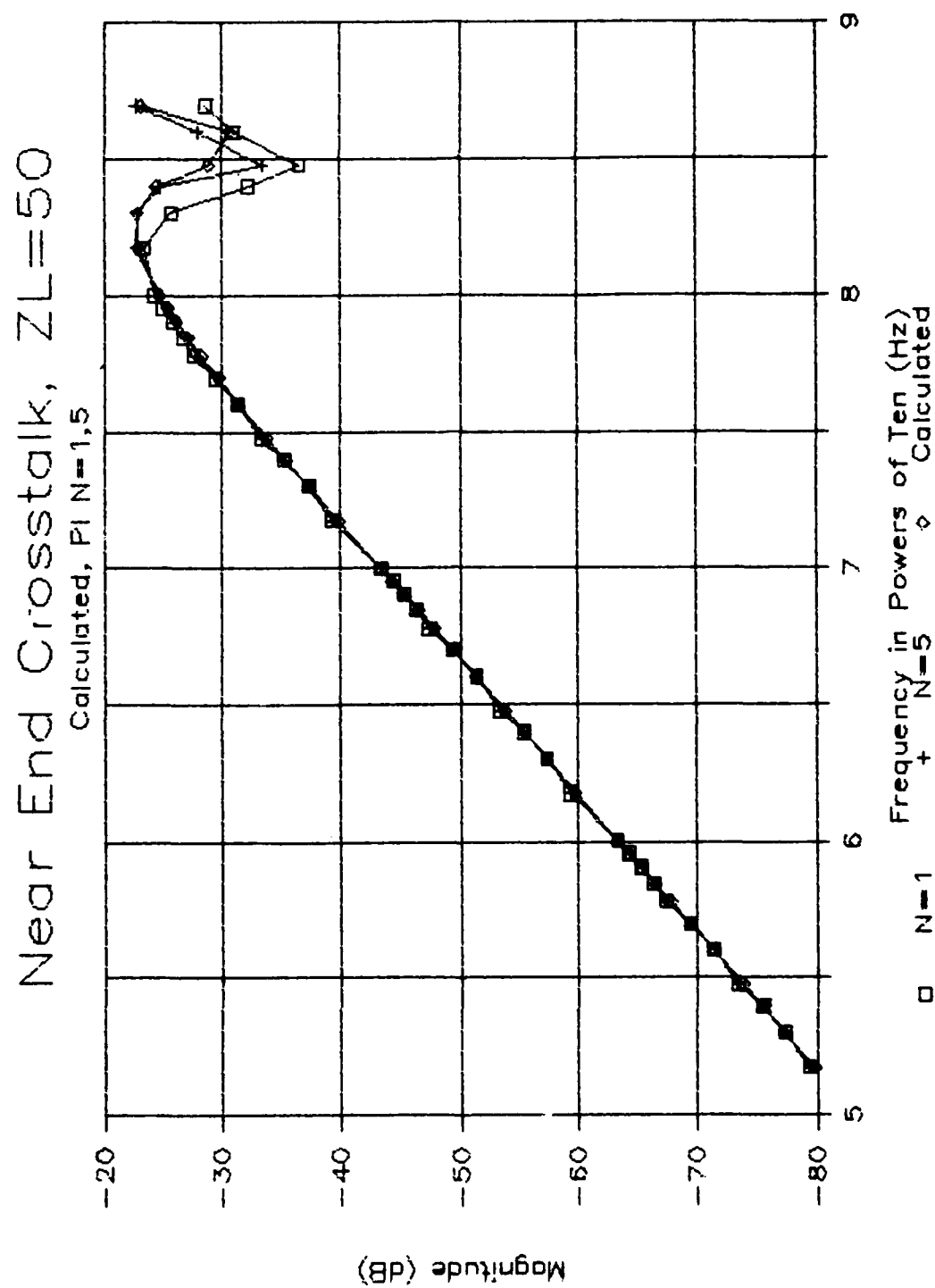


Fig. 4.7. Lumped iterative model vs. MTL model predictions.
Near End, P_i , 50Ω .

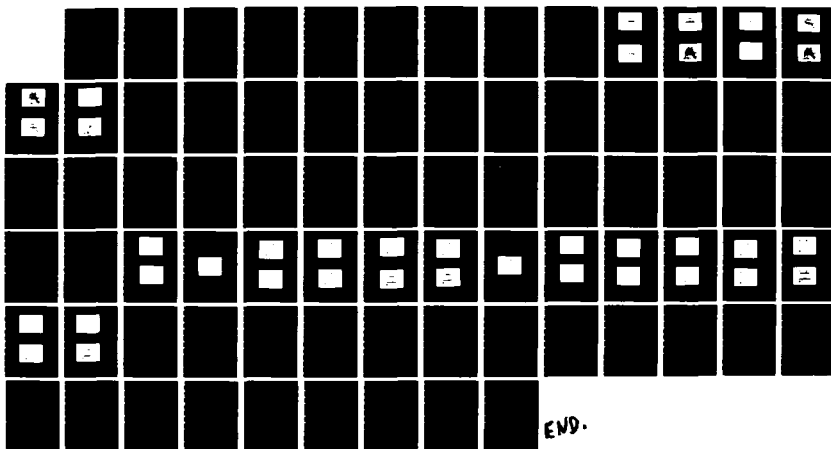
AD-A160 657

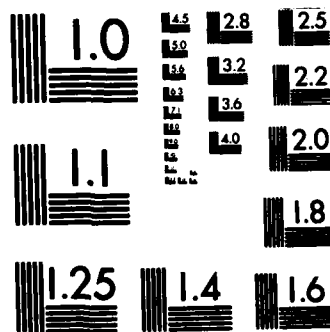
MODELING CROSSTALK ON PRINTED CIRCUIT BOARDS(U) GEORGIA 2/2
INST OF TECH ATLANTA C R PAUL ET AL JUL 85
RADC-TR-85-107 F30602-81-C-0185

UNCLASSIFIED

F/G 20/14

NL





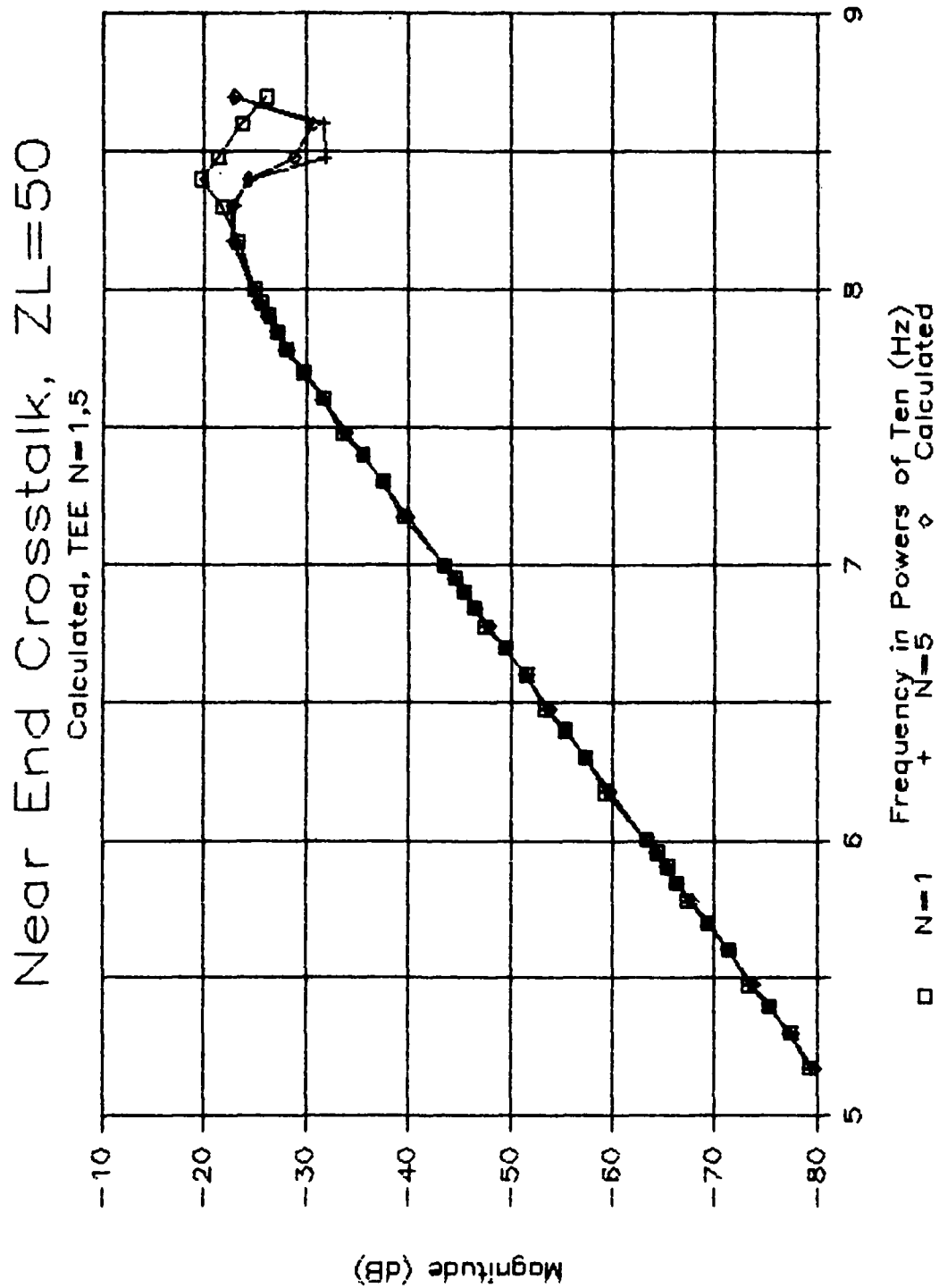


Fig. 4.8. Lumped iterative model vs. MTL model predictions.
Near End, Tee, 50 Ω .

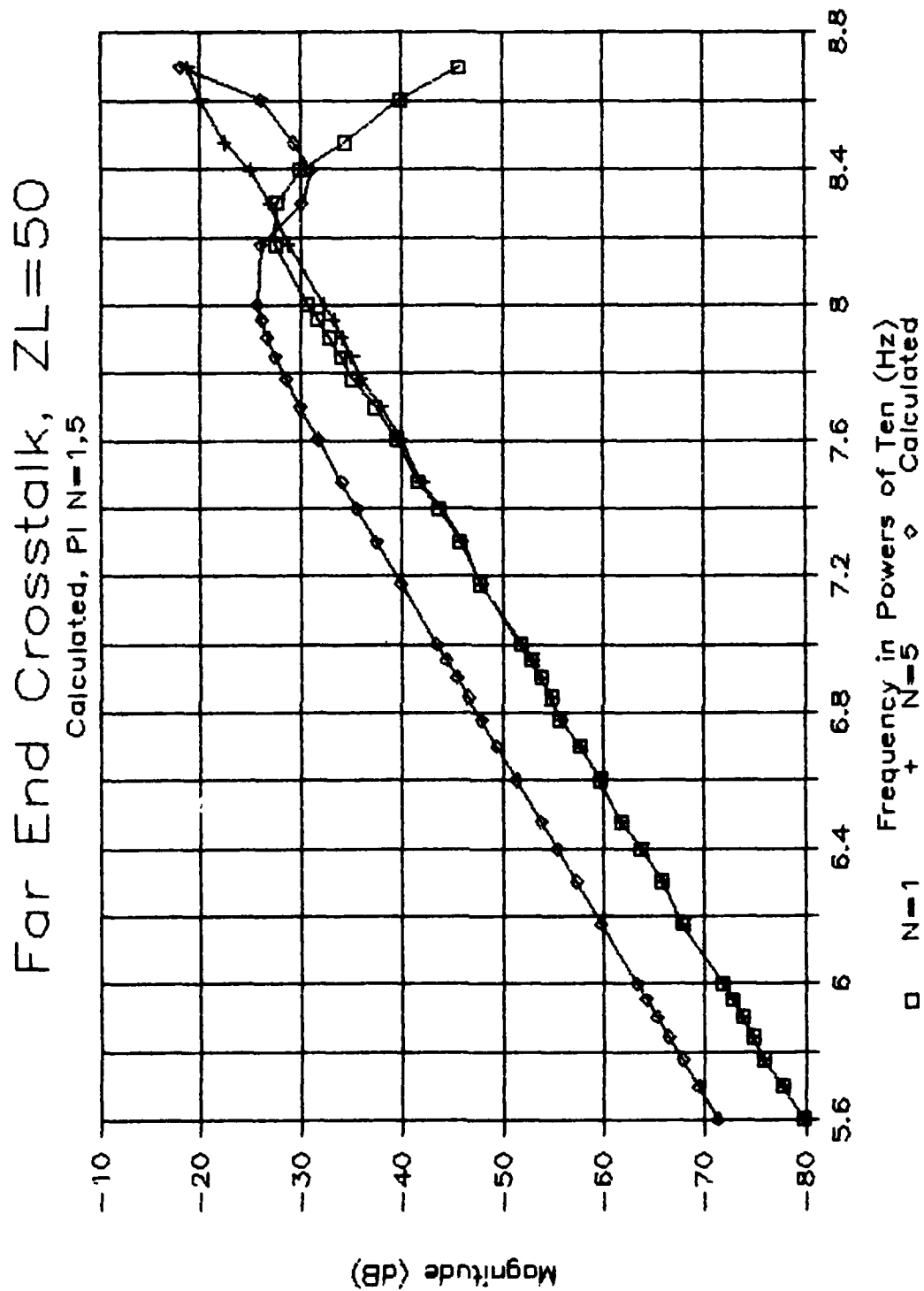


Fig. 4.9. Lumped iterative model vs. MTL model predictions.
Far End, P_i , 50Ω .

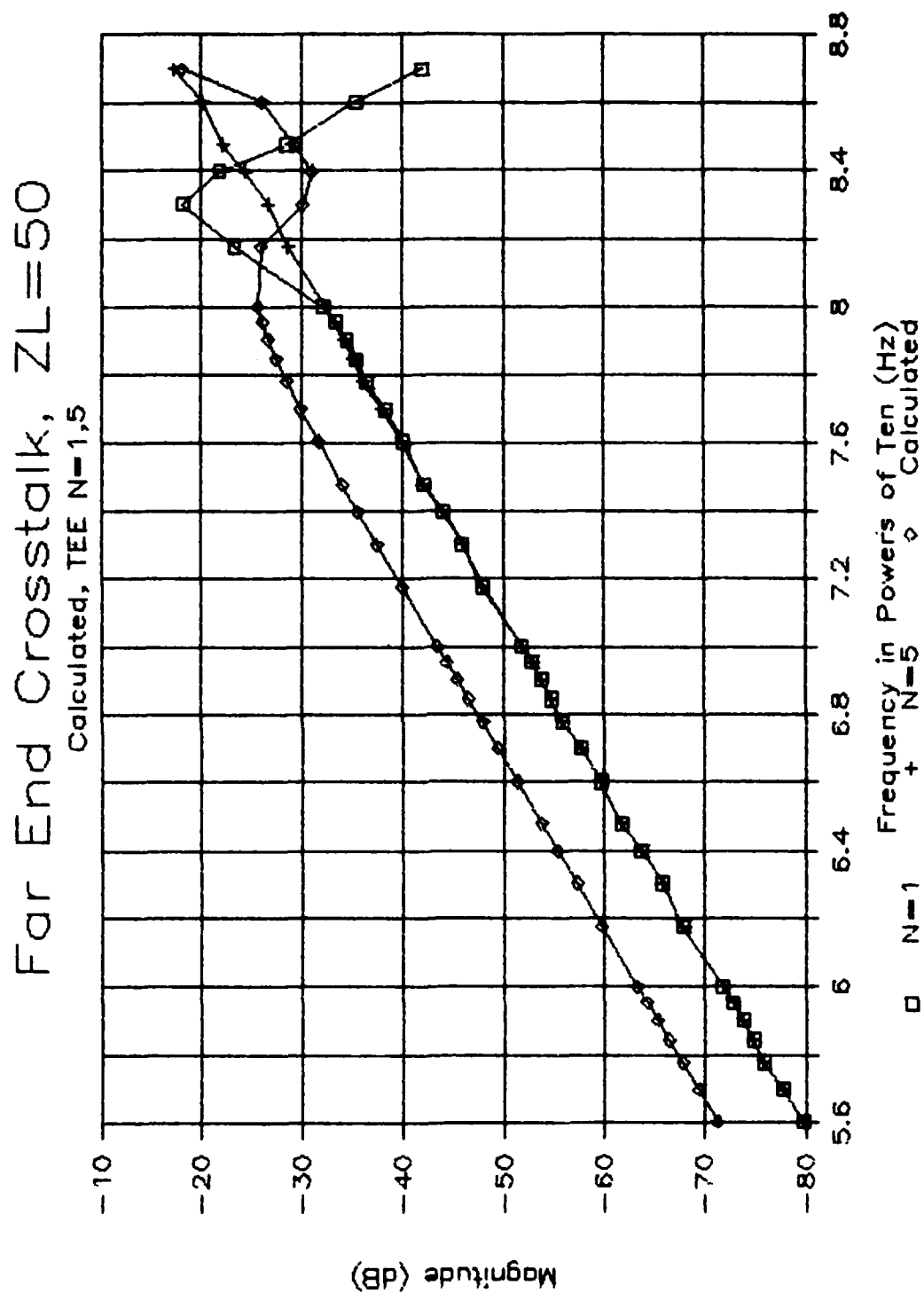


Fig. 4.10. Lumped iterative model vs. MTL model predictions.
Far End, Tee, 50Ω.

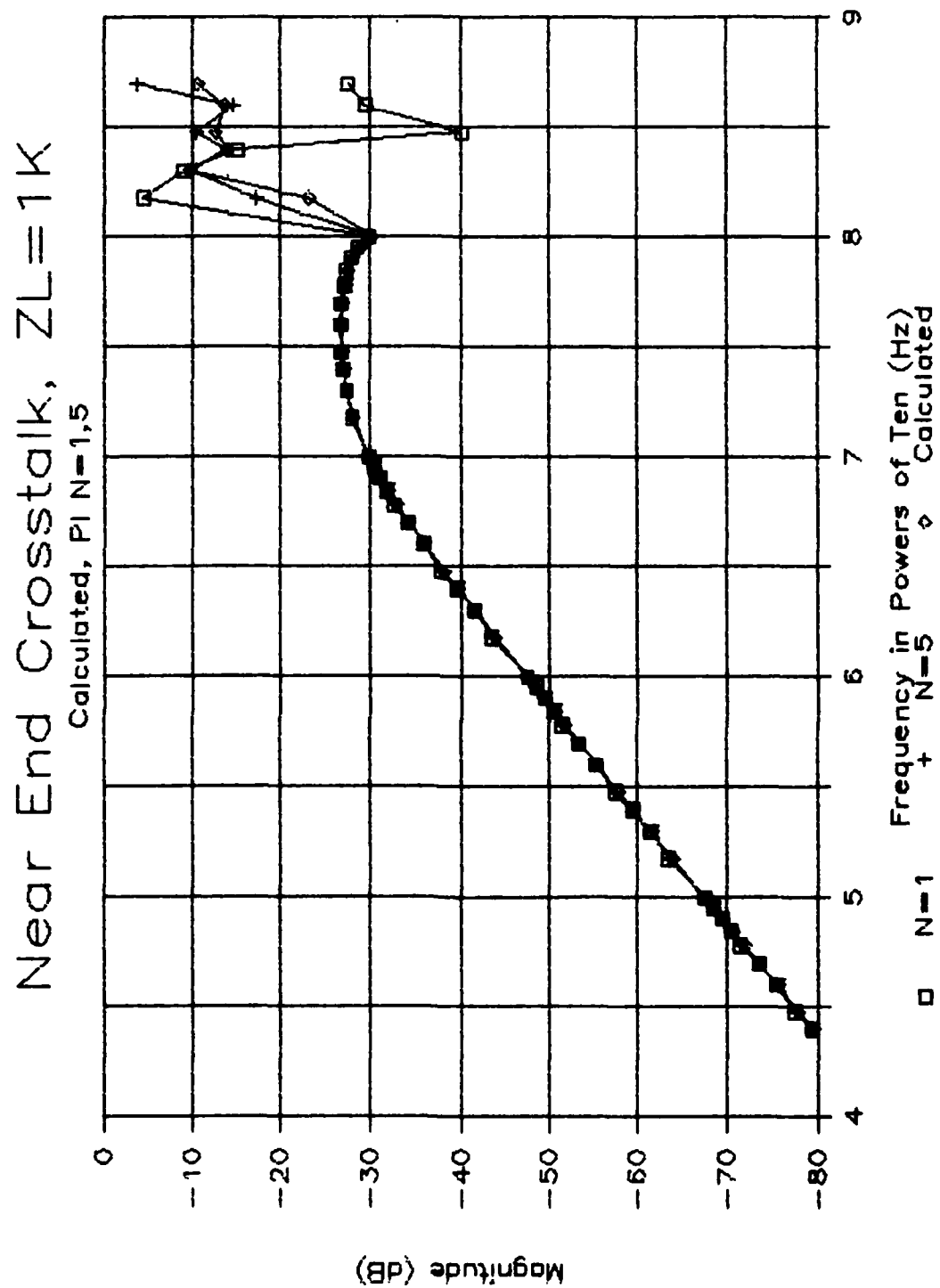


Fig. 4.11. Lumped iterative model vs. MTL model predictions.
Near End, P_i , 1 k Ω .

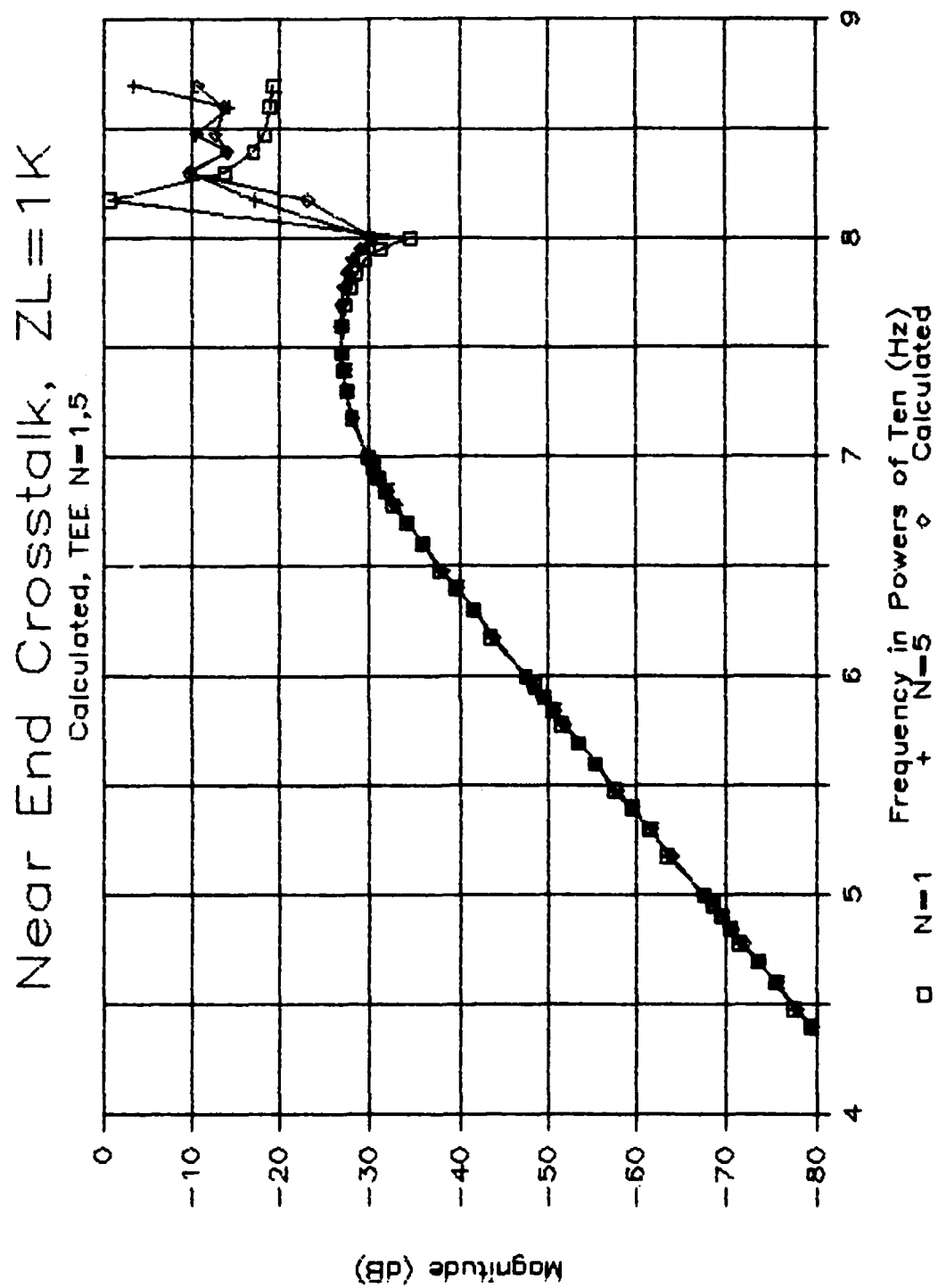


Fig. 4.12. Lumped iterative model vs. MTL model predictions.
Near End, Tee, 1 k Ω .

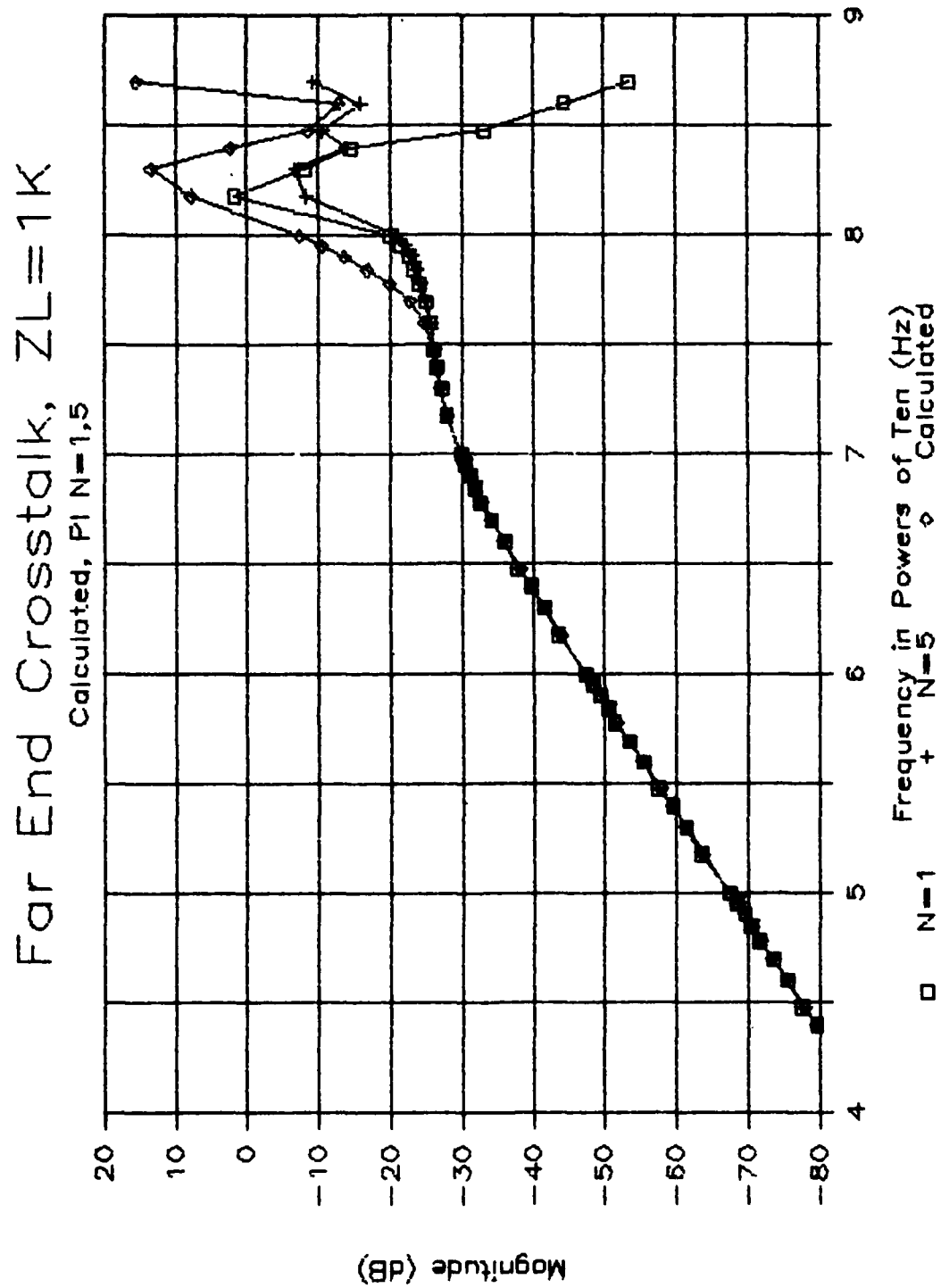


Fig. 4.13. Lumped iterative model vs. MTL model predictions.
Far End, P_i , 1 k Ω .

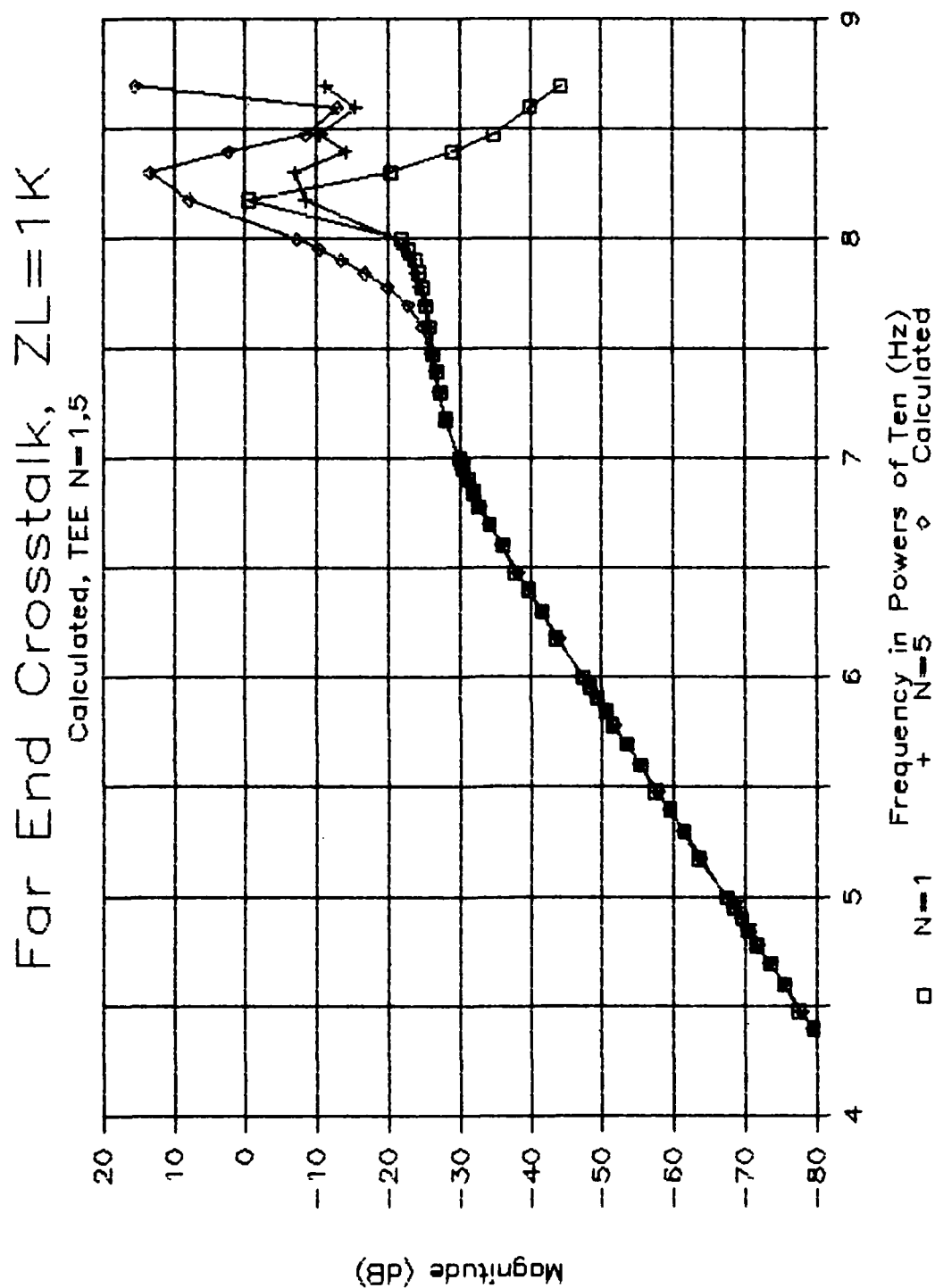


Fig. 4.14. Lumped iterative model vs. MTL model predictions.
Far End, Tee, 1 k Ω .

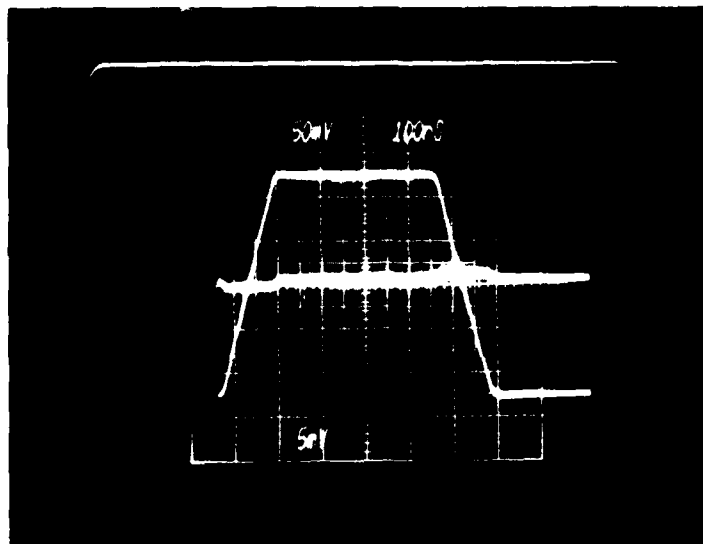
the approximate lower limit on applicability of the model.

The results will be shown with two photographs--one for the near end crosstalk and one for the far end crosstalk. The input voltage $v_S(t)$ will be shown on each photograph. The results for $R=50\Omega$ and $\tau_r=\tau_f=100$ ns, 50 ns and 10 ns are shown in Fig. 4.15, Fig. 4.16 and Fig. 4.17, respectively. The results for $R=1$ k Ω and $\tau_r=\tau_f=100$ ns, 50 ns and 10 ns are shown in Fig. 4.18, Fig. 4.19 and Fig. 4.20, respectively.

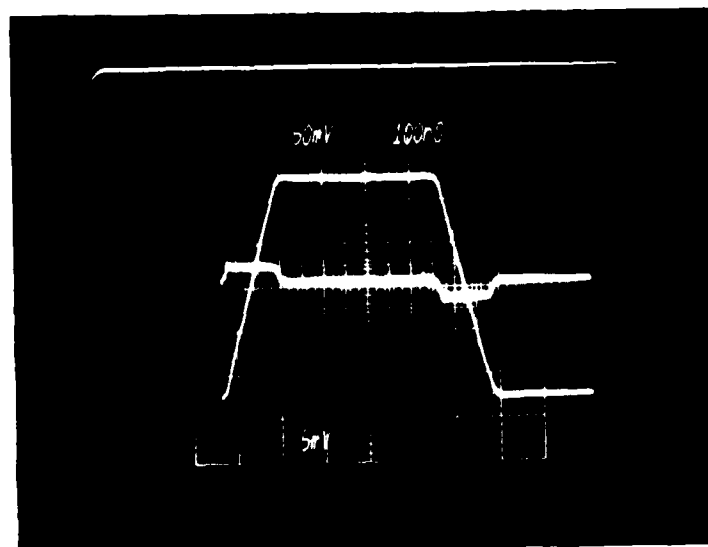
From the frequency-domain results for M and ω_u , we compute the maximum crosstalk using the model in section 3.3 as

Table 4.2
Maximum Crosstalk Levels
($R=50\Omega$)

		Predicted	Measured
$\tau_r=\tau_f=100$ ns	V_{NE}	2.12 mV	2.5 mV
	V_{FE}	- .9 mV	- 1 mV
$\tau_r=\tau_f=50$ ns	V_{NE}	4.24 mV	4.5 mV
	V_{FE}	-1.8 mV	- 2 mV
$\tau_r=\tau_f=10$ ns	V_{NE}	21.2 mV	21 mV
	V_{FE}	-8.9 mV	- 8 mV

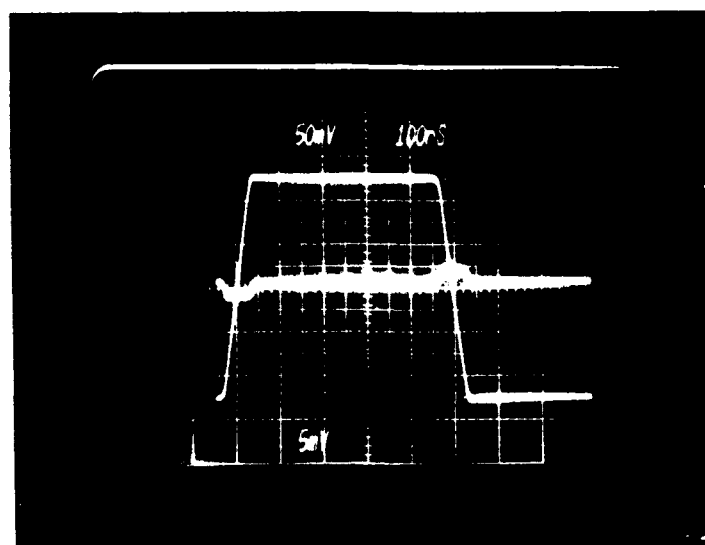


V_{FE}

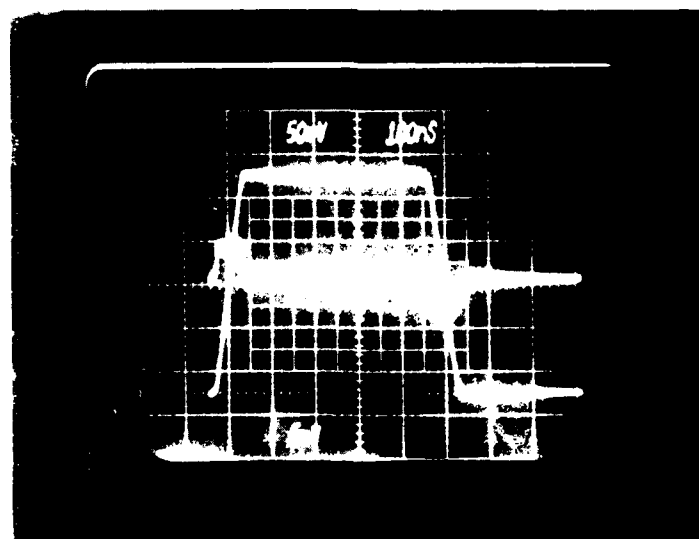


V_{NE}

Fig. 4.15. Experimental results 500, $\tau_r = \tau_f = 100$ ns
(top, near end, bottom, far end)

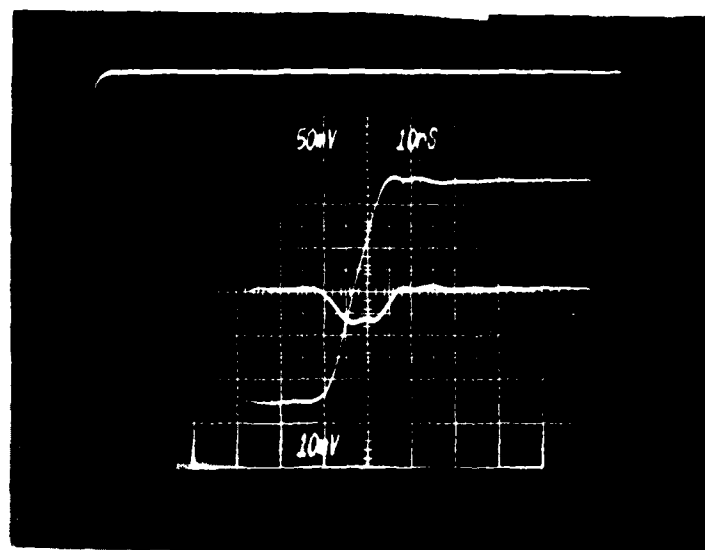


V_{FE}

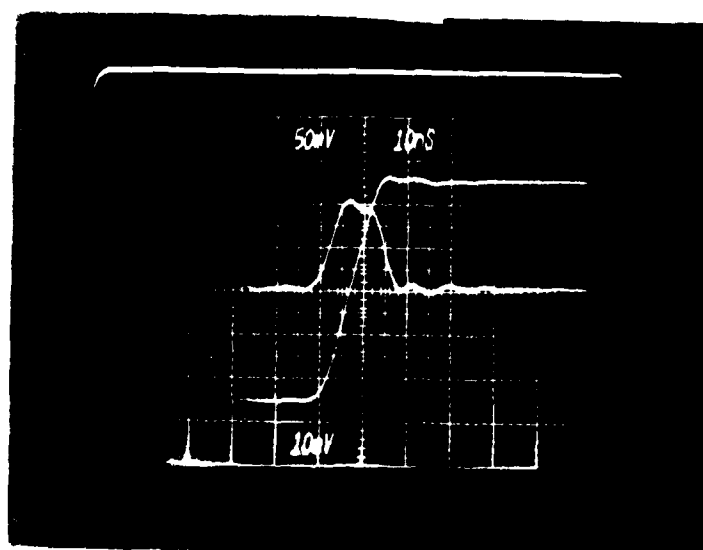


V_{NE}

Fig. 4.16. Experimental results 50Ω , $\tau_r = \tau_f = 50$ ns
(top, near end, bottom, far end)



V_{FE}



V_{NE}

Fig. 4.17. Experimental results 50Ω , $\tau_r = \tau_f = 10$ ns
(top, near end, bottom, far end)

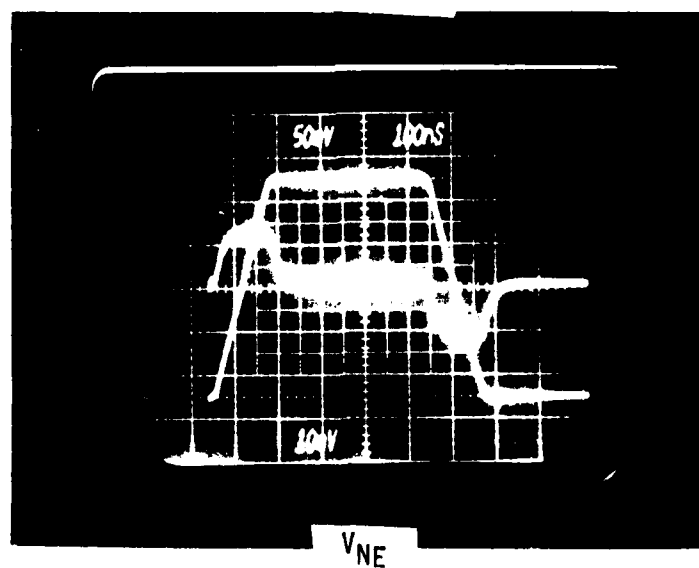
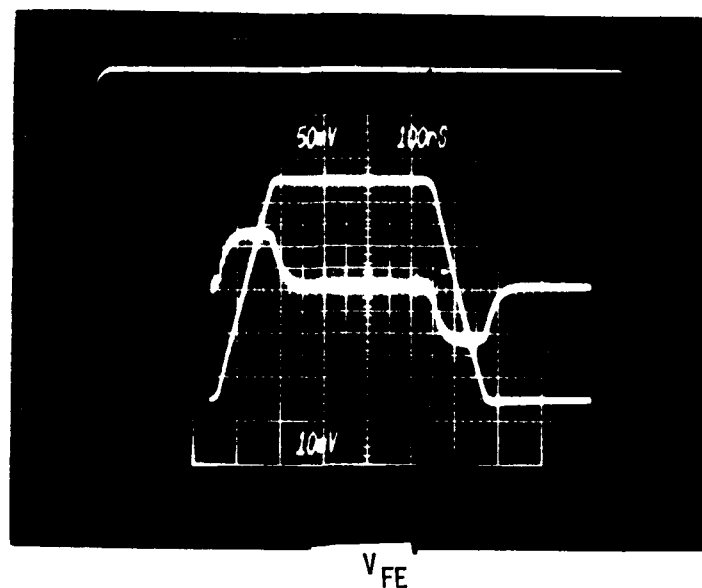
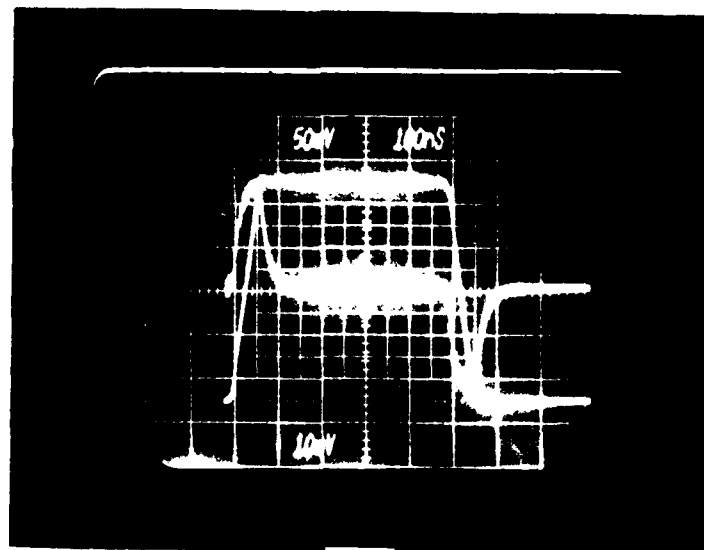
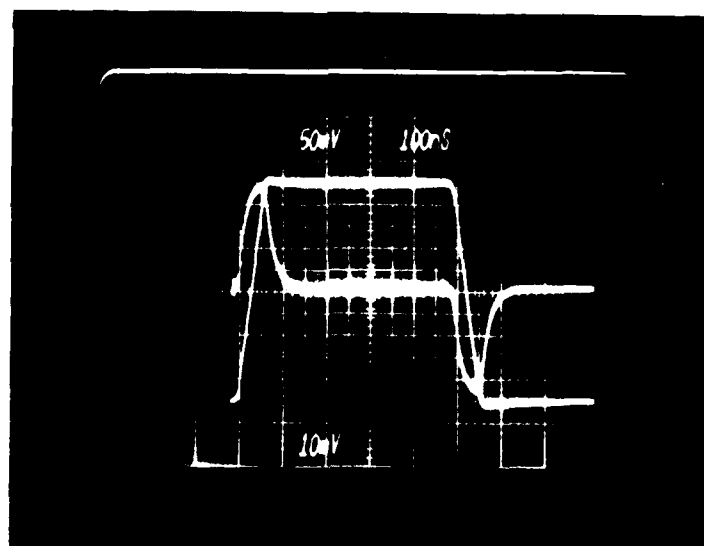


Fig. 4.18. Experimental results 1 k Ω , $\tau_r = \tau_f = 100$ ns
(top, near end, bottom, far end)

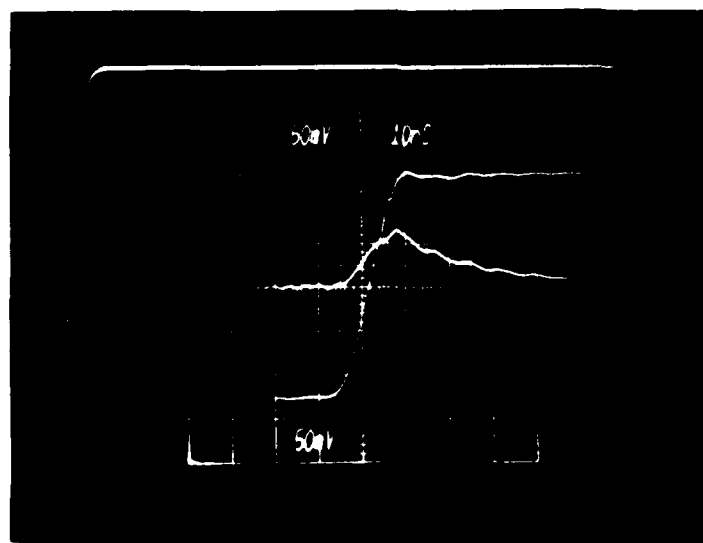


V_{FE}

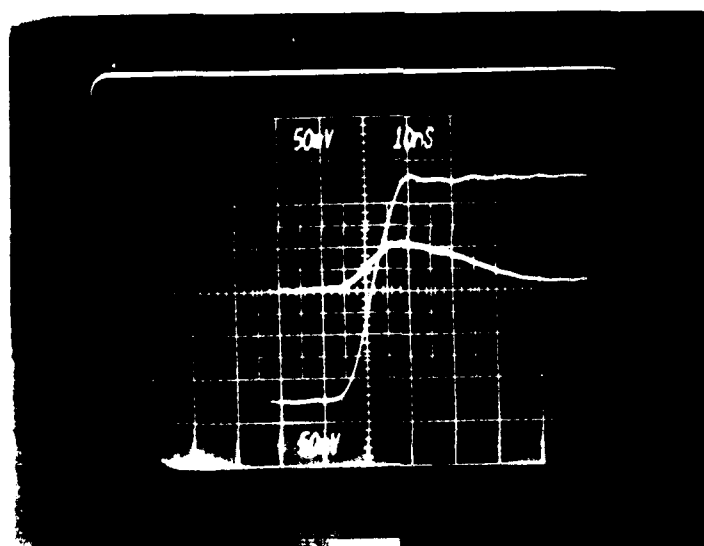


V_{NE}

Fig. 4.19. Experimental results $1\text{ k}\Omega$, $\tau_r = \tau_f = 50\text{ ns}$
(top, near end, bottom, far end)



V_{FE}



V_{NE}

Fig. 4.20. Experimental results $1\text{ k}\Omega$, $\tau_r = \tau_f = 10\text{ ns}$
(top, near end, bottom, far end)

Table 4.3

Maximum Crosstalk Levels

(R=1 k Ω)

		Predicted	Measured
$\tau_r = \tau_f = 100$ ns	V_{NE}	12.7 mV	14 mV
	V_{FE}	12.7 mV	14 mV
$\tau_r = \tau_f = 50$ ns	V_{NE}	24.4 mV	25 mV
	V_{FE}	24.4 mV	25 mV
$\tau_r = \tau_f = 10$ ns	V_{NE}	59.4 mV	55 mV
	V_{FE}	59.4 mV	65 mV

The predicted maximum levels are remarkably accurate. The exponential factor $(1 - e^{-v_u \tau_r})$ was of no consequence for R=50 Ω . The experimental results show this--the crosstalk pulses are virtually rectangular and show no significant rounding of the corners. Thus for R=50 Ω one can predict the crosstalk as simply the slope of the frequency response, M, multiplied by the slew rate of $v_s(t)$. However, this factor was important for all of the R=1 k Ω results. The experimental results show this in that all pulses show exponential rise and decay.

Note that all crosstalk pulses have the same polarity as the slope of the input signal except for R=50 Ω and far end crosstalk. It was pointed

out in Chapter 3 that this would be the case if inductive coupling dominated capacitive coupling so that M_{FE} is negative.

The predictions of the lumped-circuit iterative Pi and Tee models using 5 sections are shown in Fig. 4.21 through Fig. 4.32. The predictions of the simple model using the frequency-domain parameters of Table 4.1 and the circuit analogue in Fig. 3.7 are also shown on these figures. The simple model provides reasonable predictions and requires considerably less computational expense than the lumped iterative models.

4.2. Ribbon Cables

A three-wire ribbon cable was tested. All wires were #28 AWG (7x32) and the line length was 4.737 m (15'6½"). The dielectric insulation was polyvinyl chloride. The wires are separated (center-to-center) by 50 mils. The center wire was chosen as the reference conductor and the other wires were terminated as shown in Fig. 4.33. Once again $R_S=0$ and

$$R_L = R_{NE} = R_{FE} = R$$

with two values of R being used, $R=50\Omega$, $1\text{ k}\Omega$.

4.2.1. Frequency Domain Results

The frequency domain crosstalk was measured from 100 Hz to 100 MHz. The results are shown for near end crosstalk and $R=50\Omega$ in Fig. 4.34, for far end crosstalk and $R=50\Omega$ in Fig. 4.35, for near end crosstalk and $R=1\text{ k}\Omega$ in Fig. 4.36, and for far end crosstalk and $R=1\text{ k}\Omega$ in Fig. 4.37. The predictions of the multiconductor transmission line model are also shown [1,2,3].

Near End Crosstalk, $Z_L=50$, $t_r=100\text{ns}$
 Analog, PI & TEE $N=5$

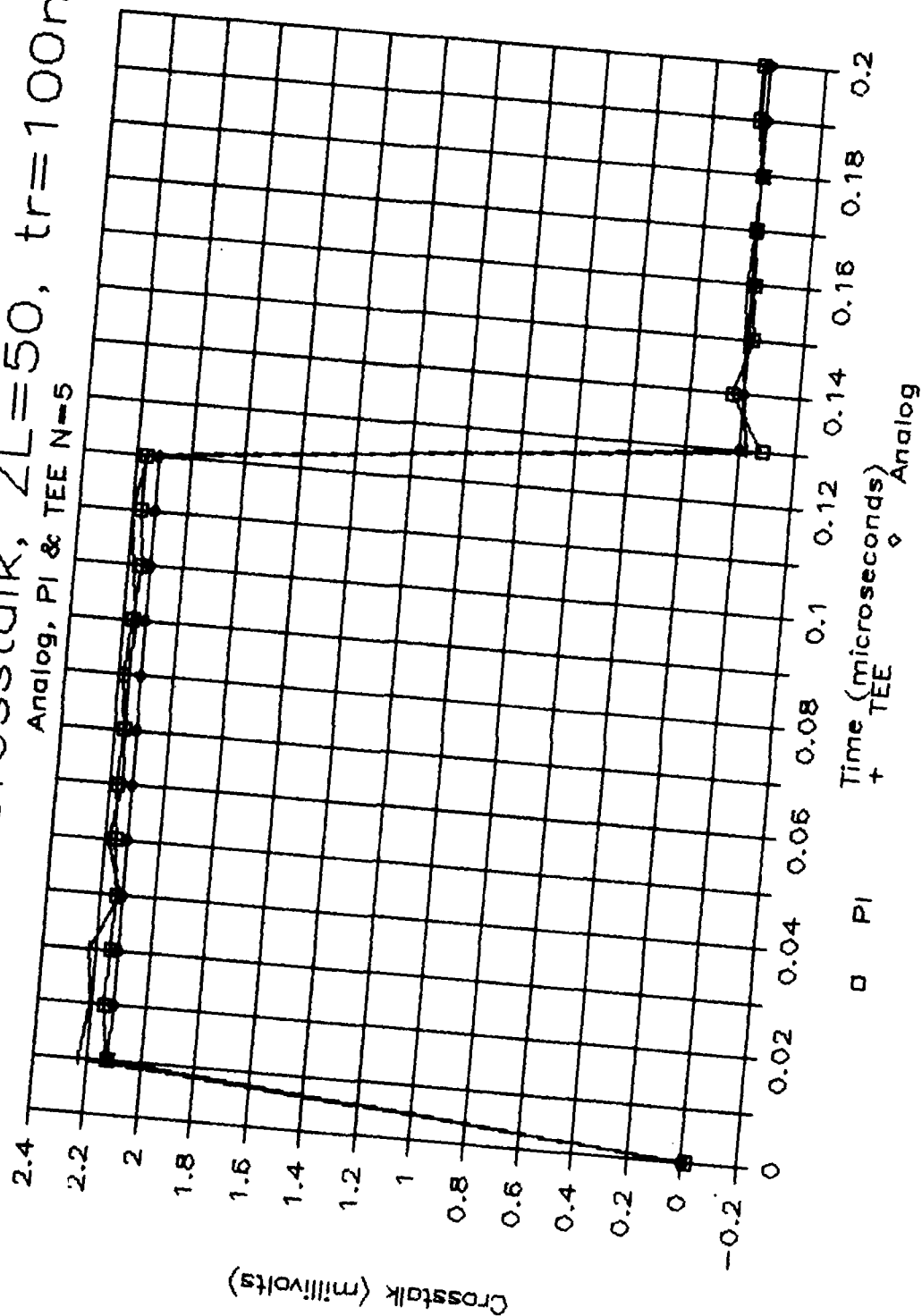


Fig. 4.21. Time-domain predictions
 50Ω, Near End, $\tau_r=\tau_f=100\text{ ns}$

Far End Crosstalk, $Z_L=50$, $t_r=100\text{ns}$
 Analog, PI & TEE $N=5$

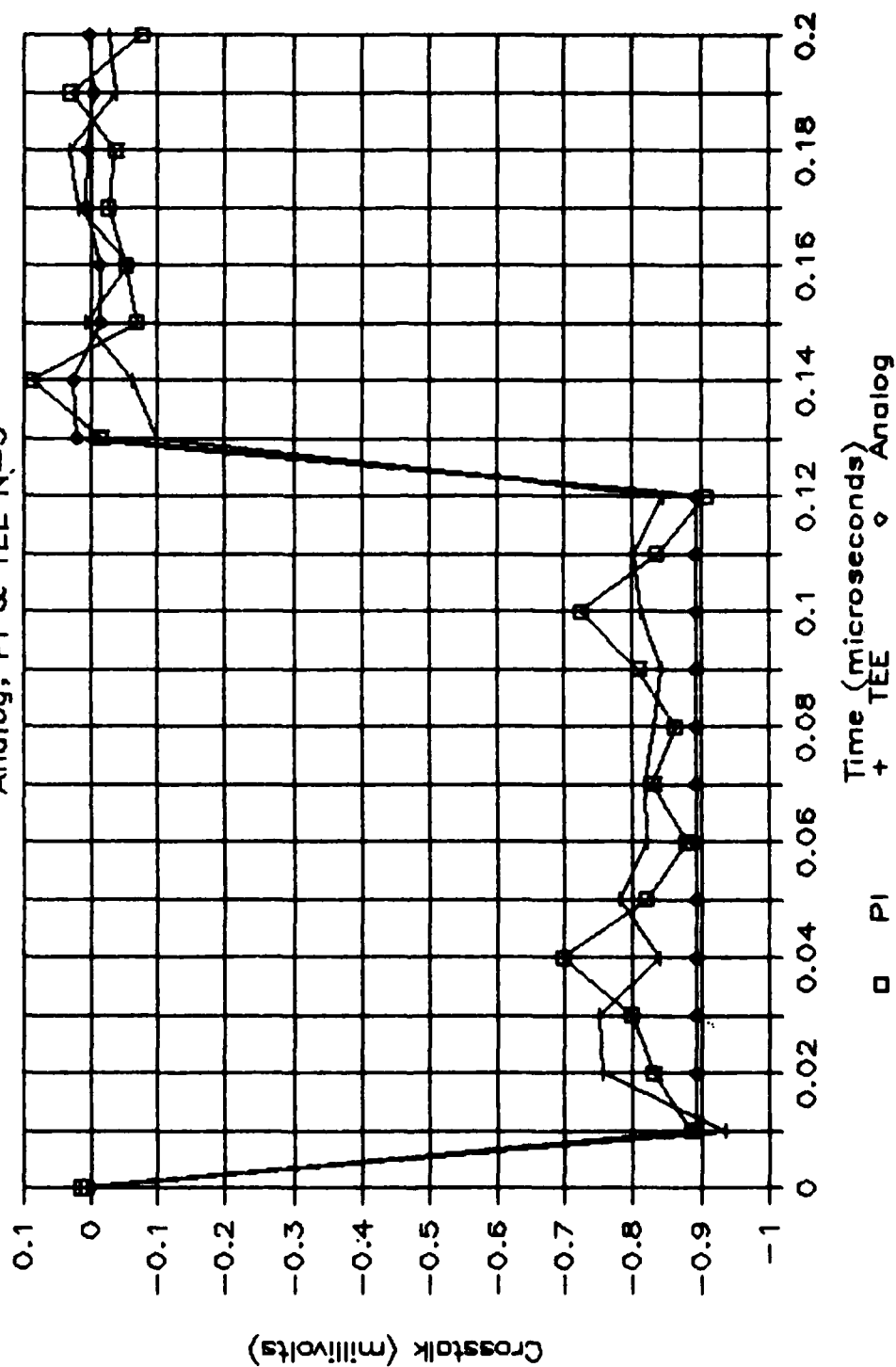


Fig. 4.22. Time-domain predictions
 50Ω , Far End, $\tau_r = \tau_f = 100\text{ ns}$

Near End Crosstalk, $Z_L=50$, $t_r=50\text{ns}$

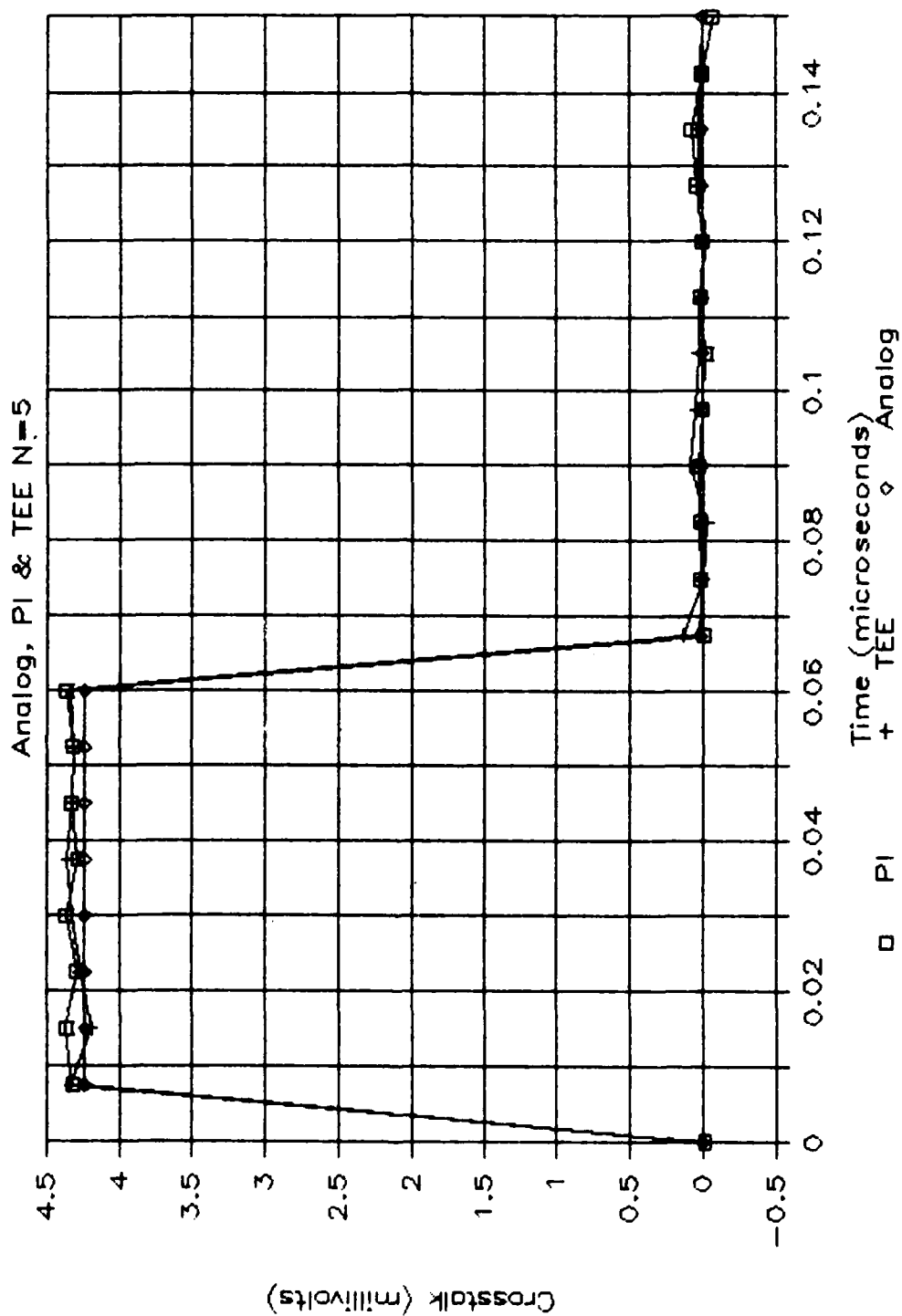


Fig. 4.23. Time-domain predictions
 50Ω , Near End, $\tau_r=\tau_f=50\text{ ns}$

Far End Crosstalk, $Z_L=50$, $\tau_r=50\text{ns}$
 Analog, PI & TEE $N=5$

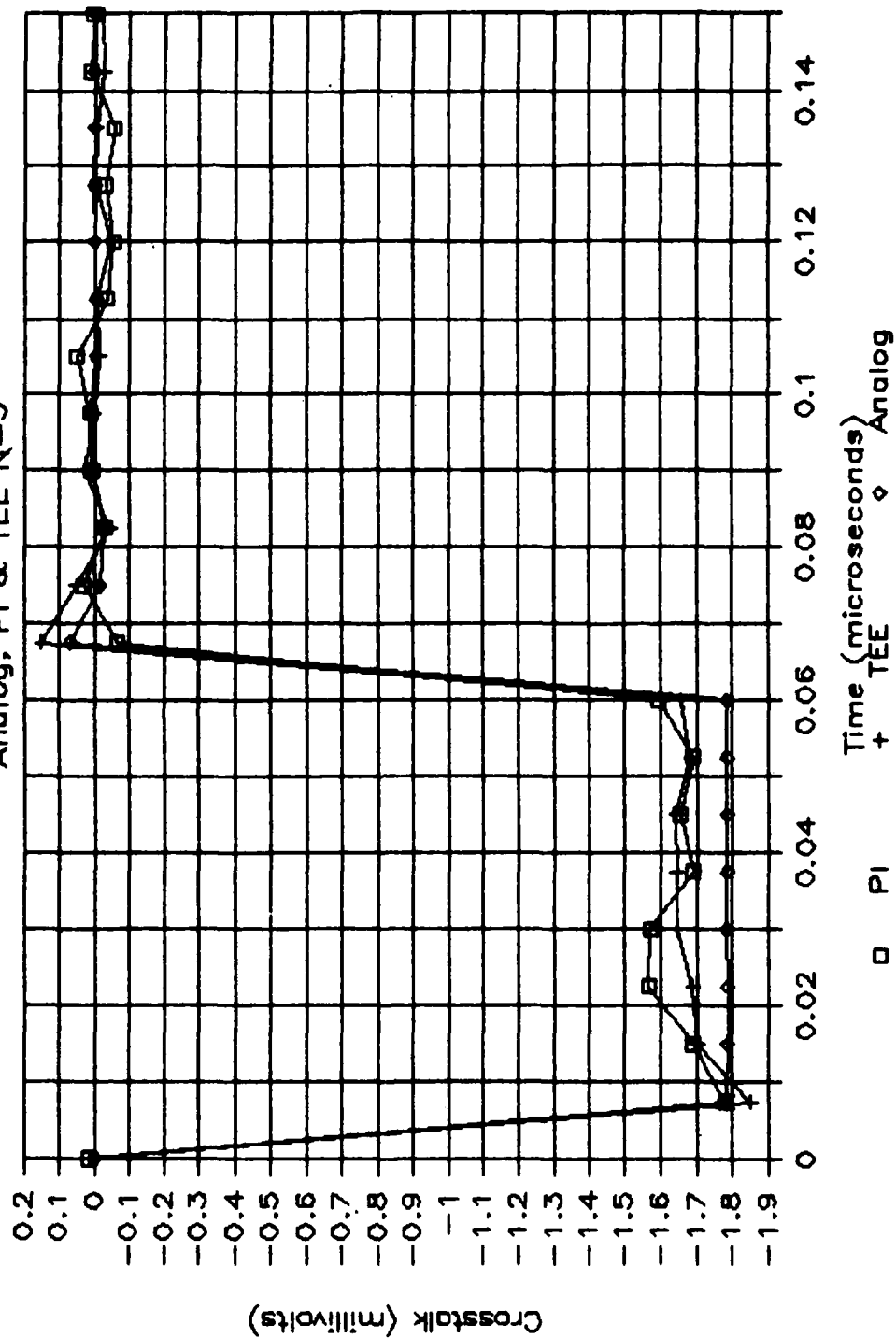


Fig. 4.24. Time-domain predictions
 50Ω , Far End, $\tau_r = \tau_f = 50\text{ ns}$

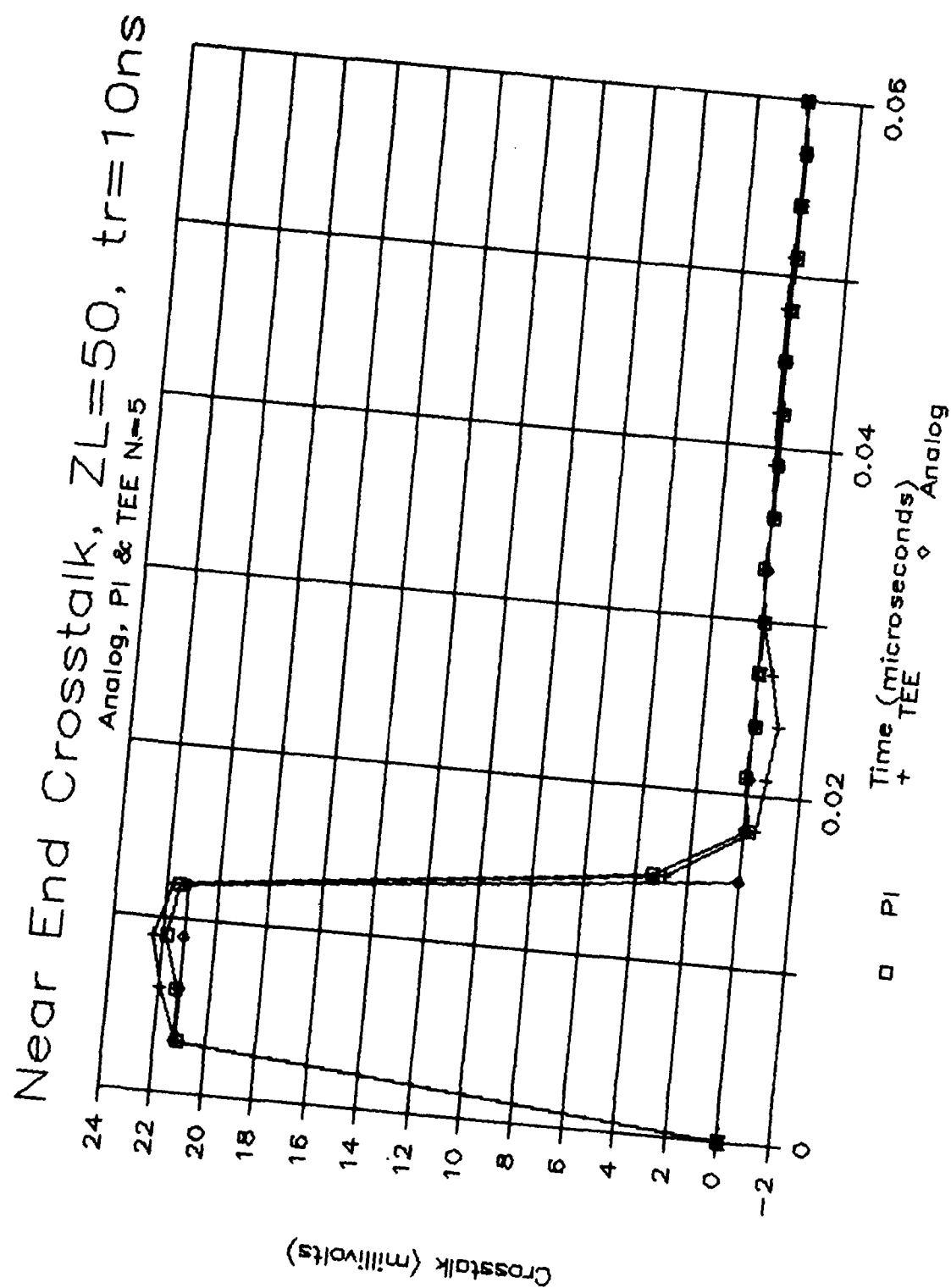


Fig. 4.25. Time-domain predictions
 50Ω, Near End, $\tau_r=\tau_f=10\text{ ns}$

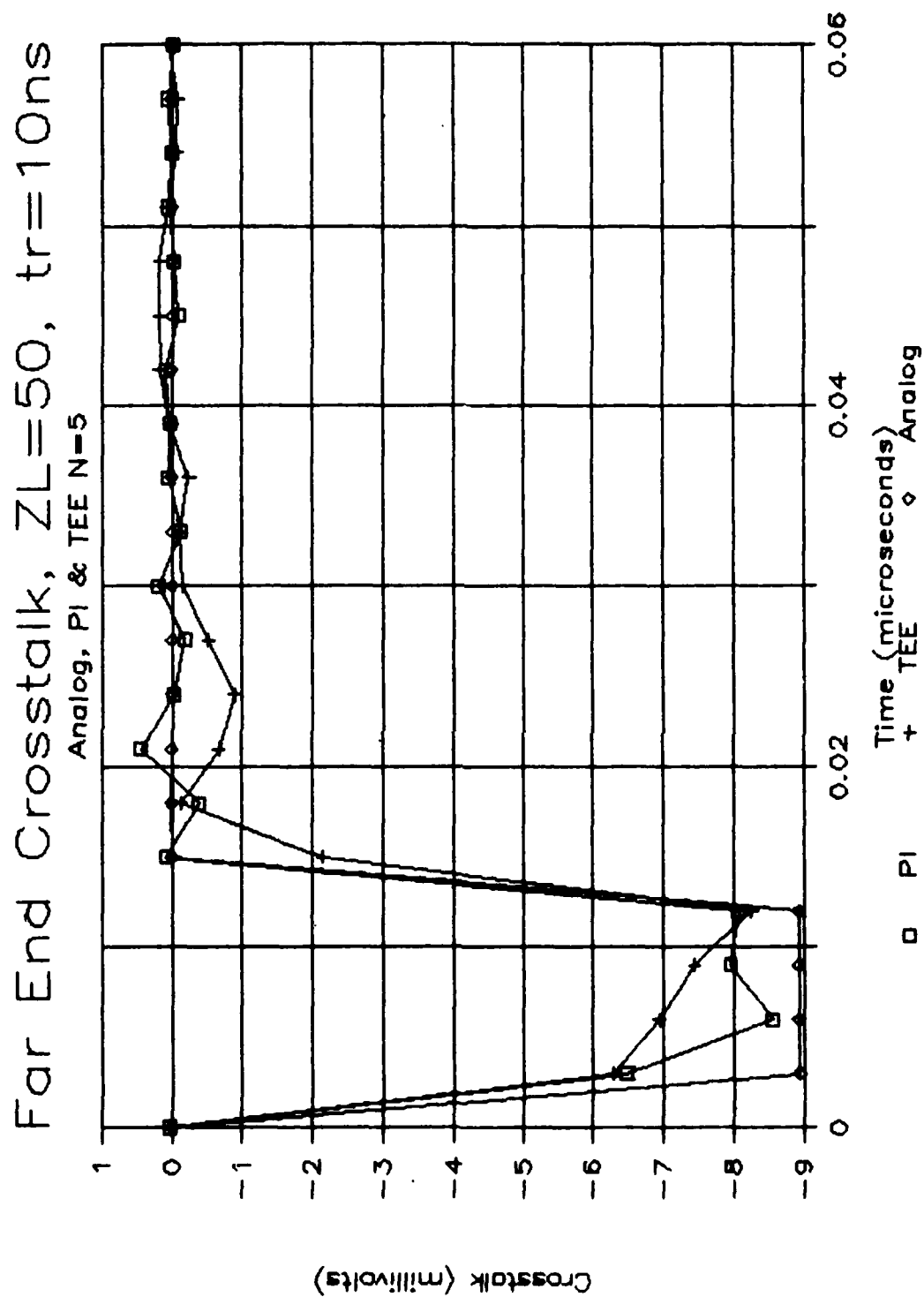


Fig. 4.26. Time-domain predictions
 50Ω , Far End, $\tau_r=\tau_f=10\text{ ns}$

Near End Crosstalk, $Z_L=1k$, $\tau_r=100ns$
 Analog, PI & TEE $N=5$

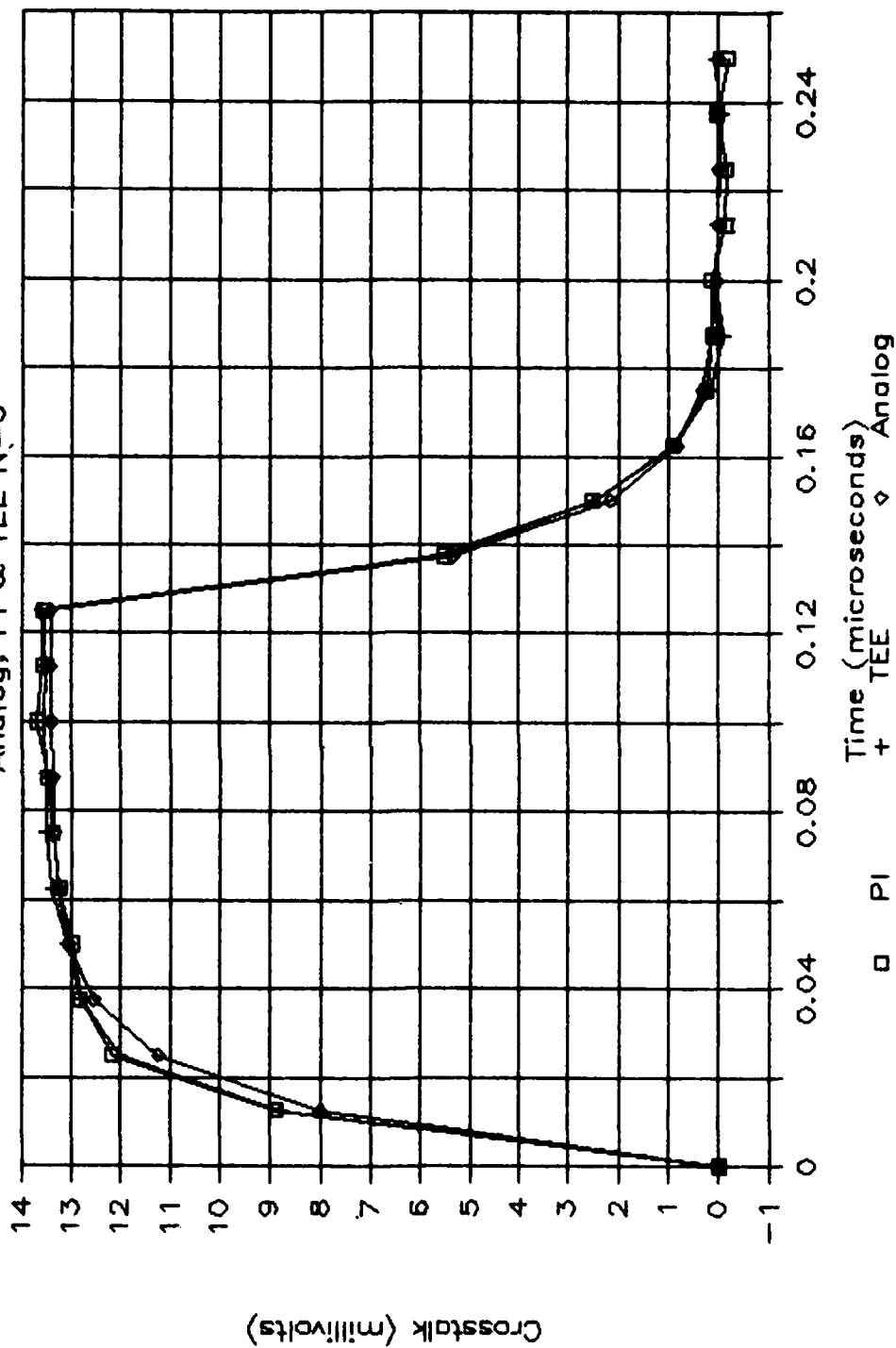


Fig. 4.27. Time-domain predictions
 1 k Ω , Near End, $\tau_r=\tau_f=100$ ns

Far End Crosstalk, $Z_L=1k$, $\tau_r=100ns$
 Analog, PI & TEE N=5

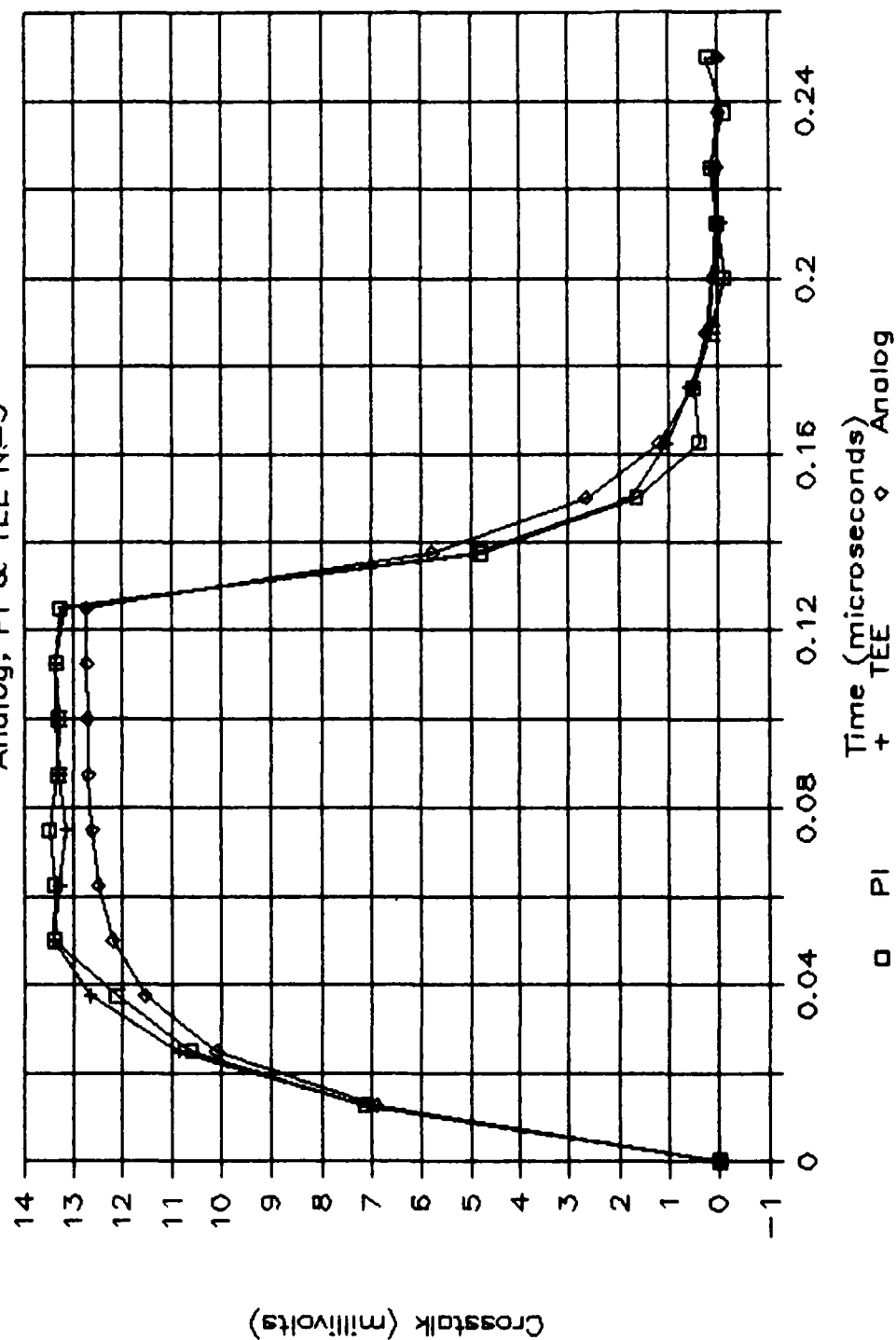


Fig. 4.28. Time-domain predictions
 1 k Ω , Far End, $\tau_r=\tau_f=100$ ns

Near End Crosstalk, $Z_L=1k$, $t_r=50ns$
 Analog, PI & TEE $N=5$

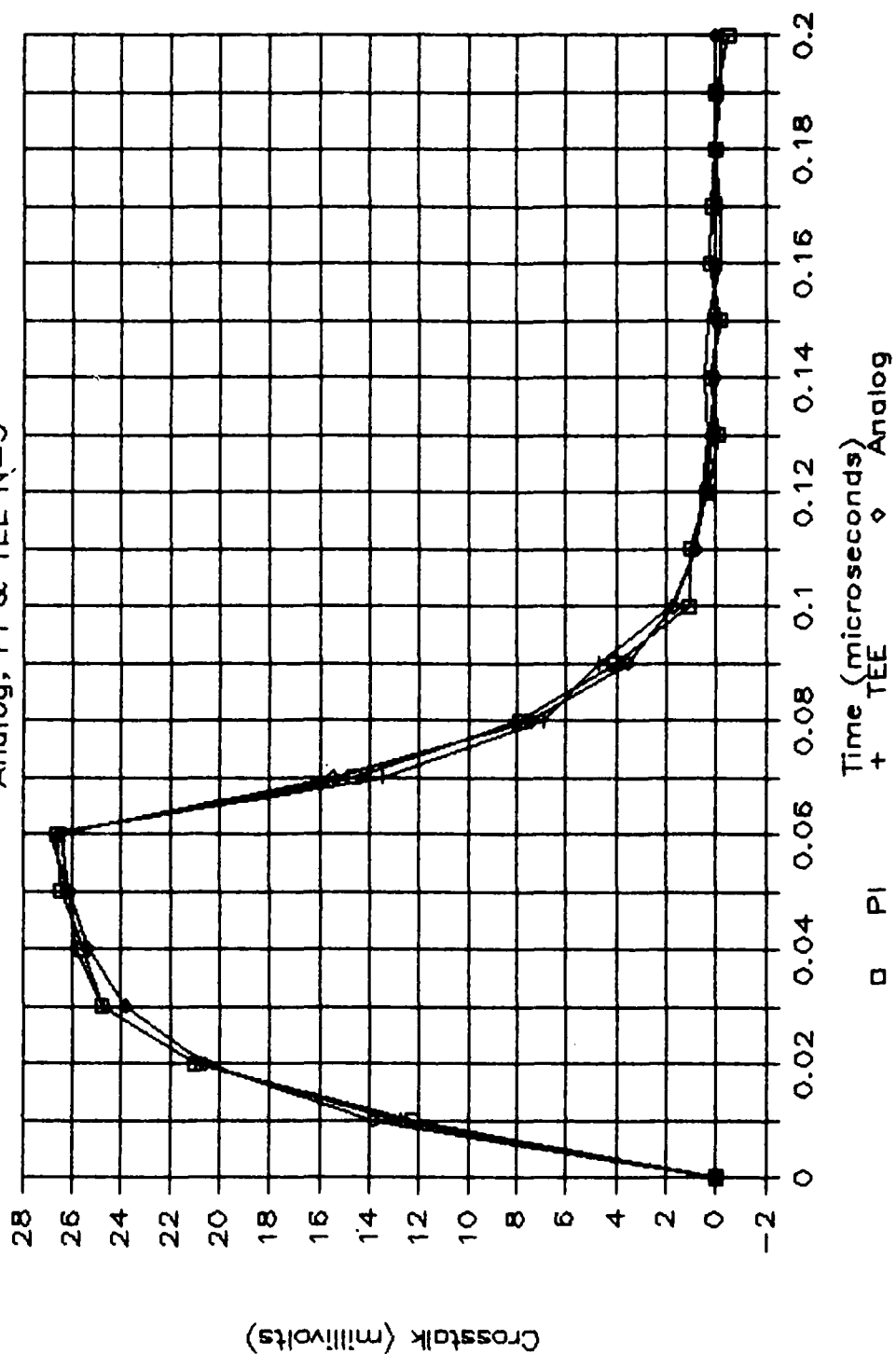


Fig. 4.29. Time-domain predictions
 $1k\Omega$, Near End, $\tau_r = \tau_f = 50ns$

Far End Crosstalk, $Z_L=1k$, $t_r=50ns$
 Analog, PI & TEE $N=5$

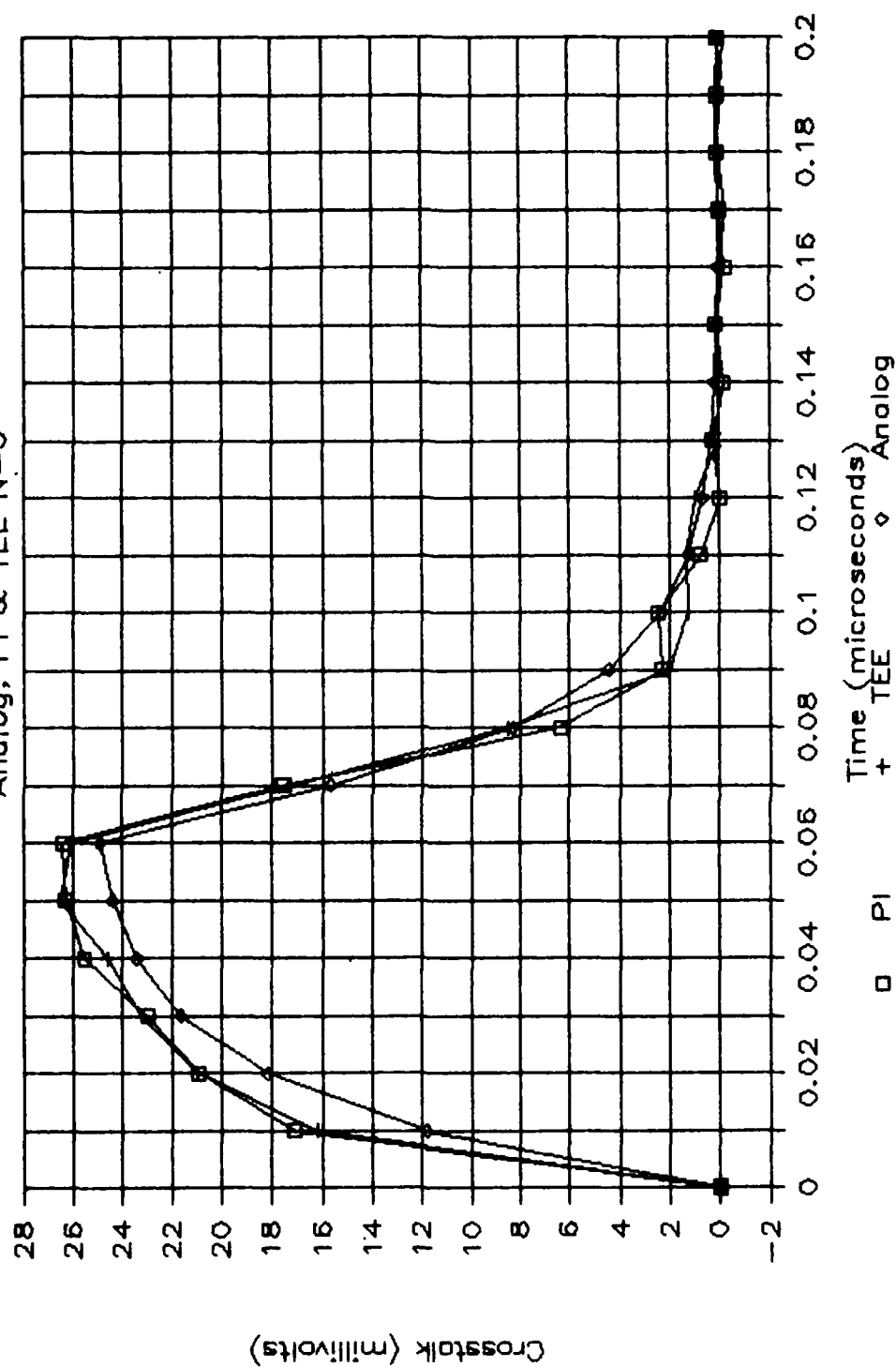


Fig. 4.30. Time-domain predictions
 $1\text{ k}\Omega$, Far End, $\tau_r=\tau_f=50\text{ ns}$

Near End Crosstalk, $Z_L=1k$, $\tau_r=10ns$
 Analog, PI & TEE $N=5$

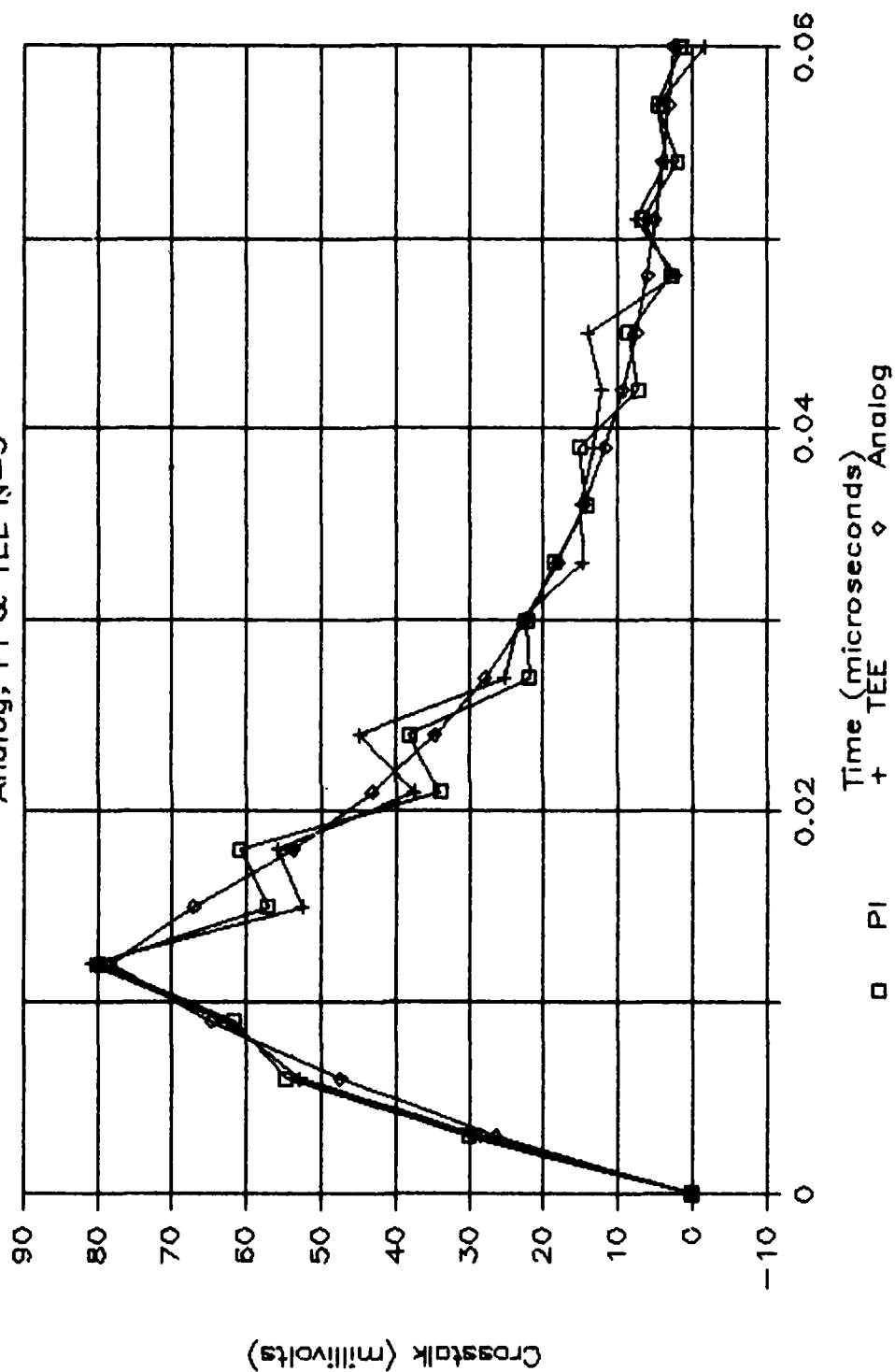


Fig. 4.31. Time-domain predictions
 1 k Ω , Near End, $\tau_r=\tau_f=10$ ns

Far End Crosstalk, $Z_L=1k$, $t_r=10ns$
 Analog, PI & TEE $N=5$

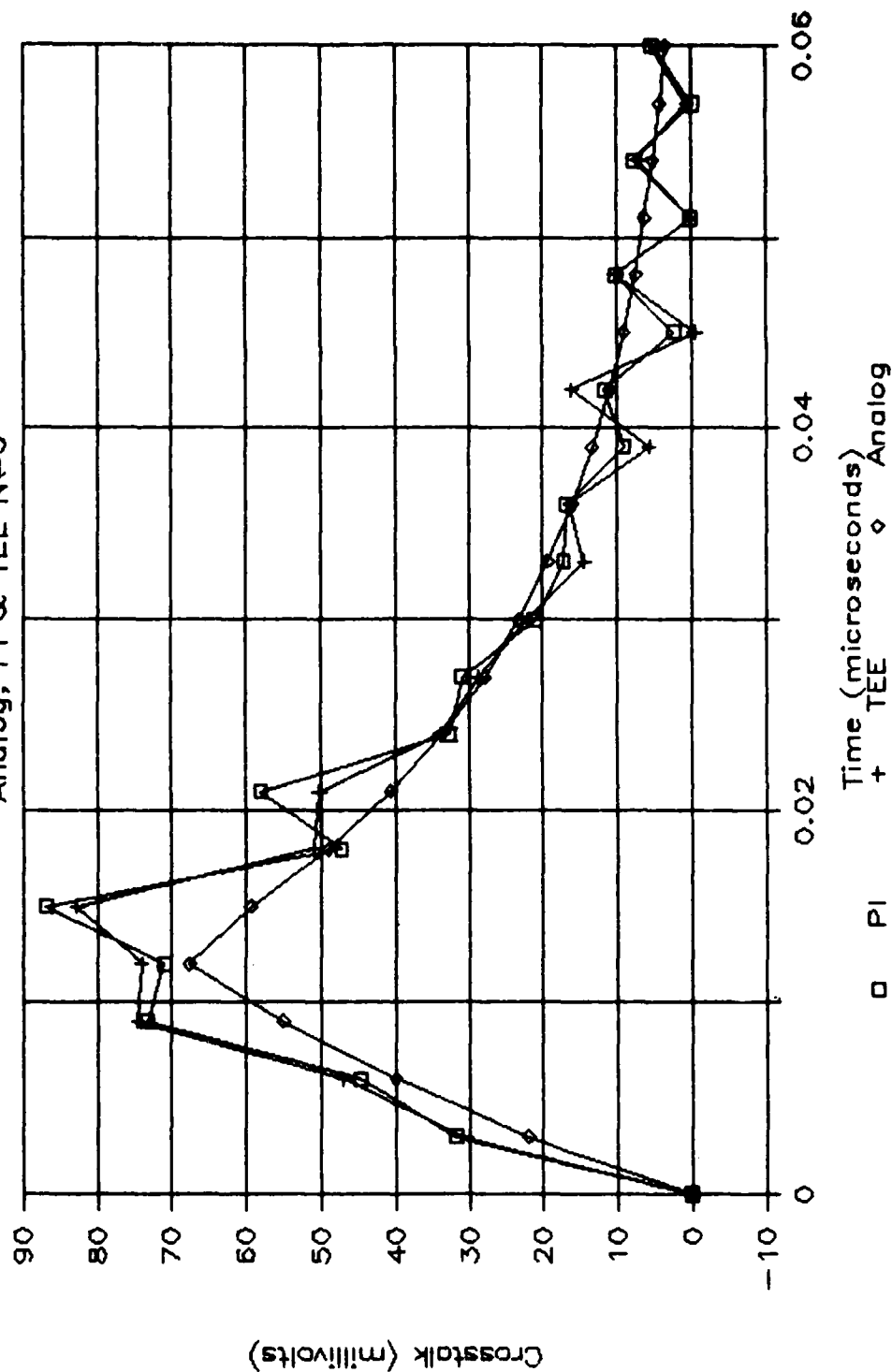


Fig. 4.32. Time-domain predictions
 $1k\Omega$, Far End, $\tau_r=\tau_f=10ns$

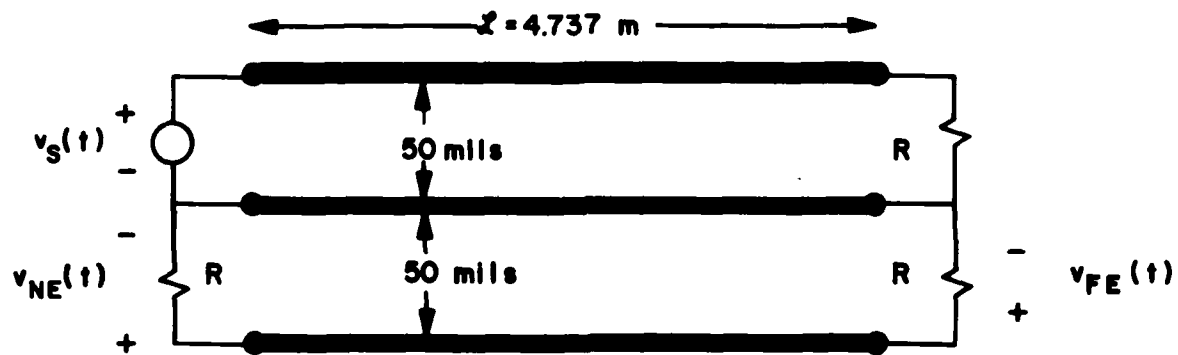


Fig. 4.33. The ribbon cable experimental configuration

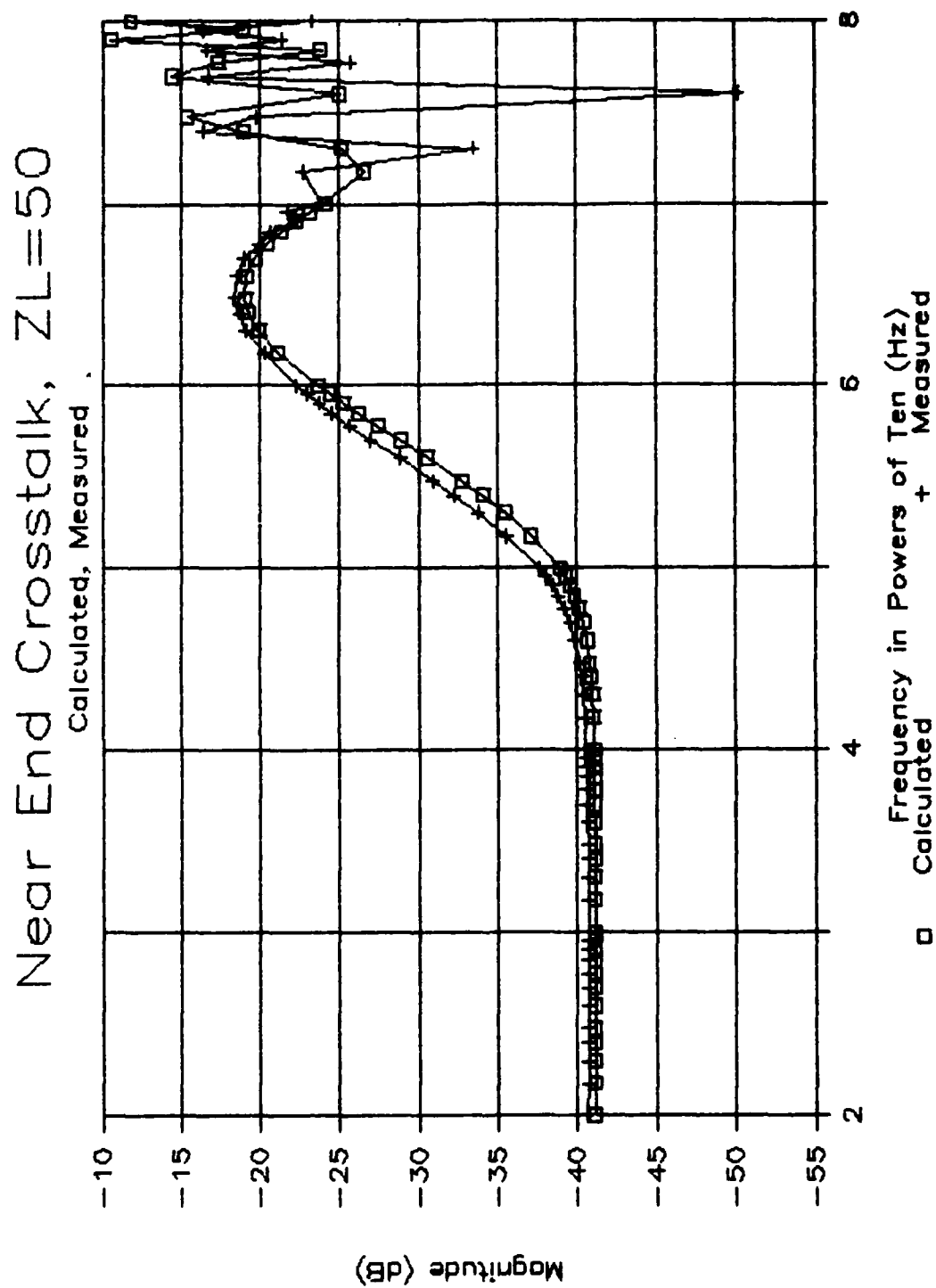


Fig. 4.34. Frequency response experimental data vs. predictions of the MTL model. Near End, 50Ω

Far End Crosstalk, ZL=50

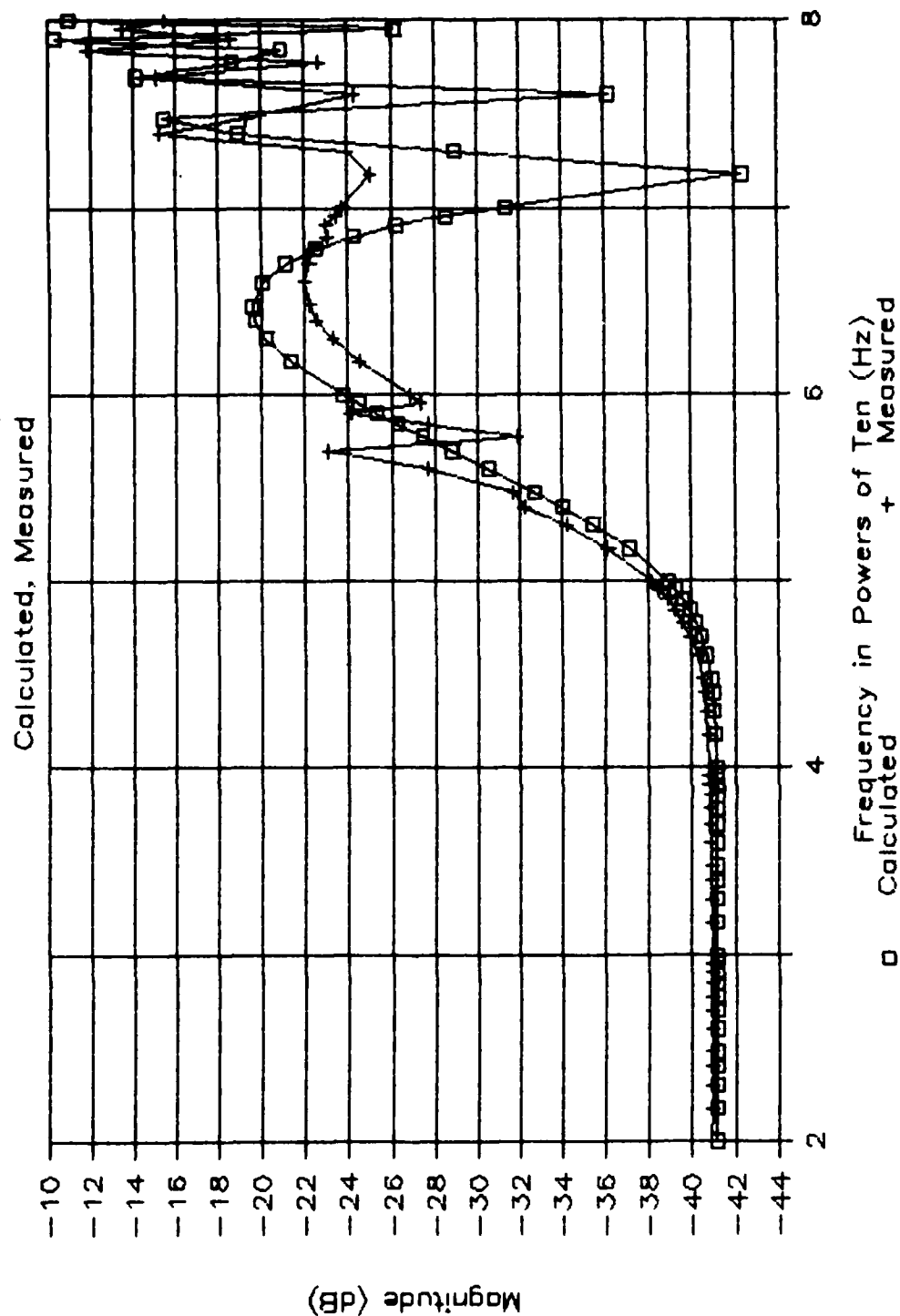


Fig. 4.35. Frequency response experimental data vs. predictions of the MTL model. Far End, 50Ω

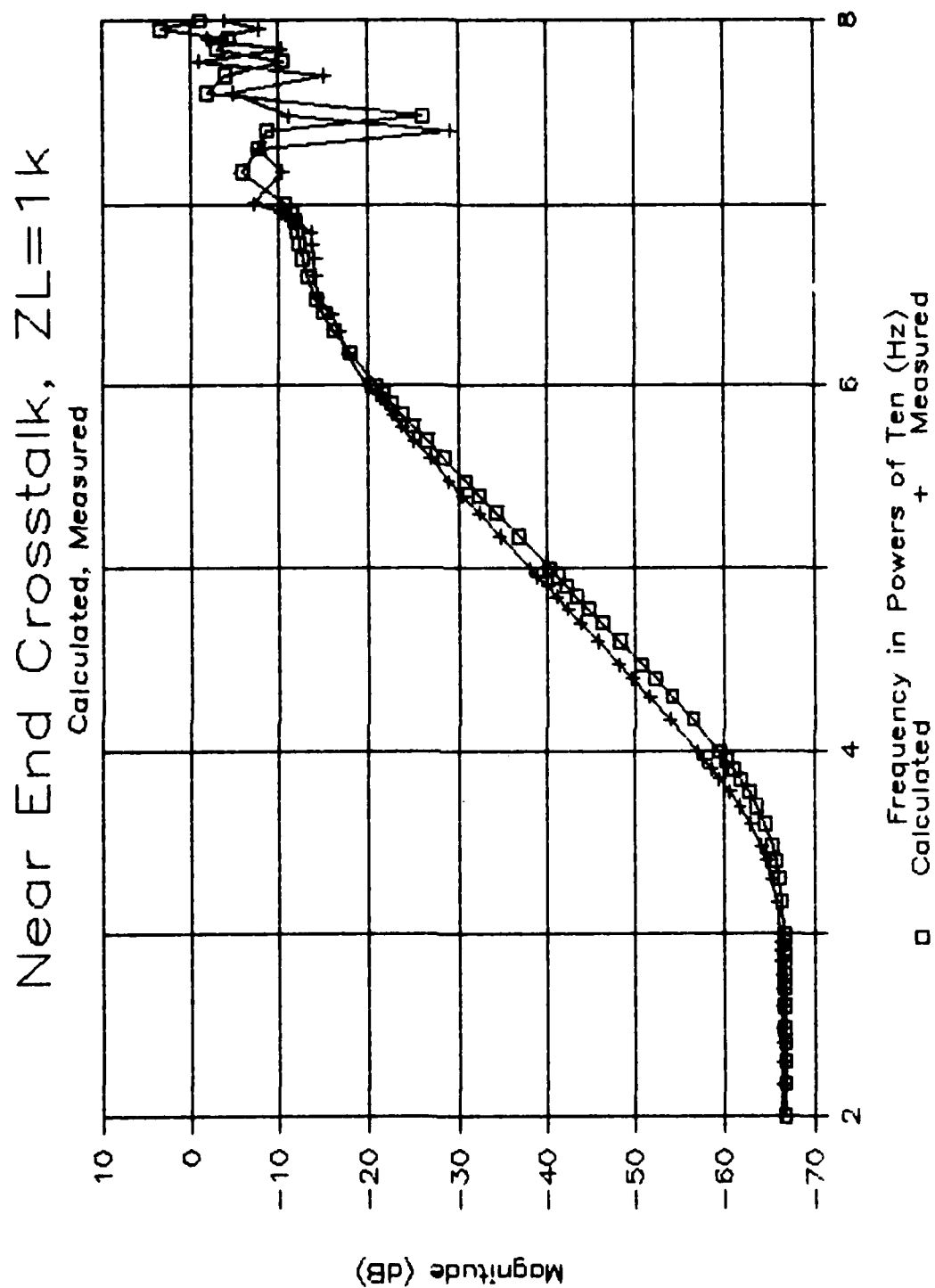


Fig. 4.36. Frequency response experimental data vs. predictions of the MTL model. Near End, 1 k Ω

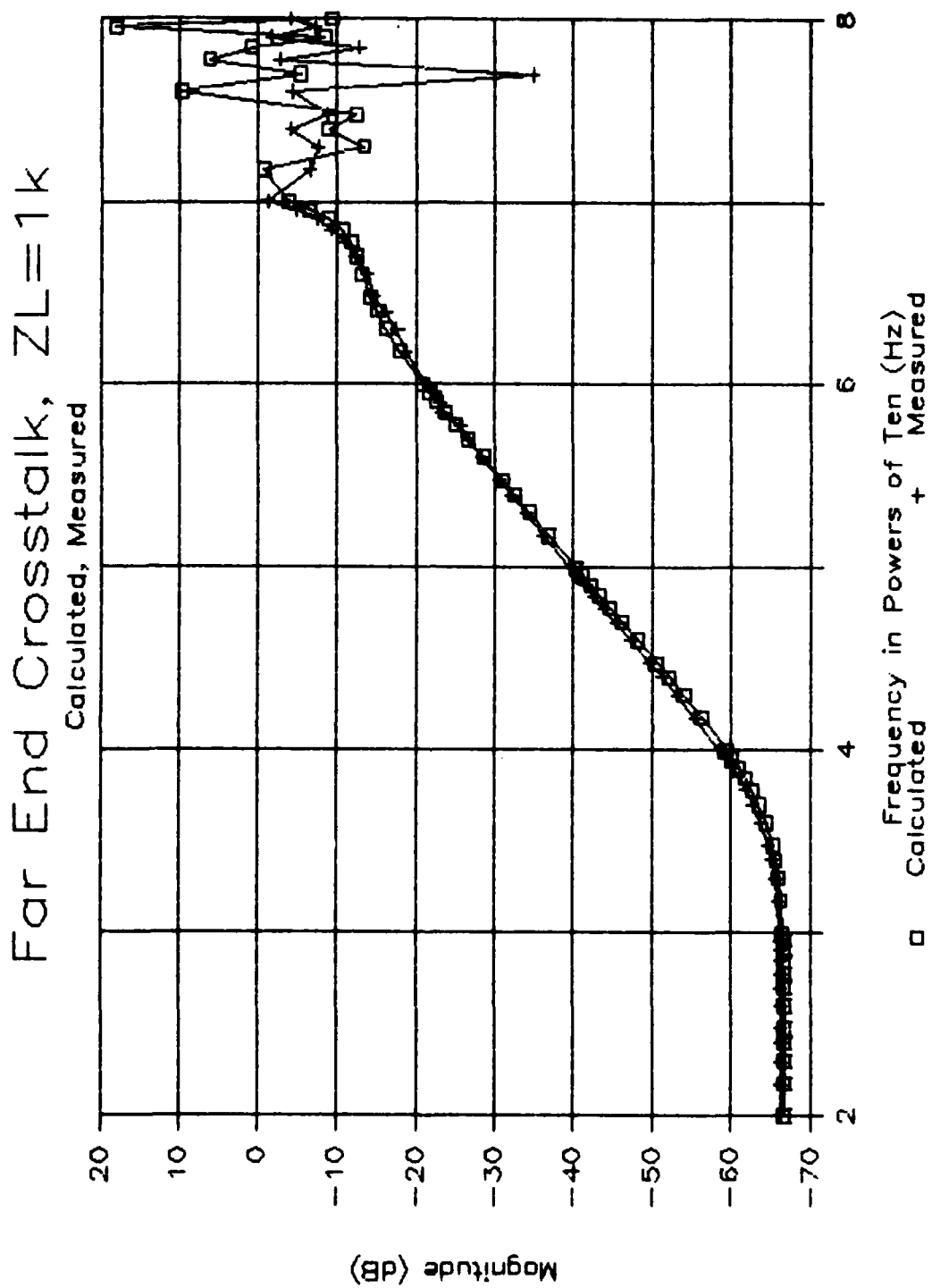


Fig. 4.37. Frequency response experimental data vs. predictions of the MTL model. Far End, 1 k Ω

From these results we obtain

Table 4.4

	R	K_L	M	w_u
near end	50 Ω	8.9E-3	1.26E-8	2E7
	1 k Ω	4.5E-4	2.16E-8	1E7
far end	50 Ω	8.9E-3	-1 E-8	2E7
	1 k Ω	4.5E-4	1.68E-8	6E7

The predictions of the lumped-circuit iterative Pi and Tee models are shown in Fig. 4.38 through 4.45. These models provide accurate predictions for one section up to a frequency where the line is on the order of $\frac{1}{10} \lambda$ in length (32 MHz).

4.2.2. Time-Domain Results

A 20 kHz trapezoidal pulse train typical of RS-232C data transmission was applied to the cable. The pulse transitioned from -1.25 V to +1.25 V. The rise/fall times used were 6 μ s, 1 μ s, 700 ns, 400 ns, 100 ns, 60 ns and 20 ns. The one-way line delay is 32 ns. Thus the 100 ns rise/fall time is approaching the limit of applicability of the model. The results are shown in Fig. 4.46 through Fig. 4.59.

From the frequency-domain results for M and ω_u , we compute the maximum crosstalk using the model in section 3.3 as seen in Table 4.5 and Table 4.6.

The predicted maximum levels are quite accurate except for the very short rise/fall times. For $\tau_r = \tau_f = 10$ ns and 20 ns we have more errors than encountered with the PCB. Since the line one-way delay time is on the

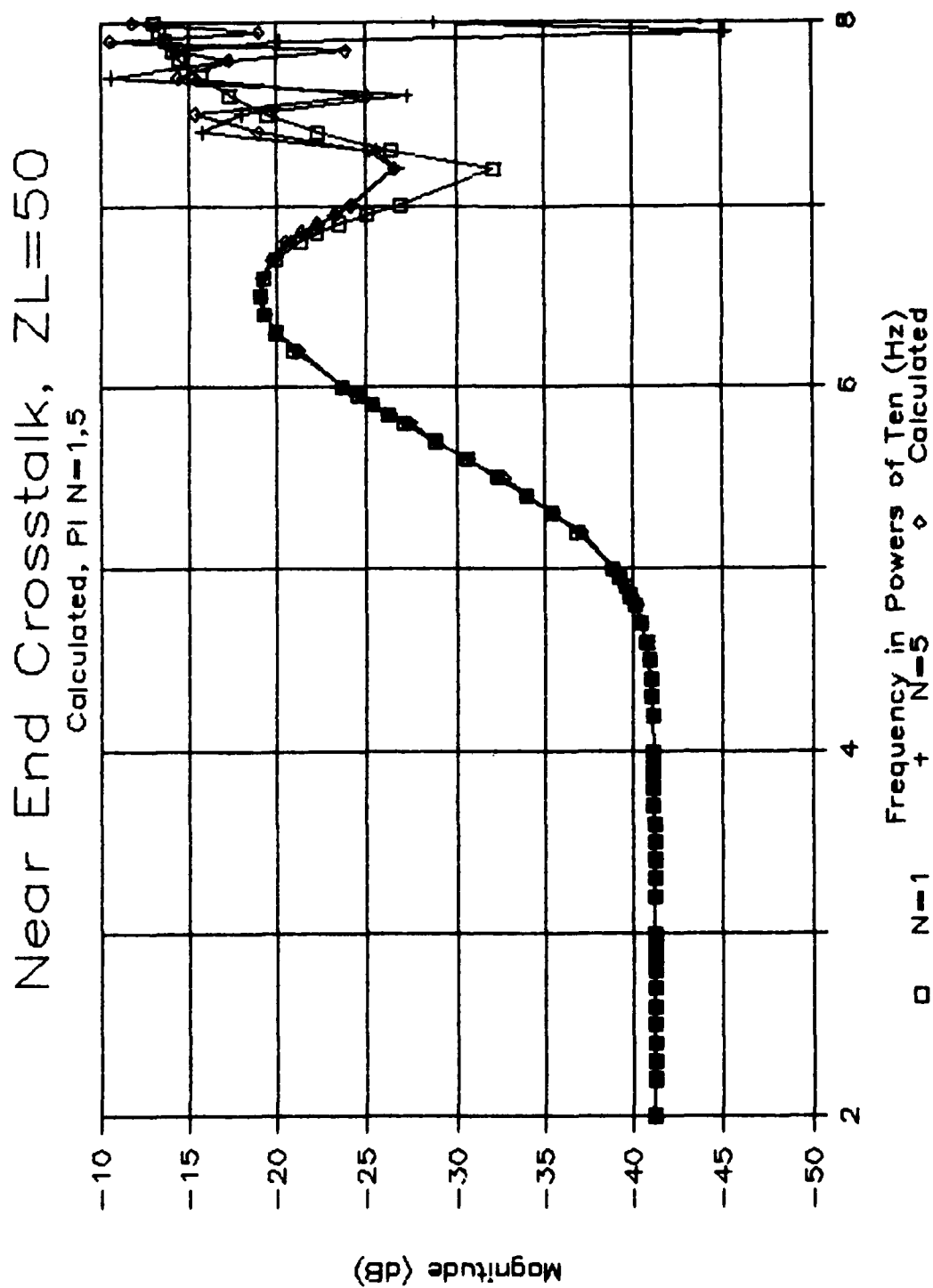


Fig. 4.38. Lumped iterative model vs. MTL model predictions
Near End, P_i , 50Ω

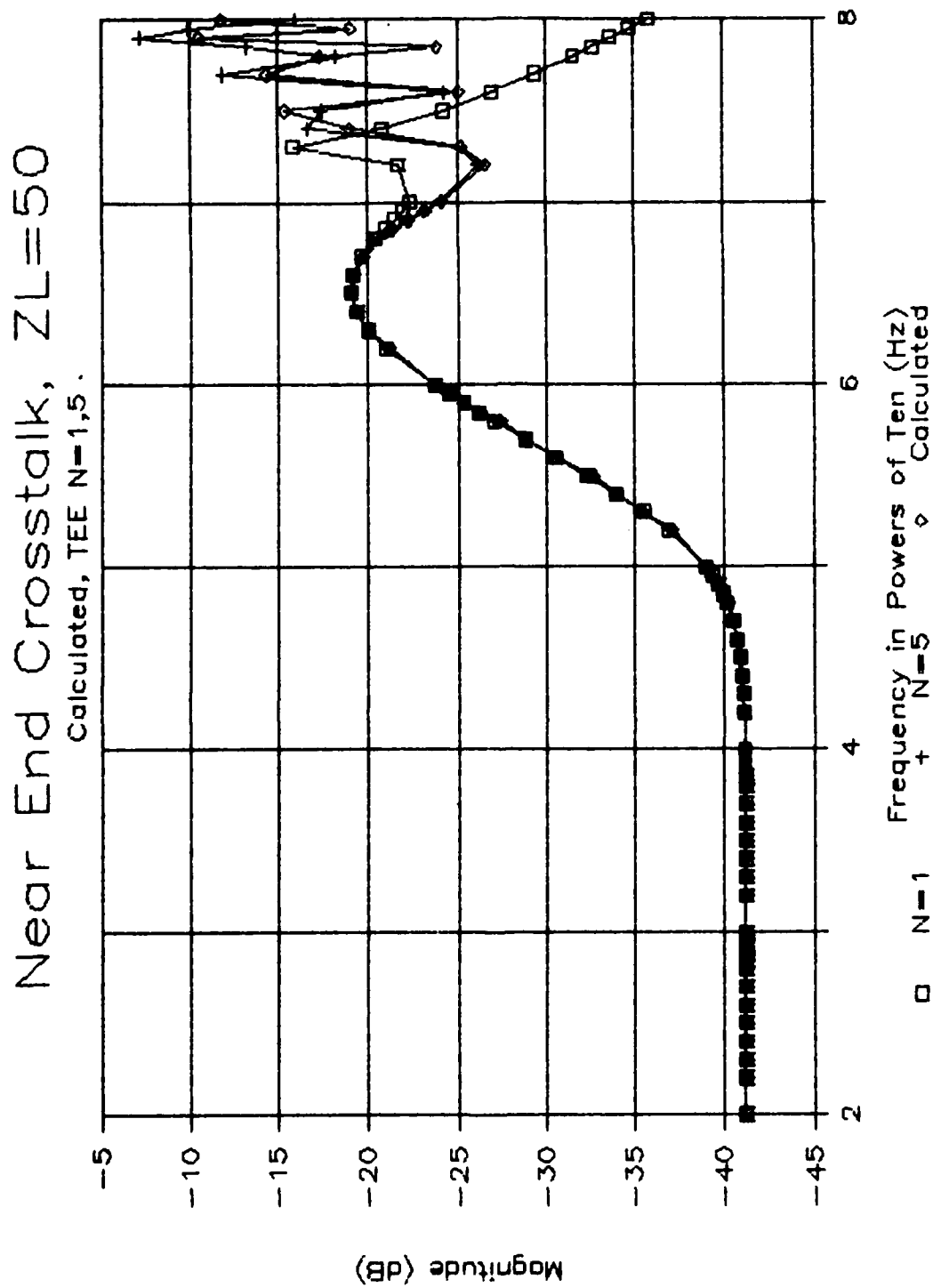


Fig. 4.39. Lumped iterative model vs. MTL model predictions
Near End, Tee, 50Ω

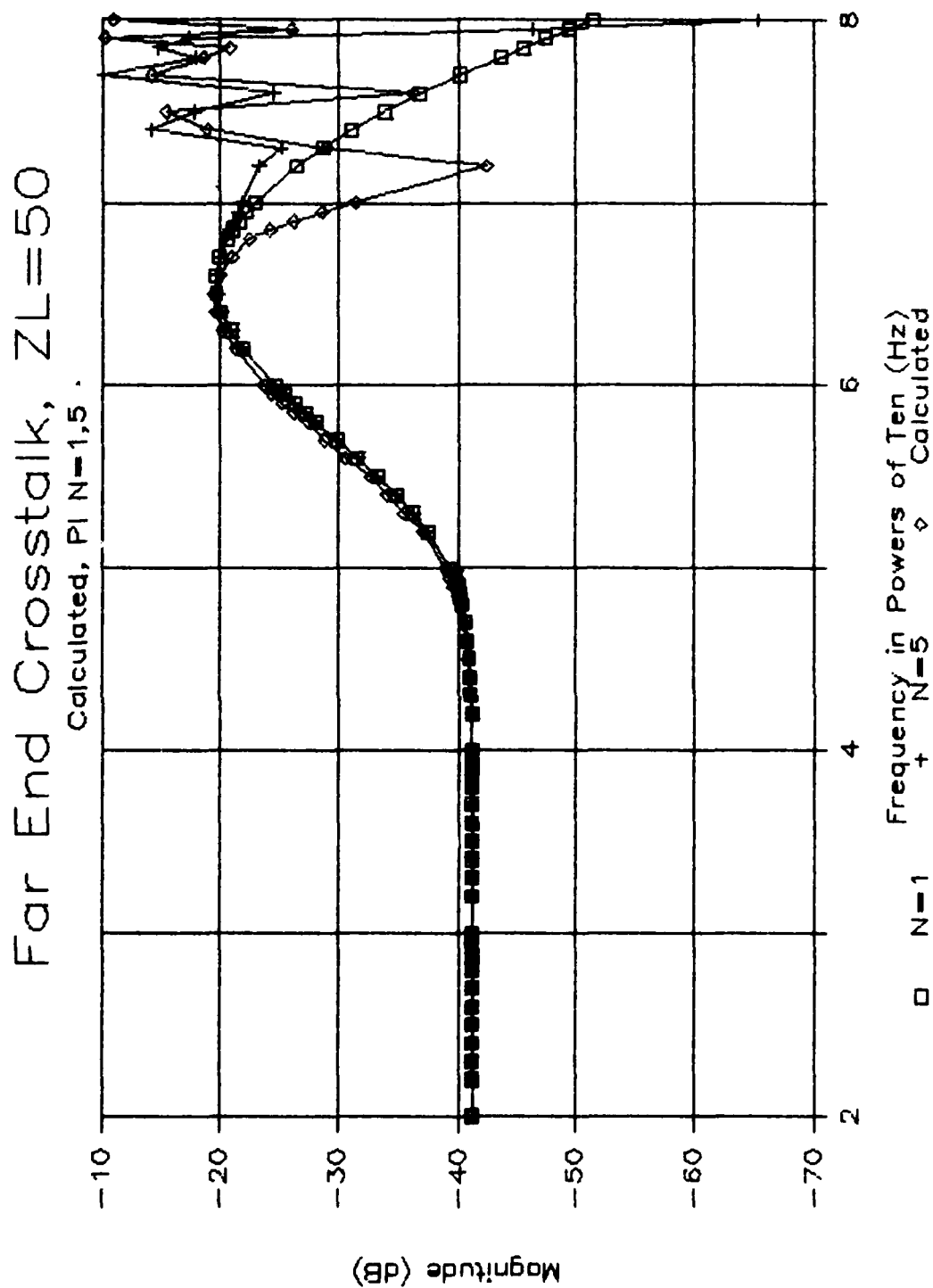


Fig. 4.40. Lumped iterative model vs. MTL model predictions
Far End, P_i , 500

Far End Crosstalk, $ZL=50$

Calculated, TEE $N=1.5$

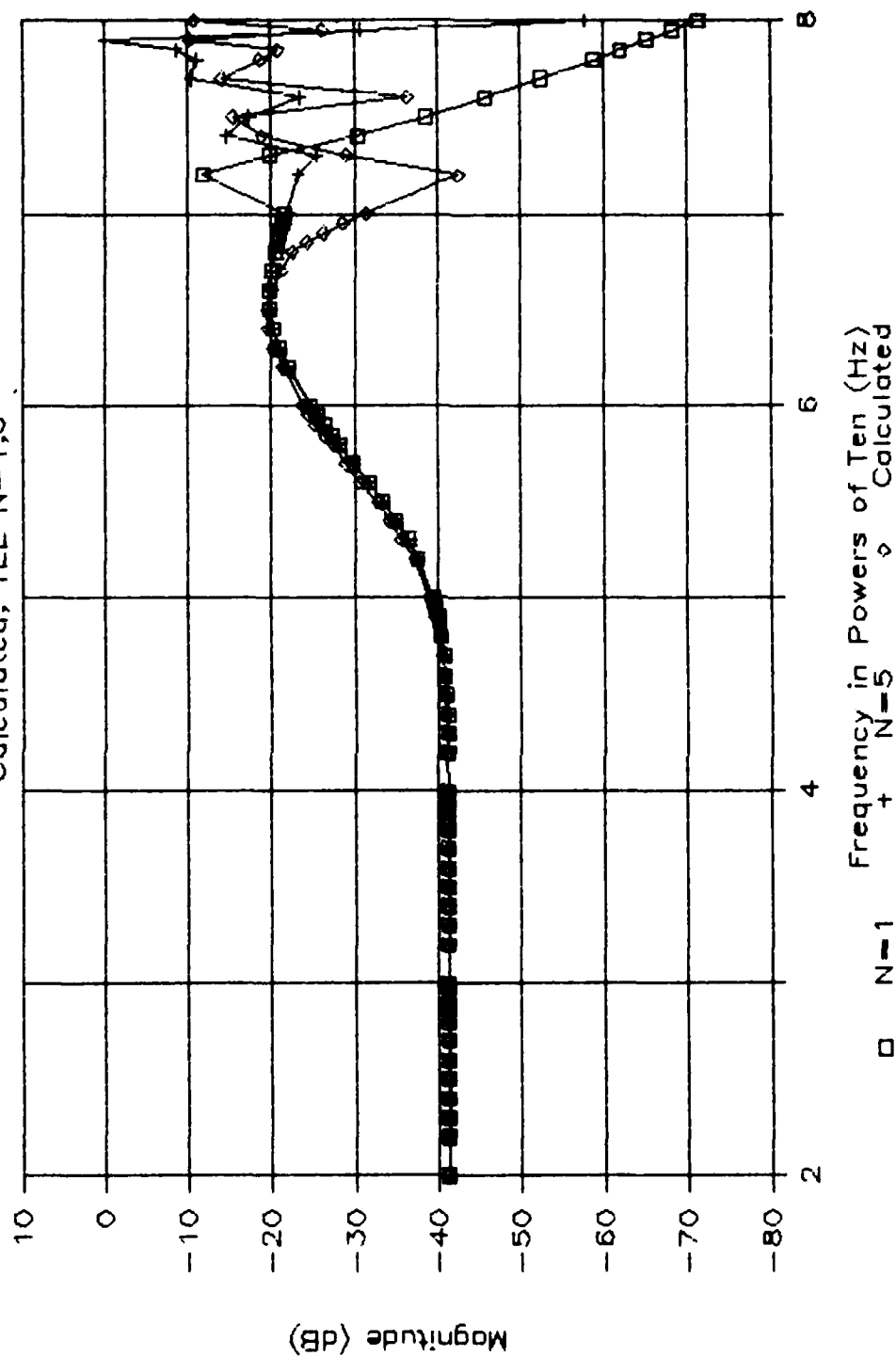


Fig. 4.41. Lumped iterative model vs. MTL model predictions
Far End, Tee, 50 Ω

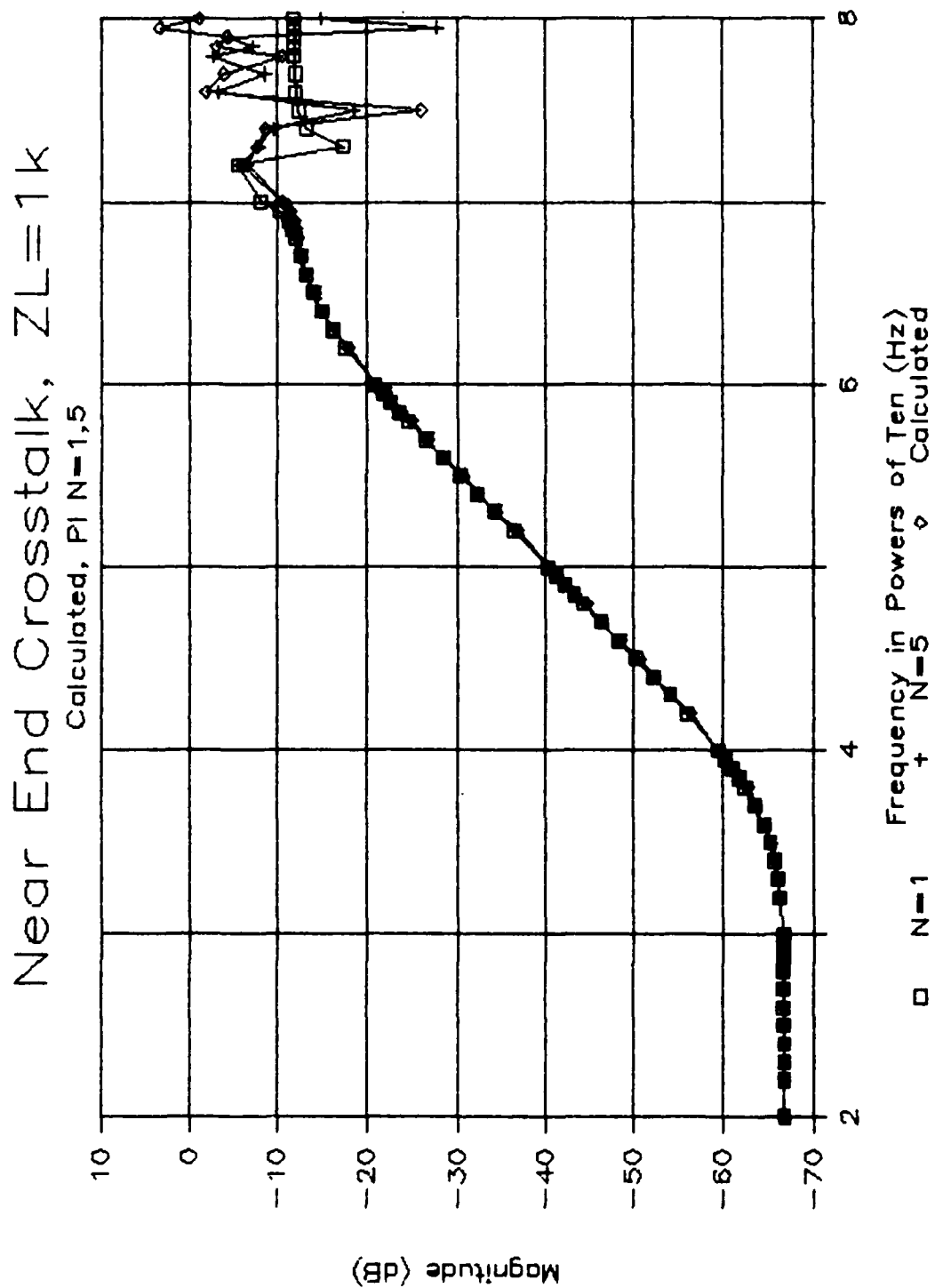


Fig. 4.42. Lumped iterative model vs. MTL model predictions
Near End, P_i , 1 k Ω

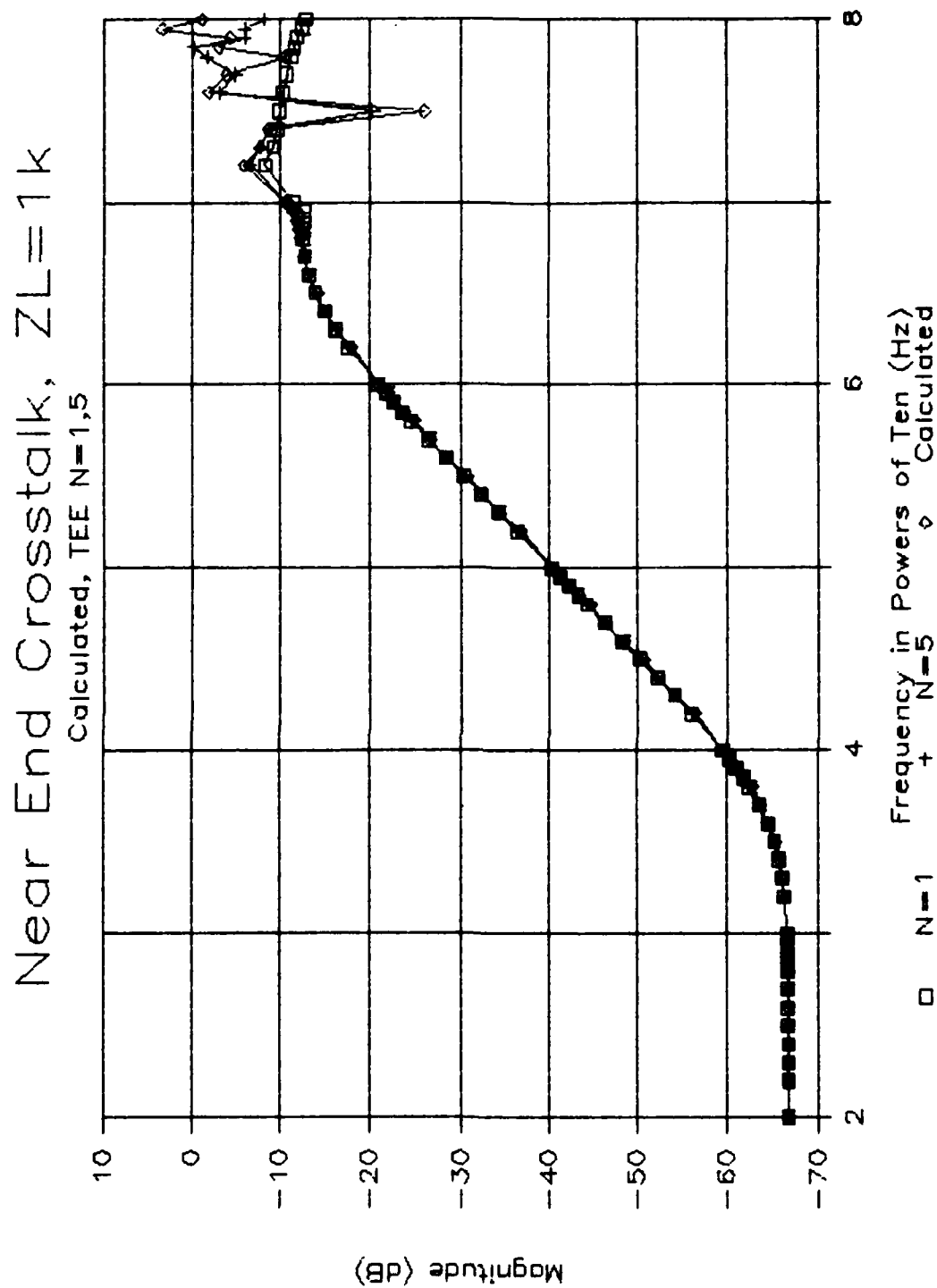


Fig. 4.43. Lumped iterative model vs. MTL model predictions
Near End, Tee, 1 k Ω

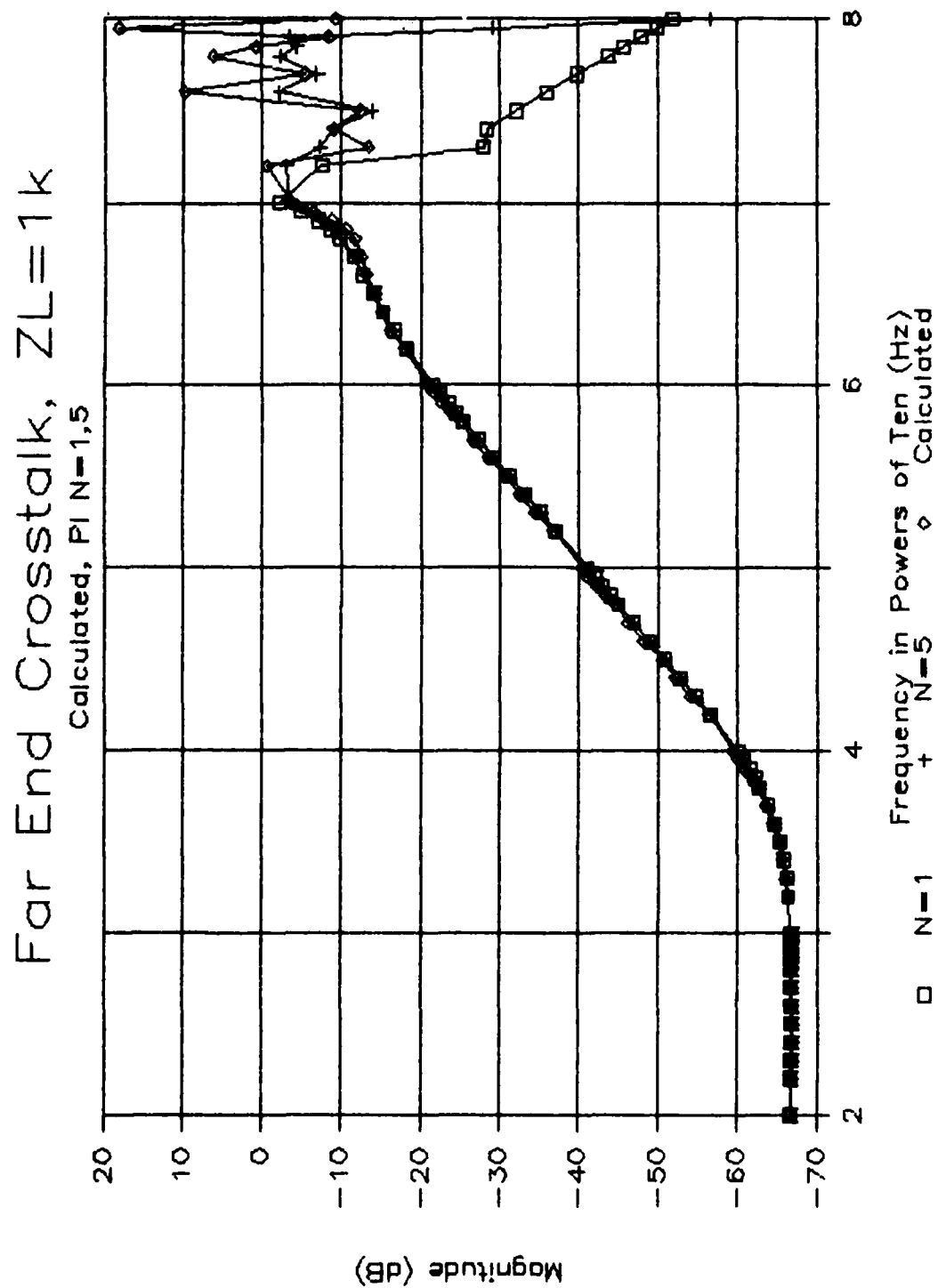


Fig. 4.44. Lumped iterative model vs. MTL model predictions
Far end, P_i , 1 k Ω

Far End Crosstalk, $Z_L=1k$

Calculated, TEE $N=1.5$

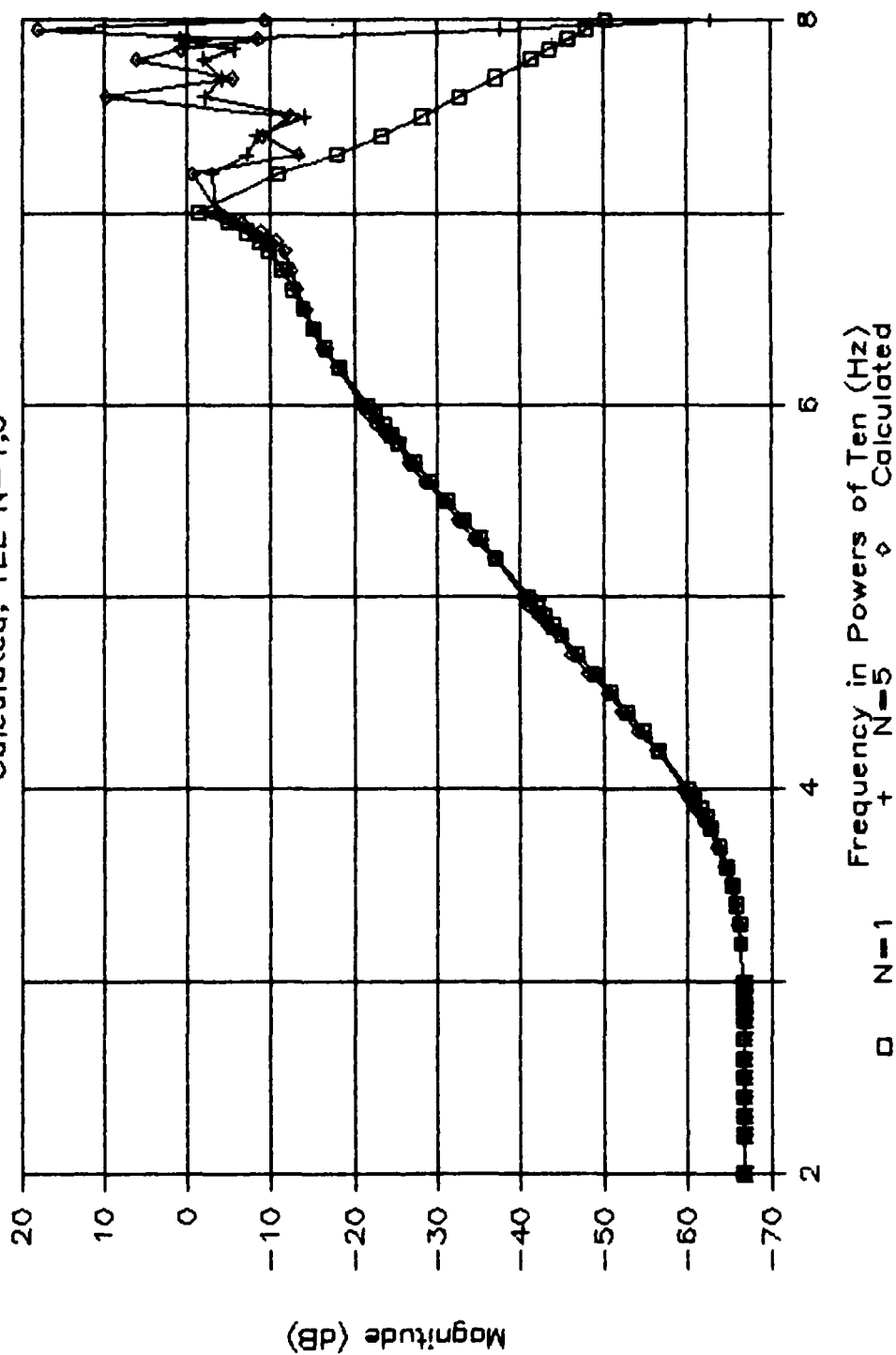
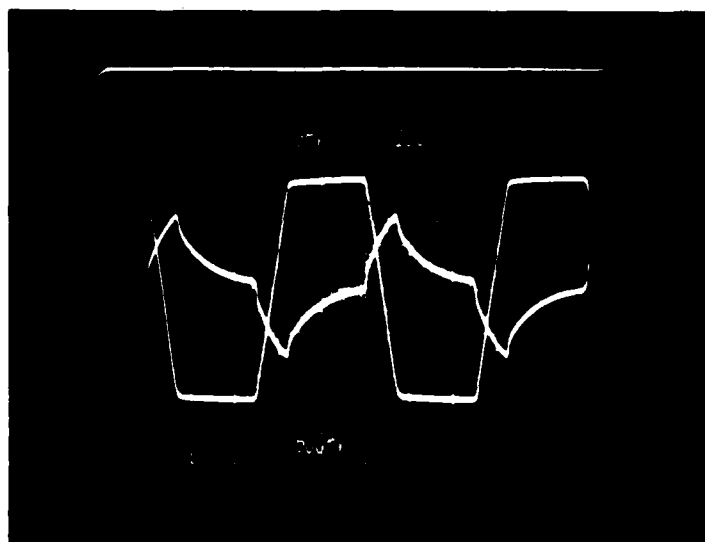
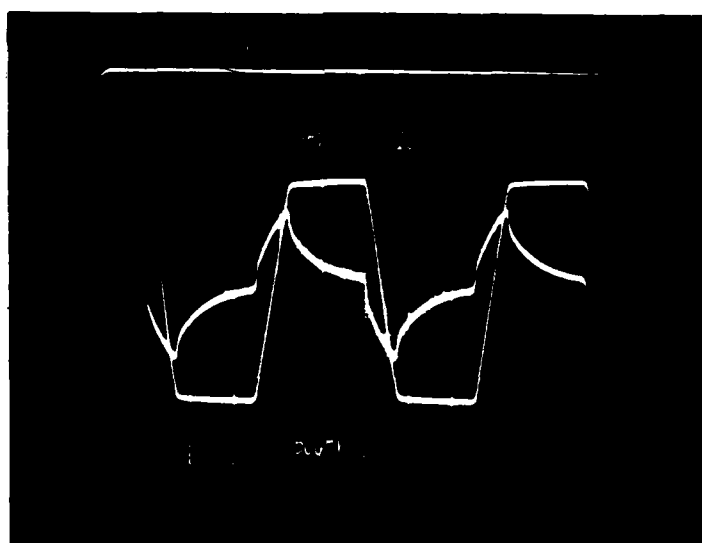


Fig. 4.45. Lumped iterative model vs. MTL model predictions
Far End, Tee, 1 k Ω

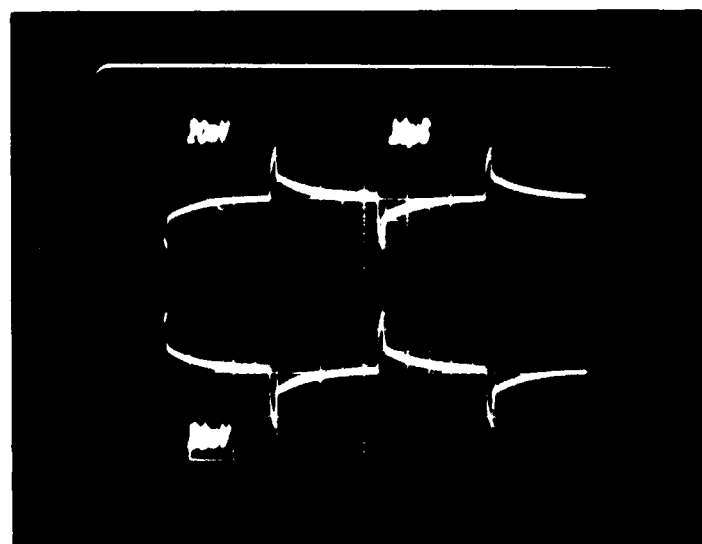


V_{FE}



V_{NE}

Fig. 4.46. Experimental results 50Ω , $\tau_r = \tau_f = 6 \mu s$



V_{FE}

V_{NE}

Fig. 4.47. Experimental results 50Ω , $\tau_r = \tau_f = 1 \mu s$

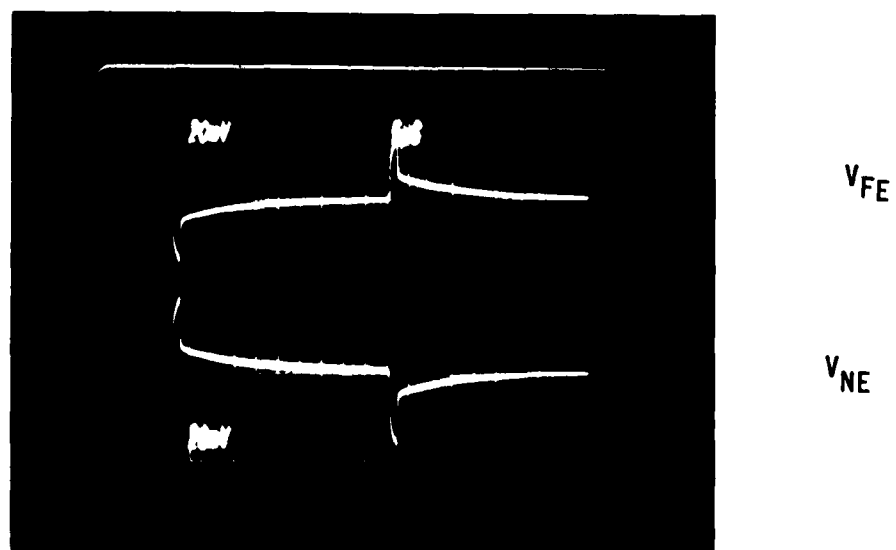
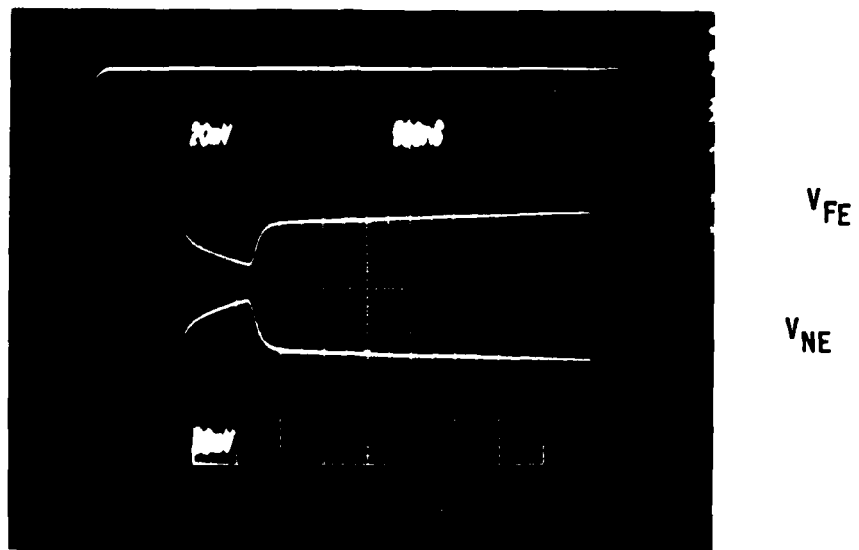


Fig. 4.48. Experimental results 50Ω , $\tau_r = \tau_f = 700$ ns

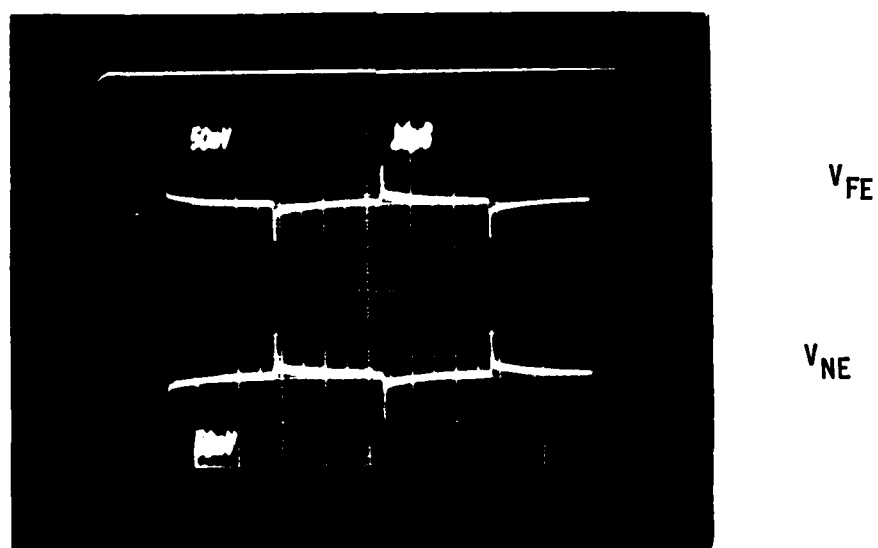
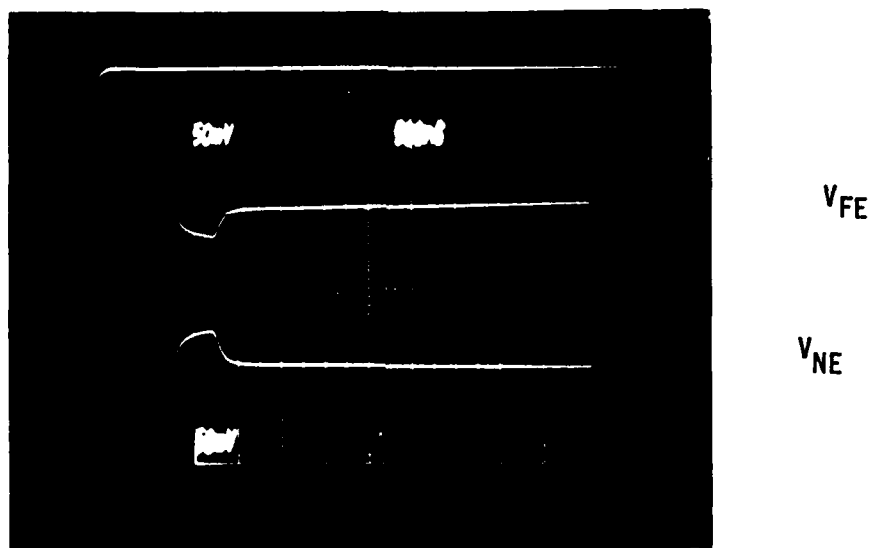


Fig. 4.49. Experimental results 50Ω , $\tau_r = \tau_f = 400$ ns

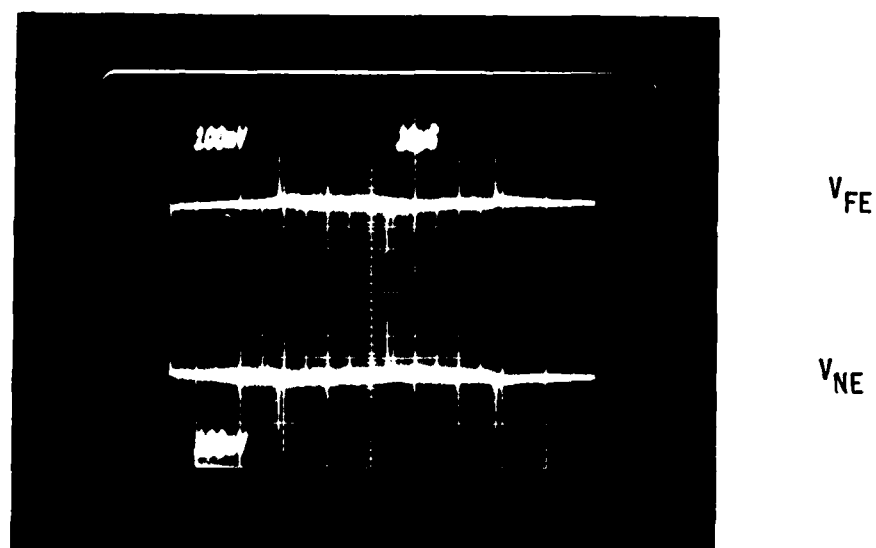
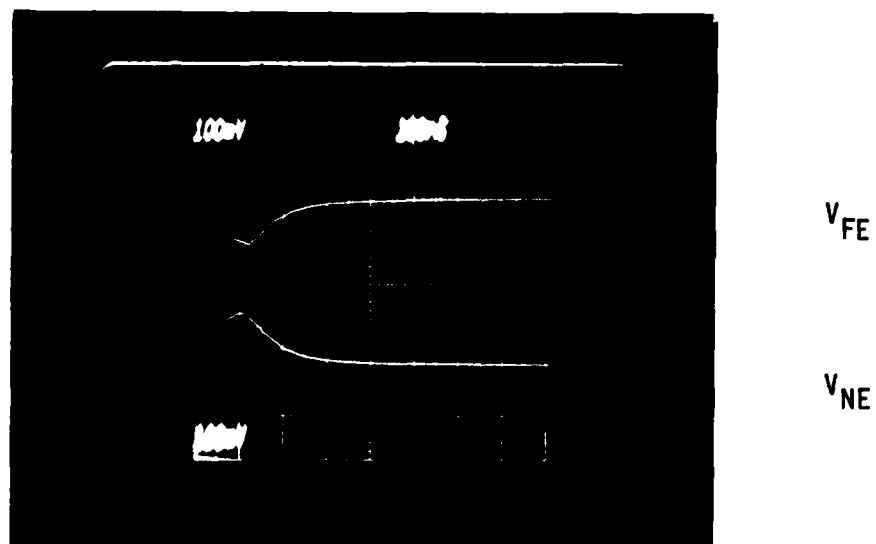


Fig. 4.50. Experimental results 50 Ω , $\tau_r = \tau_f = 100$ ns

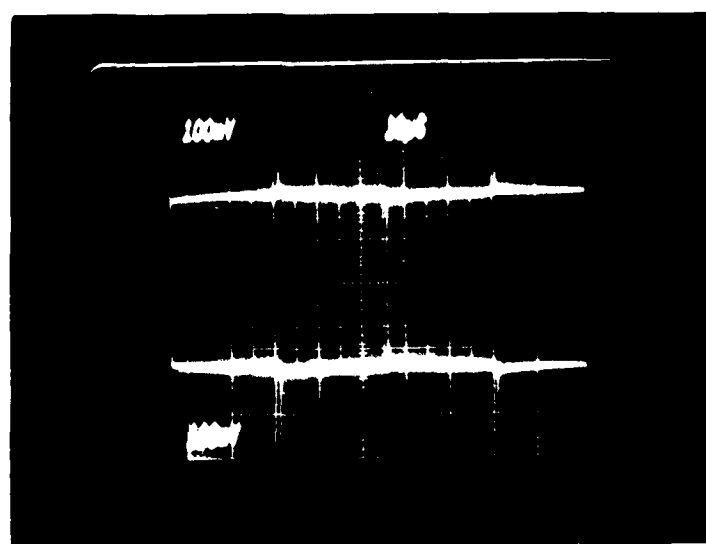
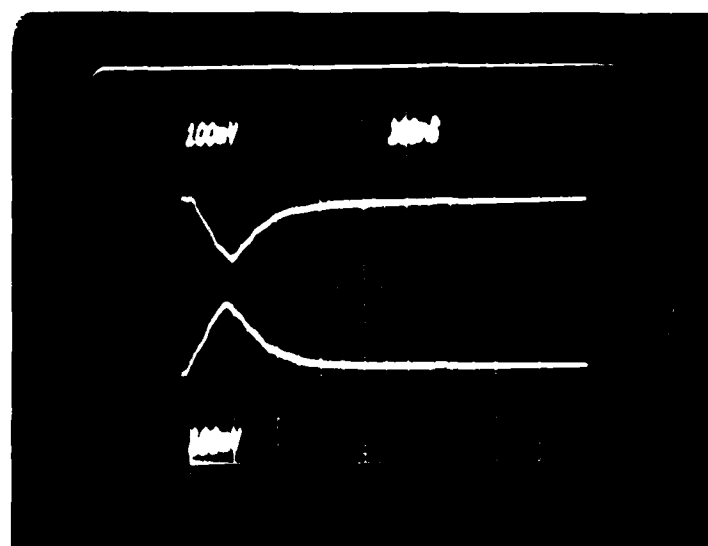


Fig. 4.51. Experimental results 50Ω , $\tau_r = \tau_f = 60$ ns

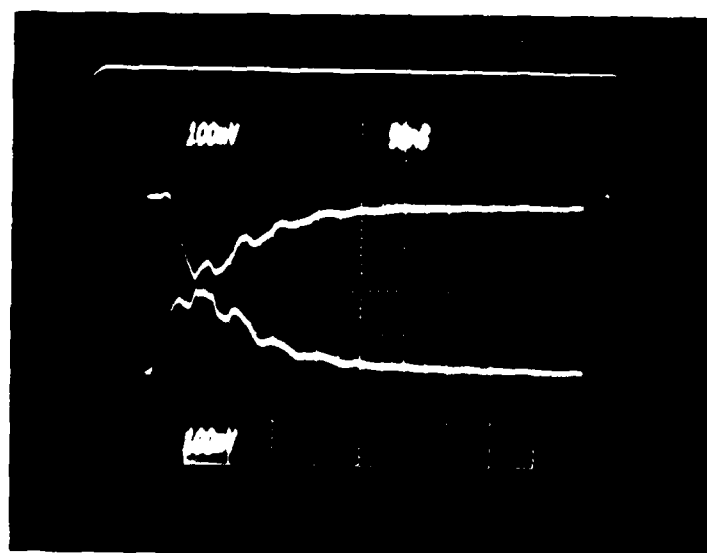
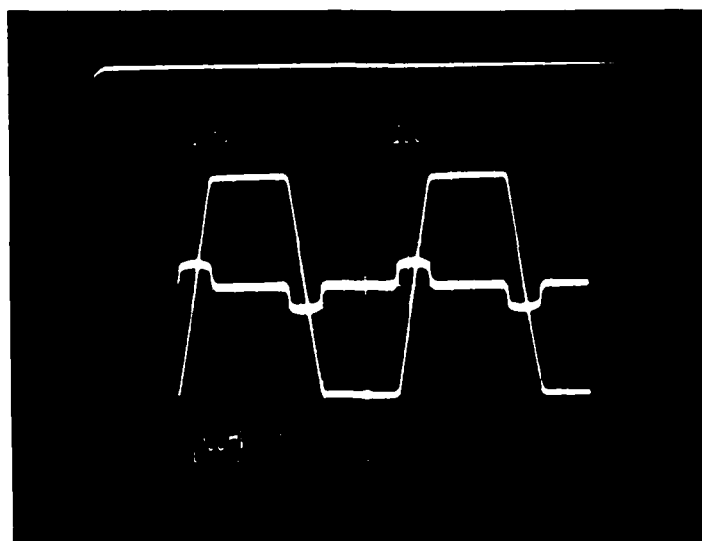
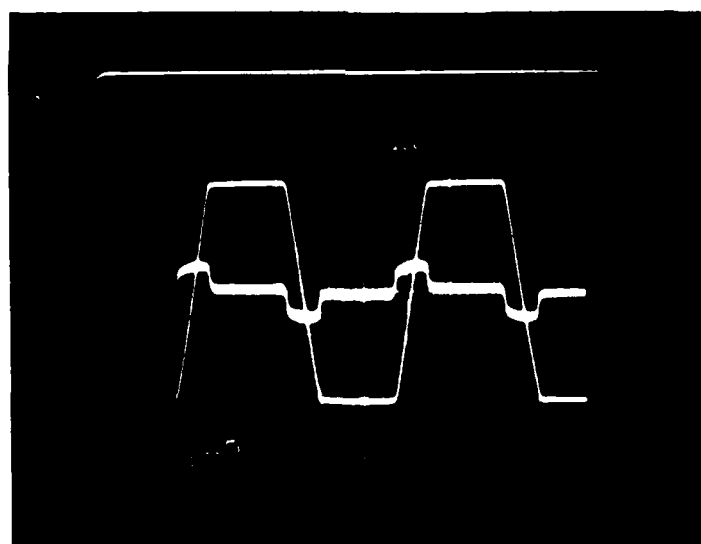


Fig. 4.52. Experimental results 50Ω , $\tau_r = \tau_f = 20$ ns



V_{FE}



V_{NE}

Fig. 4.53. Experimental results $1\text{ k}\Omega$, $\tau_r = \tau_f = 6\text{ }\mu\text{s}$

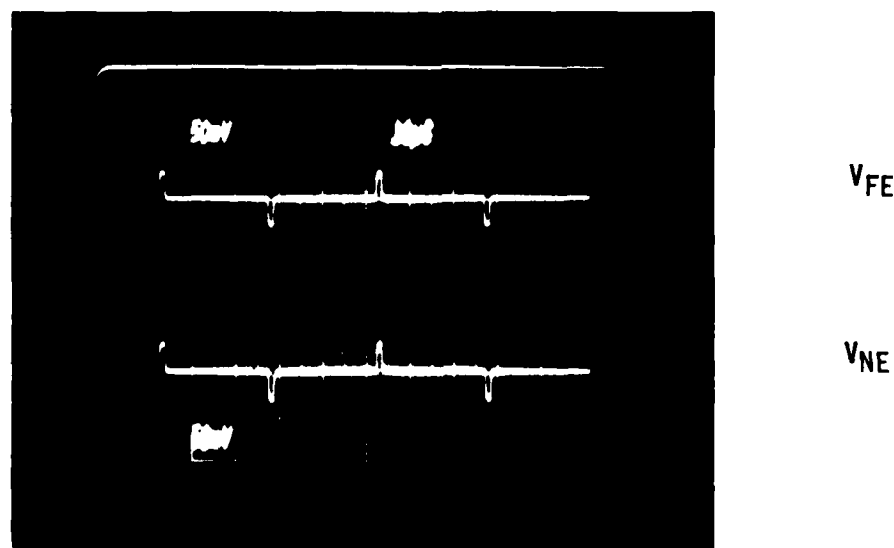
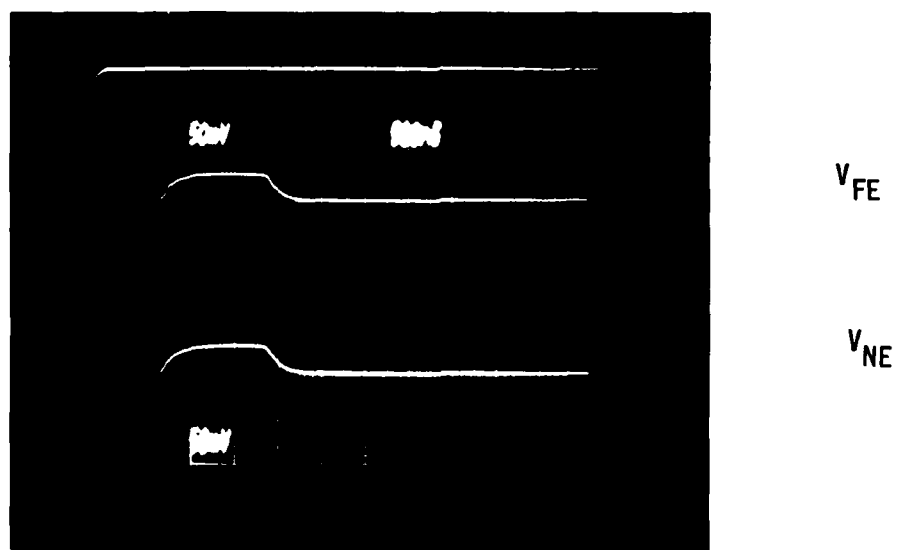
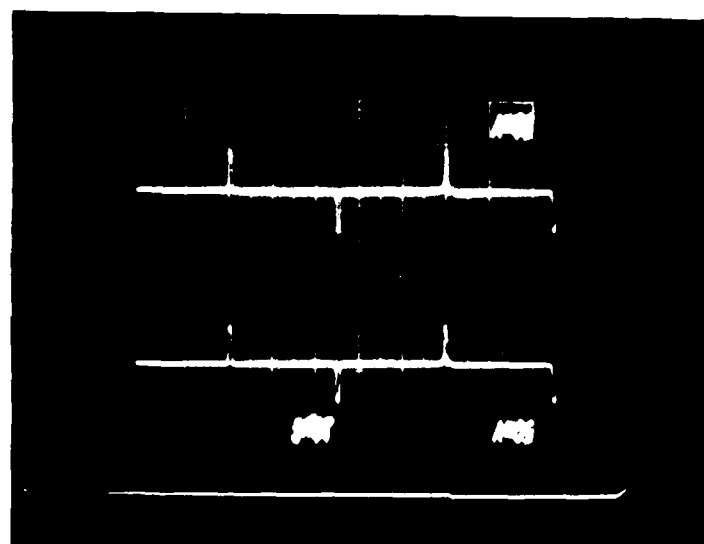
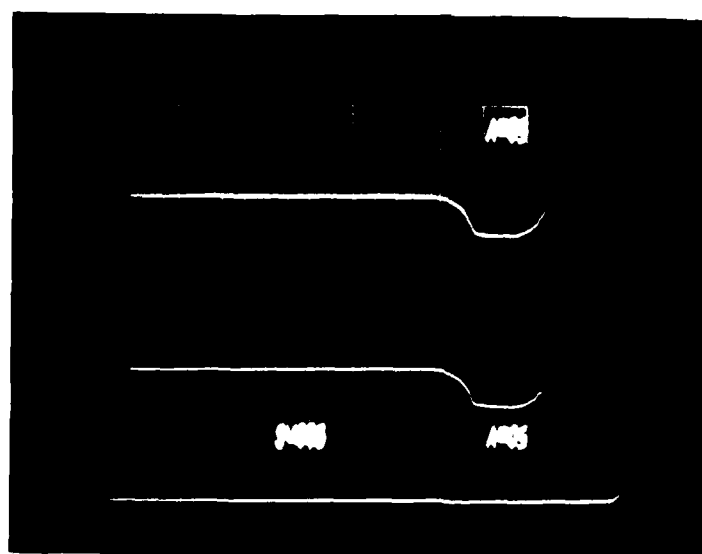


Fig. 4.54. Experimental results 1 k Ω , $\tau_r = \tau_f = 1 \mu s$



V_{FE}

V_{NE}



V_{FE}

V_{NE}

Fig. 4.55. Experimental results 1 k Ω , $\tau_r = \tau_f = 700$ ns

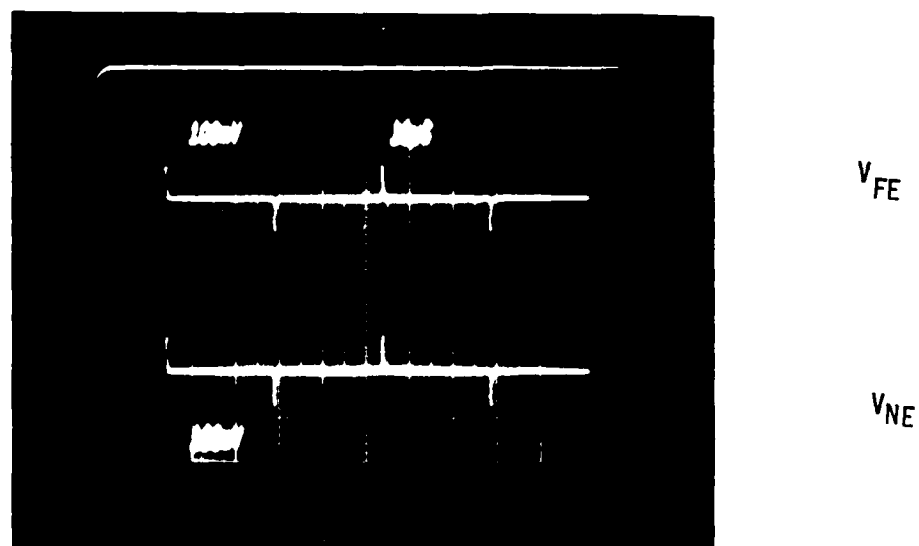
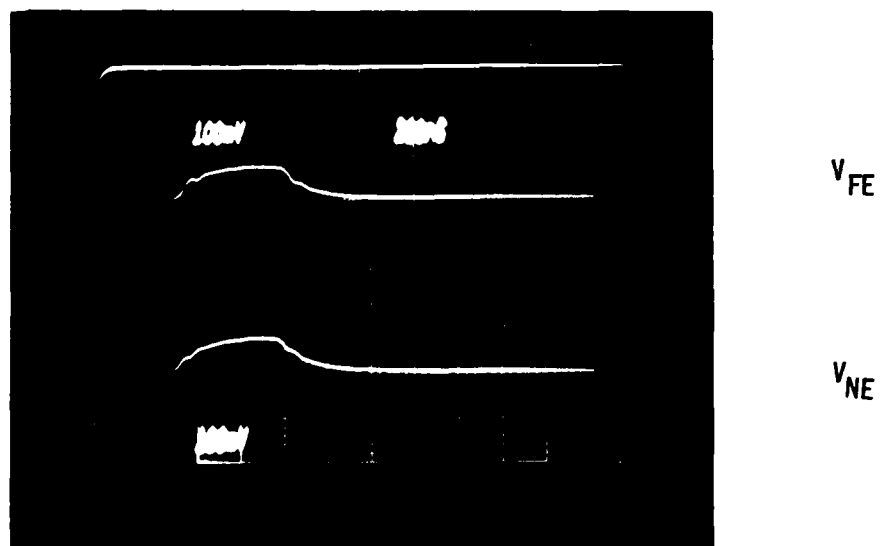
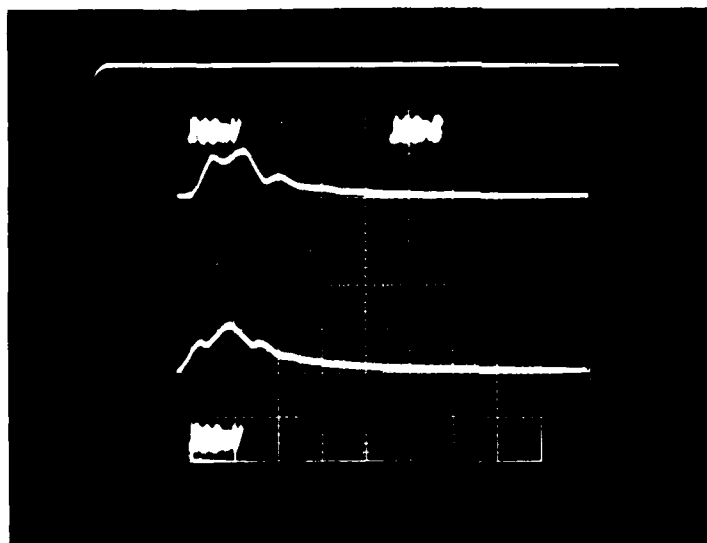
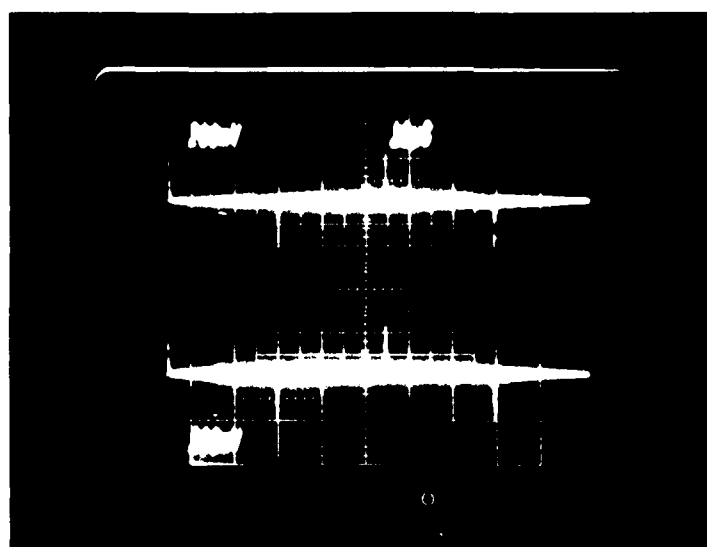


Fig. 4.56. Experimental results 1 k Ω , $\tau_r = \tau_f \cdot 00$ ns



V_{FE}

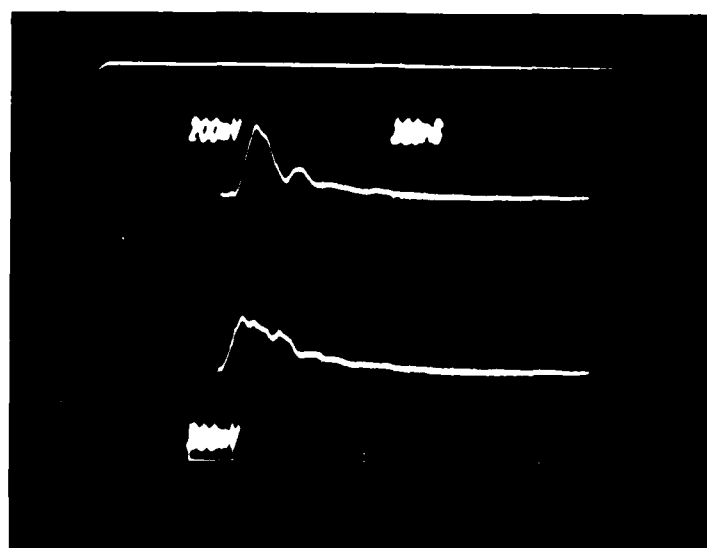
V_{NE}



V_{FE}

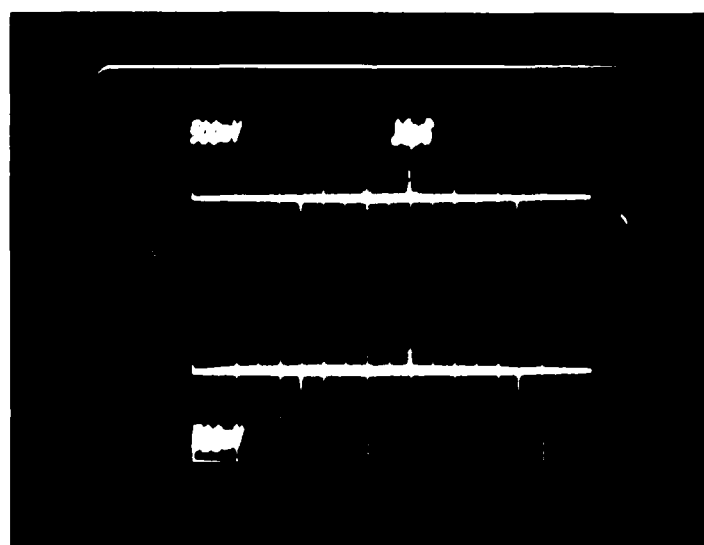
V_{NE}

Fig. 4.57. Experimental results $1\text{ k}\Omega$, $\tau_r = \tau_f = 100\text{ ns}$



V_{FE}

V_{NE}



V_{FE}

V_{NE}

Fig. 4.58. Experimental results 1 k Ω , $\tau_r = \tau_f = 60$ ns

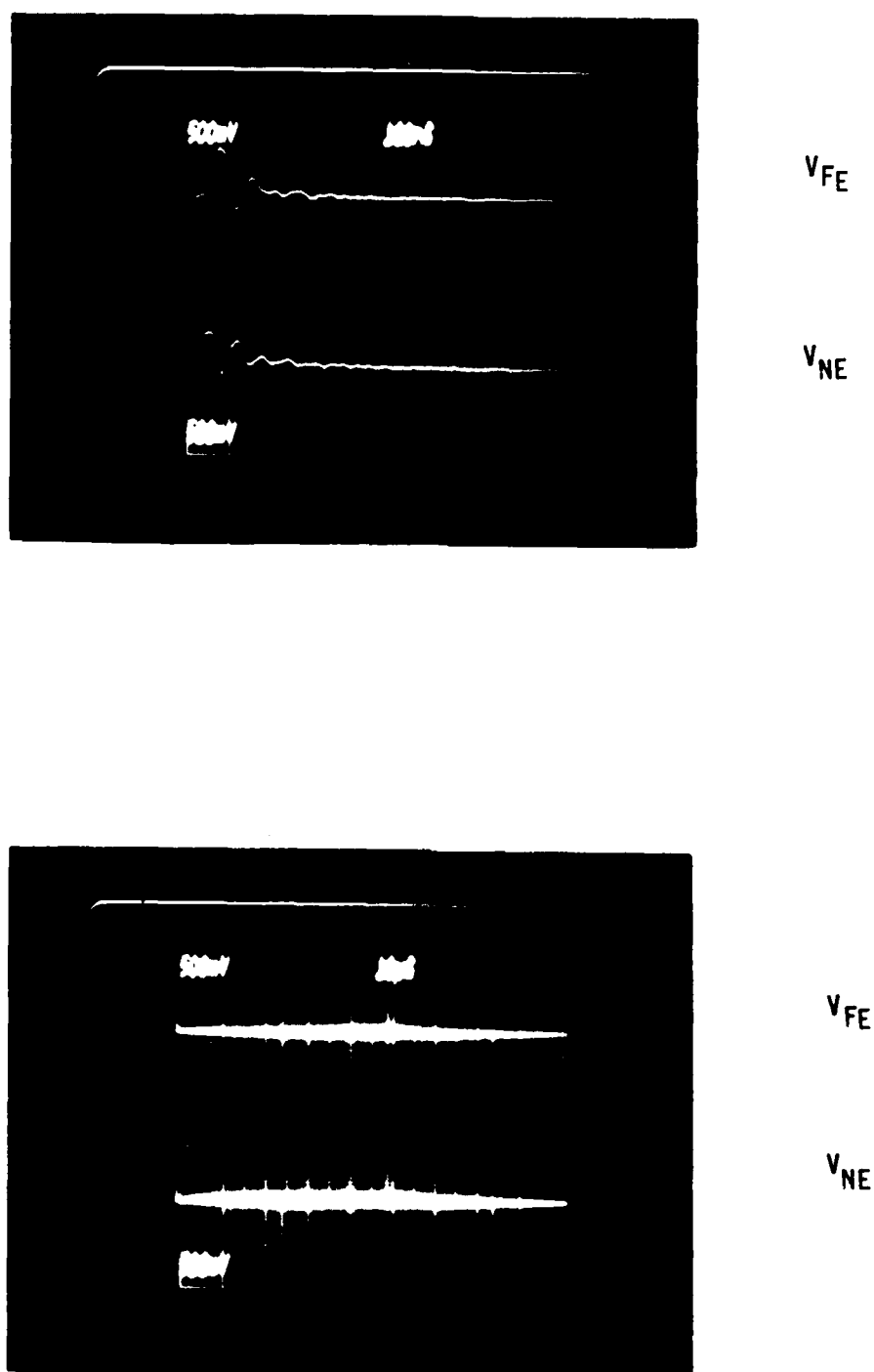


Fig. 4.59. Experimental results 1 k Ω , $\tau_r = \tau_f = 20$ ns

Table 4.5

Maximum Crosstalk Levels

(R=50 Ω)

		Predicted	Measured
$\tau_r = \tau_f = 6 \mu s$	V_{NE}	4.2 mV	9 mV
	V_{FE}	- 3.3 mV	- 9 mV
$\tau_r = \tau_f = 1 \mu s$	V_{NE}	25.2 mV	28 mV
	V_{FE}	- 20 mV	- 24 mV
$\tau_r = \tau_f = 700 ns$	V_{NE}	36 mV	34 mV
	V_{FE}	- 28.6 mV	- 30 mV
$\tau_r = \tau_f = 400 ns$	V_{NE}	63 mV	55 mV
	V_{FE}	- 50 mV	- 45 mV
$\tau_r = \tau_f = 100 ns$	V_{NE}	217.9 mV	140 mV
	V_{FE}	-172.9 mV	- 110 mV
$\tau_r = \tau_f = 60 ns$	V_{NE}	293.5 mV	170 mV
	V_{FE}	-232.9 mV	- 140 mV
$\tau_r = \tau_f = 20 ns$	V_{NE}	415.4 mV	200 mV
	V_{FE}	-329.7 mV	- 180 mV

Table 4.6

Maximum Crosstalk Levels

(R=1 k Ω)

		Predicted	Measured
$\tau_r = \tau_f = 6 \mu s$	V_{NE}	7.2 mV	6 mV
	V_{FE}	5.6 mV	5 mV
$\tau_r = \tau_f = 1 \mu s$	V_{NE}	43.2 mV	35 mV
	V_{FE}	33.6 mV	30 mV
$\tau_r = \tau_f = 700 ns$	V_{NE}	61.7 mV	50 mV
	V_{FE}	48 mV	45 mV
$\tau_r = \tau_f = 400 ns$	V_{NE}	106 mV	90 mV
	V_{FE}	84 mV	80 mV
$\tau_r = \tau_f = 100 ns$	V_{NE}	273 mV	240 mV
	V_{FE}	335.2 mV	220 mV
$\tau_r = \tau_f = 60 ns$	V_{NE}	325 mV	260 mV
	V_{FE}	544.7 mV	340 mV
$\tau_r = \tau_f = 20 ns$	V_{NE}	391.5 mV	450 mV
	V_{FE}	1174 mV	600 mV

order of 32 ns, this is not surprising. For rise/fall times of 400 ns and longer, the predictions are very good. For 400 ns rise/fall times $\tau_r = 12.5 \tau_d$.

Note again as with PCB's, the near end and far end crosstalk polarities are the same as the appropriate slope of the input pulse except for $R=50\Omega$ and far end crosstalk. Once again this is due to inductive coupling dominating capacitive coupling so that M_{FE} is negative.

The predictions of the lumped-circuit iterative Pi and Tee models for 5 sections are shown in Fig. 4.60 through 4.71 for rise/fall times of 700 ns, 100 ns, and 20 ns. The predictions are reasonably accurate. Also we have shown the predictions of the simple model using the measured, frequency-domain parameters of Table 4.4 and the lumped circuit analogue of Fig. 3.7.

4.3 Summary

The lumped-circuit iterative models predicted frequency-domain results for frequencies up to the point at which the line was $\frac{1}{10} \lambda$ in length. Above that point more sections are needed but very little extension of the valid frequency range is obtained.

The simple model of Chapter 3 provided quite accurate predictions of the maximum crosstalk levels so long as the pulse rise/fall time was longer than 10 to 20 times the one-way line delay. In addition, considerable insight into the coupling phenomenon is gained with the simple model. The lumped-circuit iterative models provide no such insight.

Near End Crosstalk, $Z_L=50$, $t_r=700\text{ns}$
 Analog, PI & TEE $N=5$

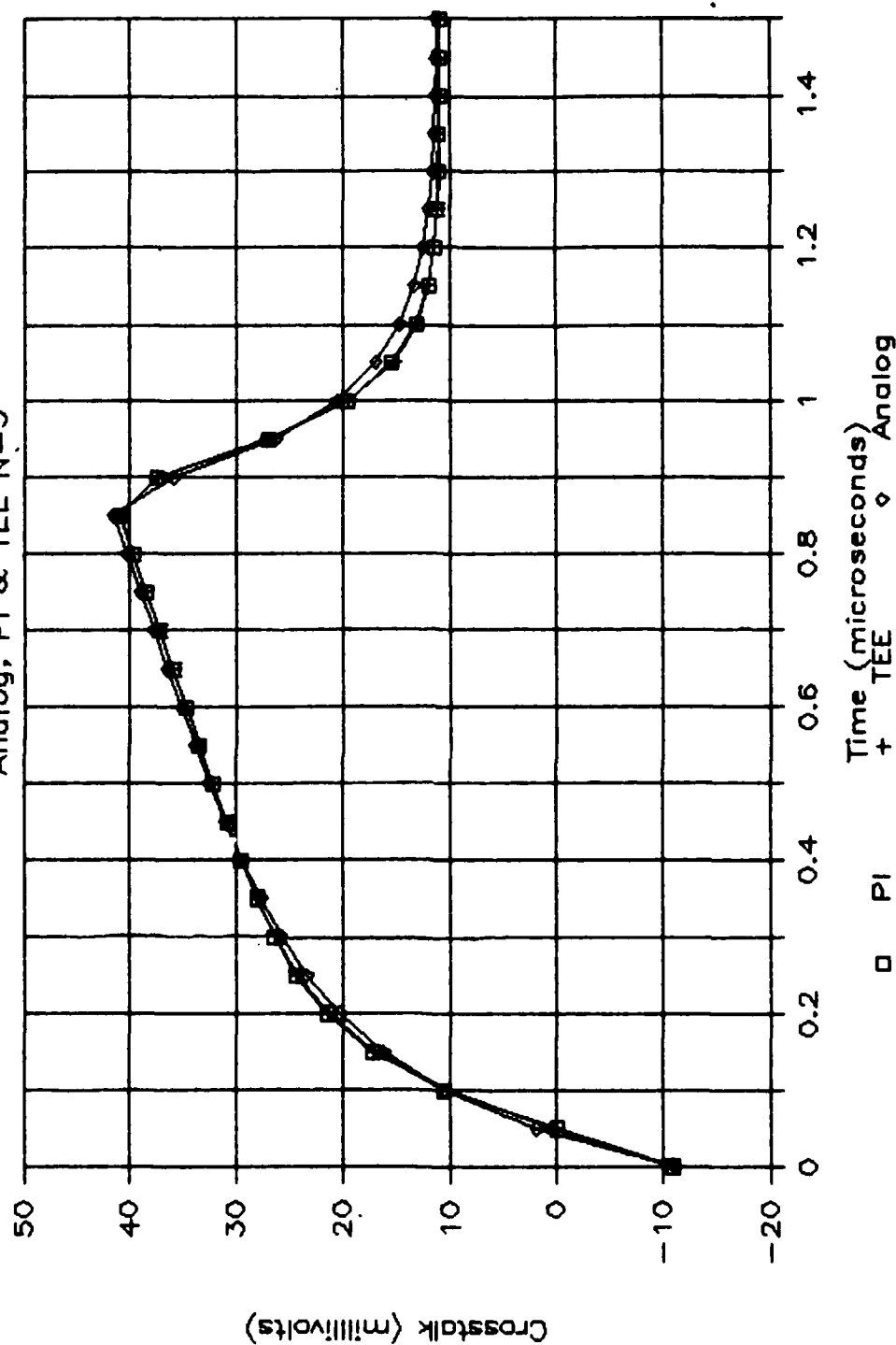


Fig. 4.60. Time-domain predictions 50 Ω , Near End, $\tau_r=\tau_f=700\text{ ns}$

Far End Crosstalk, $Z_L=50$, $\tau_r=700\text{ns}$ Analog, PI & TEE $N=5$

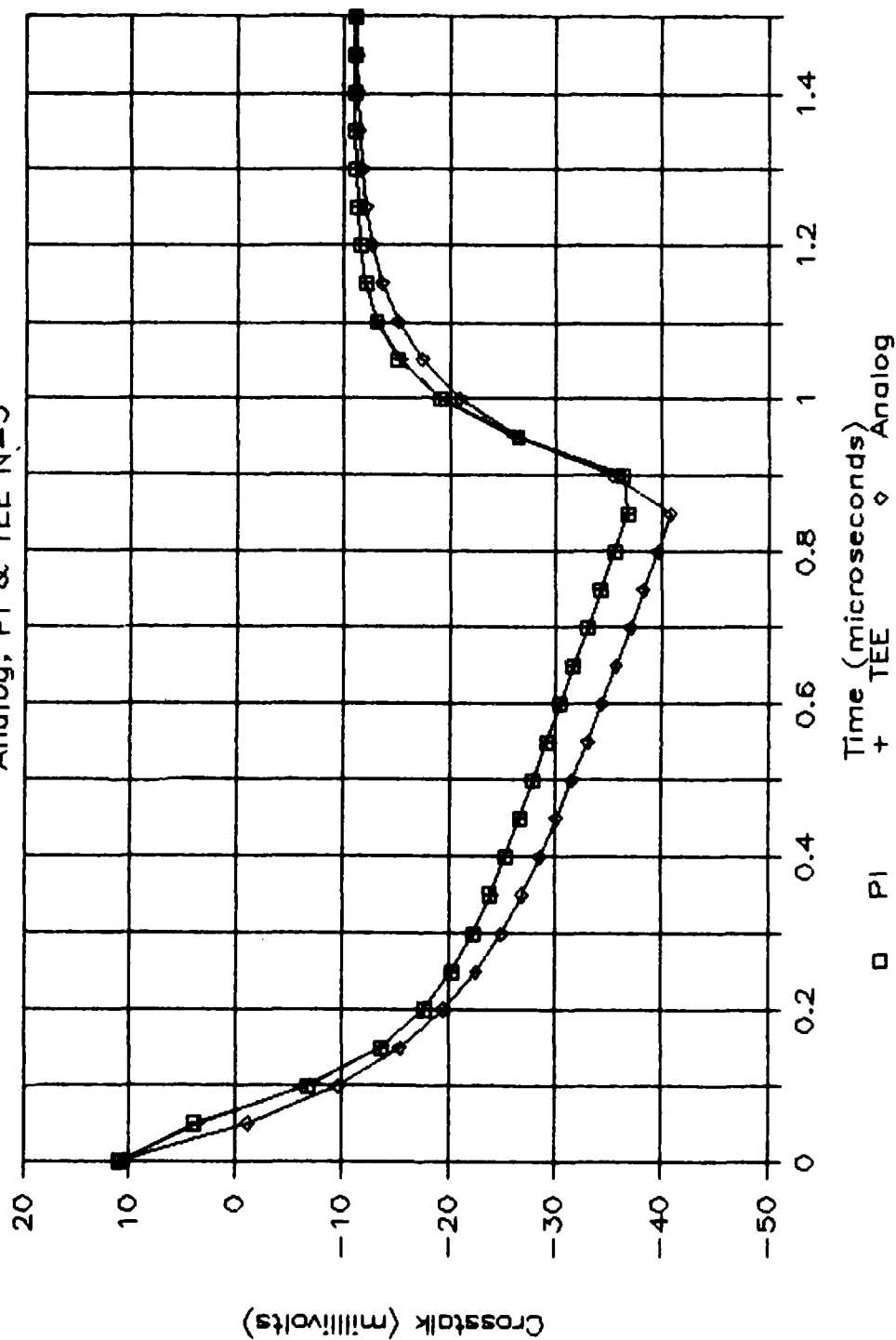


Fig. 4.61. Time-domain predictions 50Ω , Far End, $\tau_r=\tau_f=700\text{ ns}$

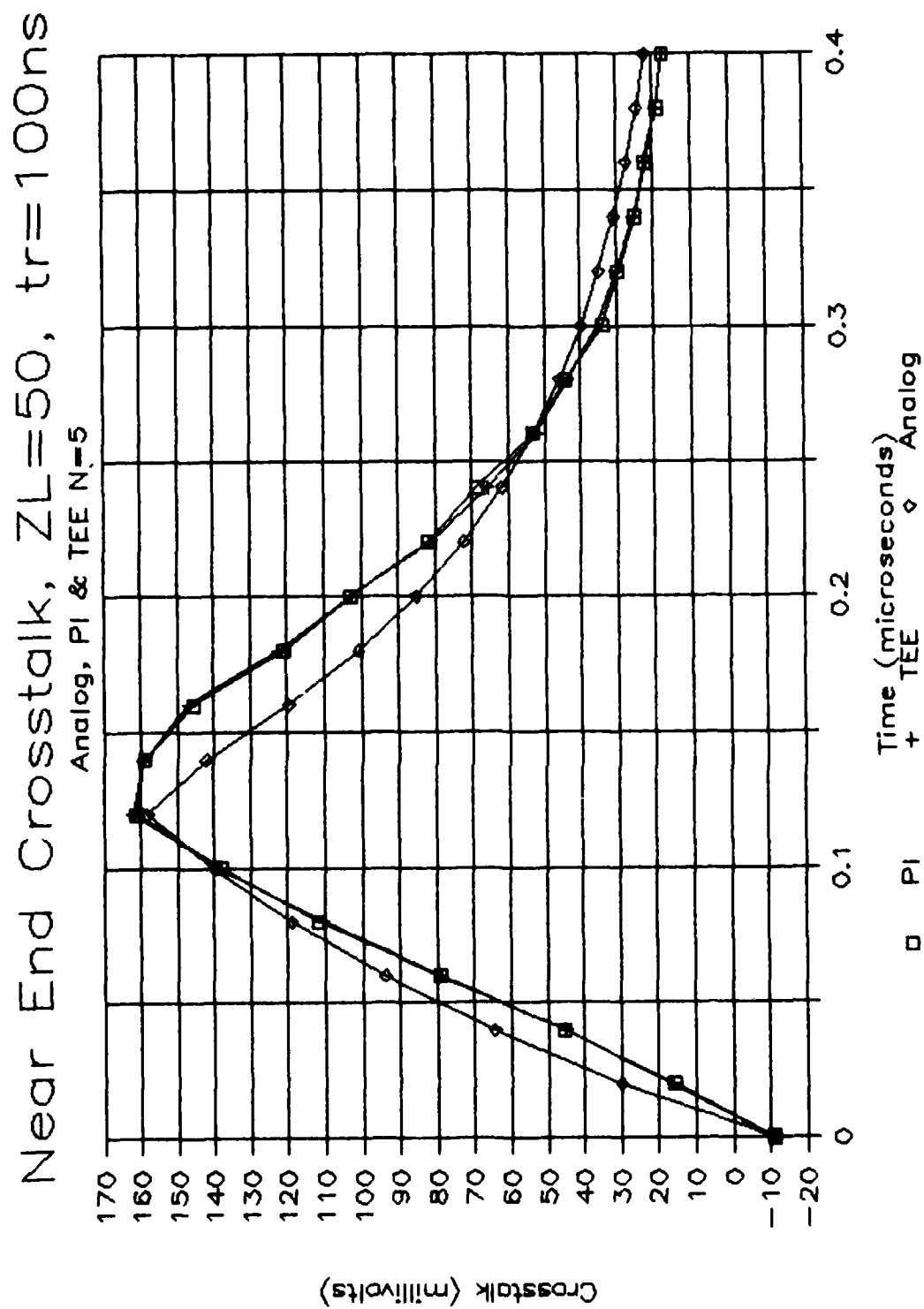


Fig. 4.62. Time-domain predictions 50 Ω , Near End, $\tau_r = \tau_f = 100\text{ ns}$

Far End Crosstalk, $Z_L=50$, $t_r=100\text{ns}$
 Analog, PI & TEE $N=5$

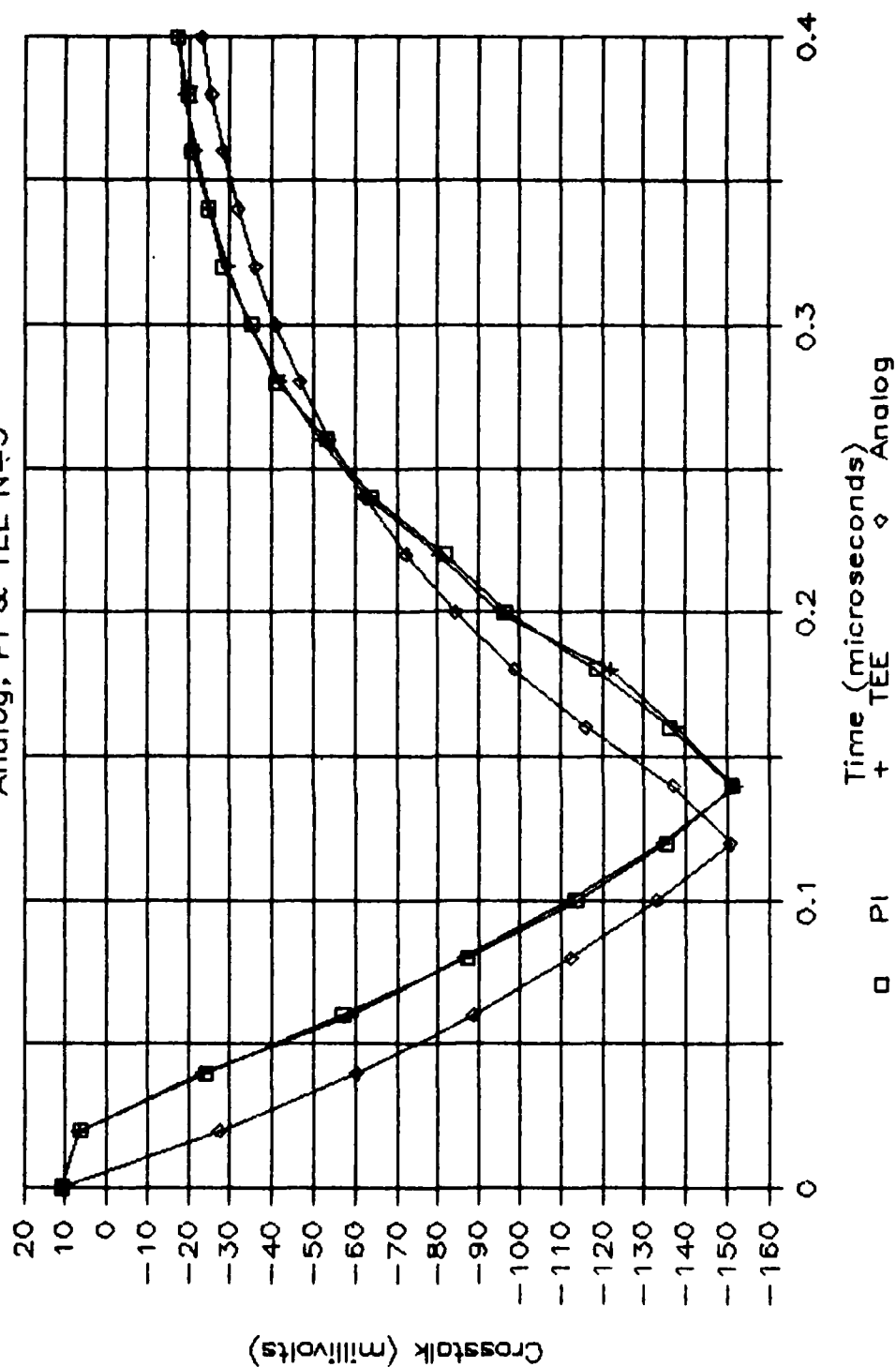


Fig. 4.63. Time-domain predictions 50Ω , Far End, $\tau_r=\tau_f=100\text{ ns}$

Near End Crosstalk, $Z_L=50$, $\tau_r=20\text{ns}$
 Analog, PI & TEE N=5

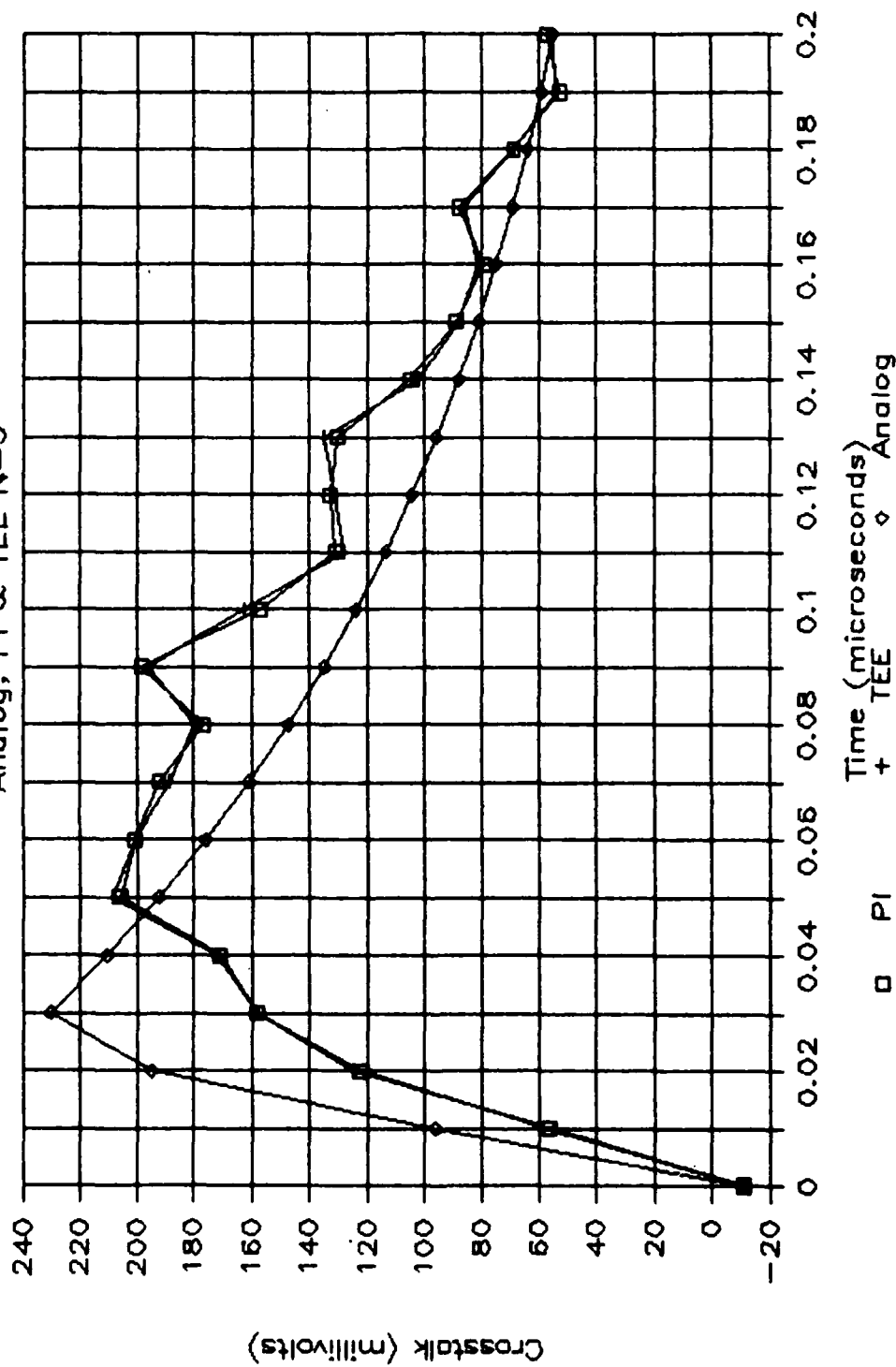


Fig. 4.64. Time-domain predictions 50Ω, Near end, $\tau_r=\tau_f=20\text{ ns}$

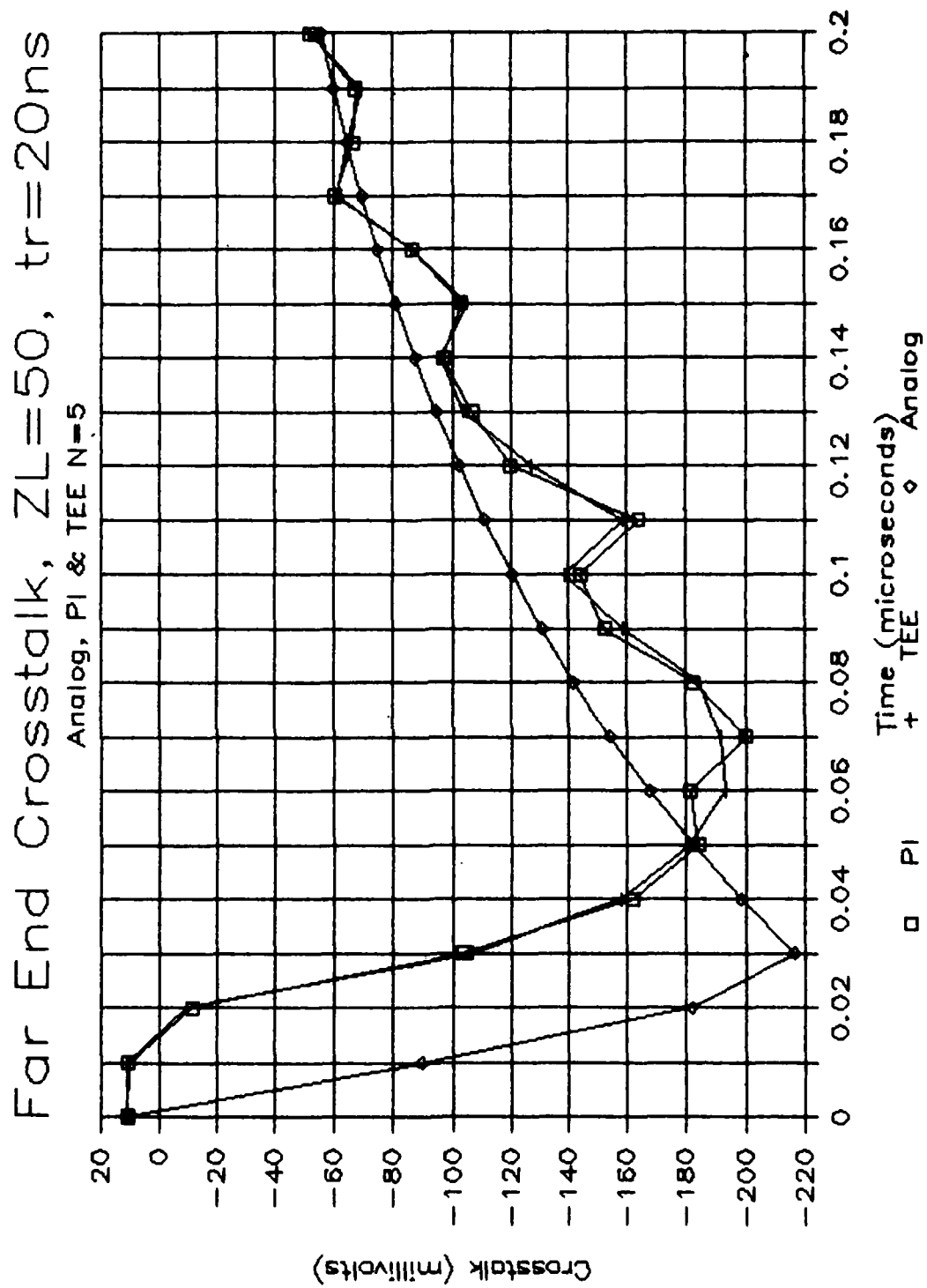


Fig. 4.65. Time-domain predictions 50 Ω , Far End, $\tau_r=\tau_f=20\text{ ns}$

Near End Crosstalk, $Z_L=1k$, $t_r=700ns$

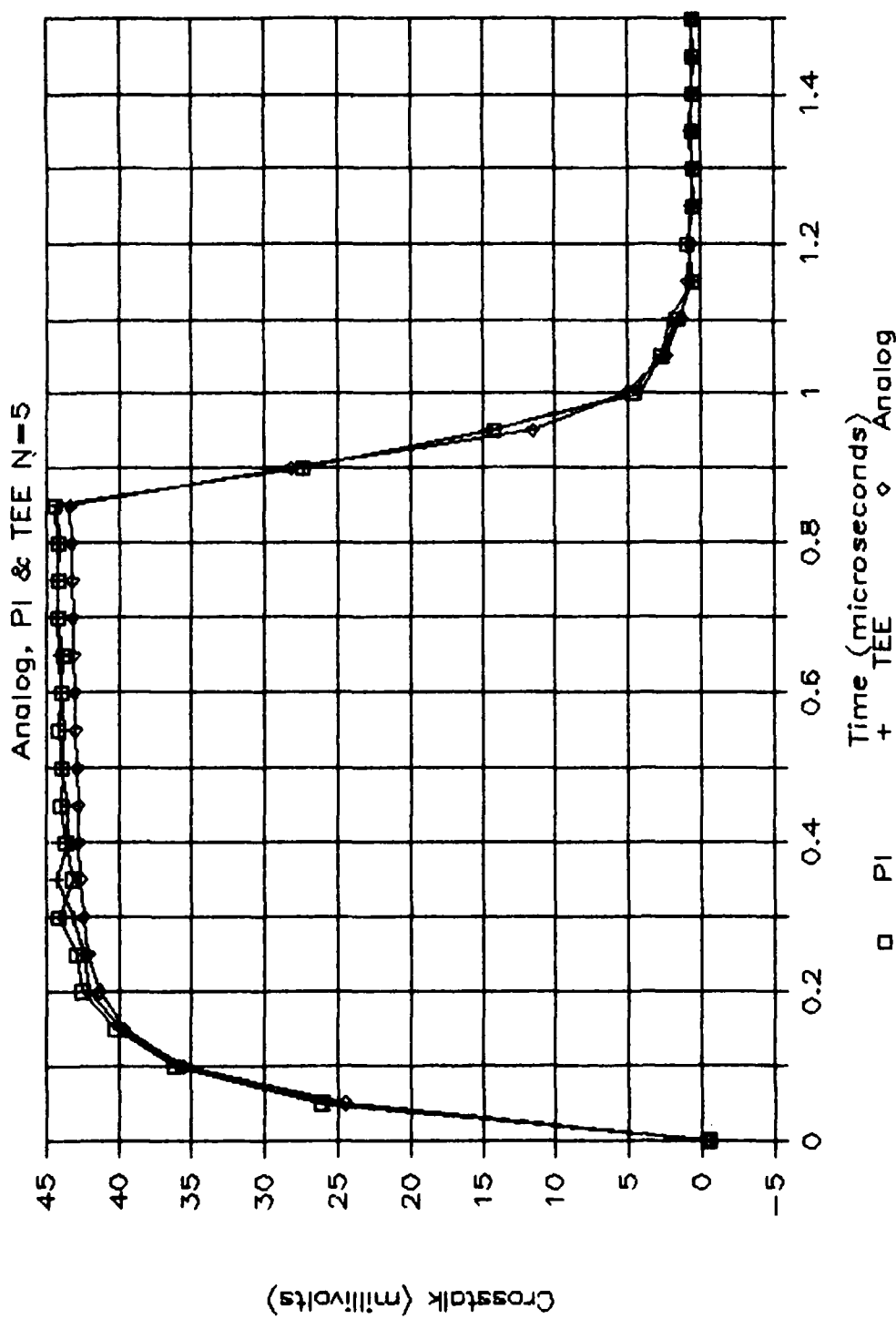


Fig. 4.66. Time-domain predictions $1k\Omega$, Near End, $\tau_r=\tau_f=700\text{ ns}$

Far End Crosstalk, $Z_L=1k$, $\tau_r=700ns$
 Analog, PI & TEE N=5

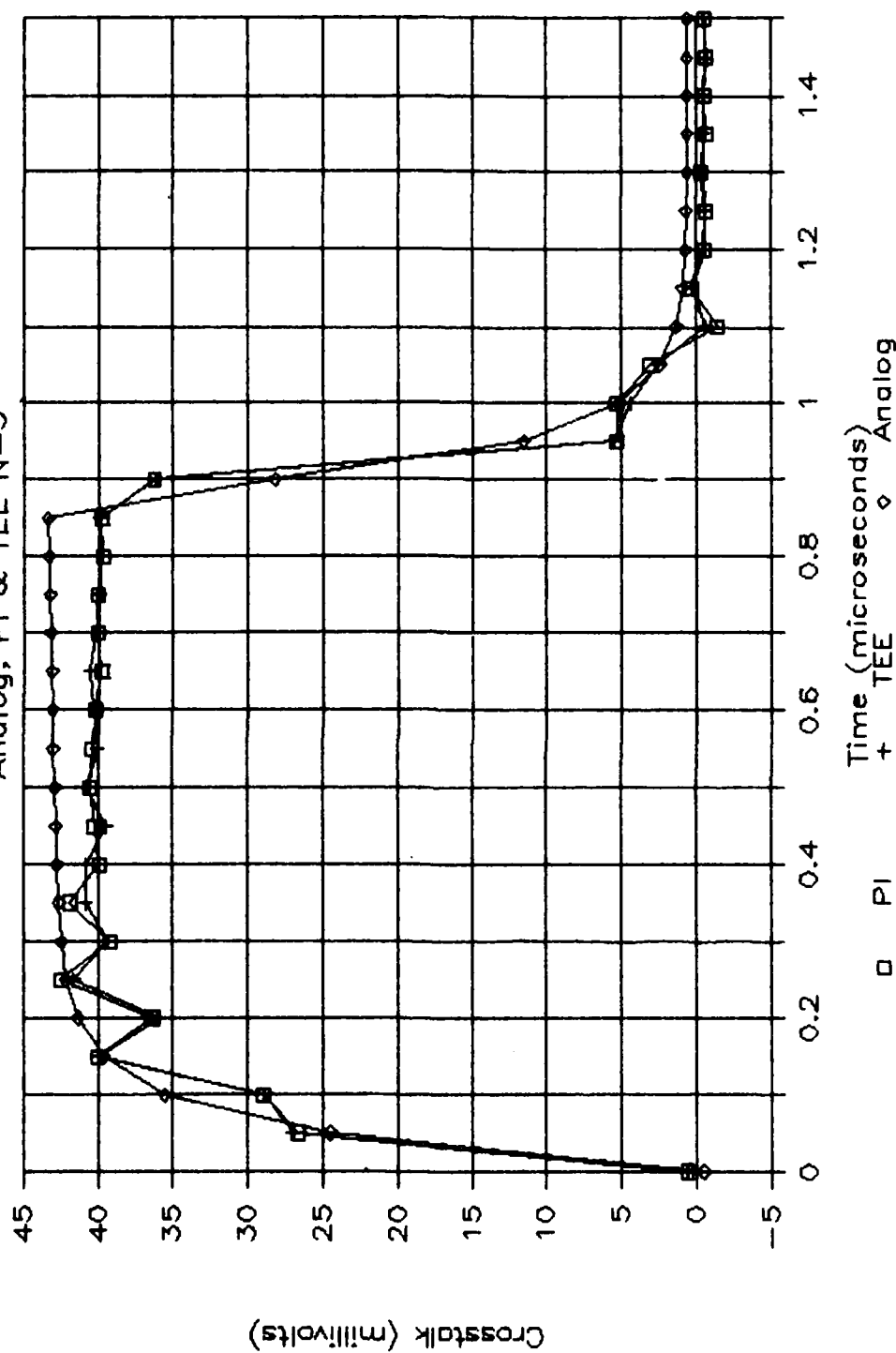


Fig. 4.67. Time-domain predictions $1k\Omega$, Far End, $\tau_r=\tau_f=700$ ns

Near End Crosstalk, $ZL=1k$, $\tau_r=100ns$

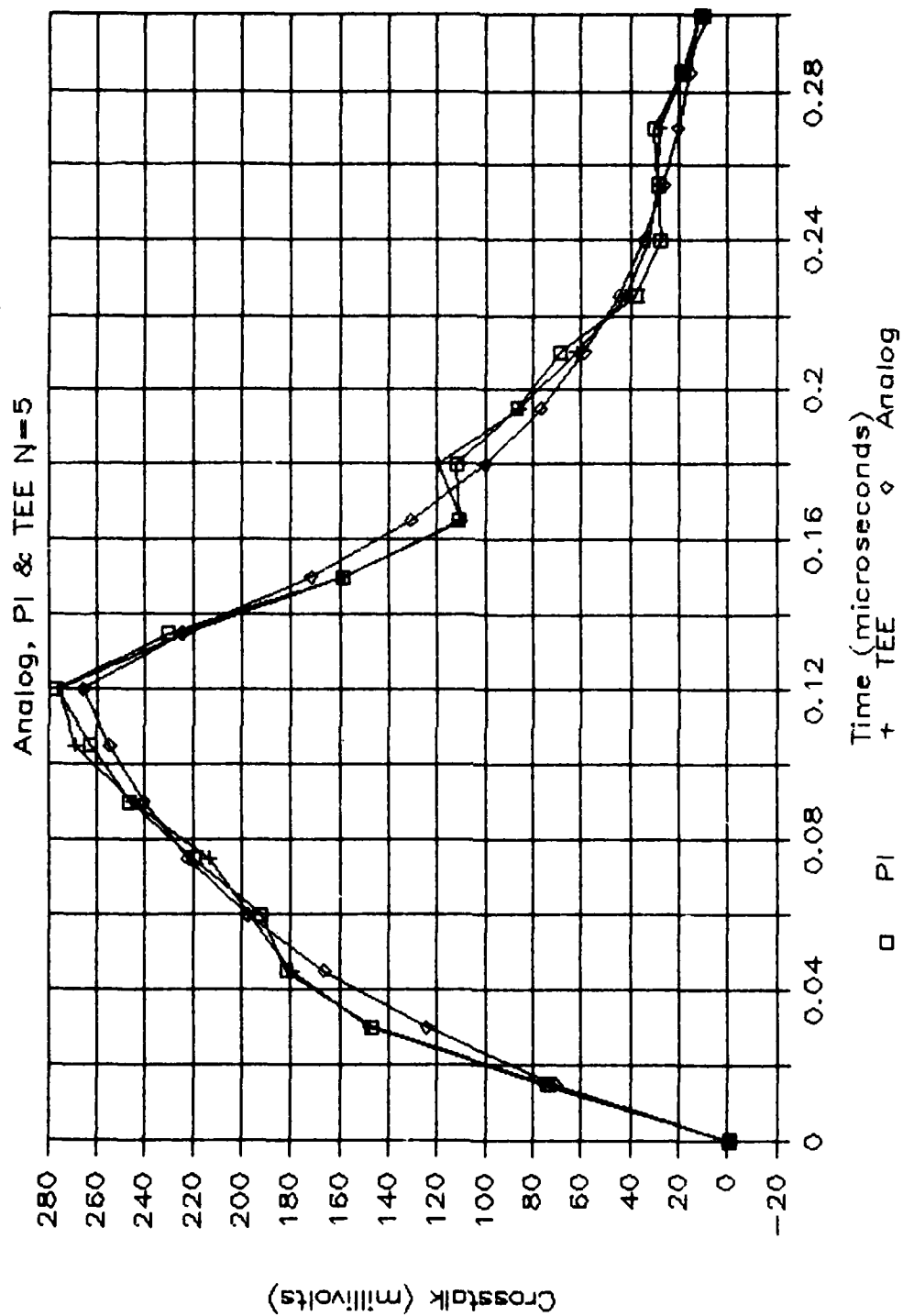


Fig. 4.68. Time-domain predictions $1k\Omega$, Near End, $\tau_r=\tau_f=100$ ns

Far End Crosstalk, $Z_L=1k$, $\tau_r=100ns$
 Analog, PI & TEE N=5

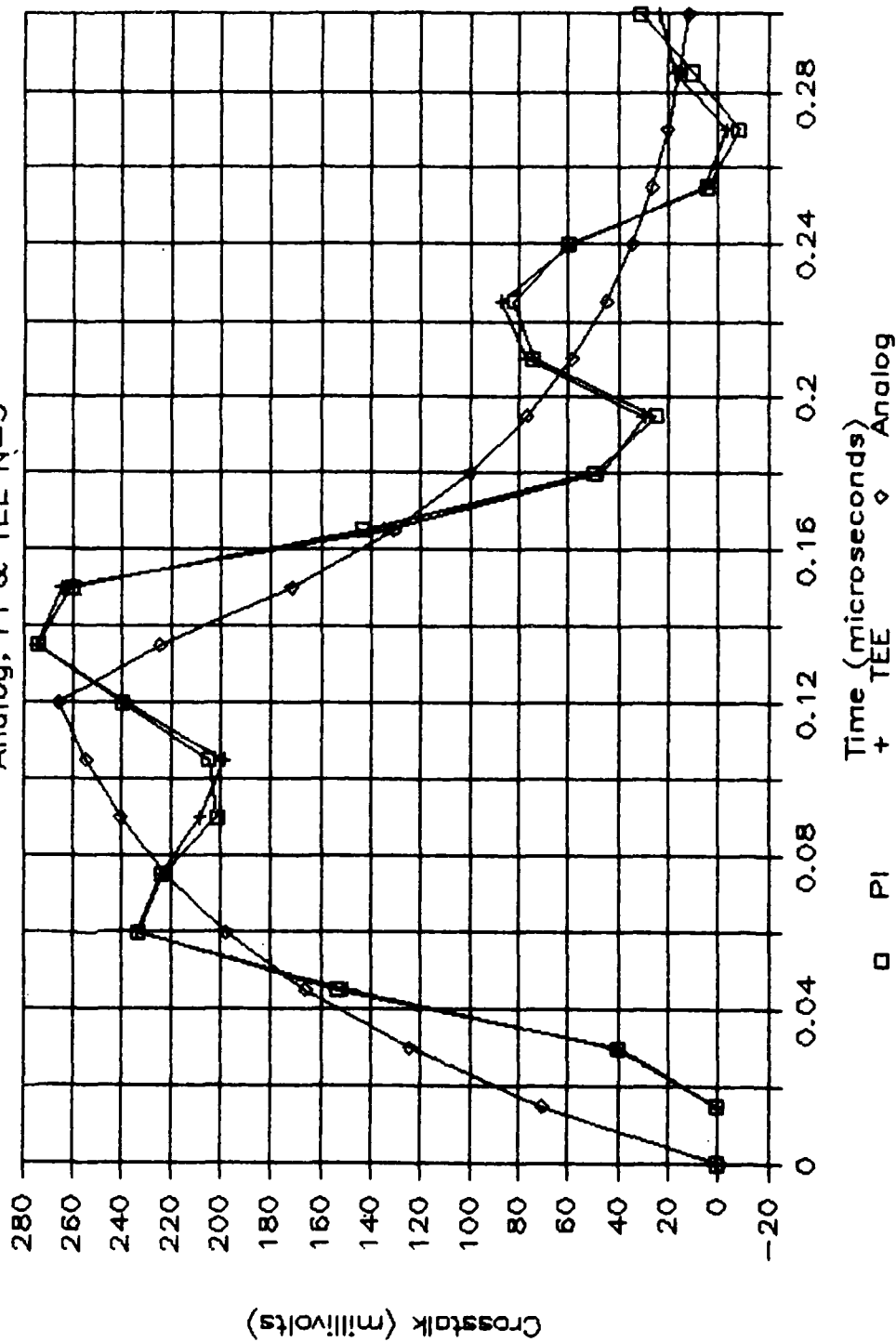


Fig. 4.69. Time-domain predictions $1k\Omega$, Far End, $\tau_r=\tau_f=100\text{ ns}$

Near End Crosstalk, $Z_L=1k$, $\tau_r=20ns$

Analog, PI & TEE N=5

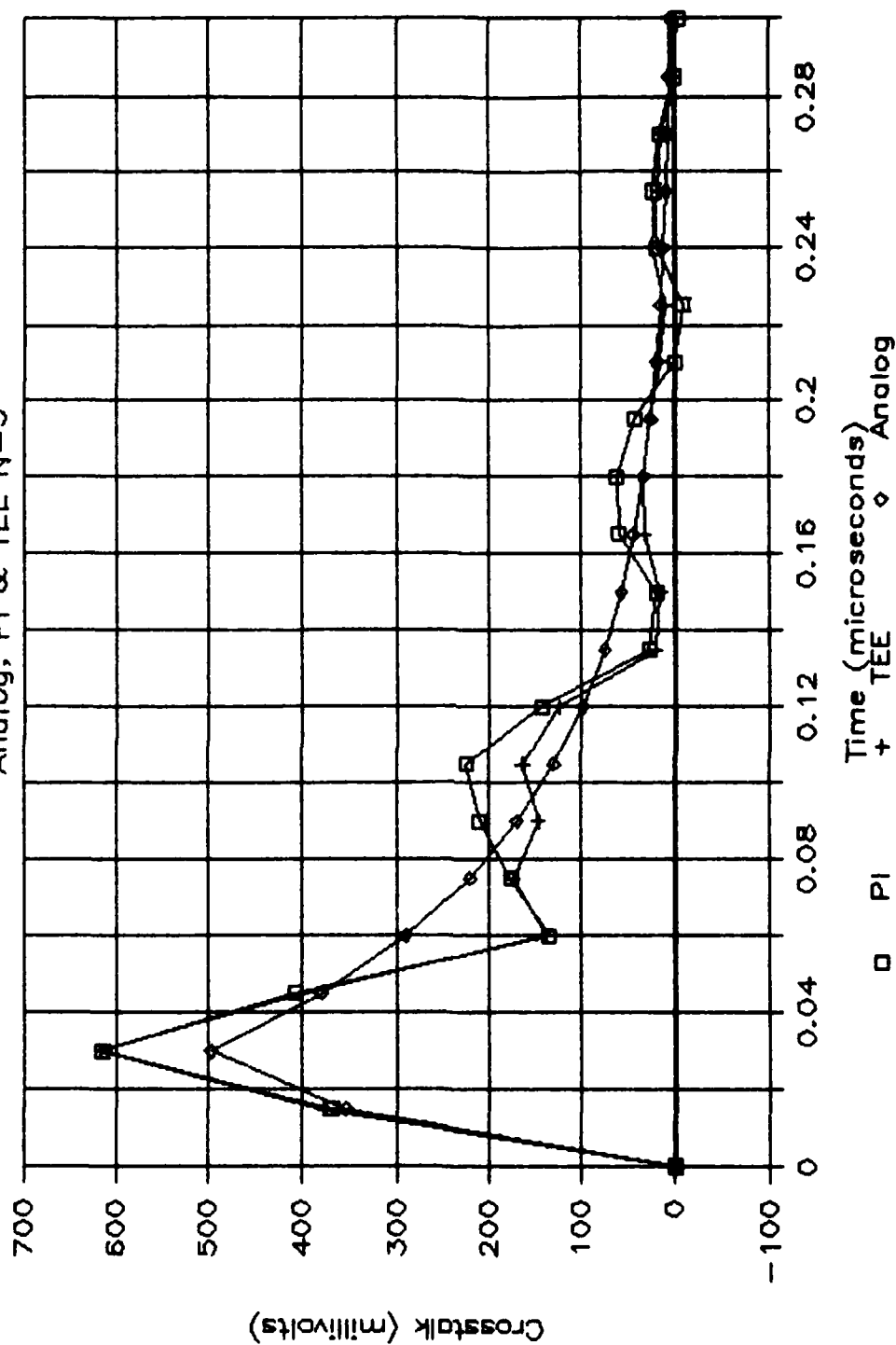


Fig. 4.70. Time-domain predictions $1k\Omega$, Near End, $\tau_r=\tau_f=20\text{ ns}$

Far End Crosstalk, $Z_L=1k$, $\tau_r=20ns$
 Analog, PI & TEE $N=5$

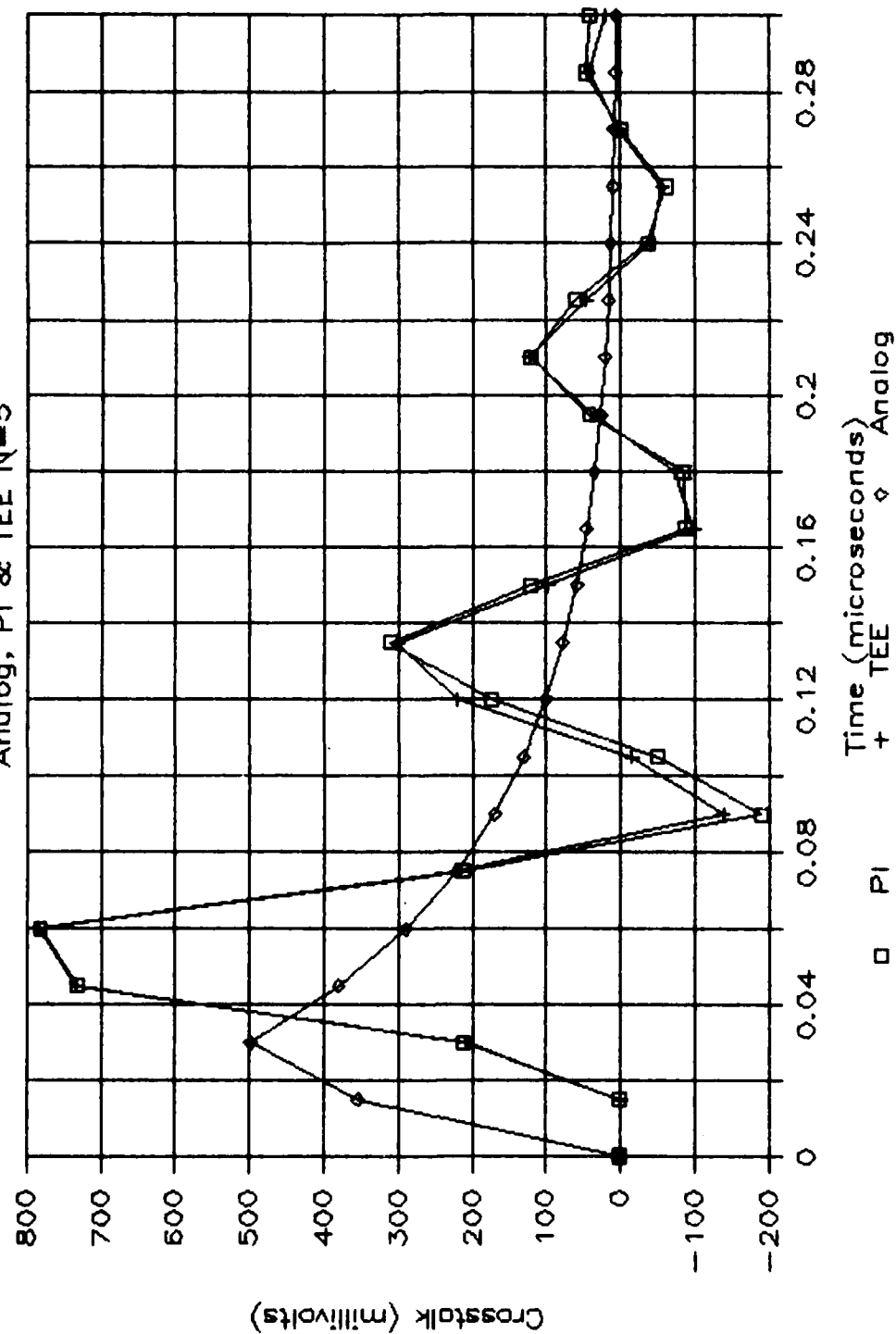


Fig. 4.71. Time-domain predictions $1k\Omega$, Far End, $\tau_r=\tau_f=20\text{ ns}$

V. Summary and Conclusions

The purposes of this report have been (1) to investigate the ability of available, time-domain, crosstalk prediction models and (2) to determine a simple time-domain crosstalk prediction model which is suitable for inclusion in CAD codes. The primary type of transmission line structure which these models were to address was the typical printed circuit board with signals which represent typical bit rates and rise/fall times.

Within these objectives and restrictions, a simple model suitable for inclusion in CAD codes was developed. The model requires two groups of information. The first set is related to the cross-sectional structure of the lines and are contained in the per-unit-length mutual inductances and capacitances between all lines. The other set are the voltages and currents on the interfering lines. The first set of data, the mutual inductances and capacitances can be obtained from direct calculation, direct measurement or inferred from frequency-domain crosstalk measurements. The second set of data--the voltages and currents on the interfering lines--are normally calculated by CAD codes and can be used directly. The crosstalk sources depend on these mutual elements and the slew rates of the voltages and currents on the interfering lines.

Experimental results for a typical PCB as well as a ribbon cable show that the simple model is capable of yielding prediction accuracies better than 3 dB so long as the pulse rise/fall time is at least a factor of 10 to 20 larger than the one-way line delay. Even if this restriction is exceeded the simple model provides an upper bound on the maximum crosstalk.

When one considers the complexity of even relatively simple PCB's, it becomes quite evident the sufficient computing power does not exist

for analyzing time-domain crosstalk between all lands in real time with sophisticated prediction models or even the relatively simple lumped-circuit iterative models (using only one section per line). The simple model proposed here has the potential for handling this problem.

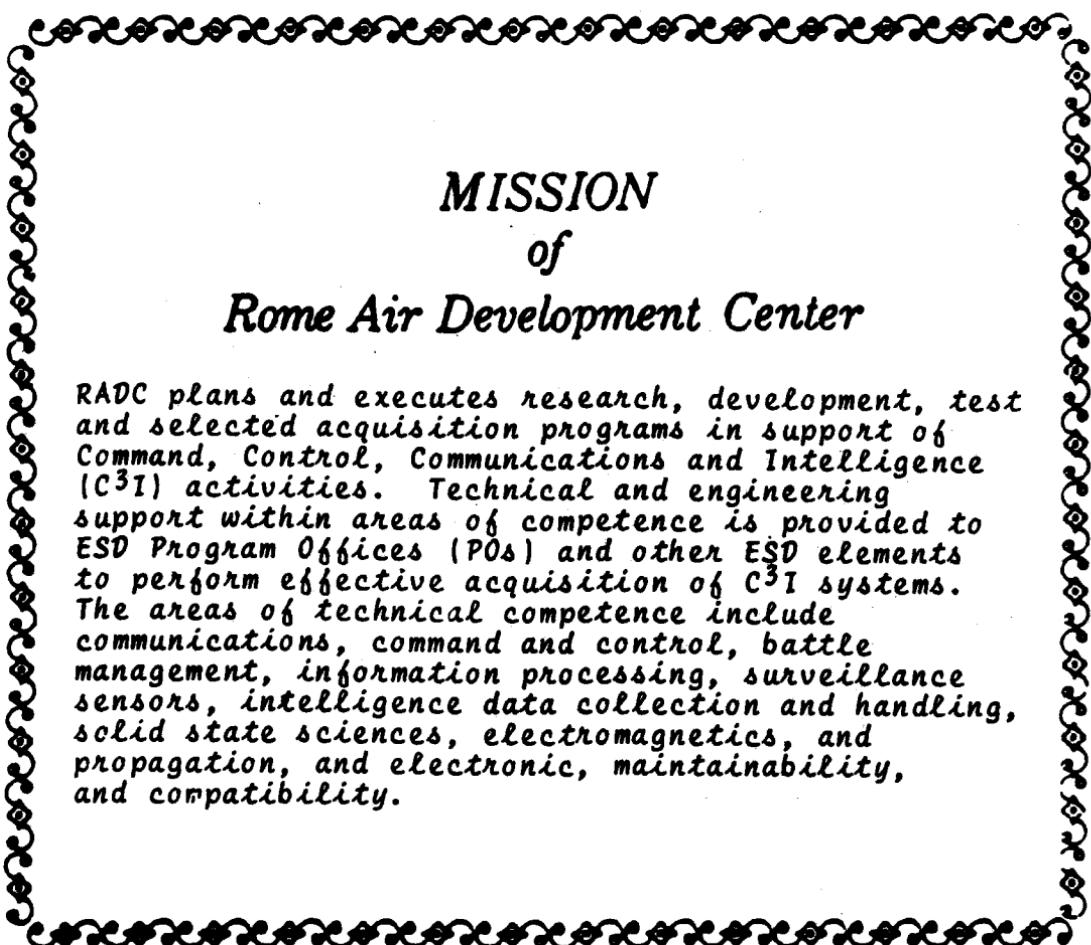
In addition, perhaps the minimum amount of information is required to be gathered by the analyst. However, it remains to provide an intermediate code to transform the physical land layout data to the mutual inductances and capacitances required by the model.

REFERENCES

- [1] C. R. Paul, Applications of Multiconductor Transmission Line Theory to the Prediction of Cable Coupling, Vol. I, Multiconductor Transmission Line Theory, Technical Report, RADC-TR-76-101, Rome Air Development Center, Griffiss AFB, NY, April 1976.
- [2] C. R. Paul, Applications of Multiconductor Transmission Line Theory to the Prediction of Cable Coupling, Vol. IV, Prediction of Crosstalk in Ribbon Cables, Technical Report, RADC-TR-76-101, Rome Air Development Center, Griffiss AFB, NY, Feb. 1978.
- [3] C. R. Paul, "Prediction of Crosstalk in Ribbon Cables: Comparison of Model Predictions and Experimental Results," IEEE Trans. on Electromagnetic Compatibility, Vol. EMC-20, No. 3, pp. 394-406, August 1978.
- [4] C. W. Ho, "Theory and Computer-Aided Analysis of Lossless Transmission Lines," IBM J. Research and Development, pp. 249-255, May 1973.
- [5] F. Y. Chang, "Transient Analysis of Lossless Coupled Transmission Lines in Inhomogeneous Dielectric Medium," IEEE Trans. Microwave Theory and Techniques, Vol. MTT-18, No. 9, pp. 616-626, Sept. 1970.
- [6] K. D. Marx, "Propagation Modes, Equivalent Circuits, and Characteristic Terminations for Multiconductor Transmission Lines with Inhomogeneous Dielectrics," IEEE Trans. Microwave Theory and Techniques, Vol. MTT-21, No. 7, pp. 450-457, July 1973.
- [7] H. Amemiya, "Time-Domain Analysis of Multiple Parallel Transmission Lines," RCA Review, pp. 214-276, June 1967.

- [8] A. K. Agrawal, H. M. Fowles, L. D. Scott, and S. H. Gurbaxani, "Application of Modal Analysis to the Transient Response of Multi-conductor Transmission Lines with Branches," IEEE Trans. on Electro-magnetic Compatibility, Vol. EMC-21, No. 3, pp. 256-262, August 1979.
- [9] H. W. Dommel and W. S. Meyer, "Computation of Electromagnetic Transients," Proc. IEEE, Vol. 62, No. 7, pp. 983-993, July 1974.
- [10] H. W. Dommel, "Digital Computer Solutions of Electromagnetic Transients in Single and Multiphase Networks," IEEE Trans. Power App. Syst., Vol. PAS-88, p. 388, 1969.
- [11] Y. K. Liu, "Transient Analysis of TEM Transmission Lines," Proc. IEEE, pp. 1090-1092, June 1968.
- [12] A.J. Gruodis and C. S. Chang, "Coupled Lossy Transmission Line Characterization and Simulation," IBM J. Res. Develop., Vol. 25, No. 1, pp. 25-41, Jan. 1981.
- [13] C. S. Yen, Z. Fazarinc, and R. L. Wheeler, "Time-Domain Skin-Effect Model for Transient Analysis of Lossy Transmission Lines," Proc. IEEE, Vol. 70, No. 7, pp. 750-757, July 1982.
- [14] W. W. Everett, III, Lumped Model Approximations of Transmission Lines: Effect of Load Impedances on Accuracy, Technical Report, Rome Air Development Center, Griffiss AFB, NY, to appear.
- [15] F. H. Branin, Jr., "Transient Analysis of Lossless Transmission Lines," Proc. IEEE, Vol. 55, No. 11, pp. 2012-2013, Nov. 1967.
- [16] Y. K. Liu, "Transient Analysis of TEM Transmission Lines," Proc. IEEE, pp. 1090-1092, June 1968.
- [17] J. L. Allen, "Analysis of Lumped-Distributed Networks," IEEE Trans. on Microwave Theory and Techniques, Nov. 1979.

- [18] Von Horst Nielinger, "Die Verzögert Spannungsgesteuerte Stromquelle-
ein Netzuert Element zur Simulation von Leitungen," Nachrichtentech
Nische Zeitschrift, Vol. 29, No. 11, pp. 820-824, Nov. 1976.
- [19] C. R. Paul, "Solution of the Transmission Line Equations for Three-
Conductor Lines in Homogeneous Media," IEEE Trans. on Electromagnetic
Compatibility, Vol. EMC-20, No. 1, pp. 216-222, Feb. 1978.
- [20] C. R. Paul, "Estimation of Crosstalk in Three-Conductor Transmission
Lines," IEEE Trans. on Electromagnetic Compatibility, Vol. EMC-26,
No. 4, pp. 182-192, Nov. 1984.
- [21] C. R. Paul, "On the Superposition of Inductive and Capacitive Coupling
in Crosstalk Prediction Models," IEEE Trans. on Electromagnetic
Compatibility, Vol. EMC-24, No. 3, pp. 335-343, August 1982.



*MISSION
of
Rome Air Development Center*

RADC plans and executes research, development, test and selected acquisition programs in support of Command, Control, Communications and Intelligence (C³I) activities. Technical and engineering support within areas of competence is provided to ESD Program Offices (POs) and other ESD elements to perform effective acquisition of C³I systems. The areas of technical competence include communications, command and control, battle management, information processing, surveillance sensors, intelligence data collection and handling, solid state sciences, electromagnetics, and propagation, and electronic, maintainability, and compatibility.